Study of catalytic and biological activity of gold-containing metal nanoparticles

A thesis submitted in partial fulfilment of the
requirements for the Degree
of Doctor of Philosophy in Chemistry
in the University of Canterbury
by Baira Donoeva

University of Canterbury

June 2014

Abstract

Small particles of gold (< 100 nm) have attracted great interest among researchers due to the unique combination of their physicochemical properties. Among various research areas catalysis and bio-nanotechnology represent the largest areas of growth for gold nanoparticle research.

Catalysts play a crucial role in the life of the modern society. More than 85 % of all chemical processes are catalytic, and this number is increasing every year. There is a constant demand to develop more efficient and durable catalysts in order to address increasing energy demands and environmental requirements. The first part of the thesis is focused on the study of catalytic activity of supported gold and mixed-metal catalysts, derived from atomically precise phosphine-stabilised gold and mixed-metal clusters in the liquid-phase oxidation of cyclohexene and one-pot synthesis of imines. Various characterisation techniques (TEM, diffuse-reflectance UV-vis, XPS, etc.) as well as kinetic studies were used in order to establish the optimal structure of gold catalysts. The effect of catalytic support, nature of hetero-metal atom for mixed metal-systems and type of catalyst pre-treatment were also examined.

Gold nanoparticles are actively studied in various biomedical applications as they are offering new approaches to the detection and treatment of life-threatening diseases, such as cancer. The second part of this work discusses our preliminary investigations of biological activity of gold nanoparticles, stabilised with cancer-targeting molecules. In particular, the cytotoxicity of gold nanoparticles was studied using 11 different cancer and normal cell types. Gold uptake and particle localisation inside the cells were also investigated.

Contents

Table of figures

Table of tables

Acknowledgements

I would like to thank my supervisors Dr Vladimir Golovko and Prof John Evans for the guidance during my studies, as well as MacDiarmid Institute for the generous funding. I am very grateful to Dr Kenny Chitcholtan for kind sharing his knowledge of methods and procedures used in biological research.

I would like to thank Dr Matthew Polson, Dr Marie Squire, Dr Meike Holzenkämpfer and Alistair Duff for instrument trainings and other help during my studies; Dr Sally Gaw and Robert Stainthorpe for the ICP-MS analysis; Dr Takanori Sato and Mike Flaws from Department of Mechanical Engineering for TEM and SEM training, Campbell McNicoll and Dr Tim Kemmitt for PXRD and surface area analysis. I would also like to thank Prof Bryce Williamson for the help with proof-reading manuscripts.

Thanks to my fellow colleagues from the Golovko group, the Laboratory for cell and protein regulation and Chemistry Department for the great company and making my PhD project more enjoyable.

Finally, I would like to thank my husband and family for the encouragement and enormous support during my studies.

Declarations

I declare that the work presented in this thesis is based on my own research, except where specifically acknowledged in the text. Parts of the work reported in this thesis have been previously published in:

1. Donoeva B. G., Ovoshchnikov D. S., Golovko V. B., *Establishing a Au Nanoparticle Size Effect in the Oxidation of Cyclohexene Using Gradually Changing Au Catalysts*, ***ACS Catalysis***, 2013, 3, 2986 − 2991
2. Ovoshchnikov D. S., Donoeva B. G., Williamson B. E., Golovko V. B., *Tuning the selectivity of a supported gold catalyst in solvent- and radical initiator-free aerobic oxidation of cyclohexene*, ***Catalysis Science and Technology***, 2014, 4, 752 − 757

List of abbreviations

AAS – Atomic absorption spectroscopy

CTAB – cetyl trimethylammonium bromide

CyOOH – cyclohexenyl hydroperoxide

DCM – dichloromethane

DMEM – Dulbecco's Modified Eagle Medium

DR UV-vis – diffuse reflectance UV-vis spectroscopy

EGFR – epidermal growth factor receptor

EPR effect – enhanced permeability and retention effect

EXAFS – Extended X-ray absorption fine structure

GC-FID – gas chromatography

GC-MS – gas chromatography mass-spectrometry

HAADF STEM – high-angle annular dark-field scanning transmission electron microscopy

HAP – hydroxyapatite

HER-2 – human epidermal growth factor receptor 2

KA oil – mixture of cyclohexanol and cyclohexanone

LSPR/SPR – localised surface plasmon resonance/ surface plasmon resonance

N-BBA – N-benzylidene benzylamine

NMR – nuclear magnetic resonance

PBS – phosphate buffered saline

PVA – polyvinyl alcohol

PVP – polyvinylpyrrolidone

SEM – scanning electron microscopy

tBuOOH – tert-butyl hydroperoxide

TEM – transmission electron microscopy

TEOS – tetraethyl orthosilicate

TGA – thermal gravimetric analysis

TOF – turnover frequency

XPS – X-ray photoelectron spectroscopy

Chapter 1. Introduction

1.1 Catalysis

It is hard to overestimate the role of catalysis in the modern industry – approximately 85 – 90 % of all chemical products (bulk and fine chemicals, fuels) are produced in catalytic processes.[1, 2] The use of catalysts allows addressing energy and environmental problems by offering more energetically efficient mechanisms, by preventing pollution from automotive/industrial exhausts and eliminating formation of waste and unwanted by-products in various industrial processes. Due to the importance of catalytic processes, tremendous efforts are dedicated to the development of new catalytic materials and improvement of the existing ones.

F.W. Ostwald defined a catalyst as "a substance that increases the rate at which a chemical system approaches equilibrium, without being consumed in the process".[2] Catalysts accelerate thermodynamically favourable chemical reactions by lowering the activation energy of the process. Figure 1.1 demonstrates how the use of a catalyst changes the reaction pathway to the one with lower activation energy. The overall energy change of the process remains the same as in the absence of a catalyst; however the transition state could be achieved more easily. At the end of the reaction catalyst remains unchanged and is ready for the next cycle.

The three main criteria for the development of new catalysts are the high activity, the high selectivity towards the desired product and good stability.

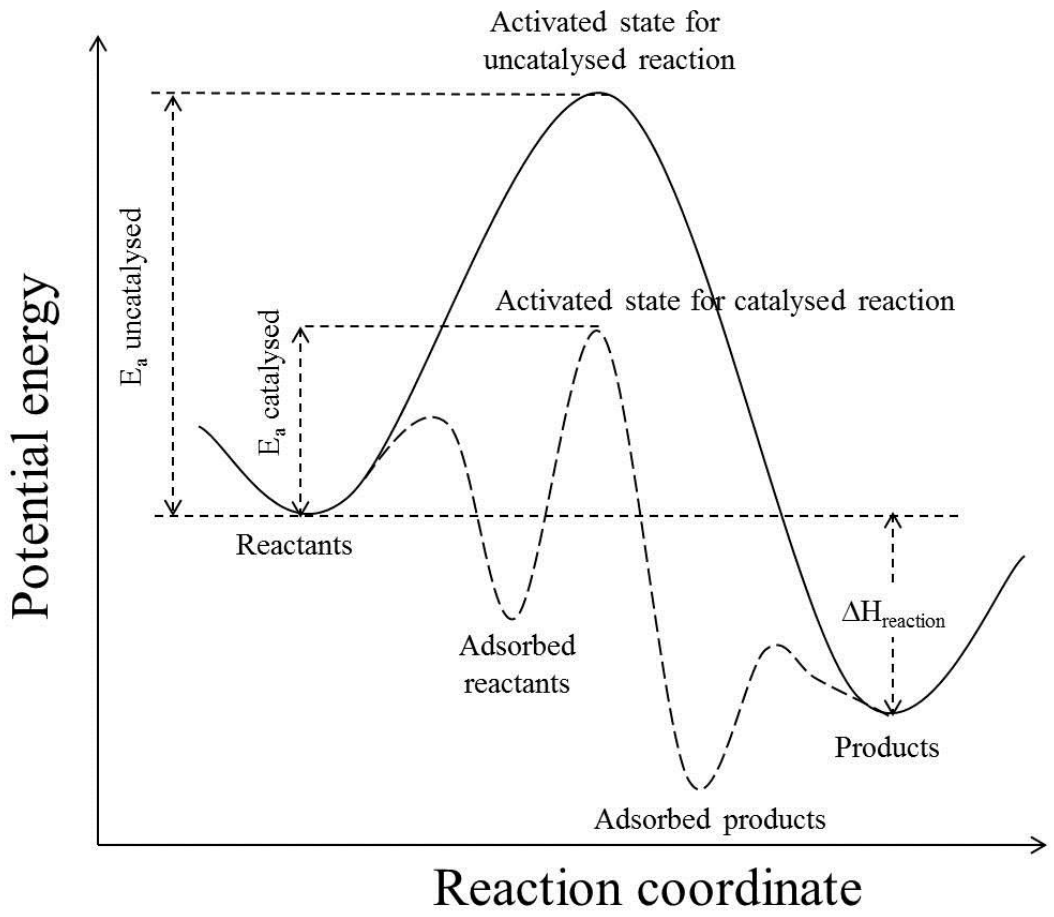

Figure 1.1. Potential energy diagram for the catalytic reaction, where E_a uncatalysed and E_a catalysed are the activation energies for uncatalysed and catalysed reactions, respectively.

1.1.1 Types of catalysts

There are three main types of catalysis: homogeneous, heterogeneous and bio-catalysis.[1]

Biocatalysis

Enzymes are large biological molecules, mostly proteins, catalysing various biological processes, such as food digestion or synthesis of DNA. Similarly to other catalysts, enzymes catalyse only thermodynamically favourable reactions, do not alter the reaction equilibrium and are not consumed during the reaction. However, enzymes are highly specific for the particular substrate/reaction, which results in a very high selectivity and efficiency of these catalysts. For example, the rate of H_2O_2 decomposition in the presence of catalase enzyme can reach up to 10^7 peroxide molecules per second.[1]

Homogeneous Catalysis

Homogeneous catalysts are catalysts which are in the same phase as the reactants, *e.g.* all molecules are in the gas phase or, more often, liquid phase. The rate of the reaction catalysed by a homogeneous catalyst is proportional to the concentration of catalyst. Homogeneous catalysis is typically employed in production of fine chemicals, where a delicate control over product structure is needed.[3] For example, soluble metal complexes with labile ligands are used in asymmetric synthesis, where judicious choice of ligands can allow formation of only one stereoisomer. Additionally, relatively easy control over their structure and characterization make homogeneous catalysts perfect for the study of reaction mechanisms. The problem with homogeneous catalysts is their typically low stability and, more importantly, difficulty of catalyst separation from the reaction mixture resulting in product contamination and poor catalyst recyclability.

Heterogeneous catalysis

In heterogeneous catalysis catalyst and reactants are in different phases: typically catalyst is solid, while reactants are in liquid or gas phase. The reaction in heterogeneous catalysis occurs at the surface of a solid, and thus reaction rate is proportional to the area of active surface. That is why many precious metal-based catalysts are typically nanometre-scale particles, because it allows creation of larger active surface area for the same amount of metal.[4, 5] In heterogeneous catalysis mass and heat transfer is an important factor determining the overall reaction rate, while this is not an issue in homogeneous catalysis.

The main advantages of heterogeneous catalysis are the ease of catalyst separation from the product mixture and facile recyclability, which allow the use of continuous flow reactors instead of batch reactors. There are two main types of heterogeneous catalysts: bulk and supported catalysts.

Bulk (carrier-free) catalysts

Such catalysts consist entirely of the catalytic material. Examples of bulk catalysts are oxide mixtures (bismuth molybdates), skeletal metal catalysts (Raney Nickel), zeolites, metal-organic frameworks, ion-exchange resins, *etc.*

Supported Catalysts

Supported catalysts typically consist of metal nanoparticles, deposited onto a surface of a porous material with a large surface area in order to protect particles from sintering. Various materials, that are thermally stable and chemically inert, can be used as a support, with alumina, silica and carbon being the most common. Other materials used as catalytic supports include titania, zirconia, zinc oxide, magnesia, zeolites, *etc.*

Probably the most commonly known example of a supported catalyst is the automotive catalytic converter. This catalytic system, which employs platinum group metals, was developed to reduce the amount of harmful compounds in vehicle exhaust, *i.e.* to oxidize carbon monoxide and hydrocarbons and reduce nitrogen oxides. The active phase of the converter includes platinum, rhodium and palladium particles, supported on ceramic monolith having a honeycomb-like structure.

1.2 Gold

Gold has always been considered as a valuable metal due to its beautiful shiny yellow colour and non-tarnishing properties that preserve its appearance for centuries. Additional factors which add value to gold are its medium rarity, easy handling/smelting and inertness towards other elements. Gold was the first metal used by early civilizations for coinage, jewellery and arts. Archaeological discoveries demonstrated the advanced gold craftsmanship in ancient civilizations such as Egypt and the Persian Empire.

Gold nanoparticles have a much longer history than those of any other metal. The oldest documented example of their use is the Lycurgus cup from 4th century A.D., where red colour of the glass is due to the doping with gold nanoparticles < 20 nm.[6] Despite the fact that gold nanoparticles were known for millennia, it was M. Faraday who demonstrated in 1857 that the red colour was due to the finely divided metallic particles of gold.[7] His pioneering work inspired the growth of knowledge of colloid science, where gold nanoparticles played a prominent role.

Today gold is one of the most expensive metals (Table 1.1).

Table 1.1. Prices of precious metals as of February 2014 (from infomine.com).

Metal	Au	Ag	Pt	Pd	Ir	Rh	Ru
Price, USD/g	40.75	0.64	44.53	22.86	14.50	33.76	2.03

Despite the variety of the uses of gold, it did not present much interest for the chemists since it was always considered to be chemically inert, and the most attention in gold chemistry was paid to its metallic state, *i.e.* to the methods of its concentration, recovery and purification. The situation, however, changed drastically about 30 years ago, when the exceptional catalytic properties of nano-sized gold particles were discovered.

1.2.1 Preparation of Au catalysts

1.2.1.1 Preparation of small unsupported particles of gold

Colloidal gold can be prepared by reduction of gold precursor ($HAuCl_4$), sometimes in the presence of stabilising agents. Turkevich and his associates used sodium citrate to reduce $AuCl_4^-$ ion in boiling aqueous solution.[8] Particles of 10 – 20 nm can be prepared this way. Various reducing agents, such as phosphorous, sodium thiocyanate, sodium borohydride, *etc.*, were demonstrated to give gold particles of small size and narrow distribution.[9] Stabilising ligands are not essential for preparation of gold colloids, but they can significantly increase

particle stability. The most commonly used stabilisers include polyvinyl alcohol (PVA), polyvinylpyrrolidone (PVP), cetyl trimethylammonium bromide (CTAB) and amines.

Gold cluster compounds. There are numerous methods to prepare gold cluster compounds with a certain number of gold atoms, such as 6, 8, 9, 11, 55, *etc.*[10, 11] They are typically stabilised with phosphines, with PPh_3 being the most common one, and thiols. Additionally, clusters containing two or more different metals can be synthesised.[12-14]

Other methods include attrition, chemical vapour synthesis and many others.[9]

1.2.1.2 Preparation of supported Au catalysts

Method of gold catalysts preparation is extremely important because it could affect catalytic activity. There are a number of methods to deposit gold on to catalytic supports, which generally fall into two categories: 1) support and gold precursor form at the same time and 2) the gold precursor is deposited onto pre-formed support.[9] The most commonly used techniques are outlined below.

Co-precipitation is a term, generally applied to the Category 1. Catalyst preparation by a co-precipitation involves adjusting pH of the solution containing $HAuCl_4$ and the nitrate of the metal – precursor of the metal oxide (Fe, Ni, Co, *etc.*). Adjustment of the solution pH results in the simultaneous precipitation of both the support and the active phase. The co-precipitates obtained are washed, dried and calcined, resulting in highly dispersed gold particles < 10 nm on metal oxide (Table 1.2). The method was first reported in 1987 by Haruta.[15] That is an easy and widely applied one-step preparation method, however, it can only be used for a limited number of metal oxides and, more importantly, gold particles are often embedded in the bulk of the support. Considering the price of gold, this method is undesirable, because a fraction of gold is not being used in catalysis. In general, the category

1 methods do not offer the variety of alternative procedures compared to the Category 2 methods.

Table 1.2. Characteristics of Au/Oxide catalysts prepared by co-precipitation. Reproduced with permission from ref. [16]. Copyright Elsevier.

Oxide support	Au, wt%	T calc. (K)	d_{Au}, nm
MgO	2	473	< 2
TiO_2	5	873	5
Fe_2O_3	5	673	4
Co_3O_4	5	673	6
NiO	10	673	8
ZnO	5	673	5
Al_2O_3	5	573	5
In_2O_3	5	673	5
SnO_2	5	673	3
SiO_2	5	573	20
Cr_2O_3	5	673	>30
CdO	5	295	21

Impregnation. Pores of the catalytic support are filled with the solution of gold precursor, typically $HAuCl_4$ or $AuCl_3$, with the subsequent solvent evaporation and calcination.[17, 18] The method is very simple and any support can be used. However, in most cases this preparation method leads to large Au particles of 10 - 35 nm with poor catalytic activity. The formation of large gold particles could be due to the presence of Cl^- ions, which are known to promote gold mobility and aggregation during heat treatments.[19, 20] Reduction in hydrogen seems to remove Cl^- in the form of HCl, however, large particles may still form.[21]

Deposition-precipitation has been widely used to prepare gold catalysts with small particles. Typically, metal oxide support is suspended in the solution of $HAuCl_4$ and the pH of suspension is raised by addition of NaOH or Na_2CO_3. Next, the suspension is heated at 70 – 80 ˚C for 1 h, which results in the deposition of gold hydroxide species. After thorough washing to remove Cl^-, the catalyst is dried and calcined at elevated temperature. The method works well for the supports with isoelectric points higher than 5, *i.e.* for MgO, TiO_2, Al_2O_3,

ZrO_2 and CeO_2, but it is not suitable for SiO_2, SiO_2-Al_2O_3, WO_3 or activated carbon.[19, 22, 23] Total catalyst gold loading and the size of gold particles were shown to be dependent on the pH of the precursor solution. Gold loading and particle size decrease upon pH increase, thus the range of pH around 7 – 8 is considered to be optimal, because it corresponds to the best compromise between particle size and gold loading.[9]

Anion adsorption. $[AuCl_4]^-$ is adsorbed at the surface of oxide when pH of the solution is lower than the point of zero charge of the support since the support surface is positively charged in these conditions. The main problem associated with this method is that only *ca.* 20 % of gold is deposited when equilibrium is reached. Study of Au/TiO_2 preparation by anion adsorption showed that 1.5 wt% was the maximum achievable Au loading and Au particle sizes were within 4 – 6 nm range.[24]

Cation adsorption is a method similar to anion adsorption.[9] However in this case pH of the solution must be higher than point of zero charge of the oxide support to make it negatively charged. Au^{III} bis-ethylenediamine complex is used as a cation. Additionally, cation exchange is an efficient method to introduce highly dispersed metal nanoparticles into zeolites or activated carbon by exchange with protons of the surface groups.

Chemical vapour deposition. In this method vapour of volatile organogold compound, dimethylgold acetylacetonate [$Me_2Au(acac)$], is introduced onto a support, on which it is decomposed upon calcination to form metallic Au particles.[25] Particles as small as 2 – 3 nm could be obtained (even on SiO_2); however size distribution is typically broader than that for deposition-precipitation.

Deposition of colloidal gold nanoparticles and gold clusters. In this method pre-formed colloid gold nanoparticles and gold clusters, stabilised with PPh_3 or thiols, are deposited onto a support by impregnating the support with a colloidal suspension/cluster solution, followed by washing and drying.[9] The catalyst can be further calcined at high temperatures to remove

molecules of stabilising agent. Using pre-formed particles is advantageous because their size can be easily controlled by well-established methods and the size-distribution is narrow. It is also one of a few methods to obtain small silica-supported Au particles. The disadvantages of this method are the difficult synthesis of clusters and necessity to remove stabiliser molecules which can lead to particle aggregation.

1.2.2 Catalysis by gold

The first hints of the catalytic activity of gold appeared in as early as 1906, when the combination of hydrogen and oxygen over gold gauze was studied,[26] however, the next reports on catalysis by gold appeared only in the second half of the 20th century.

1.2.2.1 Hydrogenation

Among the earliest reports demonstrating catalysis by gold were the works on its activity in reactions involving hydrogen. Various studies demonstrated catalytic activity of both gold foil and supported gold particles in hydrogen-deuterium exchange.[27-30] The reaction typically requires elevated temperature due to the need for thermal excitation of Au electrons from the filled 5d level to 6s level with the creation of d-band vacancies and, therefore, greater tendency towards chemisorption.[9] At high temperatures hydrogen is chemisorbed at the surface of metallic gold with the formation of hydrogen atoms. The exchange proceeds by a Rideal-Eley mechanism:

$$H^* + D_2 \rightarrow H\cdots D\cdots D \rightarrow HD + D^*$$

One of the first studies of gold-catalysed hydrogenation of unsaturated hydrocarbons was the study by Erkelens and co-authors which demonstrated the formation of benzene and cyclohexane from cyclohexene on gold films at elevated temperatures in the presence of hydrogen.[31] In this reaction cyclohexene was acting as both the substrate and the source of

hydrogen, with benzene being the main product. The yield of benzene can be increased by either raising reaction temperature or lowering H_2 pressure.

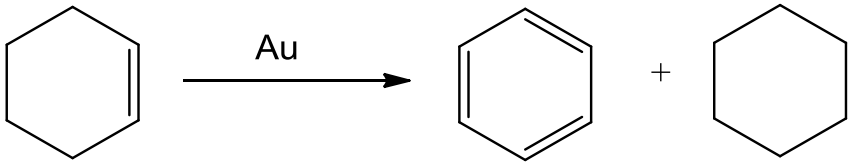

Figure 1.2. Au-catalysed formation of benzene and cyclohexane from cyclohexene.

Overall, the amount of research focusing on gold-catalysed hydrogenation of unsaturated hydrocarbons is relatively small, because it is generally admitted that activity of gold catalysts in reactions, requiring hydrogen dissociation, is considerably lower compared to metals of Group 8-10.[9] However, in some cases lower activity of gold catalysts allows achieving better selectivity.

Selective reduction of C=O bond in α,β-unsaturated aldehydes/ketones represents a major challenge in synthetic chemistry, because double C=C bond is typically much more reactive than carbonyl group, which leads to the formation of saturated aldehydes or ketones along with saturated alcohols.[9] There is an industrial interest in the synthesis of unsaturated alcohols directly from α,β-unsaturated aldehydes as they are important intermediates in pharmaceutical synthesis and can be used as fragrances and flavours.[9] Conventional monometallic hydrogenation catalysts, such as Pt, Rh and Pd supported on silica or alumina, mainly convert unsaturated aldehydes to saturated aldehydes with a minor yield of unsaturated alcohol.[32] Some very promising results were obtained for chemoselective hydrogenation of unsaturated aldehydes in the presence of gold catalysts.[33-37] Hutchings and co-workers reported formation of crotyl alcohol (2) from crotonaldehyde (1) over Au/ZnO and Au/ZrO_2 with the selectivity towards unsaturated alcohol (2) reaching up to 80% (Figure 1.3).[36, 37]

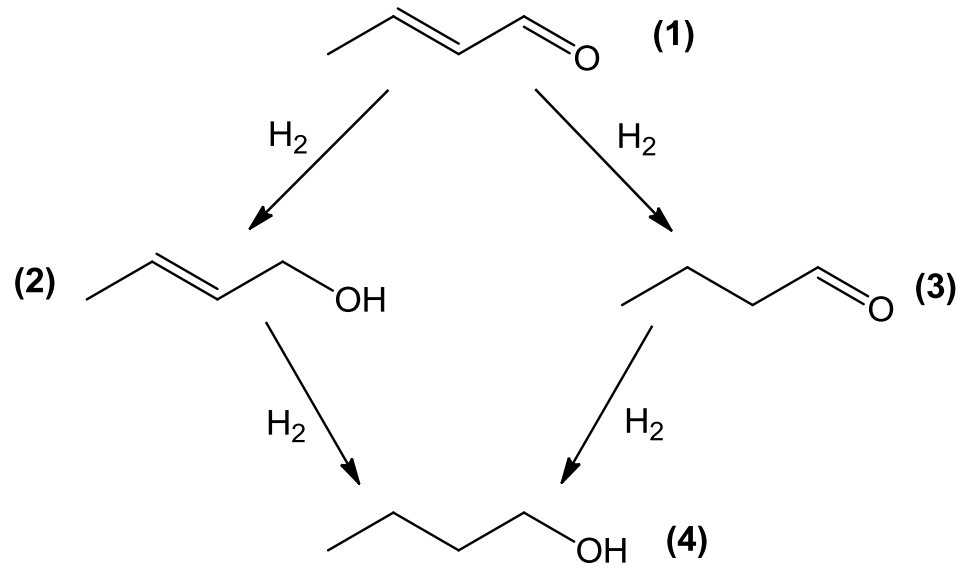

Figure 1.3. Hydrogenation of crotonaldehyde.

Activity of gold catalysts was also demonstrated in selective hydrogenation of alkynes and alkadienes to alkenes.[9, 38] The high selectivity towards alkenes without their further reduction to alkanes was found to be due to the strong adsorption of alkynes and dienes and weak adsorption of alkenes on the surface of gold. Other examples of reactions involving hydrogen, for which activity of supported gold catalysts has been demonstrated, include isomerisation of 1-butene to 2-butene by intramolecular rearrangement,[39] conversion of CO and CO_2 to methanol,[40-42] *etc.*

Hydrogenation is only one of the potential applications of the gold catalysts. Other applications of gold catalysts show that in many cases gold could be the catalyst of choice, *i.e.* it would outperform any other known catalysts.

1.2.2.2 *Oxidation of carbon monoxide*

Haruta and co-workers discovered in 1987 that very small gold nanoparticles are active in the oxidation of carbon monoxide even at temperatures below 0 ˚C.[43] It was the discovery that later caused enormous interest in catalysis by gold. The reason why gold is significantly better in this reaction compared to Group 8-10 metals lies in the strength of adsorption of the

reactants. Even though metals of group 8-10 easily adsorb and dissociate oxygen, they adsorb carbon monoxide too strongly, which results in poor catalytic activity in low temperature CO oxidation. On the other hand, the heat of adsorption of oxygen and carbon monoxide on gold is not too high and not too low, which creates optimal conditions for the high catalytic activity at low temperatures.

When the unusual activity was discovered by Haruta and his associates, it was initially attributed to some "composite" oxide of gold with 3d transition metals of Group 8 prepared by co-precipitation. However, later microscopy studies showed that the "composite" oxide catalyst in fact consisted of gold nanoparticles with size of 2 – 4 nm uniformly distributed on larger particles of Fe_2O_3, Co_3O_4 and NiO.[44] It was later shown that other catalyst preparation techniques, such as deposition-precipitation, gas-phase and liquid-phase grafting of organo-gold complexes, also give catalysts active in CO oxidation.[25, 45-47] The choice of support was shown to be critical: transition metal oxides, such as Fe_2O_3 or TiO_2 are the most active, whereas more commonly used SiO_2 and Al_2O_3 are poor or significantly less active.[19, 21, 48]

Carbon monoxide oxidation is one of the most studied reactions for gold catalysts and is often used as a reference reaction. To date hundreds of articles on CO oxidation have been published.[45, 49-56] Despite the simplicity of this reaction, its mechanism has proven extremely difficult to establish. Different research groups use different conditions and approaches and quite often do not specify important parameters. Several possible mechanisms of CO oxidation have been suggested: the reaction could take place between carbon monoxide adsorbed on gold particles and oxygen, activated by the support;[47, 57] or the reaction could take place on the Au surface only, that is either entirely metallic Au^0 or that also contains Au^I and Au^{III} species.[58, 59] It is generally agreed upon that catalytic activity in CO oxidation is associated with small gold particles (< 5 nm), rather than with large particles (Figure 1.4).[60]

Au deposition methods and supports, which give smaller Au particles, are generally preferred. Catalytic activity is typically higher for Au particles supported on reducible oxides.

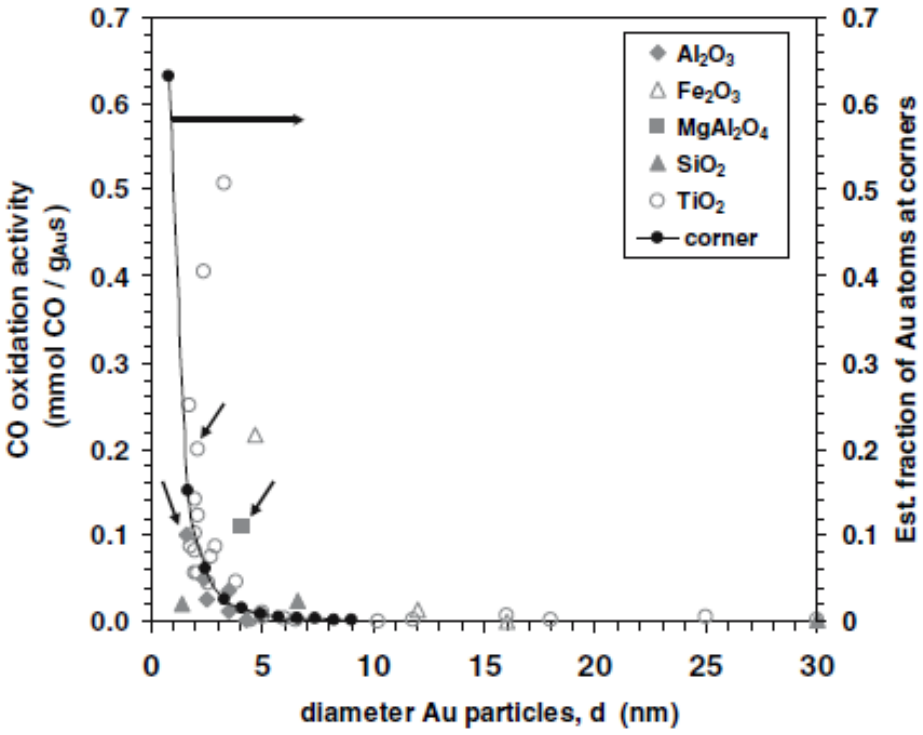

Figure 1.4. Catalytic activities of various gold-based catalysts in CO oxidation at 273 K as a function of Au particle size (nm). Image reprinted with permission from ref. [60]. Copyright Springer.

1.2.2.3 H_2O_2 synthesis

The hydrogen peroxide market is very large, contributing *ca.* 12 – 15 % of the total global chemical revenues. Production of H_2O_2 is expected to reach 4.67 tonnes/year by 2017.[61] Major areas of H_2O_2 application include pulp and paper industry, textile and the semiconductor industries. Additionally, increasing production of propylene oxide from hydrogen peroxide and propylene employed by BASF/Dow is fuelling the demand for hydrogen peroxide. Currently H_2O_2 is produced using the sequential hydrogenation and oxidation of alkyl anthraquinone.[9] This process in economically viable only when large amounts of H_2O_2 are produced, which results in the need for storage and transportation of

H_2O_2. Thus there is an increasing demand to synthesize hydrogen peroxide on a small scale where it is to be used to avoid transportation, storage and handling of this hazardous material.

Hutchings and co-authors showed that gold supported on Al_2O_3 can catalyse the direct formation of hydrogen peroxide from H_2/O_2 mixture at 2 ˚C.[62] It was shown that Au supported on alumina is significantly more active compared to Pd/Al_2O_3, and mixing Au with Pd (1:1) over alumina allows achieving the highest activity among the three catalysts in the direct synthesis of H_2O_2. Later the same group showed that as prepared Au-Pd/TiO_2 possesses high activity in the synthesis of H_2O_2, however it quickly deactivates due to full leaching of Au and Pd into the reaction solution.[63] Pre-calcination of Au-Pd/TiO_2 at 400 ˚C allows overcoming leaching and deactivation problems. Fe_2O_3 supported catalysts showed activity similar to that of Al_2O_3 supported catalysts.[64] Interestingly, catalysts active in the synthesis of H_2O_2 were completely inactive in the oxidation of CO and *vice versa*. Such an inverse correlation was suggested to be due to the effect of the particle size: while activity of gold and mixed-metal catalysts in the synthesis of H_2O_2 increases upon the increase in particle size, the opposite effect is observed for the oxidation of carbon monoxide (see Section 1.2.2.2).

1.2.2.4 Selective oxidation

Selective oxidation of organic molecules is one of the most important industrial processes. At the same time, oxidation reactions are among the most polluting and non-environmentally friendly processes: copious amounts of toxic waste are produced as a result of oxidations with stoichiometric oxidants, such as chromate, permanganate or hypochlorite. Additionally, these processes typically suffer from poor atom efficiency.[65, 66] It is beneficial to use catalytic processes from both environmental and economic points of view, because by using catalysts it is possible to employ green oxidants (O_2, H_2O_2), and thus to minimize the

amount of toxic waste, and to cut the overall cost of the process by employing milder conditions.

During the last 20 years gold has been actively studied in the oxidation of organic compounds, and greatly improved selectivity and stability of gold catalysts compared to platinum and palladium catalysts have been demonstrated in various reactions.[67] Gold catalysts were found to be highly active in the alkene, alcohol and hydrocarbon oxidation, with some cases showing possibility of industrial exploitation. The most notable cases are outlined below.

Propene epoxidation

Propylene oxide (or 1,2-epoxypropane) is an important compound which is produced industrially on a large scale. It is mainly used as a precursor to polyether polyols, which are used in the production of polyurethane plastics. Additionally, it is a building block for various organic intermediates and solvents.[68-70] Numerous attempts to produce it *via* direct oxidation of propene, similarly to silver-promoted oxidation of ethylene, have failed so far. The majority of propylene oxide is still manufactured by the chlorohydrin process and the hydroperoxide processes, which are not environmentally friendly or produce unwanted co-products (alcohols).[69] Silver catalysts, used for ethylene epoxidation, fail in the oxidation of propene because the allyl intermediate, forming as a result of the easy abstraction of the methyl hydrogen, is far more active than the reactant and is oxidised to form CO_2 only.[69] Gold catalysts were shown to be more promising in this reaction. Haruta and co-workers demonstrated that TiO_2-supported gold catalyst is capable of promoting the gas phase propene epoxidation by O_2 in the presence of H_2 at 50 ˚C.[40] The selectivity towards formation of epoxide was very high (> 99 %) at propene conversion less than 1 %. Pd and Pt mainly produced propane under the same conditions. The subsequent studies demonstrated that conversions could be increased up to 5-10 % by using higher temperatures without significant

loss of selectivity.[69, 71] Particle size was also shown to play an important role: gold nanoparticles smaller than 2 nm were shown to shift the reaction towards the formation of propane, rather than epoxidation.[68, 70] Later it was shown that the use of other supports, such as TS-1 and Ti-MCMs, could improve activity of gold in the oxidation of propene.[70, 72, 73]

Oxidation of other alkenes

Gold was employed in the aerobic oxidation of the higher alkenes. Different research groups showed that gold catalyses alkene oxidation by oxygen in the presence of catalytic amounts of peroxide initiator or by hydroperoxides used as a sole oxidant.[74-80] Activity and selectivity were shown to be dependent on the experimental conditions, the catalyst, and the substrate.

Cyclohexene was converted to 2-cyclohexen-ol (25 %) and 2-cyclohexen-one (35 %) in toluene in the presence of 1 % Au/C and 5 mol % of tert-butyl hydroperoxide (*t*BuOOH). Conversion of cyclohexene was 29 % after 24 hours. In 1,2,3,5-tetramethylbenzene comparable conversion of cyclohexene was achieved; however, the product composition was different: cyclohexene oxide and 2-cyclohexen-one formed with selectivity of 50 and 26 %, respectively (Figure 1.5).[74]

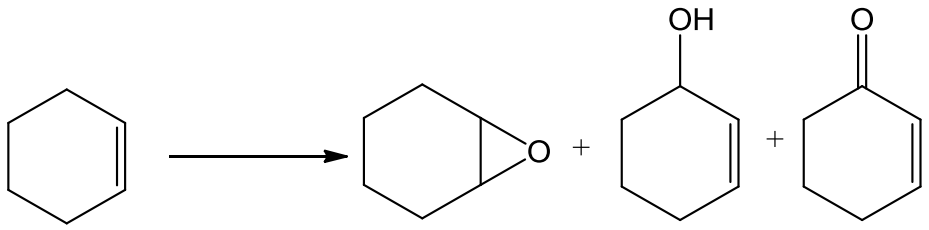

Figure 1.5. Oxidation of cyclohexene to cyclohexene oxide, 2-cyclohexene-ol and 2-cyclohexene-one.

Oxidation of styrene was studied in the presence of various supported gold catalysts by either O_2 with the addition of catalytic amount of *t*BuOOH or by *t*BuOOH as the sole

oxidant. This reaction typically produced styrene oxide, benzaldehyde and acetophenone (Figure 1.6).

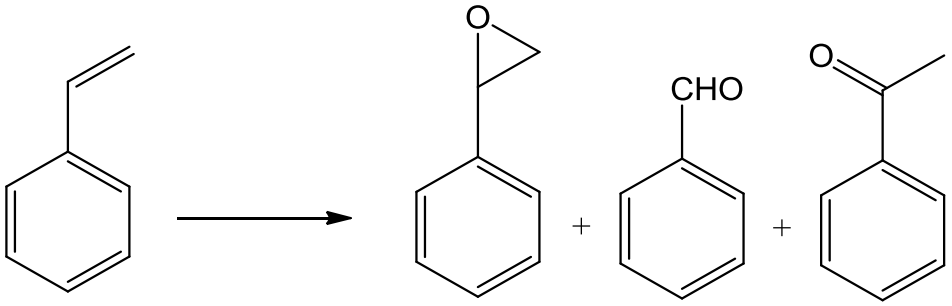

Figure 1.6. Oxidation of styrene to styrene oxide, benzaldehyde and acetophenone.

Turner and co-workers demonstrated that only small gold entities (< 2 nm) are active in the oxidation of styrene in toluene in the absence of radical initiator, suggesting that O_2 activation arises from the altered electronic structure of very small gold nanoparticles. Selectivity towards epoxide was quite poor (only *ca.* 14 %), with benzaldehyde being the main product (*ca.* 82 %).[81] Jin and co-workers studied the catalytic activity of thiolate-protected Au_{25}, Au_{38} and Au_{144} clusters in styrene oxidation with different oxidants: 1) *t*BuOOH as the sole oxidant, 2) O_2 as the sole oxidant and 3) O_2 with the addition of catalytic amounts of *t*BuOOH.[82] They found that in the case of *t*BuOOH as oxidant, there was no difference in activity between the clusters. However, when O_2 was used as an oxidant, the activity dropped upon the increase in cluster size, which correlated with the results of Turner *et al.*[81] Interestingly, the presence of thiolate ligands did not seem to affect activity of gold, and their removal led to cluster aggregation and decrease in activity. The main product of this reaction was benzaldehyde (100 % with *t*BuOOH and 80 % with O_2), while epoxide and acetophenone formed in minor quantities.

cis-Stilbene was oxidized by O_2 in isopropylbenzene in the presence of 1% Au/graphite catalyst with selectivity towards *trans*-stilbene oxide reaching 74 % at cis-stilbene conversion of 48 % (Figure 1.7).[74]

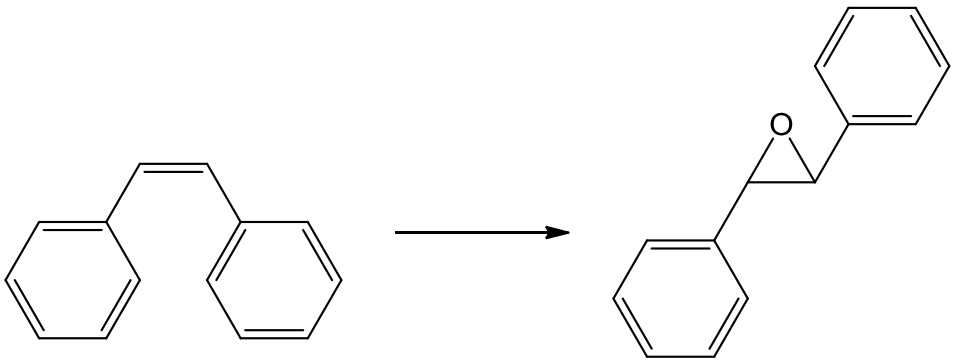

Figure 1.7. Oxidation of *cis*-stilbene to *trans*-stilbene oxide.

Oxidation of cyclohexane

Gold was also shown to be active in the oxidation of C-H bond of alkanes. Particular attention was paid to the oxidation of cyclohexane because of the growing industrial interest in this reaction.[67, 83] The products of cyclohexane oxidation, cyclohexanol and cyclohexanone (often referred to as KA oil), are mainly used as intermediates in the synthesis of ε-caprolactam and adipic acid – precursors in the production of nylon (Figure 1.8).[67]

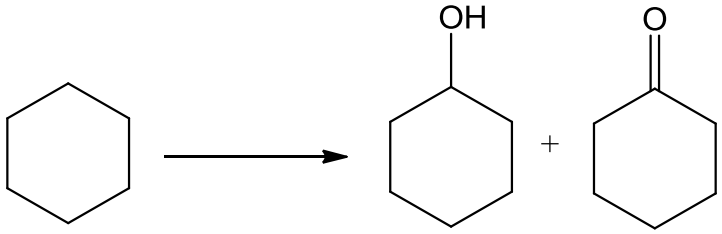

Figure 1.8. Oxidation of cyclohexane to cyclohexanol and cyclohexanone.

Current commercial processes operate in liquid-phase: non-catalytic autoxidation process and Co(II)-catalysed process, giving 4 % cyclohexane conversion with only *ca.* 70 – 85 % selectivity to KA-oil products.[67, 83] The use of gold catalysts allows obtaining much better results in terms of both activity and selectivity. For example, Zhu and co-workers showed that 20 – 30 % cyclohexane conversions and 95 % selectivity to KA-oil could be achieved when gold supported on mesoporous silica catalysts were used.[84] Tsukuda and co-authors studied the activity of hydroxyapatite-supported clusters with controlled compositions in the solvent-free oxidation of cyclohexane with oxygen.[85] No cyclohexane

conversion was observed in the absence of gold, while supported gold clusters demonstrated remarkable activity with turnover frequencies (TOF) reaching 18500 h^{-1} and selectivity to KA-oil > 90 %. It was also shown that the activity of gold clusters was dependent on their size.

Oxidation of alcohols and polyols

Alcohols and polyols are important starting materials in chemical industry as they can be obtained in large quantities from renewable resources.[67, 86] Selective oxidation of alcohols to aldehydes, ketones and carboxylic acids is one of the most important and challenging transformations in organic synthesis. Activity of gold, both in the form of supported particles and colloid dispersions, has been actively studied in the oxidation of alcohols and polyols.

It was demonstrated that unsupported polyvinylpyrrolidone-stabilised 1.3 nm Au nanoparticles are active in the oxidation of benzyl alcohol to aldehydes/carboxylic acids in aqueous solution (pH > 7) under ambient temperature.[87] Similar Pd colloid dispersions (1.5 nm) and Au colloids of larger size (9.5 nm) were shown to be less active. By performing kinetic measurements, authors suggested different mechanisms of alcohol oxidation for Pd and Au particles: while the rate-determining step for Pd nanoparticles is the transfer of H atoms from β-C to Pd, in the case of gold nanoparticles the rate-determining step is abstraction of hydrogen by superoxo-species adsorbed on Au with the formation of hydrogen peroxide. While colloidal systems represent some interest, *supported* Au nanoparticles are studied more extensively due to their easy reusability. In 2004 Nippon Shokubai Co. Ltd developed a pilot plant for the production of methyl glycolate from methanol and ethylene glycol using supported gold catalysts. Au/Al_2O_3 was shown to be more active and selective compared to Pd and Ru analogues and afforded 83 % selectivity to methyl glycolate at 63 % conversion.[88] Among various substrates in gold-catalysed oxidation, benzyl alcohol and glycerol are the most studied ones.[83, 89-99] Oxidation of benzyl alcohol proceeds relatively

smoothly due to aromatic ring activation. The reaction is often used as a reference for testing gold catalysts in liquid-phase oxidation. Even though Au catalysts are active in the oxidation of alcohols, for the practical applications the activity of gold is quite low, with typical TOF values lying within the range of 10 - 10^2 h^{-1}.[67] Thus, in order to overcome the low activity of gold, alloys of gold with other metals, in particular with Pd, were extensively studied, showing remarkable enhancement of activity of the catalysts in the oxidation of alcohols. Mixed-metal systems and synergistic effect between two or more metals are considered in detail in Section 1.2.4.

1.2.2.5 Photocatalysis on gold nanoparticles

Noble metal nanoparticles, in particular gold nanoparticles, have been recently recognised as effective systems for harvesting visible-light energy and converting it to chemical energy.[100] Gold nanoparticles were long known for their beautiful bright colour, which depends on the particle size and shape. This colour is caused by the so called localised surface plasmon resonance (LSPR) effect. LSPR absorption originates from collective oscillations of the conduction electrons, which are induced by the electromagnetic radiation of incident light when the photon frequency matches the natural frequency of metal surface electrons, oscillating against the restoring force of their positive nuclei (Figure 1.9).[100]

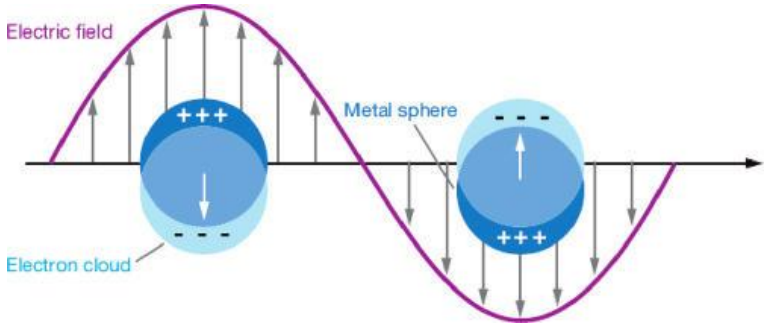

Figure 1.9. Collective oscillations of free electrons induced by electromagnetic radiation.[101]

The optical properties of gold nanoparticles are affected by various factors, such as a value of dielectric constant of the surrounding material, particle size and shape and the

surrounding environment. Au particles smaller than 2 – 3 nm do not possess LSPR, while particles of 2 – 50 nm show a strong absorption band at 520 – 530 nm. As particles become bigger, the LSPR band becomes more intense, broadens and shifts to higher wavelengths (Figure 1.10).[100, 102-104] Additionally, solvent, surfactant molecules and the nature of the catalytic support affect LSPR of gold nanoparticles.

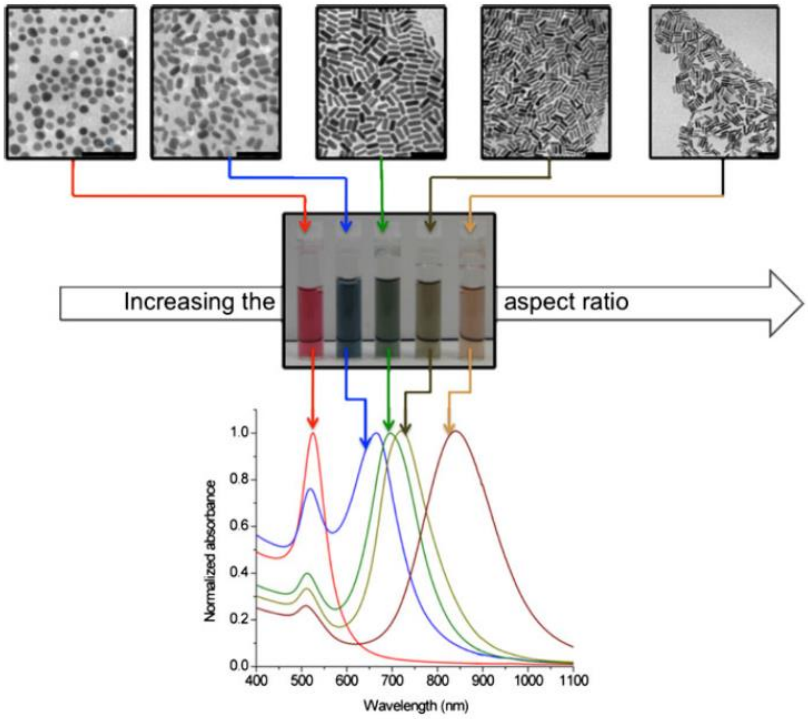

Figure 1.10. Absorption spectra of gold nanoparticles of different sizes and shapes. Reprinted with permission from ref. [105]. Copyright Springer.

Since gold nanoparticles can be used as active catalyst components for various reactions, such as hydrogenation, selective oxidation, various couplings, *etc.*, combining their light-absorption properties with their catalytic properties can give efficient visible-light photocatalysts. Au/semiconductor composites, such as Au/TiO_2 and Au/ZnO, were previously employed as efficient photocatalysts.[106-109] Au nanoparticles in these composite catalysts are used to capture visible light energy. The conduction electrons of metal, having gained this energy, can travel to the conduction band of the semiconductor material.[110] In such systems semiconductor material contributes significantly to the photocatalytic activity.

Very recently, however, various systems consisting of gold and silver nanoparticles supported on photocatalytically inactive insulator materials, such as ZrO_2, Al_2O_3, SiO_2 and zeolites, were demonstrated to be active photocatalysts.[111-113] In such systems supports cannot absorb visible light due to the wide band gap and no electron transfer from nanoparticles to the solid support is observed, thus, both the light harvesting and chemical reactions occur on the plasmonic metal nanoparticles. Such Au systems have already been shown to be active in photocatalytic degradation of dyes and volatile organic compounds; selective oxidation of organic molecules, such as oxidation of alcohols to aldehydes, amines to imines and selective reduction of organic molecules, *e.g.* reduction of nitroaromatics to azo-compounds or hydrogenation of ketones to alcohols.[100, 112, 114-117] It is expected that the area of photocatalysis on noble metal nanoparticles will be of considerable interest for the researchers in the future.

1.2.3 Catalysis by mixed-metal gold-containing systems

Despite the very promising catalytic performance of gold, some of the problems associated with gold catalysts are greatly limiting their applications. For example, gold nanoparticles are prone to aggregation with subsequent deactivation upon heat treatments, which limits their application in high temperature reactions. Thorough control of the Au particle size is often necessary as catalytic activity strongly depends on the particle size. In some cases catalytic activity of gold in not high enough for practical applications despite the great selectivity. One of the possible solutions to overcome these problems is to alloy gold with another metal. Catalysts employing nanoparticles of gold alloyed with other metals have attracted considerable interest because of their enhanced activity, more tuneable selectivity and improved resistance against sintering compared to their monometallic counterparts.[118-121] The improved resistance of gold particles against aggregation in the presence of platinum-

group metals could be due to their higher melting point compared to gold, whereas metals such as Cu or Ag could be oxidised in alloy particles and interact strongly with the oxide support, thus preventing aggregation.[122, 123]

Previous publications provide numerous examples of enhanced catalytic activity of gold particles upon alloying with another metal.[120, 124-129] The physical origin of such enhanced activity could be ascribed to electronic (also called "ligand") and/or geometric (or "ensemble") effects.[118, 130] Ligand effects describe the changes in the chemical properties of atoms at the surface of nanoparticles due to alloying, whereas geometric effects refer to changes in catalytic properties of an ensemble of atoms at the surface when chemical composition of the ensemble changes. Since gold has the highest electronegativity among the transition metals, electron transfer from another metal to gold can occur, thus affecting catalytic activity of gold by electronic modification (ligand effect). Alternatively, the presence of atoms of metals, which have a stronger tendency to activate oxygen or hydrogen (*e.g.* Ag and Pt), on the surface of Au particles can promote oxidation or hydrogenation reactions occurring at the gold-based active species by providing closely located activated oxygen or atomic hydrogen species, respectively (Figure 1.11).[118]

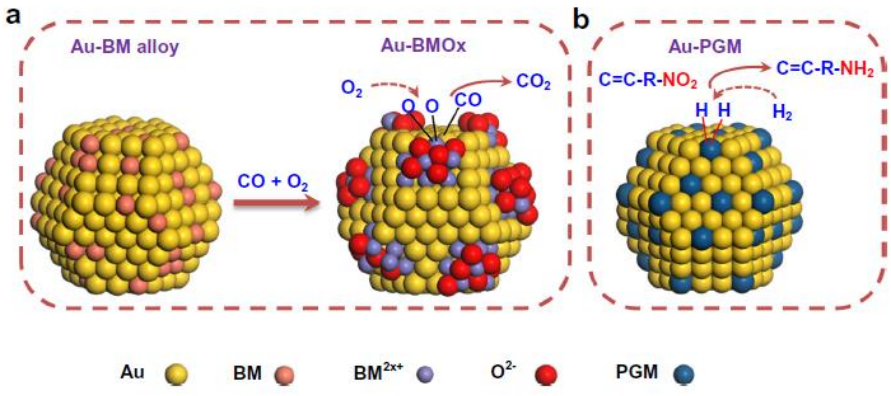

Figure 1.11. Schematic illustration of synergistic effects on gold-containing bimetallic catalysts in (a) CO oxidation and (b) selective hydrogenation of nitroaromatics. (BM and PGM stand for base metal and platinum group metal, respectively). Reprinted with permission from ref. [118]. Copyright Elsevier.

It should be mentioned that synergistic effects between Au and a second metal strongly depend on the reaction and the conditions employed, *e.g.* one metal could strongly enhance the activity of gold in a certain reaction while making no difference, or even demonstrating a negative effect in another reaction.

Selectivity is another reaction parameter that could be significantly altered by alloying gold with another metal. In some cases, manipulations with the ratio of metals in alloy nanoparticles could allow switching reaction pathways and, therefore, tune the product composition. A recent article by Zhang *et al.* reports aerobic oxidative coupling of alcohols and amines over Au-Pd/resin in water.[127] The authors demonstrated that by changing the Au:Pd ratio of the catalysts, they could efficiently switch reaction from amidation to imination: Au_6Pd/resin gave amides in high yields, while $AuPd_4$/resin produced imines with high selectivity.

1.2.4 Size-dependent activity of gold catalysts

The activity of gold catalysts has long been known to be dependent on the dimensions of gold particles. For example, only small particles of gold (< 5 nm) were shown to possess activity in the oxidation of CO.[43] In heterogeneous catalysis reactions occur on the surface of solid catalysts, therefore the use of very small nanoparticles significantly increases their surface to volume ratio, creating more reaction sites per gram of material and thus increasing the catalytic activity.[5] However, in the case of gold, the surprising change in its catalytic properties upon decrease in particle size cannot be simply attributed to the increase in the surface area, and effects intrinsic to nanoscale regime have to be considered as well. For example, when particle size is decreased to a few nm, the number of low-coordinated surface Au atoms increases, because atoms located at the particle edges and corners have fewer interatomic bonds.

There is a general agreement on the optimal size of gold particles for the low-temperature oxidation of carbon monoxide. Different studies, performed using different catalytic supports and conditions, generally agree that only Au particles with sizes below 5 nm are active, with Au particles of 1 – 3 nm showing the highest activity (see Figure 1.4).[45, 48, 131, 132] Goodman and co-authors showed that the pronounced structure sensitivity of CO oxidation on Au/TiO_2 originates from quantum size effects .[49] It was shown that smooth Au surfaces do not adsorb CO and O_2 but both molecules bind only to rough centres *i.e.* to Au atoms located at corners, edges, steps *etc.*, [133, 134] thus confirming that small particles of gold are preferred for CO oxidation.

Attempts to establish the optimal size of Au particles were made for the oxidation of larger organic molecules, such as alcohols, alkenes or alkanes. Results of these studies vary markedly depending on the reaction parameters such as substrate and oxidant. In some cases rather contradicting results are obtained.

Tsukuda and co-workers studied cyclohexane oxidation activity of sub-2 nm Au clusters composed of 10, 18, 25, 39 and ~85 Au atoms.[85] The study showed that activity of gold clusters in the sub-2 nm region is related to their size according to a volcano-type curve, with Au_{39} showing the highest activity (Figure 1.12).

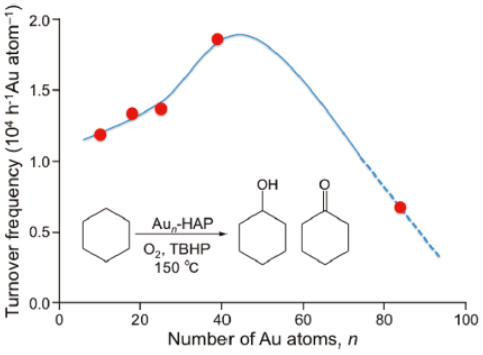

Figure 1.12. Cyclohexane oxidation TOF values as a function of Au cluster size. Reprinted with permission from ref. [85]. Copyright American Chemical Society.

As was mentioned earlier, Turner *et al.* studied the activity of Au_{55}/BN and Au_{55}/SiO_2 in the oxidation of styrene.[135] The study showed that only particles smaller than 2 nm were active, while larger gold entities were completely inactive, and the observed size effect was attributed to the altered electronic structure of small particles. This result was somewhat confirmed later by Jin and co-workers, when they showed that activity of hydroxyapatite supported gold clusters in the aerobic oxidation of styrene gradually decreased in order Au_{25} > Au_{38} > Au_{144}.[82] Recently Wang *et al.* demonstrated that positively charged bulk gold particles with sizes 20 – 150 nm were highly active in the aerobic oxidation of styrene.[136] The observed activity of large particles was attributed to Au^+ species.

Boronat *et al.* studied gold-catalysed alcohol oxidation using DFT calculations.[137] The results clearly showed that the reactivity of gold atoms in alcohol oxidation increased with decreasing Au coordination number, implying that smaller particles should possess higher catalytic activity. Tsukuda and associates demonstrated that catalytic activity of gold clusters monotonically decreased with the increase in the cluster size from 0.8 to 1.9 nm in the microwave-assisted oxidation of benzyl alcohol by H_2O_2.[92] However, the majority of studies on gold-catalysed alcohol oxidation agree that medium sized Au particles (4 – 8 nm) are more active compared to smaller and larger particles.[90, 91, 99, 138-145] For example, 5 nm gold nanoparticles supported on SiO_2 were shown to be at least three times more active than 3 nm silica-supported Au nanoparticles and 15 times more active than 10 - 30 nm particles in the aerobic oxidation of ethanol to acetaldehyde and acetic acid.[138] Similar results were obtained by Hensen *et al.*[145] for ethanol dehydrogenation catalysed by 1.7 – 15.0 nm Au particles supported on mesoporous silica. Particles of 6 nm were shown to be significantly more active compared to the smaller and the larger ones. Such size dependency was attributed to step sites at the Au surface, which provide a favourable geometry for the rate-limiting β-H elimination of adsorbed alcoholate. A series of TiO_2 and CeO_2 supported Au nanoparticles ranging from

1.3 to 11.3 nm were prepared and tested in the aerobic oxidation of benzyl alcohol.[91] The study revealed that 6.9 nm particles showed the highest activity among the studied systems. The activity did not depend on the nature of the support or the conditions employed (*e.g.* solvent), confirming that the difference in activity can be attributed to the particle size. The activity of carbon-supported gold nanoparticles in the oxidation of ethylene glycol using the series of catalysts with Au particles of different sizes gradually increased until the size of particles reached 7.5 nm.[141] Particles larger than 7.5 nm exhibited lower activity. However, lower activity of particles smaller than 7.5 nm was attributed to their limited accessibility to the reagents. Hutchings *et al.* showed that heat treatment of Au/TiO_2 at 250 ˚C in air led to an increase in Au particle size from 3.5 – 3.9 nm to 8 – 10 nm, which coincided with increase in catalyst TOF from 9780 h^{-1} to 31900 h^{-1} in the oxidation of benzyl alcohol, respectively.[89] This increase in activity, however, could be also ascribed to the removal of polyvinyl alcohol, used as a protecting agent.

1.2.5 Other applications of gold nanoparticles

Gold nanoparticles have been attracting tremendous interest in various fields of nanotechnology due to the ease of their synthesis and functionalization, chemical stability, low toxicity, and tuneable optical and electronic properties (absorption, fluorescence and conductivity).[146] In addition to catalysis, gold nanoparticles have been actively studied in various nanotechnology applications, such as sensors, electronic/optoelectronic nanodevices[147] and biomedical applications, such as diagnosis and treatment of life-threatening diseases.[148] In fact, biological applications represent one of the most rapidly growing areas of nanoparticle research, where gold nanoparticles play a prominent role.

The 5th chapter of this work is focused on the study of biological behaviour of gold nanoparticles, derived from Au_{101} nanoparticles and stabilised with different organic ligands.

Various types of applications of gold nanoparticles in biomedicine are considered in detail in the introduction to Chapter 5.

1.3 Scope of this work (chapters 2 – 4)

Ligand-stabilised gold clusters have attracted great interest in gold catalysis research in the recent years, due to their precise composition, exactly known structure and easy preparation. In this project we used triphenylphosphine-stabilised gold and mixed-metal clusters to fabricate catalysts with highly monodisperse gold particles and study their activity in selected oxidation reactions.

In particular, the aims of this project were:

- To gain better understanding of the Au catalyst structure-activity relationship using supported gold clusters in the reactions of the liquid-phase oxidation of olefins;
- To study which parameters (in addition to the catalyst structure) affect catalytic activity of gold catalysts in the liquid-phase oxidation of olefins and other types of reactions;
- To study how the addition of a heterometal, such as Pt or Pd, to gold affects the activity of nanoparticles;
- Finally, to study the effects of different pre-treatments on the activity of Au catalysts.

Chapter 2. Experimental Section

2.1 Synthesis of gold-containing compounds

$HAuCl_4 \cdot 3H_2O$[149] was prepared by dissolution of 99.99% pure gold (1 g) in freshly prepared *aqua regia* (50 mL) at 60 ˚C. After gold dissolved completely in *aqua regia*, the solution was dried on a rotary evaporator. The resulting yellow solid was collected and kept in a freezer.

$AuPPh_3Cl$ was synthesised according to the method described by Malvano *et al.*[150] A solution of $HAuCl_4 \cdot 3H_2O$ in ethanol was mixed with the 2-fold excess of PPh_3 in methanol. A white precipitate of $AuPPh_3Cl$ started appearing immediately. In 10 – 20 minutes the precipitate was collected by filtration, washed 2 times with ethanol and dried in vacuum. The white precipitate was stored in the fridge. Typical yield was 91%. ^1H NMR showed signal at δ: 7.5-7.6 ppm (m), while ^{31}P NMR showed signal at δ: 33.1 ppm (s) (see Appendices 1, 2), which matched literature data.

$AuPPh_3NO_3$ was prepared according to the procedure described by Malatesta *et al.*[151] $AgNO_3$ (8.5 g, 0.05 mol) dissolved in ethanol (300 mL) was added to $AuPPh_3Cl$ (10.0 g, 0.02 mol) dissolved in CH_2Cl_2 (150 mL). Silver chloride started to precipitate immediately. After 30 minutes of stirring AgCl was filtered off and the solution was evaporated to dryness on a rotary evaporator. Solid was washed with ethanol (50 mL) 3 times, dissolved in chloroform (60 mL), filtered from insoluble impurities and then solvent was removed on a rotary

evaporator. White powder was collected, dried in a desiccator and stored in the fridge. Yield was 5.94 g (60 %). ^{31}P NMR δ: 27.5 ppm (Appendix 3)

$[Au_9(PPh_3)_8](NO_3)_3$ (denoted as Au_9) was synthesized according to the procedure described by Wen *et al.* [11] $NaBH_4$ (0.072 g, 1.92 mmol) in ethanol (92 mL) was added to the magnetically stirred solution of $AuPPh_3NO_3$ (4.0 g, 7.60 mmol) in ethanol (160 mL). The solution became deep red within two hours. After that solution was filtered from insoluble impurities, and solvents were removed *in vacuo*. The solid was dissolved in CH_2Cl_2 (20 mL), filtered on the fritted funnel (porosity 3) and the solvent was removed on Rotavapor. The black precipitate was washed with tetrahydrofuran (50 mL). Upon washing the solid becomes dark-green. The precipitate was crystallized from methanol solution by slow diffusion of diethyl ether. Dark-green crystals, typical for an Au_9-cluster, formed within *ca.* 5 days. Yield 1.24 g (36 %). The compound was characterised using ^{31}P NMR, UV-vis spectroscopy, transmission electron microscopy (TEM) and thermal gravimetric analysis (TGA). The obtained characterisation data matched earlier published results.

^{31}P NMR (CD_2Cl_2): δ 56.9 (s) ppm (Appendix 4), UV- vis 315, 350, 380, 450 nm. TEM and TGA data are discussed in Section 3.1.

$Au_{101}(PPh_3)_{21}Cl_6$ (denoted as Au_{101}) was prepared according to the procedure described by Hutchinson *et al.*[3] A solution of $HAuCl_4$ (1.00 g, 2.54 mmol) in Milli-Q water (60 mL) was stirred vigorously for 5 minutes. Analytical grade toluene (60 mL) was added to the stirred solution, followed by the addition of tetraoctylammonium bromide (1.40 g, 2.56 mmol). The organic layer turned red, while the aqueous layer became colourless. After 5 minutes of stirring, PPh_3 (2.30 g, 8.78 mmol) was added to the solution and the organic layer turned cloudy white. After 10 minutes of vigorous stirring, a fresh solution of $NaBH_4$ (2.00 g) dissolved in Milli-Q (30 mL) water was added dropwise to the reaction mixture and the solution turned dark-brown. The aqueous and organic layers were separated using a funnel

and the organic layer was washed 3 times with deionised water (100 mL). Next, the toluene solution was filtered from insoluble impurities and solvent was removed on a rotary evaporator.

The crude dark product was dissolved in chloroform (40 mL) and precipitated upon addition of pentane (300 mL). The suspension was filtered through a fritted funnel (porosity 4) to collect the solid (crude nanoparticles). The product was washed with the following solvent combinations to remove the excess of tetraoctylammonium bromide:

- 100 mL petroleum ether followed by 100 mL 2:3 MeOH:H_2O
- 100 mL petroleum ether followed by 100 mL 1:1 MeOH:H_2O
- 100 mL petroleum ether

The above sequence of washings was repeated 2 times. Next, the product was washed on the same fritted funnel with the following solvent combinations to remove $AuPPh_3Cl$:

- 150 mL 3:1 pentane:chloroform
- 150 mL 2:1 pentane:chloroform
- 150 mL 1:1 pentane:chloroform

During the each pentane/chloroform wash the product was agitated and allowed to soak in the wash solution for 5 minutes. The purified product was rinsed through the fritted funnel with CH_2Cl_2 and the solvent was removed on rotary evaporator. To increase the yield and purity of Au_{101}, after each new particle solubilisation during the above described steps the solution was filtered through Celite-545 layer on fritted glass funnel. Final yield of Au_{101} typically was *ca.* 0.3 g. The cluster was characterised using ^{1}H NMR, TEM and TGA. The results of cluster characterisation matched earlier published data. ^{1}H NMR (CD_2Cl_2) 7.1 ppm with a minimal signal from $AuClPPh_3$ at 7.52 ppm (Appendix 5), TEM and TGA data are discussed in Section 3.1.

$[PdAu_6(PPh_3)_7](NO_3)_2$ (denoted as $PdAu_6$) was synthesized according to the method reported by Takata et al.[152] A 100 mL round-bottom flask was charged with $PdCl_2(PPh_3)_2$ (0.30 g, 0.43 mmol) and $AuPPh_3NO_3$ (1.08 g, 2.00 mmol) in CH_2Cl_2 (10 mL) with stirring. A solution of $NaBH_4$ (0.039 g, 1.03 mmol) in ethanol (10 mL) was added dropwise to the solution of metal precursors. The dark red solution was stirred at room temperature for 30 min and then Milli-Q water was added to quench the reaction. The solvents were removed under vacuum. Methanol was added to the flask and the crude mixture was filtered through Celite-545 on a fritted glass funnel to remove insoluble precipitate. The dark red filtrate was evaporated to dryness and acetone (20 mL) was added to the solid. The resulting solution was then filtered again through Celite-545 and the filtrate was evaporated to dryness using rotary evaporator. The product was dissolved in 5 mL of methanol and precipitated by the addition of 40 mL of diethyl ether. Dark brown solid was centrifuged and dried *in vacuo*. Yield 0.45 g (42 %). The cluster was characterised using ^{31}P NMR. The result matched earlier reported data. ^{31}P NMR (CD_2Cl_2, 25 °C): δ 49.7 (doublet), δ 61.4 - 62.2 (septet) (Appendix 6).

$PtAu_8(PPh_3)_8(NO_3)_2$[153, 154] **(denoted as $PtAu_8$)** was synthesised following the earlier published procedure.[149,150] $Pt(PPh_3)_3$ (0.35 g, 0.36 mmol), which was prepared in advance in air/light-free conditions following the procedure published by Ugo and co-workers,[155] was dissolved in dry THF (25 mL) in a degassed round-bottom flask wrapped in aluminium foil. $AuPPh_3NO_3$ (1.10 g, 2.11 mmol) was added to the solution of $Pt(PPh_3)_3$. Hydrogen was bubbled through the magnetically stirred solution for 2 hours. After 2 hours of H_2-bubbling, red solution was separated from insoluble precipitate by filtration and evaporated to dryness. Dark brown crystals of $PtAu_8(PPh_3)_8(NO_3)_2$ were obtained by slow diffusion of hexane into 1:1 mixture of chloroform and methanol. The typical yield was 54 %. The cluster was characterised using ^{31}P NMR (^{31}P NMR ($CDCl_3$, 25 °C): 57.3 (s), Appendix 7).

$Au_8(PPh_3)_8(NO_3)_2$ (denoted as Au_8) was synthesised from Au_9 following the procedure by Van *et al.*[156] $Au_9(PPh_3)_8(NO_3)_3$ (1.48 g, 0.36 mmol) and PPh_3 (0.96 g, 3.66 mmol, 10-fold excess) were mixed in CH_2Cl_2 (20 mL). The solution was stirred for 30 minutes. After that the red product was precipitated by addition of toluene (200 mL), isolated by filtration, washed with toluene three times and dried. The red product was crystallized from CH_2Cl_2 solution by slow diffusion of diethyl ether. Crystals, typical for Au_8-cluster, formed in 2 days. The crystallization was repeated 2 times to remove excess of triphenylphosphine. Yield 1.38 g (88 %). The cluster was characterised using ^{31}P NMR ((CD_3OD): δ 56.0 (s) ppm) and UV-vis spectroscopy (375, 415 and 454 nm) (Appendix 8). The characterisation data matched earlier reported results.

$Au_6(dppp)_4(NO_3)_2$ (denoted as Au_6) was prepared from Au_9 cluster following the procedure described by van der Velden.[157] To a solution of Au_9 (1.0 g, 0.24 mmol) in CH_2Cl_2 (25 mL) $(C_6H_5)_2P(CH_2)_3P(C_6H_5)_2$ (dppp) (2.0 g, 4.85 mmol) was added. Fast reaction occurs and colour of the solution changes from red to deep blue. After 15 min product was precipitated by the addition of 200 mL of toluene and washed with toluene and ether. Compound was recrystallized by slow diffusion of diethyl ether into dichloromethane solution of Au_6. During recrystallization, the excess of dppp ligand formed cotton-like layer at the top, while Au_6 crystals grew at the bottom of crystallizing dish. Recrystallization was repeated several times until clean product was obtained. ^{31}P NMR in CD_2Cl_2 showed signals at δ 54.4 and 63.7 ppm, which matched the NMR data in the original paper (Appendix 9).

Colloid Au nanoparticles. Various colloid Au nanoparticles of different sizes were prepared following the published procedures. Stabilizer-free gold nanoparticles were synthesized following the exact procedure reported by Martin *et al.*[158] Citrate-stabilized Au nanoparticles were prepared following a protocol described by Turkevich *et al.*[8] Briefly, 450 mL of 0.24 mM $HAuCl_4$ and 1.6 mM sodium citrate solution was heated at 70 ˚C for 1 hour.

The resulting red solution containing 13.9 nm Au particles was cooled down using ice bath. 33.9 nm particles were prepared by heating 50 mL of 0.3 mM $HAuCl_4$ and 0.58 mM sodium citrate solution at 90 ˚C for 5 minutes. 47.4 nm particles were prepared by heating 50 mL 1.2 mM $HAuCl_4$ and 1.9 mM sodium citrate at 60 ˚C for 2 hours. Colloid gold solutions were used immediately for the preparation of supported gold catalysts.

2.2 Synthesis of catalyst supports

SBA-15 was synthesized according to the procedure reported by Zhao *et al.*[159] 2 M HCl solution (120 g) was added to a mixture of Pluronic P123 (4 g, M_n ~ 5800) with H_2O (30 mL) at 35 ˚C under vigorous stirring. After P123 completely dissolved, tetraethyl orthosilicate (TEOS, 8.5 g, 0.041 mmol) was added to the mixture and the resulting solution was left under stirring at 35 ˚C for 24 hours. The mixture was further aged at 80 ˚C overnight without stirring and the solid was collected by centrifugation, washed with H_2O and dried in air. To remove the copolymer surfactant the solid was calcined at 500 ˚C for 6 h in static air (heating rate 1 ˚C/min). The final white powder was characterized using N_2 adsorption/desorption technique and TEM.

Cr-MIL-101 ($Cr_3(OH)(H_2O)_2O[(O_2C)\text{-}C_6H_4\text{-}(CO_2)]_3 \cdot nH_2O$) was synthesized by Daniil Ovoshchnikov following the procedure published by Bromberg *et al.*[160] and characterized using Powder X-ray Diffraction analysis, surface area measurements, TGA and SEM.

2.3 Catalyst preparation

As made gold clusters were deposited onto SiO_2 or TiO_2 from CH_2Cl_2 solution. A calculated amount of gold cluster dissolved in CH_2Cl_2 (10 mL, 1-2 mg/mL) was added drop-wise to a vigorously stirred suspension of SiO_2, TiO_2 or WO_3 (500 mg) in CH_2Cl_2 (15 mL). The mixture was stirred for 30 min and the solid was collected by centrifugation. A colourless supernatant solution confirmed completeness of cluster deposition. The catalysts

were washed with CH_2Cl_2 (20 mL) and dried under vacuum at room temperature. Deposition of Au_9 clusters onto SBA-15 was performed using a methodology similar to the one described by Liu *et al.*[161] SBA-15 (500 mg) was suspended in the mixture of C_2H_5OH and CH_2Cl_2 (5 mL, 1:4). Solution of Au_9 cluster (2.3 mg) in the same solvent mixture (5 mL) was added dropwise to the suspension of SBA-15 under vigorous stirring. The mixture was stirred for 2.5 h. The solid was collected *via* centrifugation, washed with CH_2Cl_2 (10 mL) and dried under vacuum at room temperature. In cases when clusters did not adsorb readily to supports, such as in case of WO_3 and high Au_9 loadings, n-hexane was slowly added to the stirred suspension of oxide and Au cluster in dichloromethane until supernatant solution became colourless.

Colloid Au particles were deposited on SiO_2 from aqueous solutions. A calculated volume of freshly prepared Au colloid solution in water was added to SiO_2 (0.5 g). Mixture was sonicated for 1 minute and water was slowly removed from the suspension using rotary evaporator (T of bath *ca.* 30 ˚C). The resulting solid was collected, dried under vacuum at room temperature.

2.4 Catalyst treatments

In addition to the as made catalysts, TiO_2-based catalysts treated in different ways were studied in the one-pot synthesis of imine from alcohol and amine. Various gold and mixed-metal clusters supported on TiO_2 were treated in order to remove the PPh_3 stabilizing shell. The following treatments were employed:

Calcination. Catalyst was calcined in static air in for 2 hours at the temperature at which a particular cluster was shown to lose most of its organic moiety (based on TGA data). Typically, temperature was quickly raised to the desired one with the heating rate of 10 ˚C/ min, and clusters were kept under the target temperature for at least 2 h.

Ozonolysis (O_3). Catalyst was exposed to O_3 flow for 1 hour at room temperature under magnetic stirring using ozone generator OL100H1DS, Yanco Industries Ltd.

Ozonolysis, followed by toluene wash (O_3+W). Catalyst, treated with ozone for 1 hour, was further stirred in toluene at 100 ˚C for 1 hour.

2.5 Cluster and catalyst characterization

Catalysts were characterized using Transmission Electron Microscopy (TEM), X-ray photoelectron spectroscopy (XPS), diffuse-reflectance UV-vis (DR UV-vis). Gold loadings were established using atomic absorption spectroscopy (AAS) on a VARIAN SpectrAA 220FS. TEM analysis was performed using Philips CM200 operating at 200 kV. Samples for TEM analysis were suspended in diethyl ether and deposited on holey-carbon coated Cu grids. At least 100 particles were measured to plot particle size distributions. Diffuse-reflectance UV-visible spectra were recorded using Cintra 404 (GBC Scientific Equipment) spectrometer. UV-visible spectra were recorded in 10 mm quartz cuvette using Varian Cary 50 Probe UV-visible spectrophotometer. Thermal gravimetric analysis was performed using an Alphatech SDT Q600 instrument. The samples were heated at a rate of 1 – 10 ºC/min from room temperature to the desired temperature, and maintained at this temperature for 2 h. NMR spectra of gold clusters were recorded using Oxford/Varian AS500 500 MHz NMR spectrometer. Orthophosphoric acid was used as a standard for calibrating ^{31}P shifts.

Surface area and powder X-ray diffraction analysis measurements were performed by Campbell McNicoll at Callaghan Innovation, Wellington. Powder X-ray diffraction was performed on Philips PW 1700 automated diffractometer with CoKα radiation and graphite monochromator. Surface area measurements were performed using Micromeritics ASAP 2010.

X-Ray Photoelectron Spectroscopy

XPS was conducted on a Kratos Axis DLD spectrometer with a monochromated Al-Kα X-ray source. The samples were pressed into indium foil as the mounting medium. A supply of low energy electrons was used for charge neutralization. Survey spectra were recorded with a pass energy of 80 eV and high-resolution spectra with a pass energy of 40 eV.

Synchrotron based XPS was performed at the Soft X-ray Beamline at the Australian Synchrotron using a SPECS Phoibos 150 hemispherical electron analyser with the photon energy set to 690 eV. High resolution XPS spectra of C, O, Si, P, Ti and Au were recorded with pass energy of 10 eV. Scans were repeated several times to ensure that no photon-induced changes occurred in the samples. The stability of the X-ray energy was monitored using a bulk gold reference.

Binding energies were normalized with respect to the position of the adventitious C1s peak at 285.0 eV. Modelling of the data was performed using CasaXPS program (SiO_2 samples) or MS Excel (TiO_2 and WO_3 samples). Background was simulated using the empirical Shirley method:[162]

$$S(E) = I_2 + k\frac{A2(E)}{(A1(E)+A2(E))},$$

where S(E) is the background intensity at energy E, A_1 and A_2 – peaks areas, k defines the step in background and is equal to ($I_1 - I_2$).

To calculate a Shirley background from spectral data an iterative procedure was used. The integrated areas $A_1(E)$ and $A_2(E)$ for each point on the background E must initially be computed using an approximation to S(E), then refined using the background computed from the first approximation as input to improve the values computed for $A_1(E)$ and $A_2(E)$. The peaks were fitted using either sum of Lorentzian and Gaussian functions[163] (MS Excel, equation 1) or Gaussian/Lorentzian product[61] (CasaXPS, equation 2):

$$SGL\ (x; F, E, m) = (1-m)\exp\left(-4ln2\frac{(x-E)^2}{F^2}\right) + m/(1+4\frac{(x-E)^2}{F^2}) \quad (1)$$

$$GL(x;F,E,m) = \frac{\exp\left(-4ln2(1-m)\frac{(x-E)^2}{F^2}\right)}{1+4m\frac{(x-E)^2}{F^2}} \quad (2)$$

where F is the full width at half maximum, E – position of the peak maximum, and m is a mixing coefficient - 30.

Atomic Absorption Spectroscopy (AAS)

Actual Au loading in catalysts was established using AAS. A catalyst (typically 30 mg) was placed into a glass vial and heated at 100 ˚C for 2 hours to remove adsorbed water. After calcination, catalyst weight was measured and the sample was transferred to 50 mL polycarbonate centrifuge tube. 10 mL of freshly prepared *aqua regia* was added to the sample and the mixture was heated at 80 ˚C overnight. Next day, the suspension was centrifuged and supernatant solution was transferred into a clean polycarbonate tube. The catalyst support was washed with 4 % *aqua regia* in Milli-Q water 3 times. After each washing and centrifugation the solution was added to the *aqua regia* solution of gold. Next, the volume of gold solution was reduced to *ca.* 4 - 5 mL by evaporating the liquids at 105 ˚C. The resulting solution was transferred to a 10 mL volumetric flask and diluted to 10 mL using 4 % aqua regia in water. Gold content was established using AAS and quantified using an Au calibration curve, which was plotted using calibration solutions prepared from commercial standard Au solution (1 mg/mL) (Figure 2.1).

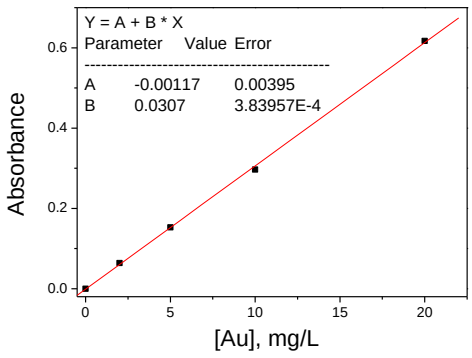

Figure 2.1. Absorbance of standard Au solutions (determined by AAS) as a function of gold concentration.

2.6 Catalytic experiments

2.6.1 Cyclohexene oxidation

Catalytic activity of Au catalysts was tested in aerobic solvent-free cyclohexene oxidation without addition of radical initiator. Kinetic studies of cyclohexene oxidation were performed in a glass reactor equipped with a reflux condenser. 10 mL of stabiliser-free cyclohexene containing 0.2 M of n-decane as an internal standard, 100 mg of catalyst and a Teflon-coated magnetic stirrer were loaded into 100 mL 2-necked glass round bottom flask. The system was flushed with O_2 three times and connected to a rubber balloon filled with O_2. The mixture was magnetically stirred at 65 °C (Figure 2.2).

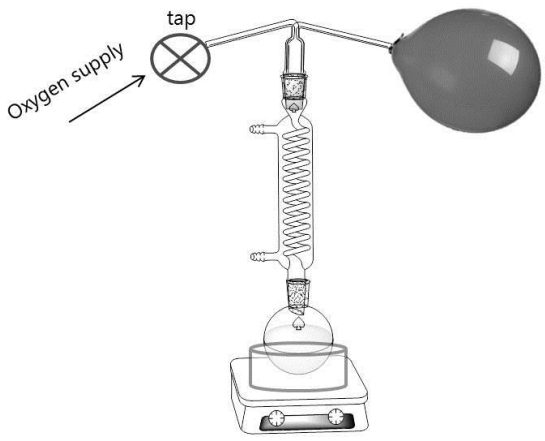

Figure 2.2. Scheme of the catalytic testing setup for cyclohexene oxidation.

Samples of reaction mixture were taken using glass syringe through the attachment with a Teflon septa connected to the second neck of the round-bottom flask. Reaction was stopped by cooling the reactor to room temperature; condenser was rinsed with 5 mL of diethyl ether and the reaction mixture was separated from the solid catalyst by centrifugation. Catalysts were washed with diethyl ether and dried under vacuum at room temperature before recycling. Each experiment was reproduced at least three times. The typical standard errors of independent catalytic tests were below 1.5 %.

2.6.2 One-pot imine synthesis

One-pot imine synthesis reactions were performed in glass reactors equipped with reflux condensers in the complete absence of light. 3 mL of toluene containing 0.1 mmol of benzyl alcohol, 0.1 mmol of benzylamine, 50 mg of catalyst, 10 mg of biphenyl as an internal standard, 0.2 mmol of base (K_2CO_3), and Teflon-coated magnetic stirrer were loaded into 25 mL glass round bottom flask, wrapped with foil. The flask was connected to a reflux condenser and the system was flushed with O_2 three times and connected to a rubber balloon filled with O_2. The mixture was magnetically stirred at 100 °C for 19 hours. Reaction was stopped by cooling the reactor to room temperature; condenser was rinsed with 5 mL of acetonitrile, the reaction mixture was separated from the solid catalyst by centrifugation and analysed using GC. Each experiment was repeated at least 2 times.

2.7 Product identification and quantitative analysis

The liquid samples were analysed by gas chromatography (GC-FID) using Shimadzu GC-2010 equipped with an Rxi-5SilMS capillary column (30 m × 0.25 mm × 0.25 μm). Helium was used as a carrier gas. The products of cyclohexene oxidation were identified by gas chromatography mass-spectrometry (GC-MS, Shimadzu GCMS-QP2010) and quantified using solutions of reference compounds with known concentrations. The following settings of GC instrument were used to analyse the cyclohexene oxidation reaction mixture (Table 2.1):

Table 2.1. GC instrument settings for the analysis of cyclohexene oxidation reaction mixture

Parameter	Value
Column program	70 ˚C (3 min), 30 ˚C/min to 200 ˚C (3 min)
FID temperature	250 ˚C
SPL temperature	250 ˚C
Pressure	95.3 kPa
Total flow	111.4 mL/min
Column flow	1.07 mL/min
Injection volume	1 μL

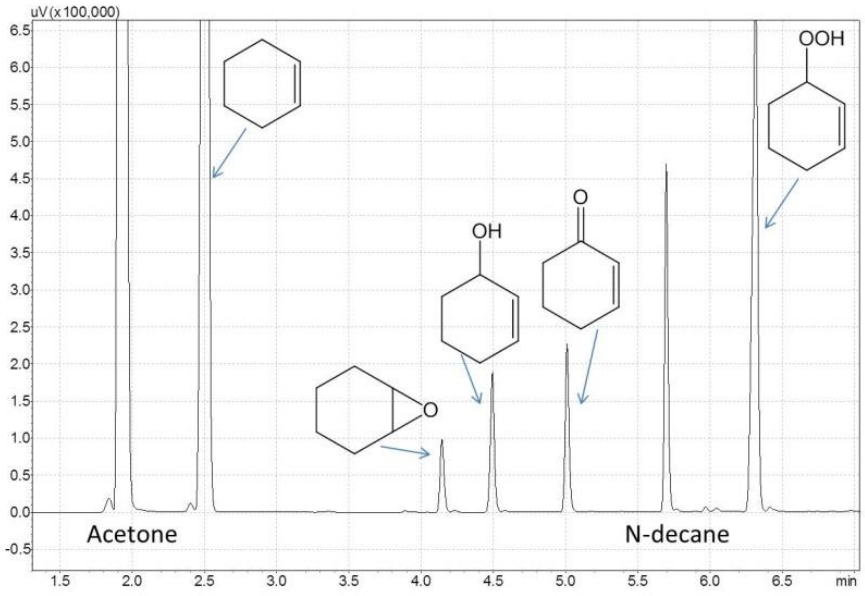

Figure 2.3. Typical chromatogram of cyclohexene oxidation reaction mixture.

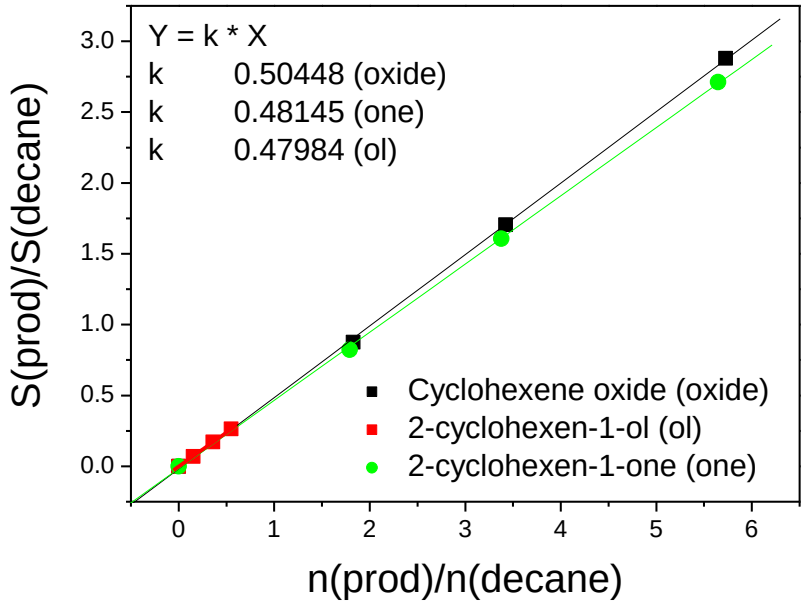

Figure 2.4. Calibration curves for cyclohexene oxidation products.

Conversion of cyclohexene was calculated using the following equation:

Conversion, % = $100 \cdot \frac{n(init) - n(final)}{n(init)}$; where n(init) is an initial amount of cyclohexene (moles) and n(final) is a final amount of cyclohexene (moles).

Product yields were calculated using the following equation:

Yield, % = $100 \cdot \frac{0.021 \cdot Sprod}{Sdecane \cdot k}$; where Sprod and S decane are the peak areas determined from GC analysis of the reaction mixture, k is a calibration coefficient for a product (see

Figure 2.4) and 0.021 is a ratio between initial number of moles of cyclohexene and number of moles of decane.

Product selectivity was calculated using the equation:

Selectivity, % = Yield (%)/Conversion.

Turnover frequencies (TOFs) were calculated using formula:

$$TOF, h^{-1} = (n^0_{substrate} - n_{substrate})/time\ (h) \cdot n_{Au},$$

where $n^0_{substrate}$ is initial number of moles of the substrate, $n_{substrate}$ is the number of moles left in the reaction after time (h) and n_{Au} is the number of moles of Au introduced to a catalytic reaction.

The concentration of cyclohexenyl hydroperoxide (CyOOH) was established using iodometric titration following the methodology described by Mair *et al.*[164] Reverse titration was performed as follows: 200 μL of reaction solution was placed into conical flask, followed by the addition of *ca.* 30 mg of KI and 1 mL of 80 % acetic acid. The mixture was left for 5 minutes, after which the I_2 formed was titrated with 0.05 M $Na_2S_2O_3$ (eq. 1 and 2).

$$2I^- + CyOOH + 2H^+ = I_2 + CyOH + H_2O \qquad \text{(eq. 1)}$$

$$2S_2O_3^{2-} + I_2 = S_4O_6^{2-} + 2I^- \qquad \text{(eq. 2)}$$

Prior to titration the concentration of $Na_2S_2O_3$ solution was standardized using 0.1 M $K_2Cr_2O_7$ solution according to the following equations:

$$Cr_2O_7^{2-} + 6I^- + 14H^+ = 3I_2 + 2Cr^{3+} + 7H_2O \qquad \text{(eq. 3)}$$

$$2S_2O_3^{2-} + I_2 = S_4O_6^{2-} + 2I^- \qquad \text{(eq. 4)}$$

Addition of PPh_3 to the reaction mixture prior to GC analysis did not change the concentration of 2-cyclohexene-1-one, determined from GC analysis, which implies that there was no cyclohexenyl hydroperoxide decomposition during GC analysis (*vide infra*).[165] Concentration of cyclohexenyl hydroperoxide was calibrated by comparison of GC data and iodometric titration results and was further calculated directly from GC results.

One-pot imine synthesis from alcohols and amines

Similarly to cyclohexene oxidation, liquid samples were analysed by gas chromatography using Shimadzu GC-2010 equipped with an RTX-50 capillary column, and helium was used as a carrier gas. The products were identified and quantified by GC analysis using solutions of reference compounds with known concentrations. The following settings of GC instrument were used to analyse reaction mixture of one-pot imine synthesis (Table 2.2):

Table 2.2. GC instrument settings for the analysis of imine synthesis reaction mixture

Parameter	Value
Column program	70 ˚C (2 min), 20 ˚C/min to 90 ˚C (2 min), 40 ˚C/min to 200 ˚C, 15 ˚C/min to 230 ˚C (5.5 min)
FID temperature	250 ˚C
SPL temperature	250 ˚C
Pressure	95.3 kPa
Total flow	111.4 mL/min
Column flow	1.07 mL/min
Injection volume	1 µL

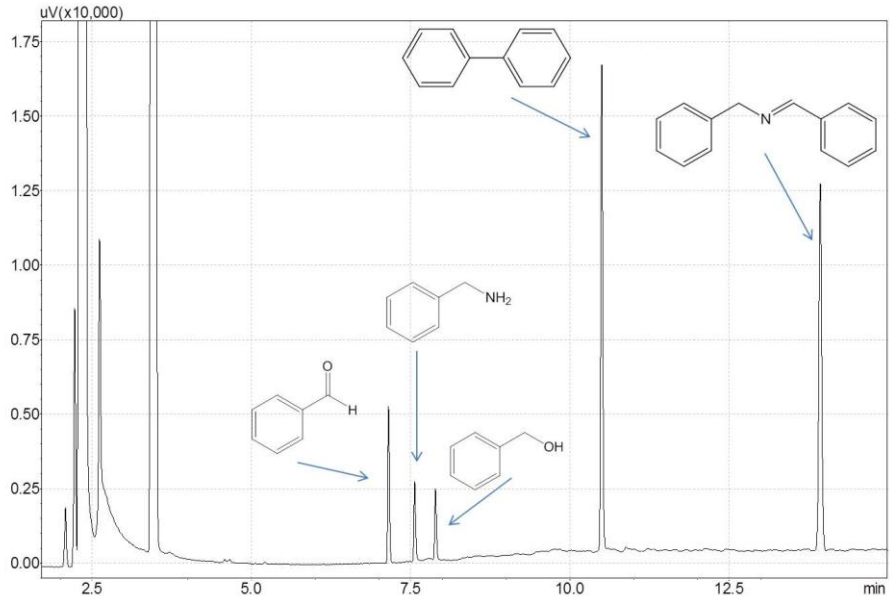

Figure 2.5. Typical chromatogram of one-pot synthesis of N-benzylidene benzylamine from benzylalcohol and benzylamine.

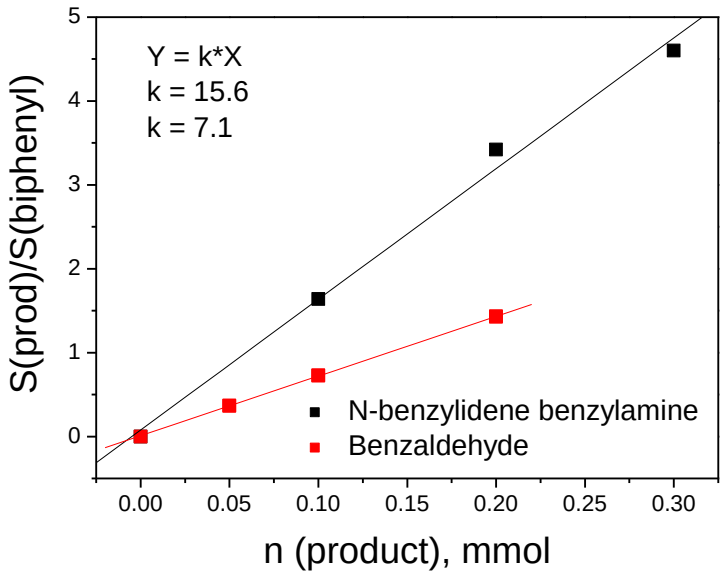

Figure 2.6. Calibration curves for the products of one-pot N-benzylidene benzylamine synthesis.

Yields of N-benzylidene benzylamine and benzaldehyde were calculated using the following equation:

Yield, % = $100 \cdot \frac{Sprod}{0.1 \cdot Sbiphenyl \cdot k}$; where k is a corresponding calibration coefficient (Figure 2.6).

Chapter 3. Gold-catalysed oxidation of cyclohexene

Work reported in this chapter was performed in collaboration with Daniil Ovoshchnikov. In Sections 3.2 - 3.5 TGA, AAS analysis, TEM studies of some WO_3-based catalysts and catalytic testing of WO_3-based catalysts, as well as TEM studies of some SiO_2-based catalysts were performed by Daniil. Also, discussions and formulation of ideas regarding the work on this chapter were done together with Daniil.

3.1 Cluster and support characterization

$Au_9(PPh_3)_8(NO_3)_3$ (Au_9) and $Au_{101}(PPh_3)_{21}Cl_5$ (Au_{101}) were synthesized and characterized using ^1H, ^{31}P NMR, TGA, UV-visible spectroscopy and TEM. The NMR spectra of synthesized clusters matched previously published spectra: the ^{31}P spectrum of Au_9 clusters in DCM had a singlet at δ 56.9 ppm; the ^1H spectrum of Au_{101} in DCM had a broad phenyl resonance at 7.1 ppm, with a minimal signal (7.52 ppm) due to unbound $AuClPPh_3$ (Appendix 5). Mean diameters of Au_9 and Au_{101} were determined as 0.9 ± 0.2 nm and 1.5 ± 0.3 nm, respectively, based on TEM observations (Figure 3.1 and Figure 3.2). UV-vis spectrum of Au_9 possesses 4 bands at 450, 380, 351 and 315 nm, which correlates with the literature data (Figure 3.1C). TGA showed 52 % (Au_9) and 26 % (Au_{101}) weight loss, which agrees well with the calculated values of 52 % and 21 %, respectively, based on the loss of PPh_3 ligands (Figure 3.3 and Figure 3.4, respectively).

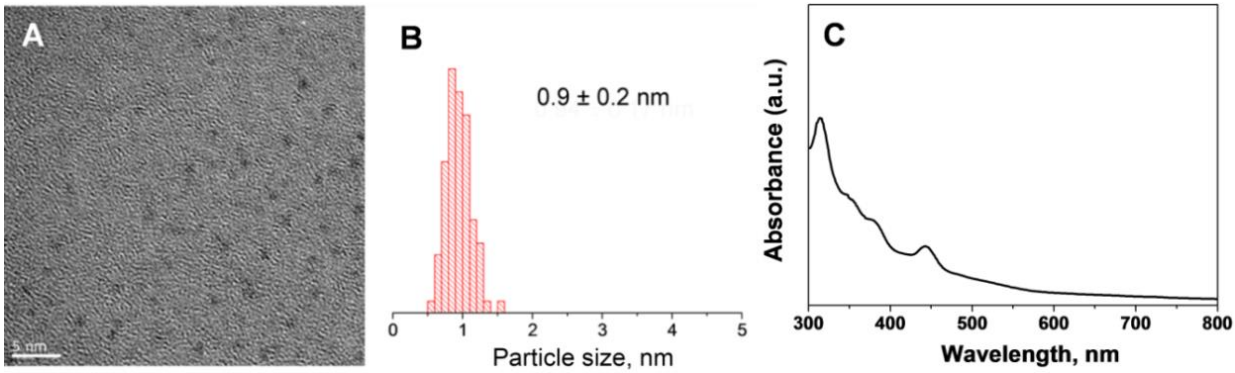

Figure 3.1. A representative TEM image of $Au_9(PPh_3)_8(NO_3)_3$ deposited onto the carbon film of the TEM grid, scale bar 5 nm (A) and corresponding particle size distribution (B). UV-vis spectrum of $Au_9(PPh_3)_8(NO_3)_3$ dissolved in CH_2Cl_2 (C).

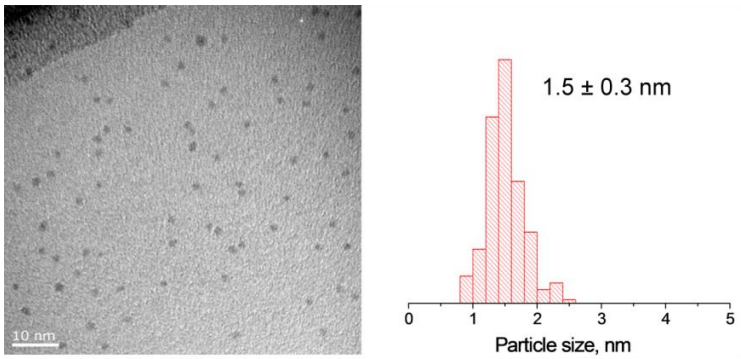

Figure 3.2. A representative TEM image of the $Au_{101}(PPh_3)_{21}Cl_5$ and the corresponding particle size distribution.

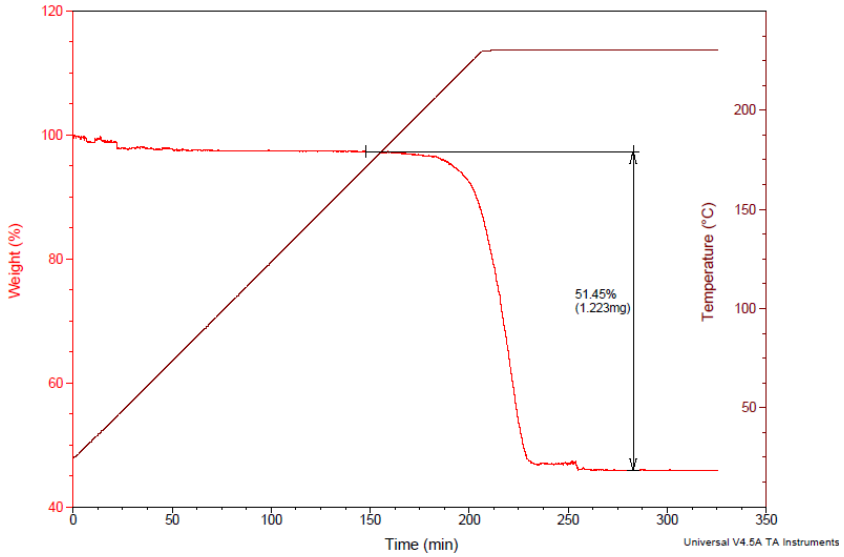

Figure 3.3. TGA of $Au_9(PPh_3)_8(NO_3)_3$. Conditions: 230 °C, 1 °C/min heating rate, hold 40 min, N_2 flow 100 mL/min.

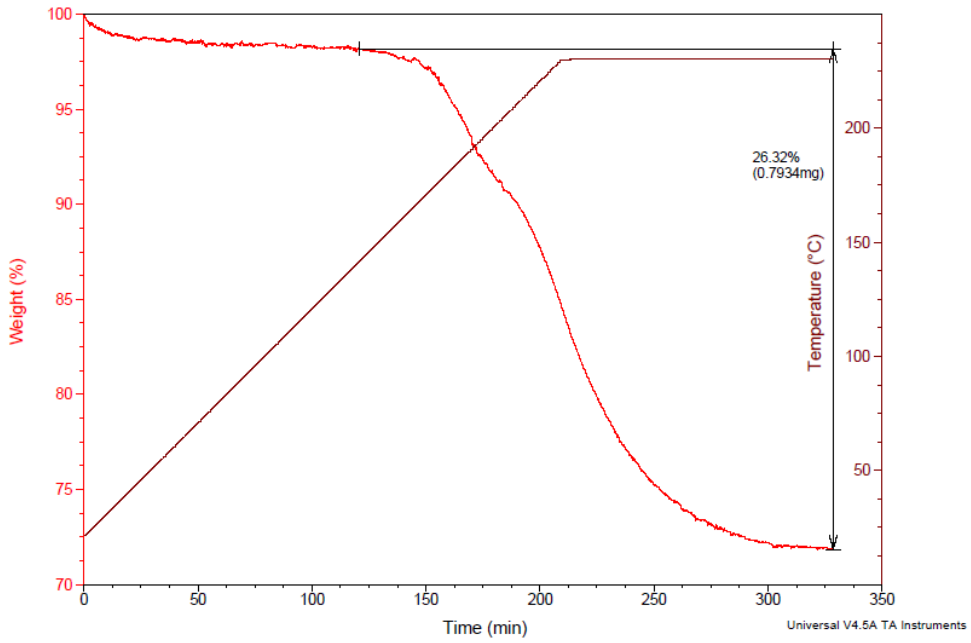

Figure 3.4. TGA of $Au_{101}(PPh_3)_{21}Cl_5$. Conditions: 230 °C, 1 °C/min heating rate, hold 2 h, N_2 flow 100 mL/min.

Other clusters and compounds used in this work were synthesized following previously published procedures and characterized using NMR, TGA, UV-vis, *etc*. In all cases, characterization results closely matched the previously reported data (see Appendices).

Surface area (BET) of SBA-15 was found to be 570 m^2/g and the average pore diameter was found to be 5 nm.

Figure 3.5 shows TEM micrograph of SBA-15.

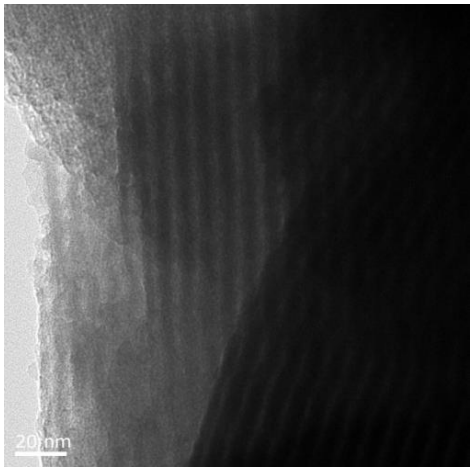

Figure 3.5. TEM micrograph of the porous structure of SBA-15.

BET surface area of CrMIL-101 was found to be 3265 m^2/g (Langmuir Surface area – 4050 m^2/g). X-Ray powder diffraction spectrum of CrMIL-101 matched the simulated spectrum (Figure 3.6). TGA showed 2 steps of weight loss (Appendix 13), corresponding to the loss of adsorbed water (46 %) and organic moiety of the MOF (39 %). Inset in the Figure 3.6 shows scanning electron microscopy (SEM) micrograph of CrMIL-101 powder.

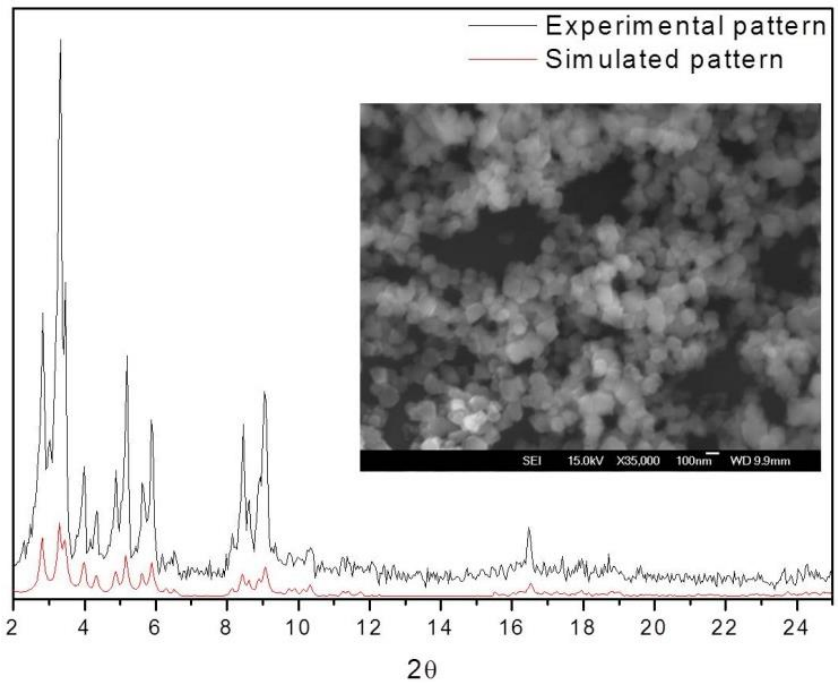

Figure 3.6. Powder X-Ray diffraction pattern of CrMIL-101: experimental (black) and simulated (red). Patterns are re-plotted for CuKα radiation source. Inset shows SEM micrograph of CrMIL-101 particles (scale bar 100 nm).

3.2 Investigation of the nature of the active Au sites in aerobic oxidation of cyclohexene

Three different types of SiO_2-based catalytic supports were used in this part of the study: Aerosil SiO_2 (Evonik, surface area ~ 50 m^2/g), fumed SiO_2 (Aldrich, surface area ~ 200 m^2/g) and SBA-15 (surface area 570 m^2/g).

Unless stated otherwise, gold clusters were deposited onto silica support by drop-wise addition of cluster solution in DCM to the suspension of silica in DCM and, typically, complete cluster deposition was easily achieved without any additional measures. When methanol or ethanol was used as a solvent for Au_9 deposition, even prolonged stirring did not result in complete cluster deposition, which was evidenced by the coloured supernatant solution. The efficient deposition of Au_9 cluster in an aprotic solvent (dichloromethane) is most likely due to the interaction between permanent dipole of OH groups of the support and dipole induced within triphenylphosphine layer of Au_9-cluster.[166] Thus, higher permittivity of methanol results in less efficient Au_9 deposition on SiO_2.

Gold loadings of catalysts were established using Atomic Absorption Spectroscopy. The established Au loading was very close to a target value (Table 3.1), confirming that in most cases clusters readily adsorb to SiO_2 supports in DCM.

Table 3.1. Gold loadings of Au/SiO_2 determined by AAS.

Catalyst name with target Au loading (%)	Actual gold loading established by AAS, %
$0.5Au_9$/Aerosil	0.49
$0.1Au_9$/Aerosil	0.098
$0.02Au_9$/Aerosil	0.021
$0.1Au_{101}$/Aerosil	0.11
$0.1Au_9$/SBA-15	0.095
0.1Au-9.1/Aerosil	0.097
0.1Au-13.7/Aerosil	0.094
0.1Au-33.9/Aerosil	0.095
0.1Au-47.4/Aerosil	0.096

Catalytic activity of various as made Au/SiO_2 catalysts with different gold loadings was studied in the solvent-free aerobic oxidation of cyclohexene at 65 ˚C (Table 3.2). No activity has been observed in either the absence of the catalyst (blank) or in the presence of pure SiO_2 materials. Au/SiO_2 catalysts demonstrated high activity in the studied reaction, which confirmed that the observed activity was due to the presence of gold. Main products were identified as cyclohexene oxide (1), 2-cyclohexen-1-ol (2), 2-cyclohexen-1-one (3) and cyclohexenyl hydroperoxide (4). Other products formed in this reaction in trace amounts were 2,3-epoxycyclohexenone, 2,3-epoxycyclohexenol and 1,2-cyclohexanediol, as determined using GC-MS analysis (See Appendices 10 – 12).

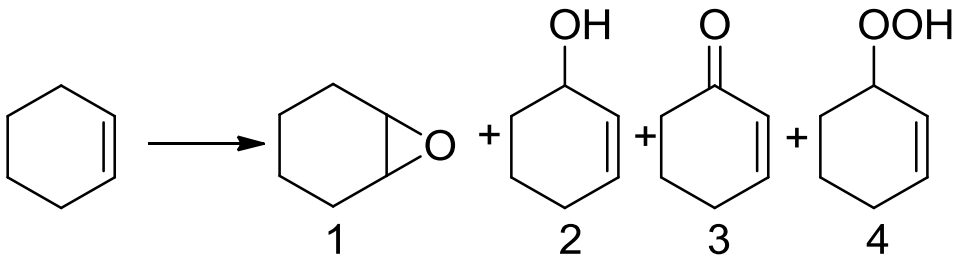

Table 3.2. Cyclohexene oxidation in the presence of various silica-supported Au catalysts.

N	Catalyst	Cyclohexene conversion, %	Selectivity, %				
			1	**2**	**3**	**4**	Other
1	Blank	2	-	-	-	-	-
2	Aerosil	2	-	-	-	-	-
3	SiO_2 fumed	2	-	-	-	-	-
4	0.5 Au_9/Aerosil	46	6	13	20	46	15
5	0.5 Au_9/SiO_2-fumed	30	6	10	15	63	6
6	0.5 Au_{101}/Aerosil	50	6	14	23	38	19
7	0.5 Au_{101}/SiO_2-fumed	43	6	14	21	42	17
8	0.3 Au_9/Aerosil	43	7	12	19	51	11
9	0.1 Au_9/Aerosil	25	6	10	14	66	4
10	0.1 Au_{101}/Aerosil	40	7	12	18	51	12
11	0.3 Au_9/Aerosil[a]	41	7	12	20	49	12
12	0.5 Au_{101}/Aerosil[a]	42	7	12	19	48	14
13	0.5 Au_9/Aerosil[b]	43	6	12	18	43	21

Reaction conditions: 65°C, 16 h, solvent-free cyclohexene, 5 mL, O_2 (~1 atm), 50 mg catalyst, 0.2 M n-decane as internal standard. [a]catalyst recycled after a 16-hour catalytic run. [b]reaction was performed in the absence of light.

We observed that Au_{101}/SiO_2 catalysts showed higher cyclohexene conversion compared to Au_9/SiO_2 (Table 3.2, entries 4 and 6, 9 and 10). Catalytic activity of Au-clusters deposited on Aerosil was higher than that of fumed SiO_2-based catalysts (Table 3.2, entries 4 and 5, 6 and 7). Catalysts with Au loadings of 0.3 and 0.5 % collected after reaction and used in the recyclability tests showed the activity close to that of as made catalysts (Table 3.2, entries 11 and 12). In all cases, clusters agglomerated during the reaction forming larger 5-10 nm particles after 16 h, as was evidenced by TEM study (*vide infra*).

Kinetic studies of aerobic cyclohexene oxidation catalysed by xAu_n/Aerosil showed that the reaction possessed an induction period. The length of the induction period depended on the Au loading of the catalyst (Figure 3.7A). The decrease of the Au loading of Au_9/Aerosil from 0.5 to 0.02 wt% led to the elongation of the induction period from *ca.* 1 to 6.5 h. The length of the induction period also depended on the type of Au cluster: $0.1Au_{101}$/Aerosil showed a significantly shorter induction period of 50 minutes compared with 3.5 hours for $0.1Au_9$/Aerosil (Figure 3.7B).

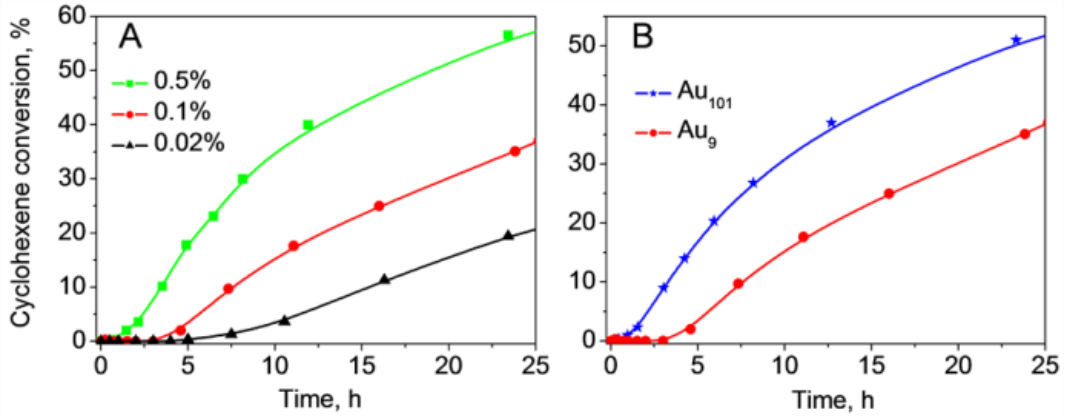

Figure 3.7. Cyclohexene oxidation catalysed by (A) Au_9/Aerosil with gold loadings of 0.5, 0.1 and 0.02% and (B) $0.1Au_{101}$/Aerosil and $0.1Au_9$/Aerosil. Conditions: solvent-free cyclohexene, 10 mL, O_2 1 atm, 65 °C, catalyst 0.1 g.

Change of the Au particle size during the reaction was monitored using TEM and diffuse-reflectance UV-visible spectroscopy. TEM micrographs of $0.5Au_9$/Aerosil sampled

from the reaction after 0.5, 1 and 16 h are shown in Figure 3.8B-D. Intact Au_9 clusters of as made $0.5Au_9$/Aerosil are not visible on bright-field TEM images because of the poor contrast for the supported Au clusters smaller than 1 nm (Figure 3.8A). During the reaction larger particles, which can be detected by TEM, gradually form and their number increases, as evidenced by the increase of the surface density of visible particles: *ca.* 40, 170 and 370 particles/μm^2 were detected in TEM micrographs of $0.5Au_9$/Aerosil sampled from the reaction after 0.5, 1 and 16 h, respectively. The mean diameter of detectable particles was 3.1 ± 0.1 (standard deviation (s.d.) 1.2) nm after 1 h and it increased further to 5.4 ± 0.1 (s.d. 1.4) nm during the next 15 h. The development of the particle size as a function of reaction time for $0.5Au_9$/Aerosil is shown in Figure 3.9.

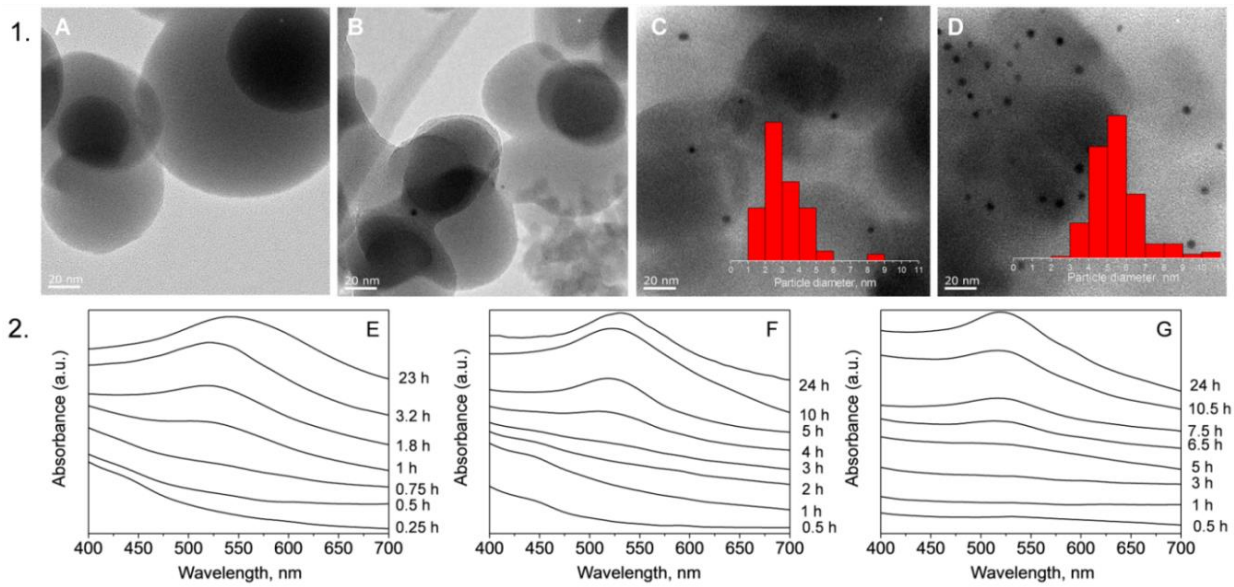

Figure 3.8. 1) TEM micrographs of $0.5Au_9$/Aerosil as made (A) and sampled from the reaction after 0.5 h (B), 1 h (C) and 16 h (D); 2) DR UV-vis spectra of $0.5Au_9$/Aerosil (E), $0.1Au_9$/Aerosil (F) and $0.02Au_9$/Aerosil (G) sampled at reaction times indicated along the right-hand ordinates.

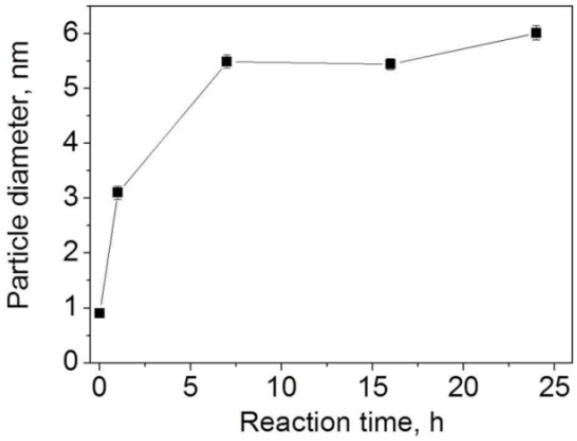

Figure 3.9. Evolution of the size of visible Au particles of $0.5Au_9$/Aerosil during cyclohexene oxidation (t = 0 – the size of the unsupported cluster)

DR UV-vis study of $0.5Au_9$/Aerosil showed the appearance of the surface plasmon resonance (SPR) band at 520 nm for samples of catalyst recovered from the reaction after 1 h. As was mentioned in the Introduction, surface plasmon resonance is a collective oscillation of electrons at the surface of metals induced by visible light, resulting in a bright red colour of gold nanoparticles. This feature is characteristic only for particles larger than 2 nm: particles smaller than 2 nm do not possess surface plasmon resonance.[102-104] Thus, the appearance of an SPR band in $0.5Au_9$/Aerosil after 1 h indicates the formation of gold particles larger than 2 nm (Figure 3.8E).

Hence, both TEM and DR UV-vis studies of $0.5Au_9$/Aerosil show a similar time of formation of particles larger than 2 nm. DR UV-vis studies of catalysts with different gold loadings, *i.e.* $0.1Au_9$/Aerosil and $0.02Au_9$/Aerosil showed that particles larger than 2 nm form only after *ca.* 4 and 6.5 h, respectively. Slower gold agglomeration for catalysts with lower Au loadings is most likely due to the lower density of Au particles on Aerosil surface, because it takes longer for particles to collide and form of agglomerates. As seen from the kinetics of cyclohexene oxidation (Figure 3.7A) and DR UV-vis data, in all cases formation of a sufficient number of particles larger than 2 nm was accompanied by the appearance of

catalytic activity, which indicates that such particles are active in cyclohexene oxidation. The absence of an induction period for Au_9/Aerosil, recycled after 16 h catalytic run, supports this conclusion (Figure 3.10).

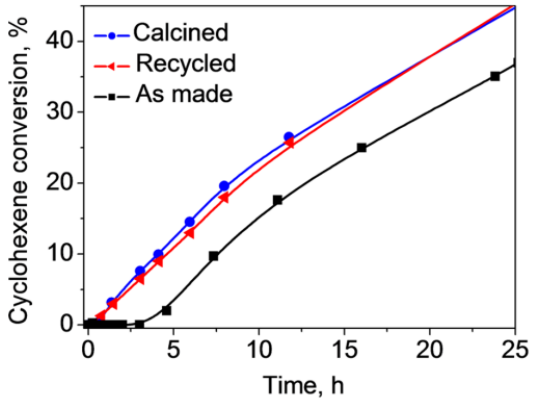

Figure 3.10. Cyclohexene oxidation catalysed by as made, recycled and pre-calcined 0.1Au_9/Aerosil.

Importantly, the cyclohexene used for catalytic oxidation did not contain 2,6-di-tert-butyl-4-methylphenol, which is typically added as a stabilizer by chemical suppliers. When cyclohexene containing the stabilizer was used, the Au_9 clusters did not agglomerate after 16 hours under typical reaction conditions (65 °C, 1 atm O_2) and no cyclohexene conversion was observed. Stirring 0.5Au_9/Aerosil for 16 hours under typical reaction conditions, but in n-hexane instead of cyclohexene, also did not lead to cluster agglomeration. These results imply that thermal treatment at 65 °C alone is not enough to induce agglomeration of Au_9 supported on silica. Recently, Kilmartin *et al.* reported the removal of phosphine ligands from silica-supported $Au_6(Ph_2P(o\text{-tolyl}))_6(NO_3)_2$ by tert-butyl hydroperoxide.[167] It could be suggested that in our study phosphine ligands were removed from the cluster *via* reaction with cyclohexenyl hydroperoxide, which is present in trace amounts in the stabilizer-free cyclohexene (*ca.* 0.015 wt% by GC). Agglomeration did not occur in n-hexane or stabilizer-containing cyclohexene because neither of them contained even traces of peroxides. Thus, cluster agglomeration is possible only when PPh_3 ligands are removed from the gold core of

Au_9. An indication of such step-by-step in situ transformation of gold clusters, which includes ligand removal from the cluster cores and subsequent particle agglomeration, can also be seen in Figure 3.8F. DR-UV-vis spectra of catalyst sampled in the initial stages of the reaction possessed a weak band at 450 nm, originating from intact supported Au_9 clusters (Figure 3.1C). The features in the optical spectra of small phosphine-stabilized gold clusters are known to be due to the effects of the ligand shell bound to the gold core of the cluster.[168] Therefore, the disappearance of the band at 450 nm before the SPR band emerges indicates that agglomeration occurs after the ligand shell is at least partially removed. Because sintering is not possible when ligands are still bound to the gold cores of the clusters, it could be concluded that particles forming during the reaction are predominantly phosphine-free.

Additionally, Synchrotron-based XPS study of a post-reaction $0.1Au_9/WO_3$, a catalytic system in which similarly sized Au particles form during cyclohexene oxidation and similar activity in cyclohexene oxidation is achieved (*vide infra*), showed at least 70 % phosphorous removal from the catalyst after the reaction (Figure 3.11) as indicated by the disappearance of the signal at 132 eV (phosphorous detection limit of 0.03 wt% was calculated from the spectrum of a post-reaction catalyst).

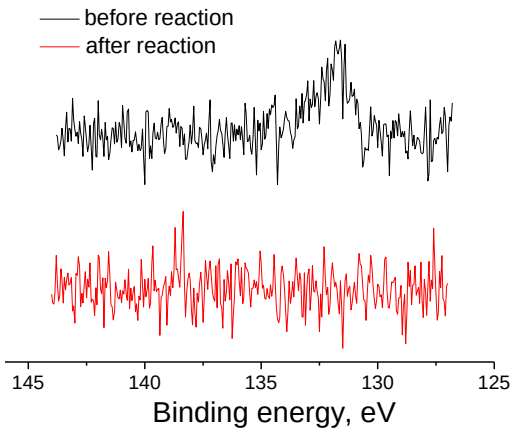

Figure 3.11. XPS $P2p_{3/2}$ spectra of as made $0.1Au_9/WO_3$ (black) and $0.1Au_9/WO_3$ (red) recovered after 16 h catalytic cycle of cyclohexene oxidation.

Pure Au_9 clusters lose phosphine ligands upon calcination at 230 °C for 40 min in Ar flow according to TGA (Figure 3.3). Calcination of $0.1Au_9$/Aerosil under the same conditions in order to remove phosphine ligands from supported Au_9 clusters led to the formation of 8.0 ± 0.3 (s.d. 2.6) nm particles (Figure 3.12). Catalyst treated this way showed a cyclohexene conversion profile similar to that of the recycled $0.1Au_9$/Aerosil (particle size 9.6 ± 0.6 (s.d. 3.9) nm, Figure 3.13), which indicates that phosphine-free particles of similar size and larger than 2 nm obtained in different ways have similar activity in the reaction (Figure 3.10).

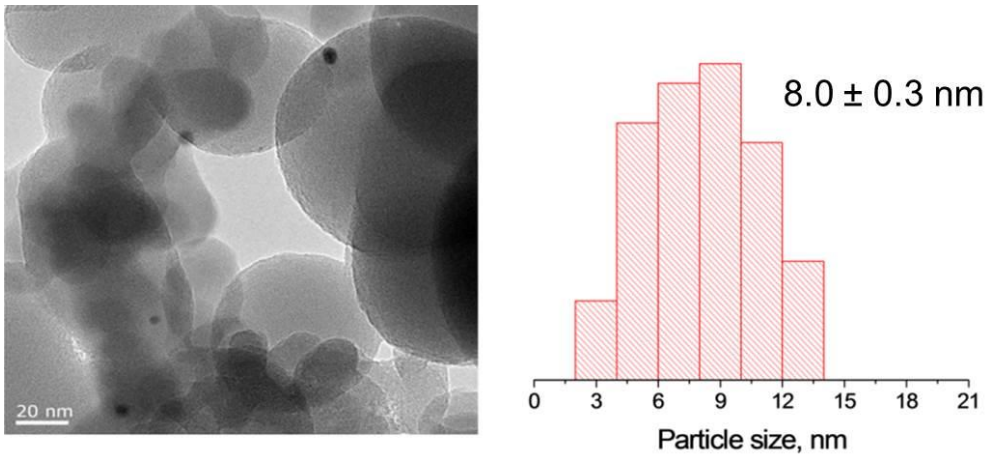

Figure 3.12. A representative TEM image of $0.1Au_9$/Aerosil calcined at 230 °C for 40 min, 1 °C/min, Ar flow 100 mL/min and the corresponding particle size distribution.

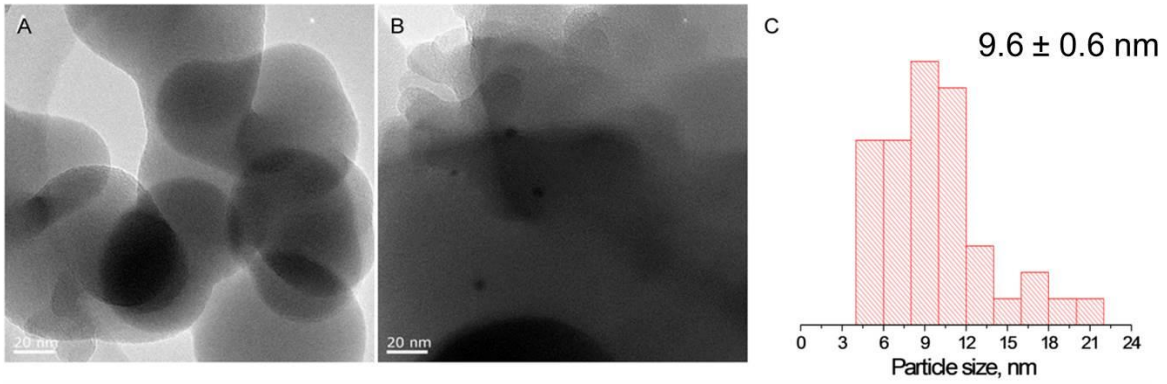

Figure 3.13. Representative TEM images of $0.1Au_9$/Aerosil before (A) and after (B) cyclohexene oxidation and particle size distribution of $0.1Au_9$/Aerosil after cyclohexene oxidation (C).

Inasmuch as two catalyst parameters change during the reaction, *i.e.* Au particle size and the presence of phosphine ligands, the initial inactivity of the as made catalysts could be due to one of the following: a) stabilizing ligands cover active gold sites, thus hindering the catalytic activity; once the phosphine ligands are removed, the particles become active b) sub-2 nm gold particles, even without phosphine ligands, are inactive in cyclohexene oxidation and activity appears only after the particle size reaches a certain threshold. Results of this study indicate that removal of phosphine ligands is not a sufficient condition for the appearance of catalytic activity and particle size plays a significant role:

a) As seen from Figure 3.8F, the PPh_3 ligand shell was at least partially removed from Au_9 after 2 hours, as indicated by disappearance of the band at 450 nm, but no activity was observed until particles larger than 2 nm had formed after *ca.* 4 hours of reaction (Figure 3.7A).

b) Because the core of Au_{101} is larger than that of Au_9, gold particles derived from Au_{101} need significantly less time to overcome the threshold in particle size, which leads to shorter induction period for Au_{101} catalyst (Figure 3.7B).

To confirm that small (sub-2 nm) and phosphine-free Au particles are inactive in cyclohexene oxidation, Au_9 was deposited on SBA-15,[169] a mesoporous silica-based material with large surface area (see Section 3.1), which was prepared in advance. A mixture of ethanol and dichloromethane was used to ensure homogeneous distribution of clusters throughout the surface of the support.[166] As was mentioned earlier, the high permittivity of alcohol results in only partial cluster deposition, thus allowing more homogeneous surface distribution of clusters, than in the case pure dichloromethane, where clusters immediately adsorb to the surface of silica once they meet it.

To remove phosphine ligands from the cluster core, the catalyst was calcined at 230 °C for 40 min in Ar flow (denoted as $0.1Au_9$/SBA_c230) – the conditions at which pure Au_9

loses its ligands, as determined from TGA (Figure 3.3). The large surface area of the support and the homogeneous distribution of clusters prevented particles from sintering during calcination, as evidenced by the absence of the SPR band in the DR UV-vis spectrum of $0.1Au_9$/SBA_c230 (Figure 3.14). On the other hand, the absence of absorption bands at 450, 380 and 315 nm, characteristic for the Au_9 cluster, indicates successful removal of ligands during calcination. TEM of $0.1Au_9$/SBA_c230 also confirmed very minimal agglomeration – only a few particles of 2-3 nm were detected, which correlates with the results obtained for Au_{11} clusters in the similar system.[166] Thus, phosphine-free sub-2 nm gold particles supported on SBA-15 were obtained.

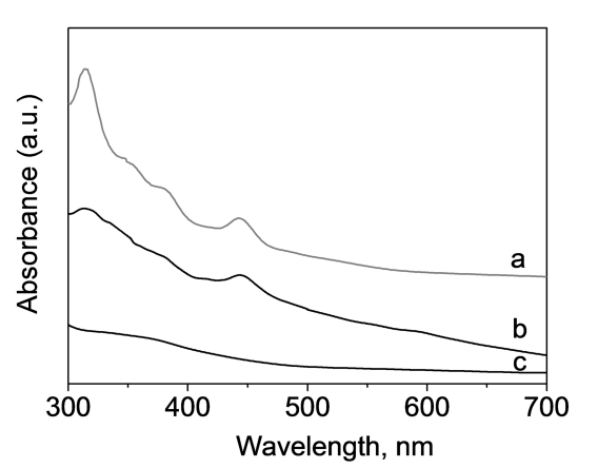

Figure 3.14. UV-vis spectrum of Au_9 dissolved in CH_2Cl_2 (a) and DR UV-vis spectra of as made $0.1Au_9$/SBA-15 (b) and $0.1Au_9$/SBA_c230 (c).

Although the Au particles were phosphine-free, the kinetics of cyclohexene oxidation in the presence of $0.1Au_9$/SBA_c230 showed an induction period of *ca.* 3.5 hours. The appearance of catalytic activity correlated with the formation of plasmonic particles (Figure 3.15), similar to the behaviour observed for Aerosil-based catalysts, as discussed earlier. Recycled $0.1Au_9$/SBA_c230 did not show an induction period in cyclohexene oxidation. This result confirmed that phosphine-free Au particles with the sizes below 2 nm are inactive in the cyclohexene oxidation. The change of catalytic behaviour of Au particles once they

become larger than 2 nm could be due to the transition from non-metallic to metallic properties, which occurs at sizes of *ca.* 2 nm.[170]

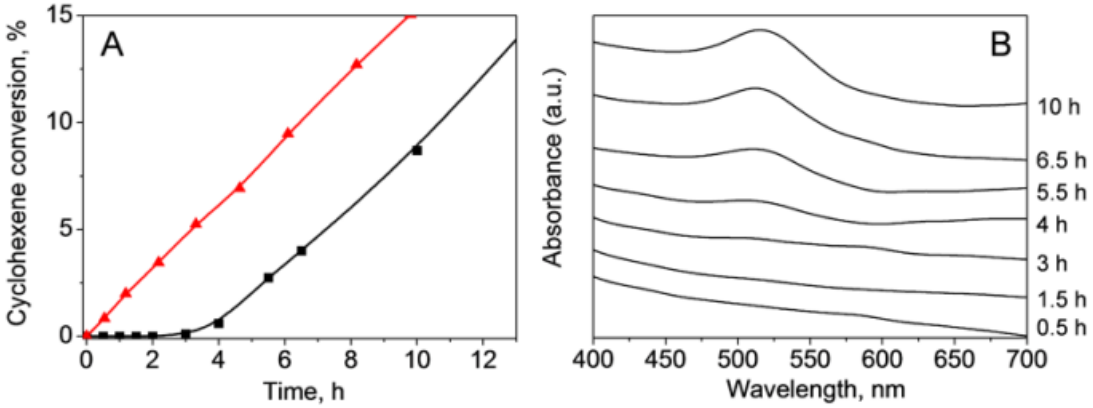

Figure 3.15. A) Cyclohexene oxidation catalysed by $0.1Au_9$/SBA_c230 (black) and recycled $0.1Au_9$/SBA_c230 (red). B) DR UV-vis spectra of $0.1Au_9$/SBA_c230 sampled from cyclohexene oxidation at different reaction times.

Numerous examples of catalysis, driven or enhanced by plasmonic photoactivity of Au nanoparticles, have been recently reported.[171-173] Because catalytic activity in this study appeared only when gold nanoparticles larger than 2 nm, *i.e.* plasmonic particles, were formed, we investigated whether the observed activity was enabled by the SPR. The activity of $0.5Au_9$/Aerosil in cyclohexene oxidation under ambient light was similar to that in the absence of light, which indicated that catalytic activity was not enhanced by the SPR in this study (Table 3.2, line 13).

The XPS spectrum of a post-reaction $0.5Au_9$/Aerosil showed the $Au4f_{7/2}$ signal centred at 84.0 eV, a binding energy characteristic of bulk neutral gold (Figure 3.16). No signal at 85.0 eV from pristine Au_9 clusters[174] was detected in the post-reaction catalyst, indicating that most of the gold present in the catalytic system is in the metallic state and no intact clusters are left after the reaction. Unlike the recently reported activity of positively charged 20 – 150 nm Au nanoparticles in styrene oxidation,[136] catalytic activity in this study was solely due to the metallic Au^0 particles, as evidenced by the activity of the post-reaction catalysts in the second catalytic cycle.

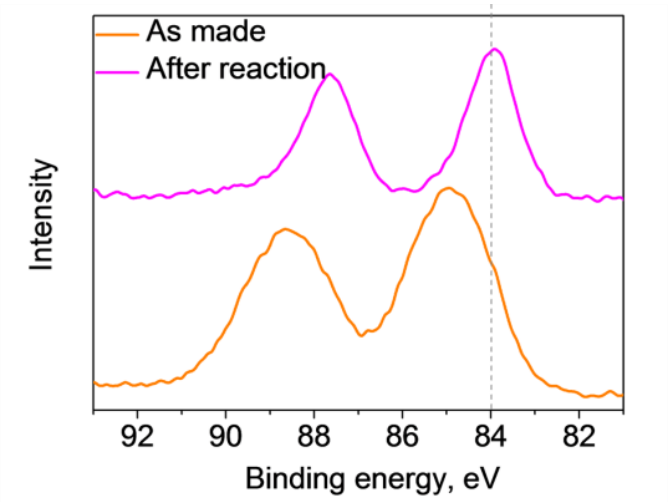

Figure 3.16. XPS Au4f$_{7/2}$ spectra of as made 0.5Au$_9$/Aerosil and 0.5Au$_9$/Aerosil recovered after 16 h catalytic cycle of cyclohexene oxidation. Dotted vertical line indicates Au4f$_{7/2}$ peak position corresponding to metallic gold.

To check whether there is an effect of particle preparation, colloid stabilizer-free[158] and citrate-stabilized[8] Au nanoparticles were synthesized and deposited onto Aerosil with the total gold loadings of 0.1 wt% (see Table 3.1). Four different catalysts 0.1Au-9.1/Aerosil, 0.1Au-13.7/Aerosil, 0.1Au-33.9/Aerosil and 0.1Au-47.4/Aerosil with particle sizes of 9.1, 13.7, 33.9 and 47.4 nm, respectively, were obtained (Figure 3.17).

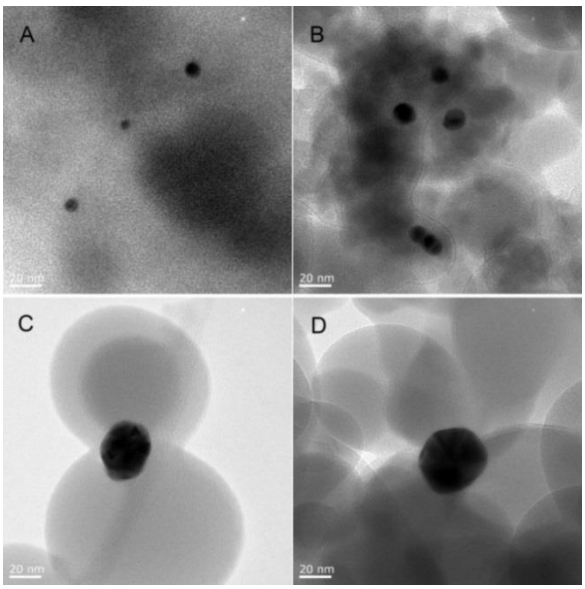

Figure 3.17. Representative TEM images of colloid Au nanoparticles supported on Aerosil: 9.1 nm (A), 13.7 nm (B), 33.9 nm (C) and 47.4 nm (D).

All the catalysts were active in cyclohexene oxidation and no induction period was observed in all cases (Figure 3.18). Comparison of initial reaction rates and turnover frequencies (TOFs) of the Au colloid-based catalysts is shown in Table 3.3 Catalytic activity of 0.1Au/Aerosil gradually decreased with the increase in Au particle size, which is in accordance with the smaller fraction of surface Au atoms for larger particles. Indeed, TOF values normalized by $Au_{surface}$ are very close for differently sized supported Au nanoparticles (Table 3.3). This result confirms that metallic Au particles larger than 2 nm are responsible for the observed catalytic activity in the oxidation of cyclohexene, and the catalytic activity does not depend on the preparation method, but it is proportional to the surface area of Au exposed to reagents.

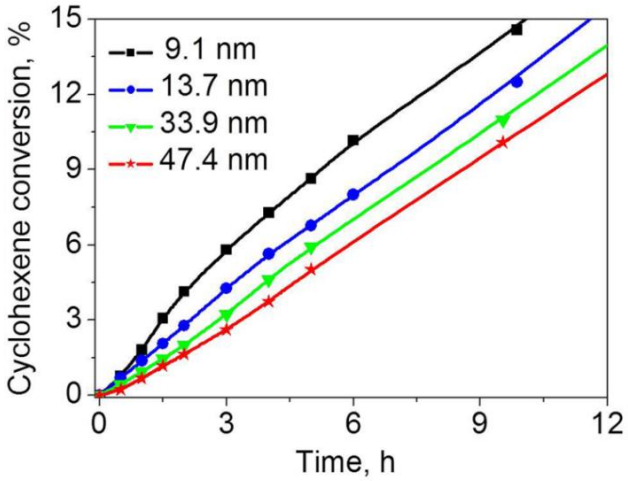

Figure 3.18. Cyclohexene oxidation catalysed by 9.1, 13.7, 33.9 and 47.4 nm Au particles supported on Aerosil with the total gold loading of 0.1 wt%.

Finally, the observations summarised in Table 3.2 are consistent with the results obtained from this size-dependency study: Au_{101}-based catalysts show higher cyclohexene conversion after 16 h compared to Au_9-based catalysts due to the shorter induction period of Au_{101}-catalysts; Aerosil-based samples give higher cyclohexene conversion after 16 h compared to fumed SiO_2 samples because of the lower surface area of Aerosil (50 *vs.* 200

m^2/g), which causes faster cluster agglomeration and consequently faster formation of active nanoparticles.

Table 3.3. Comparison of initial reaction rates and TOFs of Au/Aerosil catalysts in cyclohexene oxidation.

N	Catalyst	Reaction rate × 10^6, $mol_{substrate}/s$	TOF_{Au}, s^{-1}	$TOF_{surface\ Au}$, s^{-1}
1	0.1Au-9.1/Aerosil	0.58	1.14	17.5[a]
2	0.1Au-13.7/Aerosil	0.39	0.78	18.0[a]
3	0.1Au-33.9/Aerosil	0.28	0.53	21.7[b]
4	0.1Au-47.4/Aerosil	0.20	0.40	18.9[b]

Fraction of surface Au atoms was estimated assuming [a]spherical and [b]cuboctahedral shape of Au nanoparticles (based on TEM observations).

Product evolution kinetic study in the presence of $0.5Au_9$/Aerosil showed that first-to-appear and main product is cyclohexenyl hydroperoxide. The concentration of cyclohexenyl hydroperoxide reached its maximum at *ca.* 16 h and then it gradually dropped, most likely, due to hydroperoxide conversion to 2-cyclohexen-1-ol and 2-cyclohexen-1-one (Figure 3.19). Yield of epoxide reached *ca.* 2.5 %. Product distribution was similar for all Au/SiO_2 catalysts, with cyclohexenyl hydroperoxide being the main product (Table 3.2).

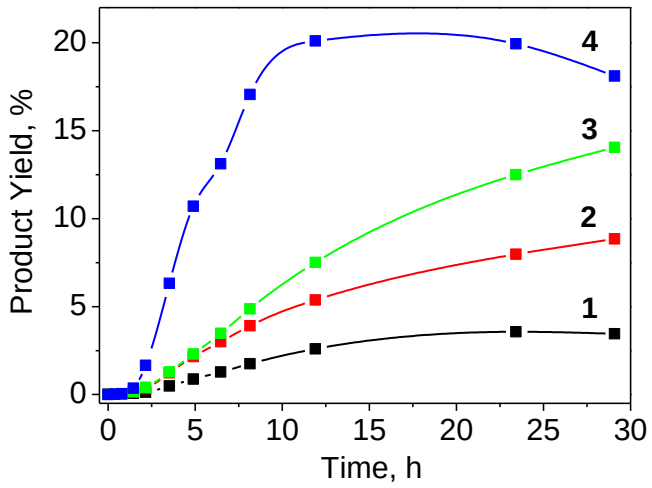

Figure 3.19. Product evolution profile in cyclohexene oxidation catalysed by $0.5Au_9$/Aerosil. Cyclohexene oxide (1), 2-cyclohexen-1-ol (2), 2-cyclohexen-1-one (3), cyclohexenyl hydroperoxide (4).

Since hydroperoxides may decompose under the conditions of GC analysis giving corresponding alcohol and ketone (2-cyclohexen-1-ol and 2-cyclohexen-1-one),[165] the following test was performed to find out whether cyclohexenyl hydroperoxide was stable during the GC analysis and to exclude the possibility of erroneous determination of product yields. After reaction was stopped, an excess of PPh_3 was added to the reaction mixture. PPh_3 readily reacts with cyclohexenyl hydroperoxide to give the corresponding triphenylphosphine oxide (PPh_3O) and 2-cyclohexen-1-ol. The resulting mixture was analysed using GC and the amount of 2-cyclohexen-1-one was compared to that in the reaction mixture before the addition of PPh_3. Because the amount of 2-cyclohexen-1-one did not change upon addition of PPh_3, it could be concluded that no cyclohexenyl hydroperoxide decomposition occurred during GC analysis.

Limitation of reaction rate due to internal mass transfer in cyclohexene oxidation in this work could be excluded because most of the support materials used in this work were non-porous. In the case of SBA-15 the reaction rate was slower than that of Aerosil-based catalysts with the same loading, and in this case diffusion of reactants into pores of SBA-15 could affect the rate of the reaction. However, this also could be due to partial blockage of pores of SBA-15 during Au particle aggregation, which may result in inaccessibility of a fraction of gold for catalysis. Nevertheless, absence or presence of limitation of the reaction rate due to the diffusion should not affect conclusions regarding the optimal structure of Au catalysts in this work.

Table 3.4 demonstrates activities of some Au-based catalysts in the oxidation of alkenes (cyclohexene, cyclooctene) in comparison with Au/SiO_2 studied in this work. The results in this table show that catalysts studied in this project were significantly more active in the oxidation of alkenes compared to the previously studied systems.

Table 3.4 Comparison of catalytic activities of various Au catalysts in the oxidation of alkenes.

Alkene	Solvent	T, ˚C	Catalyst	Ref	TOF_{Au}, h^{-1}
C_6H_{10}	No	65	0.5% Au_9/SiO_2	This work	2015
C_6H_{10}	No	65	0.1% Au_9/SiO_2	This work	5576
C_6H_{10}	No	65	0.02% Au_9/SiO_2	This work	11590
C_6H_{10}	1,4-Dimethylbenzene	80	1% Au/C	Hughes *et al.*[74]	23.8
C_6H_{10}	1,3,5-Trimethylbenzene	80	1% Au/C	Hughes *et al.*	3.6
C_6H_{10}	1,2,3,5-Tetramethylbenzene	80	1% Au/C	Hughes *et al.*	13.2
C_6H_{10}	Quinoline	80	1% Au/C	Hughes *et al.*	14.7
C_6H_{10}	Hexafluorobenzene	80	1% Au/C	Hughes *et al.*	7.0
C_6H_{10}	1,4-Difluorobenzene	80	1% Au/C	Hughes *et al.*	12.9
C_6H_{10}	No (+ TBHP 1.2 mol%)	80	Au/SiNW(66 %)	Tsang *et al.*[175]	46.1
C_8H_{14}	No (+ TBHP 1.6 mol%)	80	Au/SiNW(66 %)	Tsang *et al.*	14.5
C_6H_{10}	No (O_2 0.4 MPa)	80	Au/La-OMS-2(0.93%)	Cai *et al.*[176]	421

Mechanism of cyclohexene oxidation catalysed by Au

This work shows that only Au^0 particles larger than 2 nm are active in aerobic cyclohexene oxidation; however oxygen adsorption and its dissociative activation on large metallic gold particles were shown to be extremely impeded.[60, 177] On the other hand, extended gold surfaces were long known to catalyse hydrogen abstraction from hydrocarbons,[27] and thus activation of cyclohexene rather than O_2 by gold nanoparticles is the more probable pathway of gold-catalysed activation in this study. This suggestion is also supported by the fact that the main product of cyclohexene oxidation in this work is cyclohexenyl hydroperoxide (Figure 3.19), which is formed in the reaction between dissolved oxygen and cyclohexenyl radicals generated *via* allylic hydrogen abstraction from cyclohexene. When a sufficient amount of cyclohexenyl hydroperoxide is formed it further acts as a radical chain propagator in cyclohexene autoxidation.[178] It should be noted that the reaction is not merely an autoxidation, because the presence of gold is necessary for the initiation of the reaction. A similar mechanism was recently described for cyclohexane oxidation catalysed by Au/MgO.[179] Higher activity of Au catalysts in cyclohexene oxidation

compared to cyclohexane oxidation[85, 179, 180] can be explained by more facile H-abstraction from an allylic position because allylic C-H is weaker than alkylic C-H bond.

Thus, the following mechanism of cyclohexene oxidation catalysed by Au nanoparticles supported on SiO_2 could be suggested:

Initiation:

$C_6H_{10} \rightarrow C_6H_9\cdot$ (Hydrogen abstraction by metallic gold nanoparticles)

Propagation:

$C_6H_9\cdot + O_2 \rightarrow C_6H_9\text{-}OO\cdot$

$C_6H_9\text{-}OO\cdot + C_6H_{10} \rightarrow C_6H_9\text{-}OOH + C_6H_9\cdot$

Formation of 2-cyclohexen-one:

$C_6H_9\text{-}OO\cdot + C_6H_9\text{-}OOH \rightarrow C_6H_9\text{-}OOH + C_6H_8\cdot\text{-}OOH$

$C_6H_8\cdot\text{-}OOH \rightarrow C_6H_8{=}O + \cdot OH$

Cleavage of cyclohexenyl hydroperoxide:

$C_6H_9\text{-}OOH \rightarrow C_6H_9\text{-}O\cdot + \cdot OH$

Formation of 2-cyclohexen-ol:

$C_6H_9\text{-}O\cdot + C_6H_{10} \rightarrow C_6H_9OH + C_6H_9\cdot$

Peroxy condensation:

$2\ C_6H_9\text{-}OO\cdot \rightarrow C_6H_8{=}O + C_6H_9OH + O_2$

Such mechanism can be closely described by a kinetic model developed for this system using Mathcad. Extended reaction mechanism and the kinetic model can be found in Appendix 19.

Thus, this study shows that at low temperatures sub-2 nm particles are not able to catalyse hydrogen abstraction from the cyclohexene and metallic Au particles larger than 2 nm are the active sites associated with the observed catalytic activity. Such a size effect is opposite to that discovered for oxidation reactions where O_2 activation is involved, *e.g.* styrene oxidation, for which either sub-2 nm particles[135, 177] or large, positively charged particles[136] were suggested as the active sites.

In summary, the relationship between the size of supported gold nanoparticles and their activity in solvent-free aerobic oxidation of cyclohexene has been established by employing gradually changing catalysts. Phosphine-stabilized gold clusters and phosphine-free Au particles smaller than 2 nm were shown to be inactive in this reaction, and catalytic activity appeared only upon formation of sufficient number of metallic particles larger than 2 nm. Further increase in Au particle size results in gradual decrease in catalytic activity, which correlates with the reduction of the Au surface area. The size-dependency observed in this study is in agreement with the suggested mechanism of substrate activation through the abstraction of hydrogen catalysed by metallic gold nanoparticles.

3.3 Catalysis by supported *vs.* unsupported Au species

When heterogeneous catalysts are employed in the liquid-phase reactions it is important to check if catalysis is truly heterogeneous. In some cases the observed catalytic activity is due to the active species that have been leached into solution from the catalyst support.

Table 3.5. Recyclability of $0.5Au_9$/Aerosil and gold loading after each cycle.

Cycle N	CyH conversion, %	Au loading in $0.5Au_9$/Aerosil after cycle by AAS, wt%
0	-	0.44
1	46	0.38
2	45	0.36

Catalyst recyclability studies showed that catalysts mostly retain their activity during the subsequent catalytic cycles (Table 3.5). Gold content in $0.5Au_9$/Aerosil was monitored using AAS after each catalytic cycle. Data on Au loading in a broad scope of other Au catalysts as a function of catalytic cycle is shown in Table 3.6. The study showed that the gold content gradually decreased during recyclability studies, indicating partial gold leaching during catalytic tests. The drop of gold content was the most significant after the first catalytic cycle and it became less evident during the subsequent cycles. Because a small portion of gold leached into reaction mixture during the catalytic tests, it was important to establish whether the observed catalytic activity was due to homogeneous or heterogeneous gold species. Catalysts retained most of their activity during the recyclability tests, which may indicate that the observed catalytic activity is mostly due to Au species supported on SiO_2.

Another way to establish whether the observed catalytic activity is truly heterogeneous or it is due to the active species that were leached into reaction solution is so-called hot filtration test. Sheldon and co-workers suggested a method to establish whether the catalysis

is truly heterogeneous in their paper on stability of chromium-substituted aluminophosphates in the liquid-phase oxidations.[181] The essence of this method is in the hot filtration of a catalyst at a point when approximately 50 % maximum conversion of the substrate has been achieved. After that the reaction filtrate is placed under reaction conditions. Continuation of substrate conversion into products indicates that the observed catalysis is due to the homogeneous species that leached into solution, whereas the absence of any further conversion indicates truly heterogeneous catalysis. It is important to perform filtration at the temperature of reaction (*i.e.* hot filtration), because cooling of the reaction mixture could cause re-adsorption of leached species onto support, which could lead to the distortion of the test results.

The catalytic reaction was stopped after *ca.* 50 % of maximum achievable conversion was reached, and catalyst was quickly filtered off using 0.2 μm filter. The reaction mixture was not allowed to cool down in order to avoid re-adsorption of leached Au species on SiO_2 support. Filtrate was placed into the clean flask and placed under the reaction conditions (Figure 3.20).

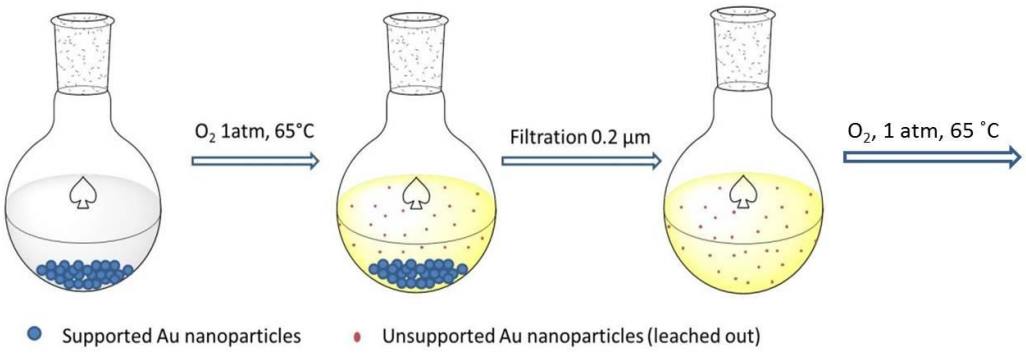

Figure 3.20. Illustration of the steps during hot filtration test

Hot filtration test, performed in our conditions, showed that in all cases cyclohexene conversion continued after the catalyst was removed (Figure 3.21), which, in principle, should indicate homogeneous nature of catalysis. However, cyclohexenyl hydroperoxide is known to catalyse cyclohexene autoxidation,[178] therefore hot filtration methodology is not

suitable for distinguishing heterogeneous and homogeneous catalysis in this case, because cyclohexenyl hydroperoxide formed during the first stage of the test would autocatalyse cyclohexene oxidation after the catalyst is removed.

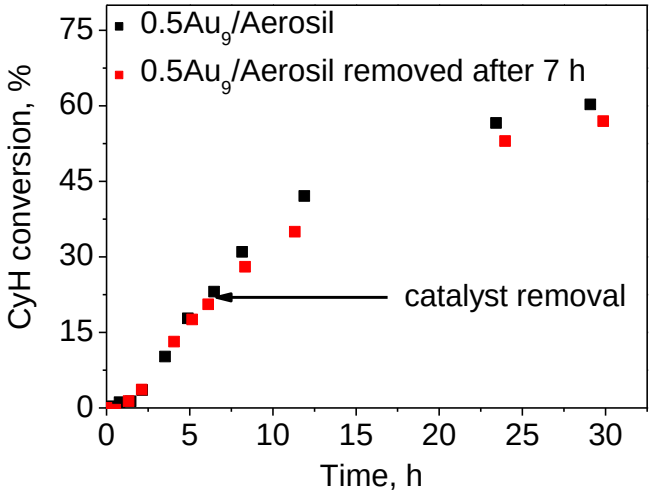

Figure 3.21. Cyclohexene oxidation in the presence of $0.5Au_9$/Aerosil (black) and $0.5Au_9$/Aerosil removed by hot filtration after 7 hours of reaction (red).

To confirm that leached Au species are inactive we performed several tests, where Au leaching occurs, but the formation of cyclohexenyl hydroperoxide is suppressed. In the first test (Figure 3.22), the reaction was conducted for 6 hours at 65 ˚C under argon atmosphere. In this case, gold leached into the reaction mixture, but oxidation products did not form due to the absence of oxygen. After 6 hours the reaction was stopped and catalyst was removed by filtration through 0.2 μm filter. The presence of gold leachate in the filtrate was confirmed using ICP-MS (*ca.* 1 ppm). No cyclohexene conversion was observed in the filtrate after it was subjected to the reaction conditions at 65 ˚C under 1 atm of O_2 for 16 hours.

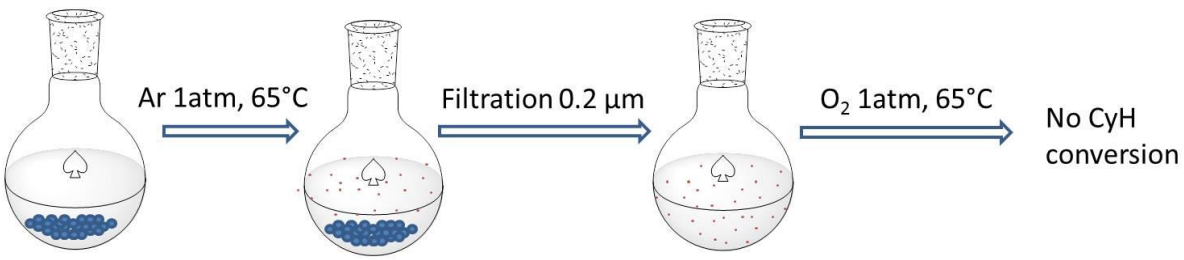

Figure 3.22. Filtration test performed under argon atmosphere.

In the second test, the formation of cyclohexenyl hydroperoxide was suppressed by the addition of n-hexane. Briefly, 50 μL of cyclohexene was mixed with 2 mL of n-hexane and the mixture was subjected to the reaction conditions. After 6 hours the liquid phase was separated from the heterogeneous catalyst by hot filtration, added to 5 mL of cyclohexene and the final mixture was subjected to the reaction conditions. No cyclohexene conversion was observed in that case. However, the catalyst which was isolated in the second stage of the test converted 11 % of cyclohexene in the mixture of 5 mL of cyclohexene and 2 mL of n-hexane.

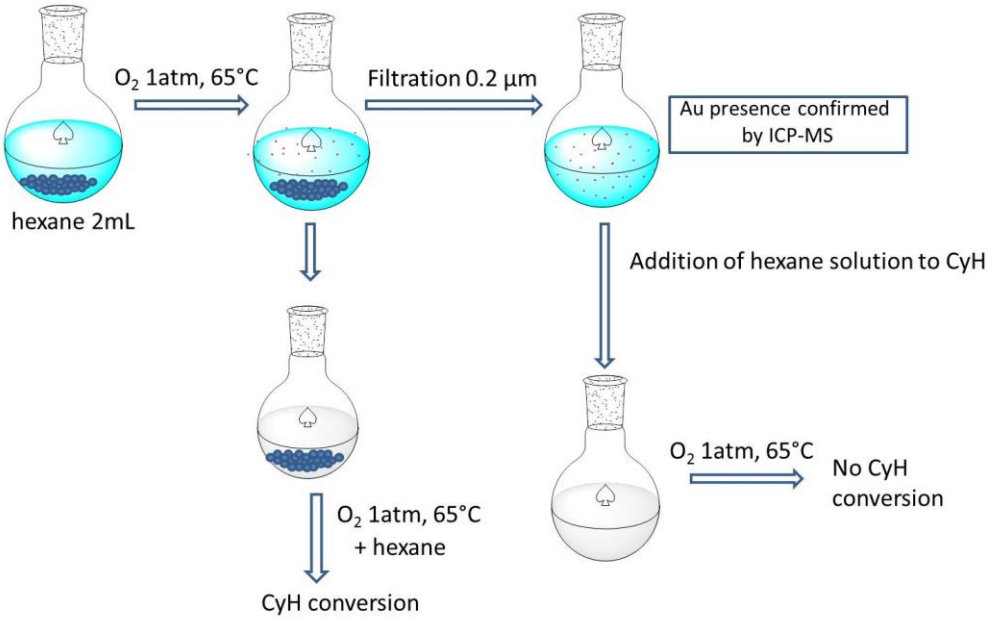

Figure 3.23. Filtration test performed with the addition of n-hexane.

In summary, the combination of recyclability studies with the simultaneous monitoring of the gold loading by AAS and various hot filtration tests showed that the activity observed in cyclohexene oxidation in the presence of supported Au catalysts is predominantly due to supported Au species. Such a result is in agreement with the fact that unsupported gold species tend to quickly form bulk agglomerates at elevated temperatures and precipitate. Since, as was shown earlier, activity is proportional to the total surface area, the contribution of leached Au to the total activity is negligible. The experiments also showed that the

standard hot filtration test is not suitable when there is a significant contribution from an autocatalytic pathway.

3.4 Study of cluster aggregation during cyclohexene oxidation

It is important to understand the behaviour of nanoparticles under the conditions of catalytic reactions in order to successfully design catalysts with desired properties. Many catalytic studies involving metal nanoparticles ignore the fact that the particles can undergo significant changes after being placed under harsh conditions of a catalytic reaction. The aim of this section was to understand the mechanisms of Au cluster agglomeration, to establish whether there is an effect of catalyst gold loading and the nature of the Au cluster and support on aggregation and reveal the relationship between gold leaching and agglomeration. Table 3.6 summarizes characterisation data (AAS and TEM) obtained for various catalysts before and after aerobic oxidation of cyclohexene.

Cluster agglomeration during cyclohexene oxidation was studied using Aerosil and WO_3 supported Au_9 and Au_{101} clusters. In all cases intact supported Au_9 clusters were not visible on TEM micrographs, indicating that Au_9 clusters mostly retain their size upon deposition onto both SiO_2 and WO_3. Au_{101} particles did not change in size when they were deposited onto Aerosil with a total Au loading of 0.1 wt%, but slightly increased to 2.0 ± 0.6 nm when the loading was increased up to 0.5 % (Table 3.6, entries 12). In the case of WO_3 support, the size of Au_{101} nanoparticles increased to 2.3 nm upon cluster immobilization for all studied Au loadings, presumably because of the low surface area of WO_3 (< 20 m^2/g) which caused particle aggregation upon deposition (Table 3.6, entries 1, 4).

As was shown earlier, both types of clusters agglomerated during the catalytic cyclohexene oxidation to form larger *ca.* 5 – 10 nm particles (Table 3.6, entries labelled by [a]). However, during subsequent catalytic cycles the size of the particles changed only slightly, which indicates that Au nanoparticles with the sizes 5 – 10 nm are mostly stable under the studied reaction conditions (Table 3.6, entries [b] and [c]).

Table 3.6. Au loadings and Au particle size distribution for various catalysts.

N	Catalyst	Au loading by AAS, %	Particle size by TEM, nm	
			mean ± s.e.[e]	s.d.[e]
1	$0.5Au_{101}/WO_3$	0.52	2.2 ± 0.1	0.7
2	$0.5Au_{101}/WO_3$[a]	0.47	5.1 ± 0.3	2.1
3	$0.5Au_{101}/WO_3$[b]	0.47	5.4 ± 0.2	1.8
4	$0.1Au_{101}/WO_3$	0.097	2.3 ± 0.1	0.5
5	$0.1Au_{101}/WO_3$[a]	0.070	4.4 ± 0.2	1.6
6	$0.3Au_9/WO_3$	0.31	<1[d]	-
7	$0.3Au_9/WO_3$[a]	0.28	5.1 ± 0.1	1.5
8	$0.3Au_9/WO_3$[b]	0.28	5.8 ± 0.3	2.1
9	$0.3Au_9/WO_3$[c]	0.28	6.1 ± 0.2	2.0
10	$0.1Au_9/WO_3$	0.093	<1[d]	-
11	$0.1Au_9/WO_3$[a]	0.087	7.9 ± 0.3	2.2
12	$0.5Au_{101}$/Aerosil	0.44	2.0 ± 0.1	0.6
13	$0.5Au_{101}$/Aerosil[a]	0.29	5.1 ± 0.2	2.0
14	$0.1Au_{101}$/Aerosil	0.12	1.6 ± 0.1	0.4
15	$0.1Au_{101}$/Aerosil[a]	0.068	4.9 ± 0.2	1.5
16	$0.5Au_9$/Aerosil	0.44	<1[d]	-
17	$0.5Au_9$/Aerosil[a]	0.38	5.4 ± 0.1	1.35
18	$0.5Au_9$/Aerosil[b]	0.36	n.d.	n.d.
19	$0.3Au_9$/Aerosil	0.27	<1[d]	-
20	$0.3Au_9$/Aerosil[a]	0.20	6.3 ± 0.2	1.6
21	$0.3Au_9$/Aerosil[b]	0.20	6.9 ± 0.2	2.3
22	$0.1Au_9$/Aerosil	0.098	<1[d]	-
23	$0.1Au_9$/Aerosil[a]	0.073	9.6 ± 0.6	3.9

[a]Recovered after the 1st catalytic cycle. [b]Recovered after the 2nd catalytic cycle. [c]Recovered after the 3rd catalytic cycle. [d]No gold particles were detected using bright-field TEM. [e]s.e. and s.d. stand for Standard error of the mean and standard deviation for the distribution, respectively.

Interestingly, opposite trends in the size of the formed particles as a function of catalyst loading were observed for Au_9 and Au_{101}. For both types of supports, the size of the particles formed from Au_{101} during the reaction *increased* with the *increase* in Au_{101} loading (Table 3.6, entries 1-2 and 4-5; 12-13 and 14-15). For example, 4.4 nm Au particles formed from Au_{101} on WO_3 when the gold loading was 0.1 %, while 5.1 nm particles formed from Au_{101} in Au_{101}/WO_3 with 0.5 % gold loading (Figure 3.24). The average size of particles formed from Au_{101} on Aerosil increased from 4.9 nm to 5.1 nm for 0.1 % and 0.5 % catalysts, respectively (Figure 3.25).

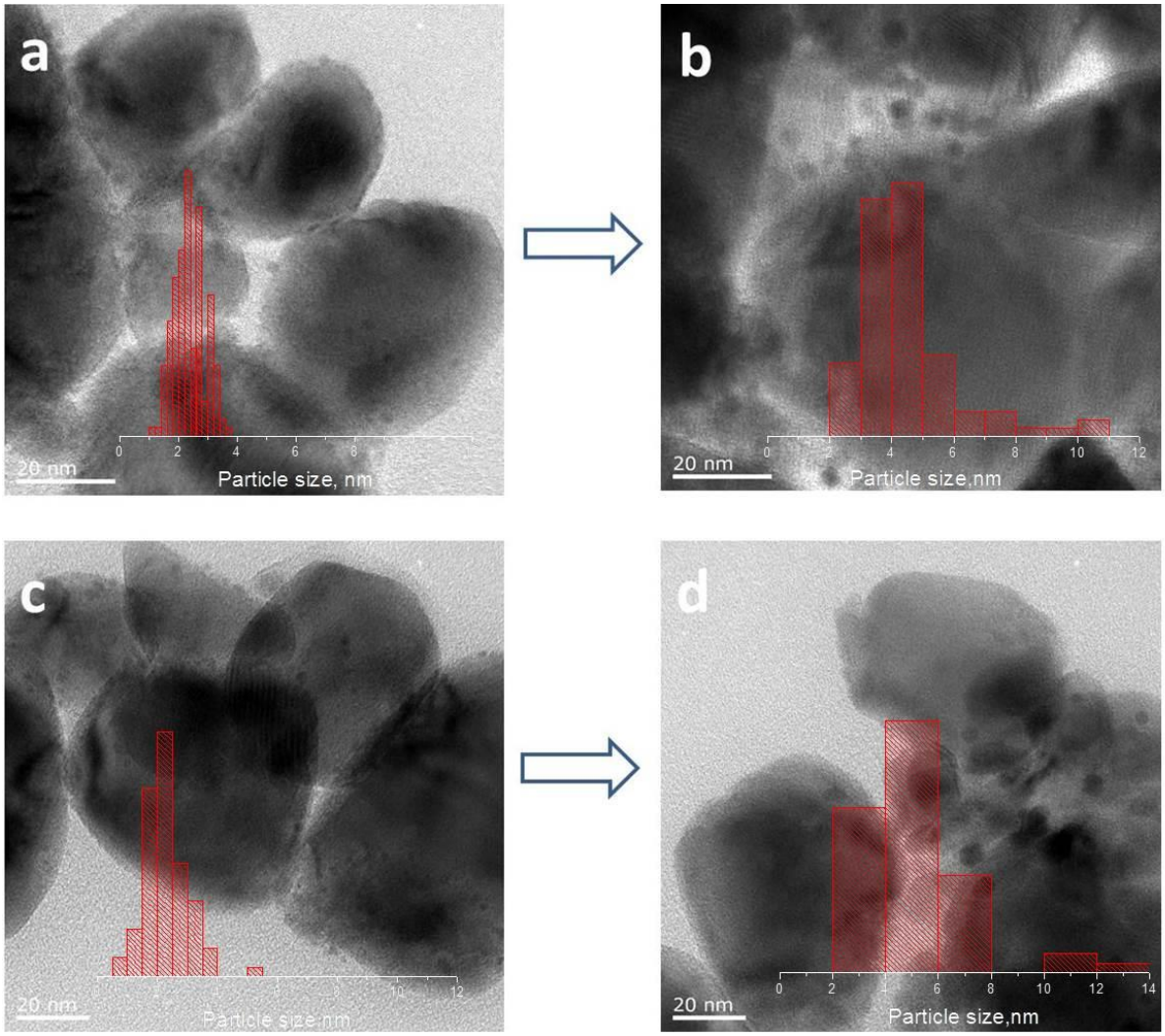

Figure 3.24. Representative TEM images of a) as made $0.1Au_{101}/WO_3$ (2.3 ± 0.1 nm) b) $0.1Au_{101}/WO_3$ after reaction (4.4 ± 0.2 nm) c) as made $0.5Au_{101}/WO_3$ (2.2 ± 0.1 nm) and d) $0.5Au_{101}/WO_3$ after reaction (5.1 ± 0.3 nm).

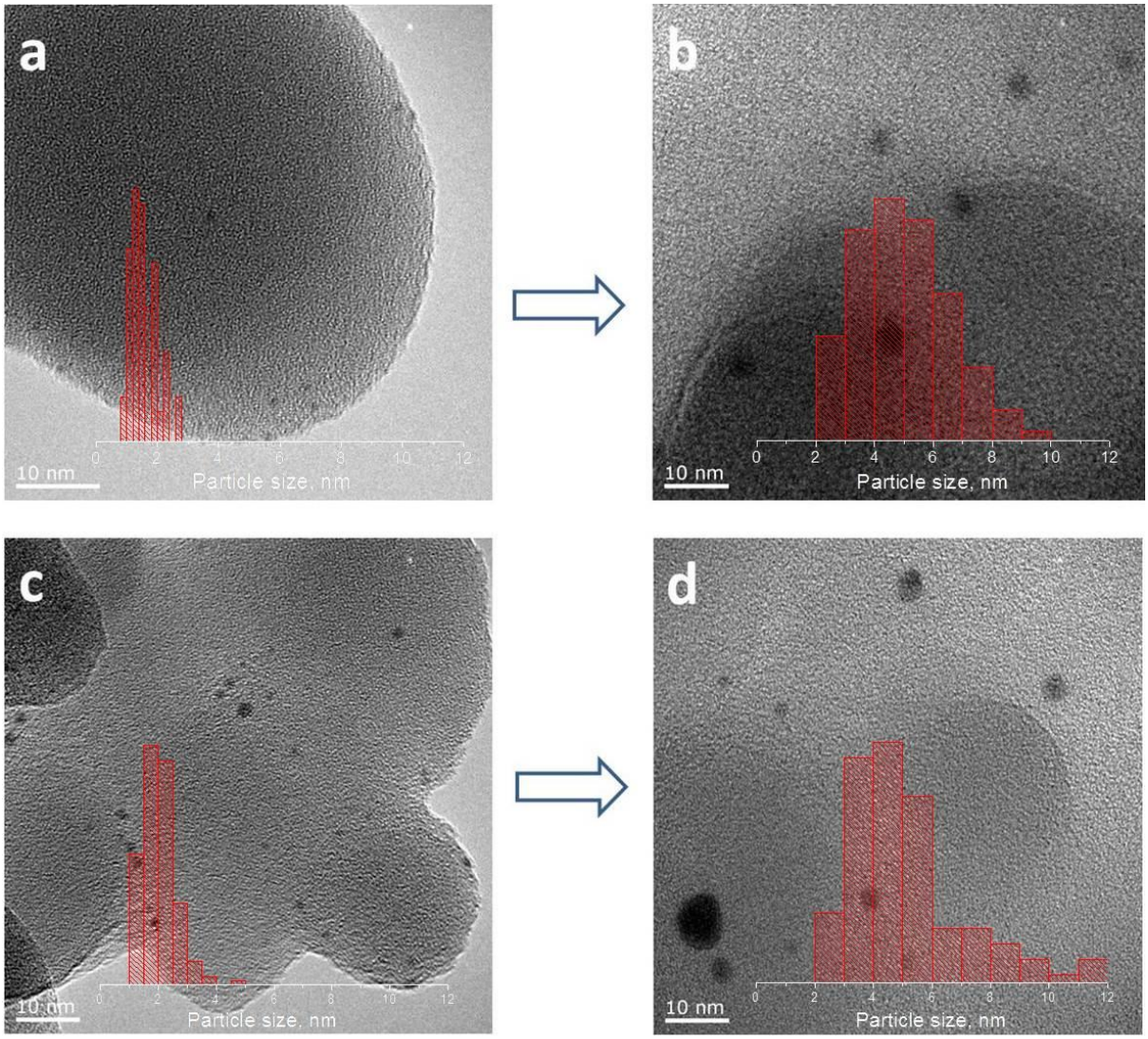

Figure 3.25. Representative TEM images of a) as made $0.1Au_{101}$/Aerosil (1.6 ± 0.1 nm) b) $0.1Au_{101}$/Aerosil after reaction (4.9 ± 0.2 nm) c) as made $0.5Au_{101}$/Aerosil (2.0 ± 0.1 nm) and d) $0.5Au_{101}$/Aerosil after reaction (5.1 ± 0.2 nm).

The opposite trend was observed in the case of supported the Au_9-cluster: for both types of supports *lower* Au_9 loadings resulted in *larger* nanoparticles formed during the reaction (Table 3.6, entries 6-7 and 10-11; 16-17 and 19-20 and 22-23). Figure 3.26 illustrates gold nanoparticles formed in Au_9/Aerosil during cyclohexene oxidation. Particles with a mean gold core diameter of 9.6 nm formed in $0.1Au_9$/Aerosil, while 6.3 and 5.4 nm particles formed in $0.3Au_9$/Aerosil and $0.5Au_9$/Aerosil, respectively.

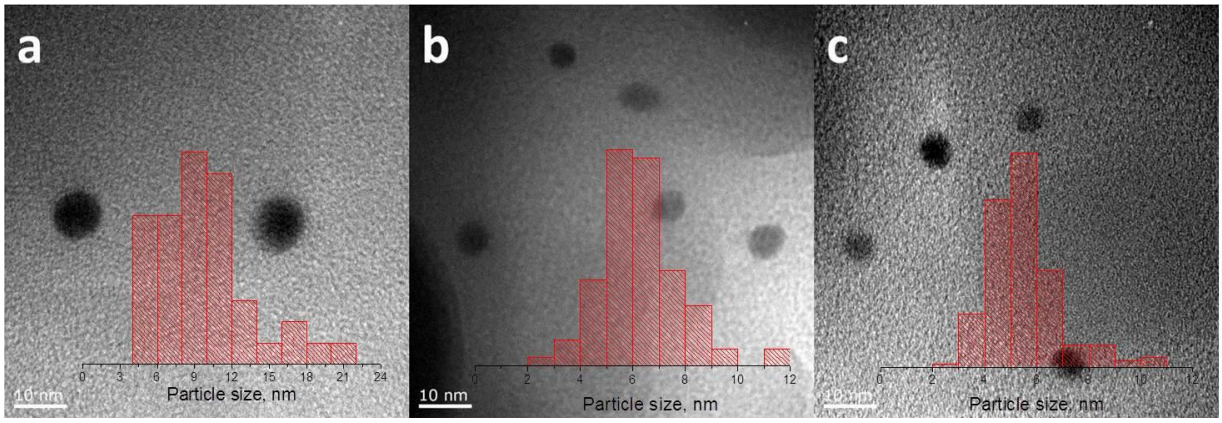

Figure 3.26. Representative TEM micrographs of Au_9/Aerosil recovered after cyclohexene oxidation with Au loadings of a) 0.1 % b) 0.3 % and c) 0.5 %.

Such different behaviour of the two clusters could suggest different sintering mechanisms – Au_9 clusters act as a feedstock for nanoparticle growth, while Au_{101} clusters collide and agglomerate through surface diffusion. It could be suggested that agglomeration of Au_9 clusters occurs similarly to the process of crystal growth, in which lower concentration of precursor leads to the creation of smaller amount of nucleation sites which produce bigger crystals. Thus, at high gold loadings the majority of Au_9 clusters rapidly sinter into relatively stable nanoparticles with mean diameters of 4-6 nm; while at lower surface concentrations clusters initially form fewer nanoparticles that act as nucleation sites that keep growing, consuming the remaining Au_9 clusters to eventually form 8-10 nm particles. As agglomeration of Au_{101} proceeds mainly *via* cluster collision, smaller Au particles form at the lower surface concentration of clusters.

Another observation based on the results summarised in Table 3.6 is that most of the leaching occurs on the first catalytic cycle, while it is almost undetectable in the subsequent cycles (see entries labelled by [a], [b] and [c]). It can be suggested that larger agglomerated nanoparticles of gold are less prone to leaching compared to smaller gold entities, probably due to poor mobility of large Au particles. Additionally, non-aggregated PPh_3-stabilised clusters could be partially soluble in the reaction mixture, which results in their leaching into

the reaction mixture. This suggestion correlates with the fact that in most cases the percentage of leached gold during the first catalytic cycle decreases with the increase in Au loading (Table 3.7): a higher surface density of gold clusters accelerates their agglomeration and hence fewer non-sintered clusters have time to leach into solution.

Table 3.7. Percentage of gold, leached into reaction during the first catalytic cycle

Catalyst	Percentage of leached gold *cf.* total initial loading, %
$0.5Au_{101}$/Aerosil	34
$0.1Au_{101}$/Aerosil	43
$0.5Au_{9}$/Aerosil	13.6
$0.3Au_{9}$/Aerosil	26
$0.1Au_{9}$/Aerosil	26
$0.5Au_{101}/WO_3$	9.6
$0.1Au_{101}/WO_3$	28
$0.3Au_{9}/WO_3$	9.7
$0.1Au_{9}/WO_3$	6.4

In summary, thorough investigation of Au particle size and catalyst Au loading of Au_9 and Au_{101} supported on SiO_2 and WO_3 with different total Au loadings before and after catalytic reaction (up to 3 cycles) was performed. The following conclusions could be drawn on the basis of the results of the study: 1) Larger particles of 5-10 nm, formed during the first catalytic cycle from Au_{101} and Au_9 clusters, are mostly stable during the following catalytic cycles with minimal increase in size; 2) It could be suggested that different mechanisms of particle aggregation as a function of the gold loading are realised for Au_{101} and Au_9. However, further investigations are required to confirm/disprove this hypothesis; 3) Larger aggregated Au particles are less prone to leaching into reaction solution compared to smaller as deposited clusters.

3.5 Effect of the catalytic support

Comparative study of support effect on the activity and selectivity of Au nanoparticles derived from Au_9 was done using various oxides: TiO_2, SiO_2 (Aerosil) and WO_3. Catalysts with different loadings were prepared and studied in the solvent-free aerobic oxidation of cyclohexene.

Table 3.8. Cyclohexene oxidation in the presence of Au nanoparticles supported on various oxides.

Catalyst	Conversion, %	Selectivity, %			
		Cy-oxide	Cy-ol	Cy-one	CyOOH
TiO_2	2	-	-	-	-
SiO_2	2	-	-	-	-
WO_3	9	33	30	4	32
$0.5Au_9/TiO_2$	2	-	-	-	-
$0.5Au_{101}/TiO_2$	2	-	-	-	-
$0.5Au_{101}/WO_3$	50	**26**	18	17	19
$0.1Au_{101}/WO_3$	36	**35**	23	12	18
$0.3Au_9/WO_3$	50	**27**	20	16	17
$0.1Au_9/WO_3$	33	**34**	24	11	21
$0.3Au_9/SiO_2$	43	7	12	19	**51**
$0.1Au_9/SiO_2$	25	5	7	12	**68**

Conditions: 65°C, 16 h, solvent-free cyclohexene, 5 mL, O_2 (~1 atm), 50 mg catalyst, 0.2 M n-decane as internal standard.

The nature of the oxide support was shown to significantly affect the activity and selectivity of supported Au nanoparticles (Table 3.8). TiO_2-supported catalysts were not active in cyclohexene oxidation under the studied conditions with the cyclohexene conversion close to that in the absence of any catalyst (*ca.* 2 %). WO_3 and SiO_2 supported catalysts showed similar activities for the catalysts derived from same clusters and with the same Au loading, however the product distributions were different for the two supports with cyclohexenyl hydroperoxide and cyclohexene oxide being the main products for SiO_2- and WO_3-supported catalysts, respectively (Table 3.8).

TEM and DR UV-vis studies (Figure 3.27) of catalysts recovered after reaction showed that particles of similar size and morphology form on both supports during the reaction. The turface plasmon band at *ca.* 520 nm in DR UV-vis spectra had similar position and shape for both SiO_2- and WO_3-supported catalysts, and TEM study showed that particles of *ca.* 5-6 nm formed during the first catalytic cycle with a slight increase in size over the subsequent cycles (Table 3.6).

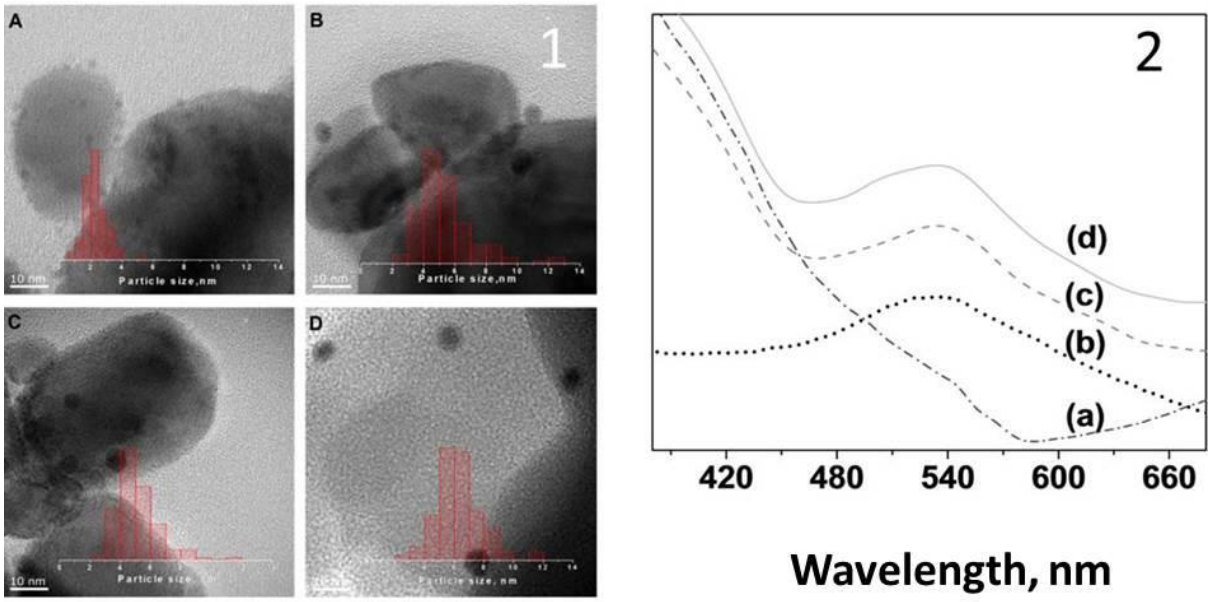

Figure 3.27. 1) Representative TEM images and Au particle size distributions of (A) as made $0.5Au_{101}/WO_3$ and catalysts recovered after the 1st catalytic cycle: (B) $0.5Au_{101}/WO_3$ (C) $0.3Au_9/WO_3$ (D) $0.3Au_9/SiO_2$. 2) DR UV-Vis spectra of (a) as made $0.3Au_9/WO_3$ and catalysts recovered after 1st catalytic cycle: (b) $0.3Au_9/SiO_2$, (c) $0.3Au_9/WO_3$ and (d) $0.5Au_{101}/WO_3$.

Moreover, a kinetic study of cyclohexene oxidation in the presence of $0.3Au_9/SiO_2$ and $0.3Au_9/WO_3$ showed that the two catalysts have close TOF values, calculated from the initial reaction rates (Figure 3.28). Both types of catalysts had similar cyclohexenyl hydroperoxide accumulation stage during first 6 hours, however, in the case of WO_3-supported catalyst, the amount of hydroperoxide started decreasing after 8 hours with epoxide becoming a major product.

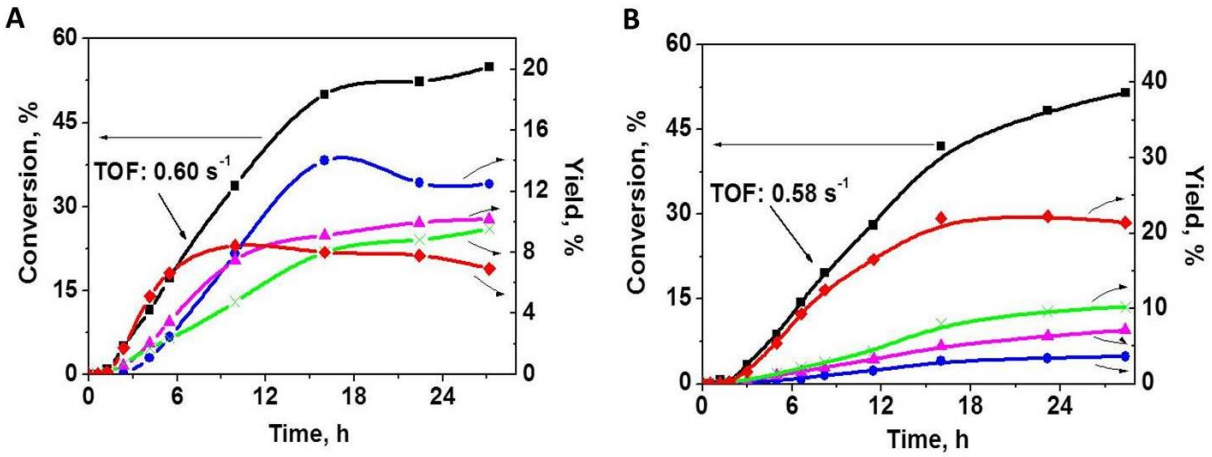

Figure 3.28. Reaction profile of cyclohexene oxidation catalysed by $0.3Au_9/WO_3$ (A) and $0.3Au_9/SiO_2$ (B). Conversion (left ordinate) of cyclohexene (black). Yield (right ordinate) of cyclohexenyl hydroperoxide (red), cyclohexene oxide (blue), 2-cylohexen-1-one (green), 2-cyclohexen-1-ol (magenta).

Based on these observations it can be suggested that gold particles catalyse the formation of cyclohexenyl hydroperoxide from cyclohexene (reaction I, Figure 3.29), while WO_3 catalyses reaction between cyclohexenyl hydroperoxide and cyclohexene, producing cyclohexene oxide and 2-cyclohexen-1-ol (reaction II, Figure 3.29).

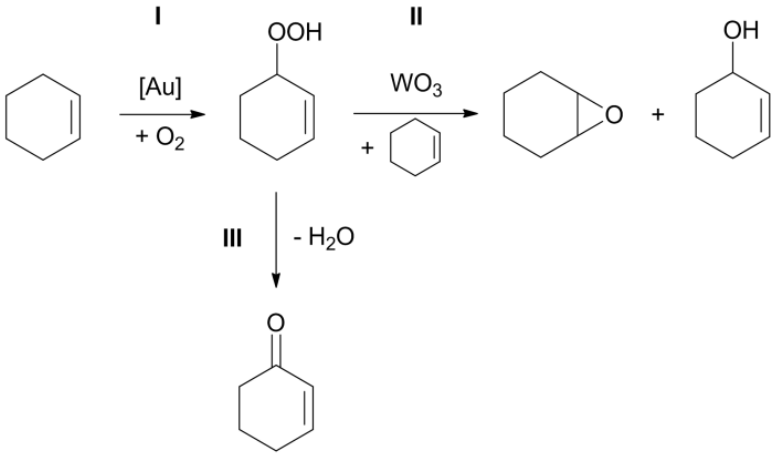

Figure 3.29. Proposed mechanism of cyclohexene oxidation in the presence of SiO_2 and WO_3 supported Au catalysts.

In order to test this hypothesis, a series of experiments in which pure WO_3 powder was mixed with $0.3Au_9/SiO_2$ at different ratios (Table 3.9) was conducted. Pure WO_3 gives 9 % cyclohexene conversion (entry 1) with selectivity towards epoxide reaching 33 %, while the selectivity towards epoxide with $0.3Au_9/SiO_2$ is only 7 % at cyclohexene conversion of 43 %. The addition of as little as 2 wt% of WO_3 (1 mg) to $0.3Au_9/SiO_2$ changed the product distribution of the reaction, with selectivity towards cyclohexene oxide increasing from 7 % to 26 % (Table 3.9, entries 4 and 5). With 10 wt% of WO_3 (5 mg) the distribution of products is almost identical to that observed for $0.3Au_9/WO_3$ (see Table 3.8). Even though the selectivity towards epoxide is slightly lower than in the case of pure WO_3, the yield of epoxide is significantly higher in the presence of gold because gold addition allows higher conversion.

Table 3.9. Effect of co-catalyst addition on product selectivity in cyclohexene oxidation.

	Mixture of catalysts	Ratio, mg:mg	Selectivity, %				Conversion, %
			Cy-oxide	Cy-ol	Cy-one	CyOOH	
1	$0.3Au_9/SiO_2$ + pure WO_3	0:50	**33**	30	4	32	9
2		5:45	**32**	28	8	20	25
3		45:5	**27**	19	13	21	48
4		49:1	**26**	17	13	26	46
5		50:0	**7**	12	19	51	43
6	$0.3Au_9/SiO_2$ + MIL-101	0:50	1	24	**59**	4	11
7		5:45	2	21	**47**	15	13
8		25:25	4	18	**42**	27	20
9		45:5	5	11	**41**	28	38
10		50:0	7	12	**19**	51	43

It is possible, however, that in this series of experiments some gold species leach from silica-based catalyst and adsorb on tungsten oxide, thus forming a catalytic system with high selectivity towards cyclohexene oxide. To exclude this possibility we performed a reaction with the silica-based catalyst, hot filtered the reaction mixture into a vial containing tungsten oxide (5 mg), which was then collected by centrifugation. Inasmuch as potentially

impregnated WO_3 was inactive in the conversion of the fresh cyclohexene, we conclude that the observed change of selectivity upon addition of WO_3 to Au/SiO_2 catalyst should be attributed to properties of pure WO_3 acting as a co-catalyst rather than to a synergistic effect between WO_3 support and Au nanoparticles. Soluble complexes of tungsten are long known for their ability to activate peroxides through the formation of electrophilic peroxo-complexes that are highly active and selective in olefin epoxidation.[182] The activation of peroxides (H_2O_2[183] and alkyl hydroperoxides[184]) by WO_3 for highly selective epoxidation of olefins[185] was discovered recently. Thus the ability of WO_3 to activate cyclohexenyl hydroperoxide found in this study is in accordance with the previous reports.

We also found that the use of different co-catalyst can shift selectivity of Au/SiO_2 towards allylic oxidation products. Metal-organic framework MIL-101, which was recently reported as a catalyst for allylic oxidation of cyclohexene with molecular oxygen, with 2-cyclohexen-1-one being the main product, was chosen as such a co-catalyst.[186, 187] Results of catalytic testing of the mixture consisting of pure MOF and $0.3Au_9/SiO_2$ in different ratios show the effect of altering the selectivity of reaction similar to the one found for WO_3, but with 2-cyclohexen-1-one becoming the main product (Table 3.9). Reaction catalysed by the mixture of MIL-101:$0.3Au_9/SiO_2$ (5:45, mg:mg) gives a maximum 2-cyclohexen-1-one yield of 16%, which is twice the yield we have been able to achieve with the pure MOF.

In conclusion, it was found that cyclohexenyl hydroperoxide, the formation of which is catalysed by Au nanoparticles, can be converted to other products in the presence of different heterogeneous co-catalysts. Cyclohexene oxide is formed *via* reaction of cyclohexenyl hydroperoxide with cyclohexene catalysed by WO_3, either present as a support or introduced to the reaction as a co-catalyst physically admixed with silica-supported gold catalyst. Selectivity towards formation of 2-cyclohexen-1-one is shifted by using MIL-101 as a co-catalyst for Au/SiO_2. It was shown that support does not alter the selectivity of the supported

Au nanoparticles, but rather acts as a co-catalyst, changing the overall selectivity of the reaction by catalysing consecutive reactions of primary products of cyclohexene oxidation. It has been shown that careful choice of support or co-catalyst for supported gold nanoparticles allows tuning of the selectivity of cyclohexene oxidation towards either cyclohexene oxide or 2-cyclohexen-1-one, allowing higher yield of a selected product under solvent-free conditions without addition of radical initiator and using oxygen as the only oxidant.

Chapter 4. Gold-catalysed one-pot synthesis of imines from alcohols and amines

Recently, heterogeneously catalysed one-pot synthesis of imines from alcohols and amines attracted wide interest among researchers.[188-194] Imines are an important class of chemicals, used as intermediates in organic synthesis and as pharmaceuticals, agricultural chemicals, *etc*.[195] Traditional ways of imine synthesis include reactions between aldehydes/ketones and amines, oxidative dimerization of primary amines, oxidation of secondary amines and direct reaction between nitroarenes and alcohols.[196-201] In this respect, synthesis of imines from alcohols and amines is the most attractive way due to the availability of the broad range of starting reagents and possibility of constructing N-alkyl imines with various alkyl substituents, as opposed to imine synthesis by dimerization of primary amines.

Different homogeneous catalytic systems were developed for the synthesis of imines, however, such systems suffer from difficult catalyst separation and recycling and the high cost of ligands.[200, 202, 203] Manganese octahedral molecular sieves,[204] palladium nanoparticles supported on boehmite nanofibers[192] and copper-based catalysts[205] were reported as heterogeneous catalysts for imine synthesis from alcohols and amines. Recently, Fan and co-workers demonstrated that 3.6 nm gold nanoparticles supported on hydroxyapatite (HAP) are efficient catalysts in the direct synthesis of imines from alcohols and amines.[190] The study

showed that Au/HAP was more active than nanoparticles of other metals (Pd, Ru) supported on HAP. Additionally, Au-based catalysts prepared using other types of supports, such as ceria, iron oxide, titania and carbon, were significantly less active. The Au/HAP catalyst was shown to be active for the broad range of substrates, both alcohols and amines. Riisager *et al.* demonstrated that Au/TiO_2 commercial catalysts with Au particles of 4 – 8 nm were active in the imine synthesis from alcohols and amines under very mild conditions: 1 atm O_2 and room temperature.[206] Addition of base was required for the catalytic activity. Kobayashi and co-authors found that alloying gold with palladium allows achieving better selectivity towards imine compared to pure Au nanoparticles. No change in selectivity was observed when gold was alloyed with platinum, and it dropped when supported Au-Co nanoparticles were employed.[194]

In this part of the study, the activity of catalysts derived from various phosphine-stabilised gold and mixed-metal clusters was studied in one-pot synthesis of imines from alcohols and amines. Since activity of the gold nanoparticles strongly depends on the preparation method,[9] we were interested whether there is an effect of cluster precursor on the activity of the gold catalyst. Previous catalytic studies show that employing alloy nanoparticles is often beneficial in terms of activity/selectivity and catalyst durability (see Introduction), and thus this work was aimed at finding out whether the addition of a single atom of another metal (Pd, Pt) to gold would affect its activity and selectivity. Finally, we were interested in how catalyst pre-treatments influence activity of gold particles. Catalyst treatments could increase catalytic activity of supported nanoparticles because of the removal of stabilising ligands and enhancement of metal-support interaction.

With regards to the necessity of the removal of stabilizing ligands from nanoparticles, the literature data are rather inconsistent. For example, Jin and co-workers observed catalytic activity of various thiolate-protected SiO_2 and HAP-supported gold clusters in alcohol

oxidation by O_2, which dropped when catalyst was pre-calcined at 200 ˚C in order to remove ligands.[82] This drop in activity was explained by the agglomeration of unprotected clusters during reaction, which did not occur when clusters were covered with thiols. Unfortunately, TEM or any other data, confirming the intactness of clusters after reaction, have not been demonstrated by the authors. The majority of studies, however, claim that capping agent/ligand removal is necessary because of inaccessibility of metal surface to reagents[167, 207, 208] and poor metal-support interaction.[209] For example, various studies reported Au catalyst deactivation upon addition of capping ligands (thiols, PVP) or inactivity of capped Au nanoparticles due to hindrance of active sites or perturbation of electronic properties of gold.[144, 210-212]

In this study 6 different gold and mixed metal clusters (Au_6, Au_8, Au_9, Au_{101}, $PdAu_6$ and $PtAu_8$) have been synthesized and supported on TiO_2 (total gold loading was 0.5 % in all cases). The activity of as made catalysts and same catalysts pre-treated by calcination (denoted as calcined), ozonolysis (denoted as O_3) and ozonolysis, followed by washing with toluene at 100 ˚C (denoted as O_3+W) was studied in the one-pot synthesis of N-benzylidene-benzylamine (N-BBA) from benzyl alcohol and benzylamine, used as a model reaction (Figure 4.1).

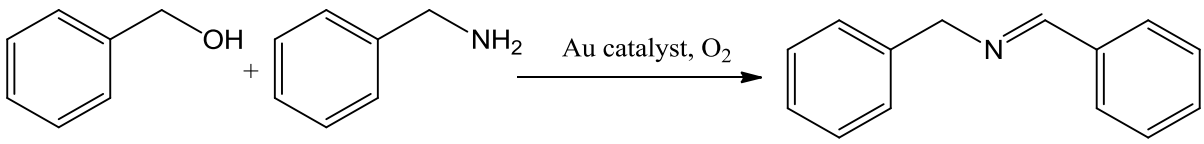

Figure 4.1. Direct synthesis of N-benzylidene benzylamine from benzyl alcohol and benzyl amine.

4.1 Optimization of conditions for one-pot synthesis of N-benzylidene benzylamine

Optimization of the reaction conditions was performed using $0.5Au_{101}/TiO_2$ catalyst. All reactions were performed in the absence of light, because TiO_2 has been recently shown to catalyse oxidation of both alcohols and amines in the presence of UV-visible light.[196, 213, 214]

Table 4.1 shows the results of optimization of reaction conditions. No imine formation and substrates conversion was observed in the absence of a catalyst, and only 3 % of N-BBA formed in the presence of pure TiO_2 powder used as a support. Addition of base was essential for the catalytic activity of supported gold and mixed-metal catalysts as no N-BBA formed in the absence of base. When reaction was performed in the presence of different types of base, *i.e.* K_2CO_3, $NaOCH_3$, KOH, KOtBu, the yield of N-BBA was 84 %, 54 %, 39 % and 11 %, respectively.

Table 4.1. Optimization of the reaction conditions.

	Catalyst	Base	Yield of N-BBA, %
1	-	K_2CO_3	-
2	TiO_2	K_2CO_3	3
3	Au_{101}/TiO_2	-	-
4	Au_{101}/TiO_2	K_2CO_3	84
5	Au_{101}/TiO_2	$NaOCH_3$	54
6	Au_{101}/TiO_2	KOH	39
7	Au_{101}/TiO_2	KOtBu	11
8	Au_{101}/TiO_2[a]	K_2CO_3	10

Conditions: benzyl alcohol 0.1 mmol, benzyl amine 0.1 mmol, base 0.2 mmol, toluene 3 mL, 19 h, catalyst 50 mg, 100 ˚C, O_2 1 atm, 10 mg of biphenyl (internal standard). [a] no alcohol added

The reaction was also performed without addition of alcohol, because gold catalysts were previously shown to be active in the aerobic oxidation of amines to imines.[199] Under conditions of this study only 10 % of imine formed after 19 h when alcohol was not added to the reaction mixture, which indicated that the majority of N-BBA formed *via* condensation of amine and aldehyde – a product of alcohol oxidation (*vide infra*). The optimised conditions,

i.e. benzyl alcohol (0.1 mmol) and benzyl amine (0.1 mmol), K_2CO_3 (0.2 mmol), 3 mL of toluene (solvent), 50 mg of catalyst, 100 ˚C, 1 atm O_2, were further employed for catalyst screening.

Table 4.2 shows the results of direct imine formation from alcohol and amine in the presence of various as made (*i.e.* no catalyst pre-treatment was employed) catalysts derived from different clusters.

Table 4.2. Catalytic activity of various gold-containing TiO_2-supported clusters in the one-pot synthesis of N-benzylidene benzylamine (N-BBA).

Catalyst	Yield of N-BBA, %	Yield of Benzyl aldehyde, %
$0.5Au_6/TiO_2$	10	-
$0.5Au_8/TiO_2$	21	-
$0.5Au_9/TiO_2$	20	-
$0.5Au_{101}/TiO_2$	84	7
$0.5PdAu_6/TiO_2$	62	21
$0.5PtAu_8/TiO_2$	15	-

Conditions: Benzyl Alcohol 0.1 mmol, Benzyl Amine 0.1 mmol, K_2CO_3 0.2 mmol, toluene 3 mL, 19 h, catalyst 50 mg, 100 ˚C, O_2 1 atm, 10 mg of biphenyl (internal standard).

The study showed that the least active catalyst was $0.5Au_6/TiO_2$ – only 10 % of N-BBA formed after 19 h. Additionally, it was found that significant cluster leaching into the reaction media occurred, which was evidenced by the brown colour of the reaction mixture and colourless catalyst powder (*vide infra* DR UV-vis data). Catalysts derived from Au_8, Au_9 and Au_{101} clusters showed N-BBA yields of 21 %, 20 % and 84 %, respectively. When Au_{101}/TiO_2 was employed 7 % of benzaldehyde was also detected as a minor product. Only 15% of N-BBA was produced in the presence of $PtAu_8/TiO_2$, which indicated that the addition of one Pt atom (with respect to Au_8) or substitution of one Au atom with Pt (with respect to Au_9) slightly decreased catalyst activity. However, addition of Pd (compared to Au_6) led to significant activity enhancement: yields of N-BBA and benzaldehyde in the presence of $PdAu_6/TiO_2$ were 62 % and 21 %, respectively.

4.2 Catalyst treatment study

In this study as made catalysts were treated in three different ways and studied using DR UV-vis spectroscopy and Synchrotron-based XPS. The treatments were performed in order to remove the triphenylphosphine shell, which can potentially prevent/decrease the activity of gold. The three treatments were a) calcination at the temperature of cluster decomposition, b) ozonolysis and c) ozonolysis, followed by washing in toluene at 100 ˚C.

Heat treatment (calcination) is probably the most common way to remove stabilising ligand shell or activate the catalyst.[89, 215-217] All clusters were analysed using TGA to find out at which conditions clusters would lose most of organic ligands (Figure 3.3, Figure 3.4, Appendices 14 – 17). Table 4.3 summarizes TGA results for different clusters.

Table 4.3. Conditions of cluster calcination in air.

Cluster	Temperature, ˚C	Time, min	Weight loss (calculated), %	Weight loss (experimental), %
Au_6	300	120	56	39
Au_8	230	120	55	56
Au_9	230	120	52	52
Au_{101}	230	120	22	26
$PdAu_6$	250	120	56	52
$PtAu_8$	230	120	52	45

Typically, temperature was quickly raised to the desired one with the heating rate of 10 ˚C/ min, and clusters were kept under the target temperature for at least 2 h. Most of clusters readily lose most of their organic ligands upon calcination at 230 ˚C for 2 h, except Au_6 and $PdAu_6$: Au_6 lost only 39 % of weight during calcination at as high as 300 ˚C, while the temperature of 250 ˚C was required to decompose ligand shell of $PdAu_6$. The conditions summarised in Table 4.3 were further employed to calcine supported clusters.

Ozonolysis, or catalyst treatment with O_3, is another way to remove ligands from cluster cores.[208, 218] Menard *et al.* studied the removal of thiol and phosphine ligands from TiO_2-supported $Au_{13}[PPh_3]_4[S(CH_2)_{11}CH_3]_4$ cluster by treating it in ozone flow at room

temperature.[208] By performing high-angle annular dark-field scanning transmission electron microscopy (HAADF STEM) studies the authors demonstrated that such treatment increased particle size only slightly – from 0.8 nm to 1.2 nm, while catalyst calcination at 400 ˚C for two hours resulted in the formation of 2.7 nm Au particles. When ozone-treated catalyst was further calcined at 400 ˚C, particles of 1.5 nm formed. The authors explained such little Au aggregation in ozone-treated catalyst upon high temperature calcination by strong metal-support interaction, established during ozonolysis, that suppresses migration of nanoparticles at the support surface. Complete removal of phosphorous and sulphur during ozonolysis was confirmed by XPS and Extended X-ray absorption fine structure (EXAFS) studies. Also, both techniques indicated the presence of Au^0 gold in ozone-treated catalyst, *i.e.* no oxidized gold species were detected, even though ozone is a strong oxidant capable, in principle, of oxidizing gold according to the standard electrode potentials.[32] In this study, catalysts were treated with ozone-flow for 1 h at room temperature.

The last treatment used in this study was a combination of ozonolysis (1 h, room temperature) and washing in toluene at 100 ˚C for 1 h (denoted as O_3+W). Catalyst washing in toluene was applied in order to remove potential ligand residues left after treatment with ozone.

DR UV-vis and XPS studies of pre-treated Au catalysts

Catalyst powders were characterized using diffuse-reflectance UV-visible spectroscopy in order to estimate the degree of Au particle aggregation during catalytic reaction or treatment. TEM is one of a few reliable techniques for establishing size of nanoparticles, however, in this study usefulness of TEM proved to be limited for several reasons:

1) The contrast of small unaggregated gold clusters on TiO_2 was very low (much worse than in the case of Au/SiO_2) on the ordinary 200 kV bright-field TEM, which is available at

the University of Canterbury, and thus we were unable to detect small unaggregated supported Au particles using TEM.

2) For this study we used TiO_2 P25 as a support with mean particle diameter of *ca.* 50 nm, meaning that there were also particles much smaller and larger than 50 nm. Typically metal nanoparticles are distinguished from support on the basis of contrast, *i.e.* metal particles appear much darker on TEM micrographs compared to the support particles. However, it was very difficult to distinguish medium-large Au nanoparticles from small P25 particles, because when piled up on top of larger P25 particles they looked very similar to each other. Additional difficulty arose from the very low gold loading employed in this study (0.5 wt%). Performing high-resolution TEM and extracting lattice space parameters of multiple nanoparticles to determine their nature and then obtain size distribution of Au particles would have made this technique expensive and time-consuming.

Thus, we used DR UV-vis spectroscopy to estimate the extent of Au particle aggregation upon treatments, bearing in mind, however, that this technique can only be used for very rough qualitative analysis. In the future, HAADF STEM and EXAFS studies would be necessary. When interpreting the results of DR UV-vis study, both the position of surface plasmon resonance band (SPR band) and its intensity were analysed to estimate the extent of gold aggregation – shift of SPR band position to higher wavelengths and the higher intensity of SPR band are both indicative of larger gold nanoparticles.[102, 103, 215]

Figure 4.2 illustrates DR UV-vis spectra of Au_9/TiO_2 catalysts: as made, treated in three different ways and as made catalyst that was recovered after imine synthesis reaction (denoted as AR). DR UV-vis spectrum of as made Au_9/TiO_2 possessed a small shoulder at *ca.* 450 nm which originates from supported intact Au_9 clusters, while no SPR band is observed in this case. After calcination at 230 ˚C a strong surface plasmon band at 540 nm appears, indicating strong particle agglomeration, whereas the band at 450 nm disappears indicating

removal of ligands. Ozone treated catalyst possessed SPR band at 540 nm as well, however, its intensity was significantly lower than that of the calcined catalyst. When ozone-treated catalyst was washed in toluene at 100 ˚C for 1 h the intensity of the SPR band slightly increased, indicating that particles had increased in size. Finally, as made catalyst recovered after the reaction possessed SPR band of high intensity, indicating strong gold aggregation during the reaction.

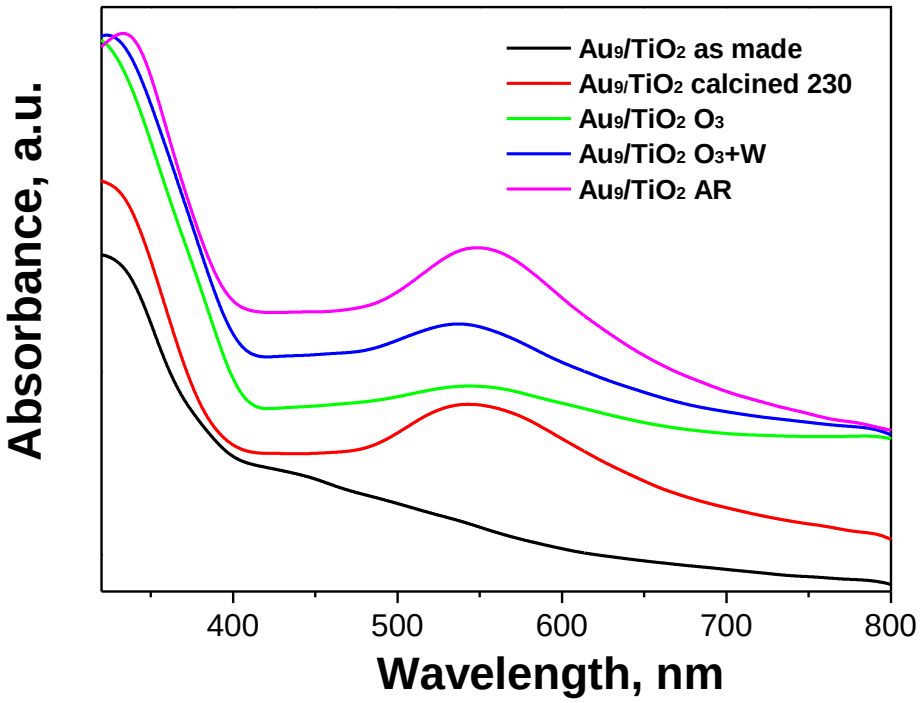

Figure 4.2. Diffuse-reflectance UV-vis spectra of $0.5Au_9/TiO_2$ before and after treatments/reaction.

The less intense SPR band of ozone-treated catalyst could indicate less pronounced aggregation upon this treatment compared to calcination. Additionally, we performed TEM study of a different ozone-treated catalyst - Au_9, supported on amorphous SiO_2 with surface area of *ca.* 80 m^2/g. The study showed that monodisperse particles of 2.3 ± 0.6 nm formed upon ozonolysis from Au_9 clusters (Figure 4.3). Considering that silica is an inert support, which is known to have a weak interaction with gold,[219] and the results of previous works involving ozone-treatment of supported clusters,[208] we could speculate that particles of at

least similar size are forming on TiO_2, which is known to have stronger interaction with the supported gold.[132]

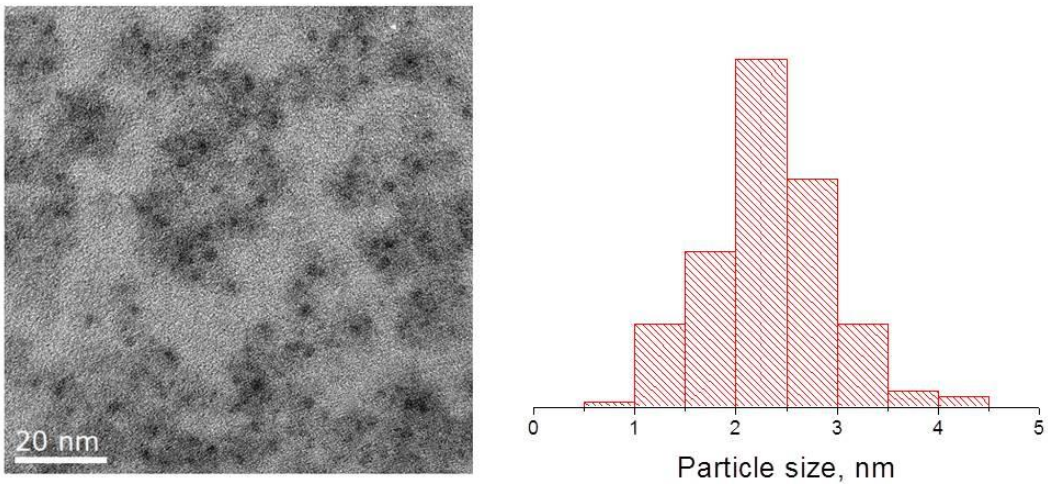

Figure 4.3. TEM micrograph of Au_9/SiO_2 after ozone treatment.

A Synchrotron-based XPS study, performed at the Australian Synchrotron, was used to monitor chemical state of gold and the presence of phosphines. Results of the XPS study for the pre-treated catalysts are summarized in Table 4.4.

Table 4.4. XPS $Au4f_{7/2}$ and $P2p_{3/2}$ data for various gold and mixed-metal clusters supported on TiO_2.

Catalyst	Au LBP[a]	Intensity Au LBP	Au HBP[a]	Intensity Au HBP	P LBP	Intensity P LBP	P HBP	Intensity P HBP
Au_9 am	83.7	778.3	85.0	4946.9	131.6	419.1	133.3	526.0
Au_9 O_3	83.6	5008.9	86.0	327.7	-	-	133.9	2170.1
Au_9 O_3+W	83.7	1130.6	-	-	-	-	133.9	2228.1
Au_6 am	83.4	410.5	85.1	8236.4	131.8	1135.8	133.2	738.7
Au_6 O_3	83.5	1937.4	85.0	379.7	-	-	133.5	5410.2
Au_6 O_3+W	83.7	980.6	85.1	1607.6	-	-	133.6	4968.9
Au_8 am	-	-	84.9	3042.3	131.8	577.3	133.4	160.2
Au_8 O_3	83.6	1023.3	-	-	-	-	134.0	2702.7
Au_8 O_3+W	83.7	682.4	84.9	2810.9	-	-	133.6	3668.2
Au_{101} am	83.8	9141.7	84.7	1504.2	-	-	-	-
Au_{101} O_3	83.6	1914.7	84.9	1281.3	-	-	133.6	473.8
Au_{101} O_3+W	83.7	2935.6	85.2	509.0	-	-	134.6	239.0
$PdAu_6$ am	83.8	9111.1	84.8	1305.6	-	-	131.3	200
$PdAu_6$ O_3	83.7	3786.1	85.7	1103.9	-	-	133.4	3357.3
$PdAu_6$ O_3+W	83.7	2309.4	-	-	-	-	133.5	2821.7
$PtAu_8$ am	83.8	1571.3	84.9	6021.7	131.6	820.6	133.1	188.9
$PtAu_8$ O_3	83.6	3167.7	85.5	274.9	-	-	133.8	3160.0
$PtAu_8$ O_3+W	83.7	881.1	84.9	2398.0	-	-	133.8	3322.1

LBP and HBP stand for low binding energy peak and high binding energy peak respectively.

XPS study of as made Au_9/TiO_2 catalysts showed the $Au4f_{7/2}$ signal at 85.0 eV originating from intact Au_9 cluster (Figure 4.4 and Table 4.4). After ozone treatment $Au4f_{7/2}$ signal is shifted towards lower binding energies (83.6 eV), thus indicating formation of Au^0 during ozonolysis, which correlates with the previously published results.[208] During subsequent washing in toluene no significant change in the peak position was observed. XPS study of the as made catalysts showed $P2p_{3/2}$ peak at 131.6 eV corresponding to the phosphorous of triphenylphosphine coordinated to the metal core of the Au_9 cluster. Interestingly, we observed strong P signal in both O_3 and O_3+W catalysts, which indicates that phosphine ligands are not completely removed from the catalyst by these treatments. $P2p_{3/2}$ binding energy of 133.9 eV indicates that phosphine remains on the TiO_2 surface in its oxidised form. The same result was previously observed for calcined Au_8, Au_9 and Au_{101} clusters supported on TiO_2.[220]

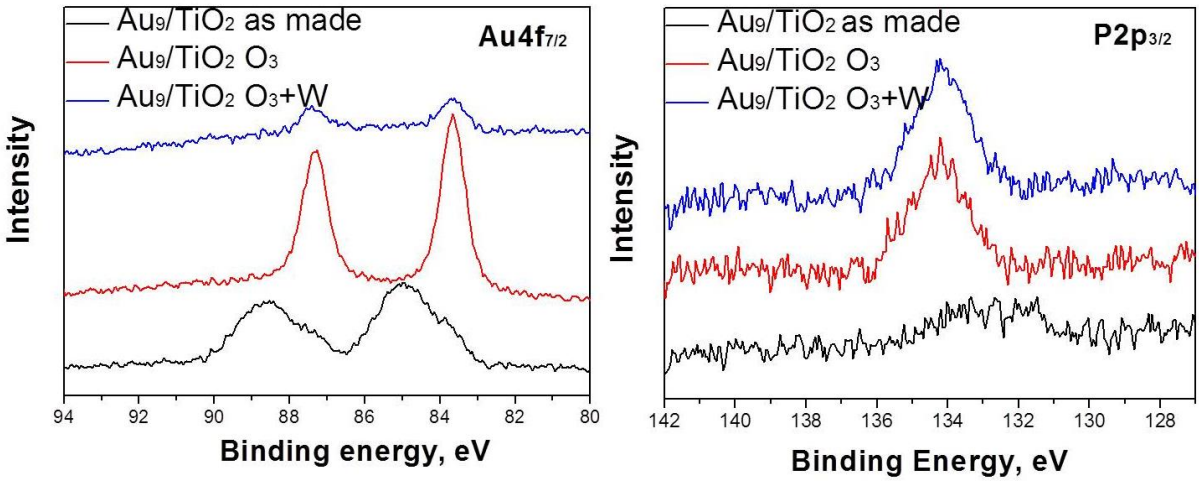

Figure 4.4. $Au4f_{7/2}$ and $P2p_{3/2}$ spectra of $0.5Au_9/TiO_2$ before and after treatments.

DR UV-vis spectrum of as made Au_6/TiO_2 possessed a band at 510 nm originating from the Au_6 cluster (Figure 4.5). As can be seen from the spectra, the cluster had leached from the as made Au_6/TiO_2 catalyst into reaction media during one-pot imine synthesis because no Au cluster/nanoparticle-related features were observed in the spectrum of the post-reaction catalyst. Thus, for Au_6 cluster catalyst pre-treatment is necessary in order to enhance metal-

support interaction and avoid gold leaching. A similar approach was previously used by Hutchings *et al.* to minimize metal leaching.[63] Calcination of Au_6/TiO_2 at 300 ˚C caused strong Au nanoparticle agglomeration, as evidenced by the broad SPR band with a shoulder at 600 nm. Similarly to Au_9/TiO_2, ozonolysis and ozonolysis with subsequent toluene wash treatments of Au_6/TiO_2 gave materials with relatively weak SPR bands.

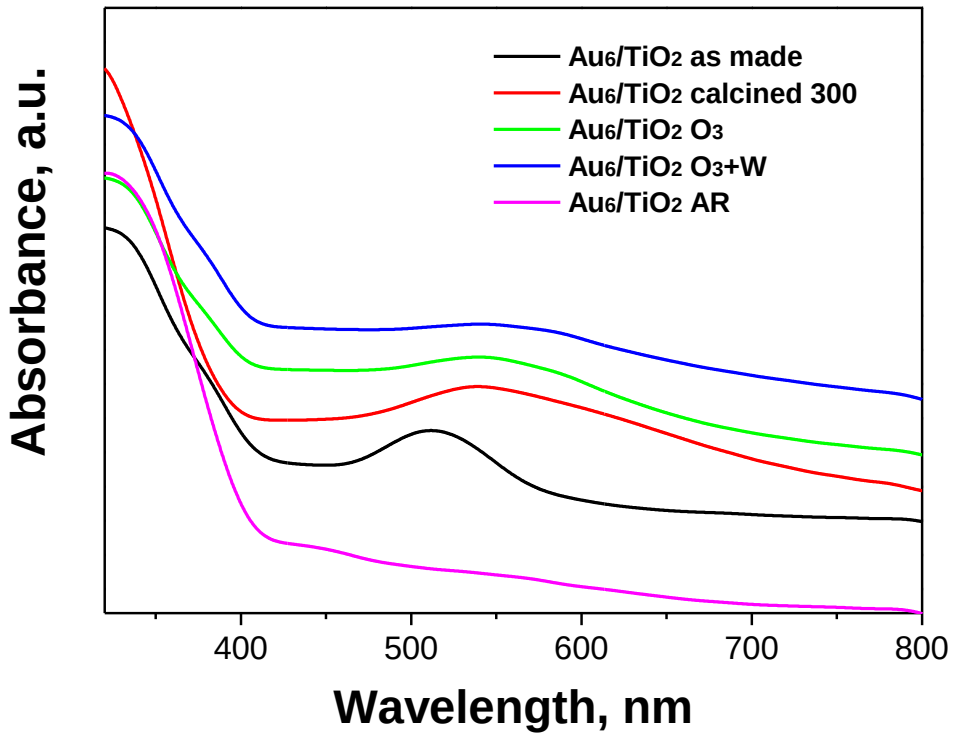

Figure 4.5. Diffuse-reflectance UV-vis spectra of $0.5Au_6/TiO_2$ before and after treatments/reaction.

XPS data of the Au_6/TiO_2 showed shift of $Au4f_{7/2}$ signal towards lower binding energies upon ozonolysis, indicating formation of Au^0 (Figure 4.6), similarly to Au_9/TiO_2 behaviour. However, in contrast to Au_9, wash in toluene leads to appearance of the higher binding energy $Au4f_{7/2}$ peak at 85.1 eV, which is most likely due to strong metal-support interaction and formation of flat raft-like nanoparticles induced by toluene wash.[208, 220] Similarly to the case of Au_9/TiO_2, phosphorous in its oxidised form was present on TiO_2 after ozone-treatments as indicated by the presence of a $P2p_{3/2}$ peak at 133.6 eV (Figure 4.6).

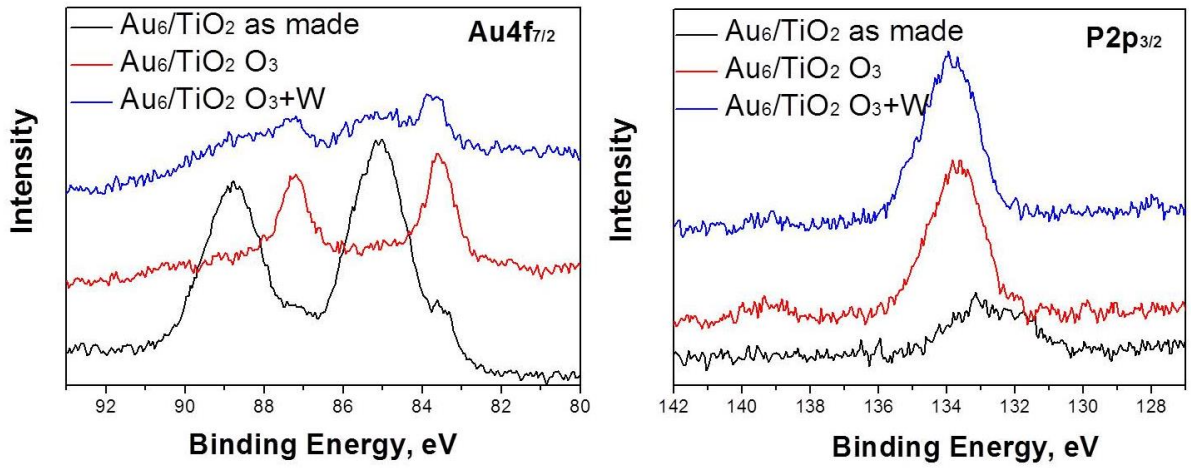

Figure 4.6. $Au4f_{7/2}$ and $P2p_{3/2}$ spectra of $0.5Au_6/TiO_2$ before and after treatments.

DR UV-vis spectra of Au_8/TiO_2 are shown in Figure 4.7. As in the case of Au_9/TiO_2, the spectra of both Au_8/TiO_2 calcined and Au_8/TiO_2 recovered after reaction possess strong SPR band at 540 nm, indicating strong Au particle aggregation, while the SPR bands of Au_8/TiO_2 O_3 and Au_8/TiO_2 O_3+W are significantly less intense.

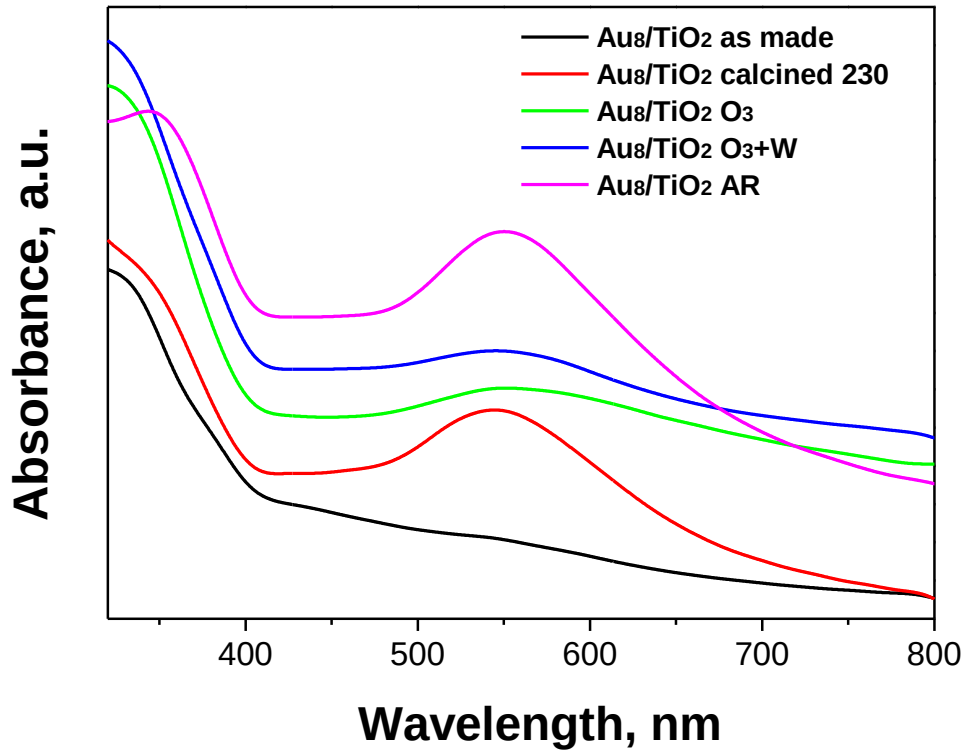

Figure 4.7. Diffuse-reflectance UV-vis spectra of $0.5Au_8/TiO_2$ before and after treatments/reaction.

XPS spectra of Au_8/TiO_2 catalysts are shown in Figure 4.8. The $Au4f_{7/2}$ peak which is positioned originally at 84.9 eV is shifted to 83.6 eV upon ozone treatment, indicating formation of Au^0 particles. Subsequent toluene wash of the ozone-treated catalyst induces stronger gold-support interaction and appearance of $Au4f_{7/2}$ peak at higher binding energy of 84.9 eV. Similarly to the above mentioned cases of Au_9- and Au_6-based systems, phosphorous is oxidised during ozone-treatment and remains on TiO_2.

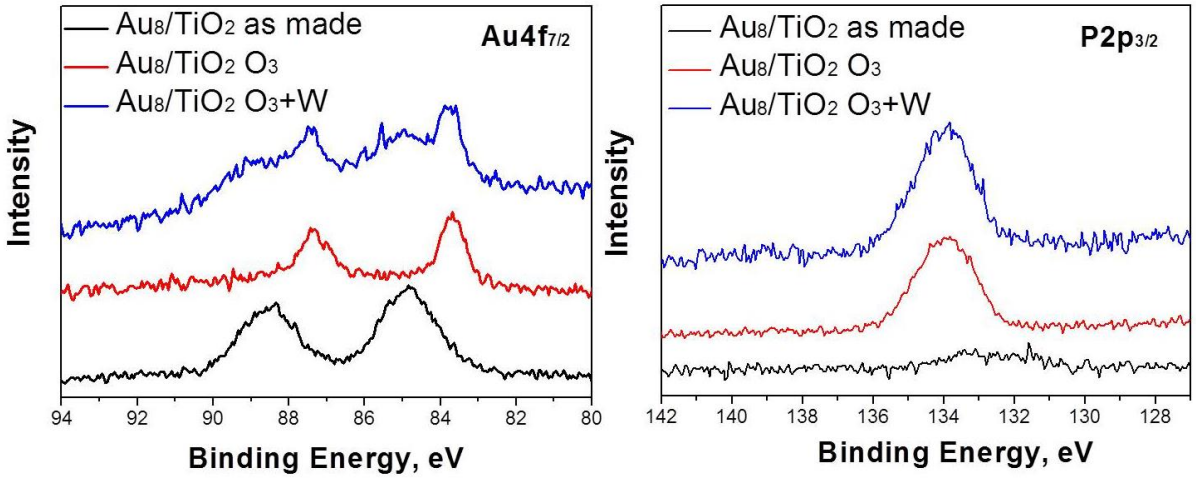

Figure 4.8. $Au4f_{7/2}$ and $P2p_{3/2}$ spectra of $0.5Au_8/TiO_2$ before and after treatments.

Results of DR UV-vis and XPS studies of Au_{101}/TiO_2 are shown in Figure 4.9 and Figure 4.10, respectively. In the studied catalyst series Au_{101} stands out from other clusters. First, the diameter of its core is larger compared to that of the other clusters (1.5 nm *vs.* 0.8-0.9 nm) and thus Au_{101} is at the interface between metallic and non-metallic Au states. Second, while other clusters exist as NO_3-salts, the anionic part of Au_{101} is Cl^-. The presence of Cl^- ions is believed to facilitate aggregation of gold nanoparticles.[221] Thus it is expected that Au_{101} might behave differently from other systems. As seen from Figure 4.9 calcination caused stronger aggregation compared to ozonolysis, as evidenced by the more intense SPR band of calcined Au_{101}/TiO_2. Relatively large particles formed during ozonolysis followed by washing in toluene, as evidenced by the increase of the intensity of SPR band compared to

Au_{101}/TiO_2 O_3. XPS study of catalysts derived from Au_{101} supported on TiO_2 showed that most of gold is in the metallic state even before treatments (Figure 4.10).

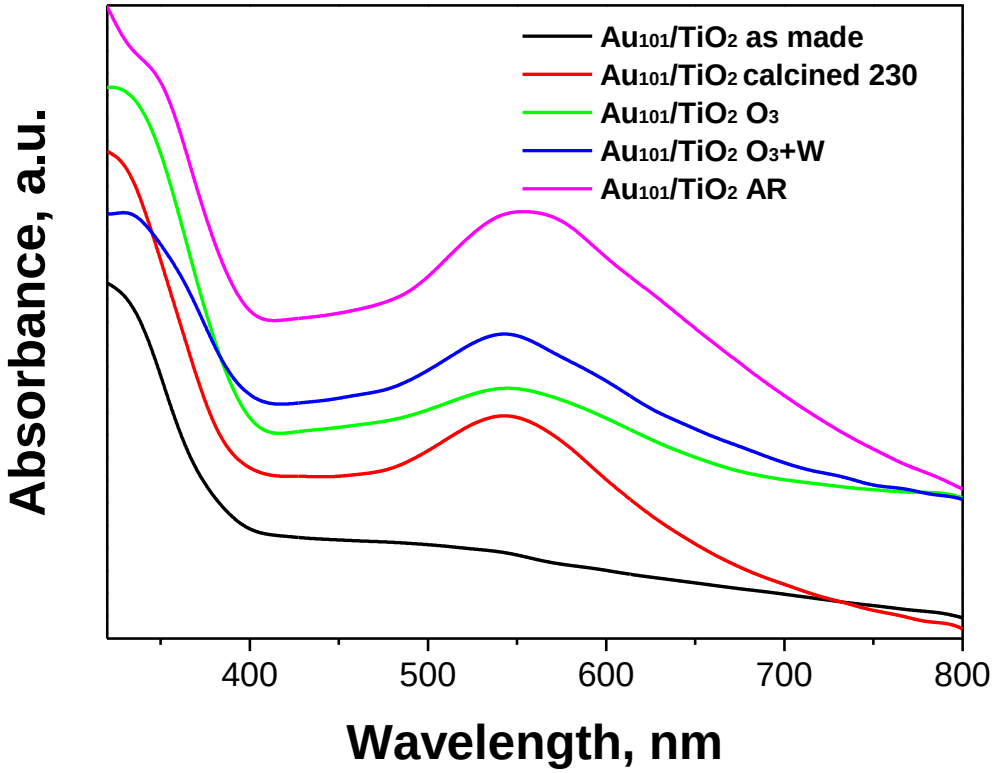

Figure 4.9. Diffuse-reflectance UV-vis spectra of $0.5Au_{101}/TiO_2$ before and after treatments/reaction.

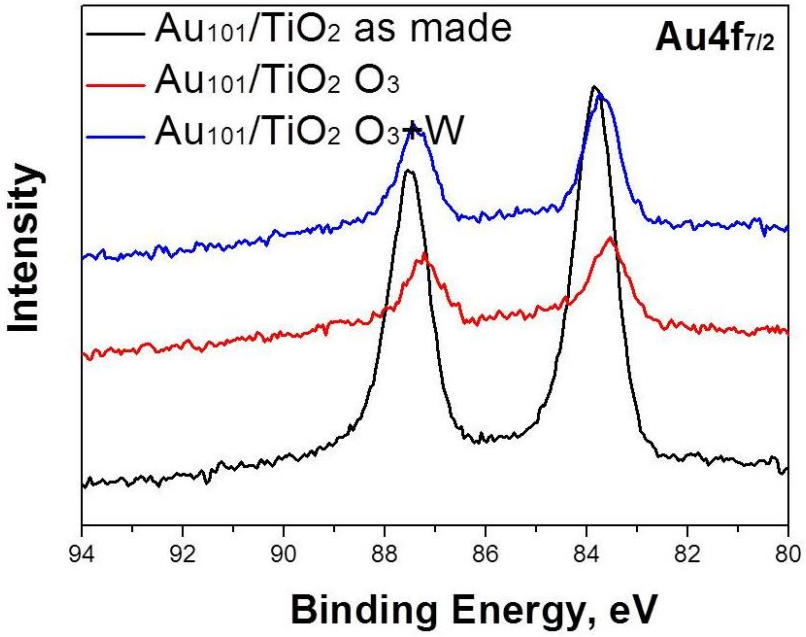

Figure 4.10. $Au4f_{7/2}$ spectra of $0.5Au_{101}/TiO_2$ before and after treatments.

Results of the DR UV-vis study of $PdAu_6/TiO_2$ catalysts are shown in Figure 4.11. Although the spectra of catalysts possess bands at *ca.* 530 - 540 nm, the bands are not as pronounced as these of pure gold catalysts. This is most likely due to the change in the electronic structure of Au upon addition of a Pd atom. Similar effects were previously observed for Au-Pd particles, where addition of a very small amount of Pd to Au particles (1:9) drastically changed absorption properties of the particles.[222, 223] However, the general trend of SPR band intensity in $PdAu_6/TiO_2$ as a function of treatment is similar to that for Au_6, Au_8 and Au_9-based catalysts: the intensity of SPR band of calcined catalyst is higher than that of ozone-treated samples.

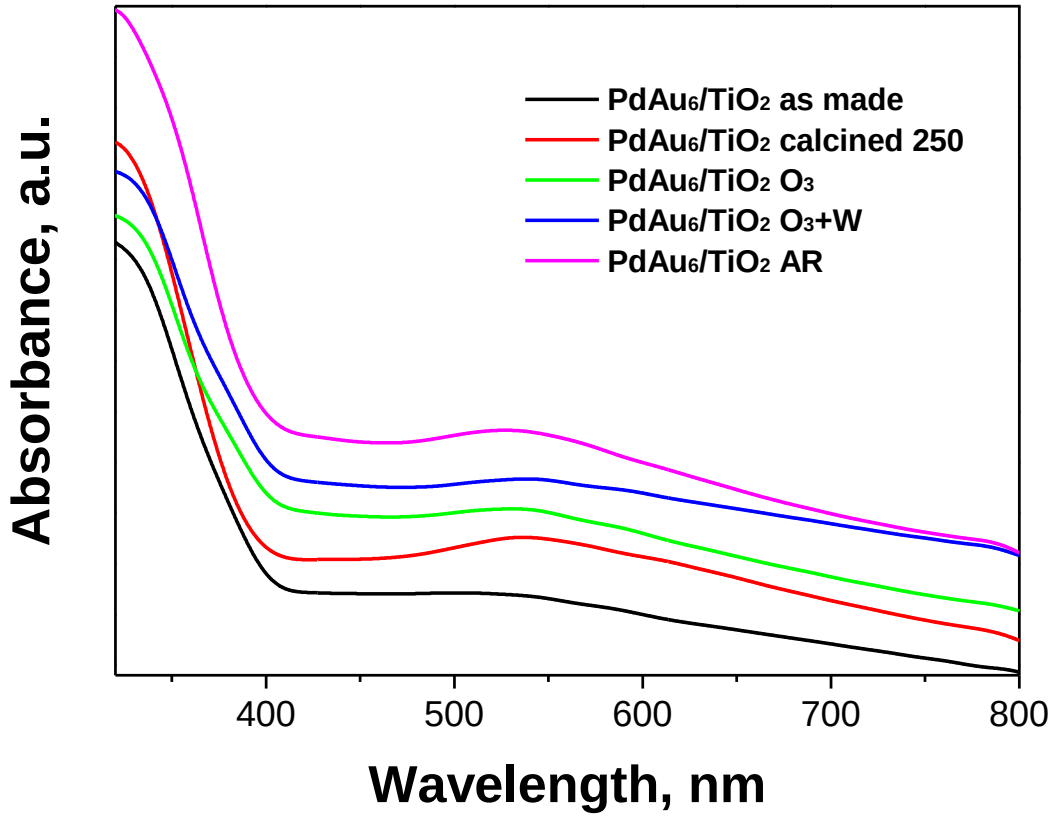

Figure 4.11. Diffuse-reflectance UV-vis spectra of $0.5PdAu_6/TiO_2$ before and after treatments.

XPS study of the as made $PdAu_6/TiO_2$ showed the $Au4f_{7/2}$ binding energy of 83.8 eV, a value very close to that of metallic gold. Such a shift of Au 4f peaks to lower binding energies upon addition of the Pd atom is in line with previously observed results for Pd-Au

nanoparticles[224-227] and it is believed to be due to the interaction and hybridization of $5d_{5/2}$ bands of gold with 4d states of Pd.[227] Upon ozonolysis the $Au4f_{7/2}$ peak of $PdAu_6/TiO_2$ shifts to lower binding energies (Figure 4.12), implying formation of metallic particles.

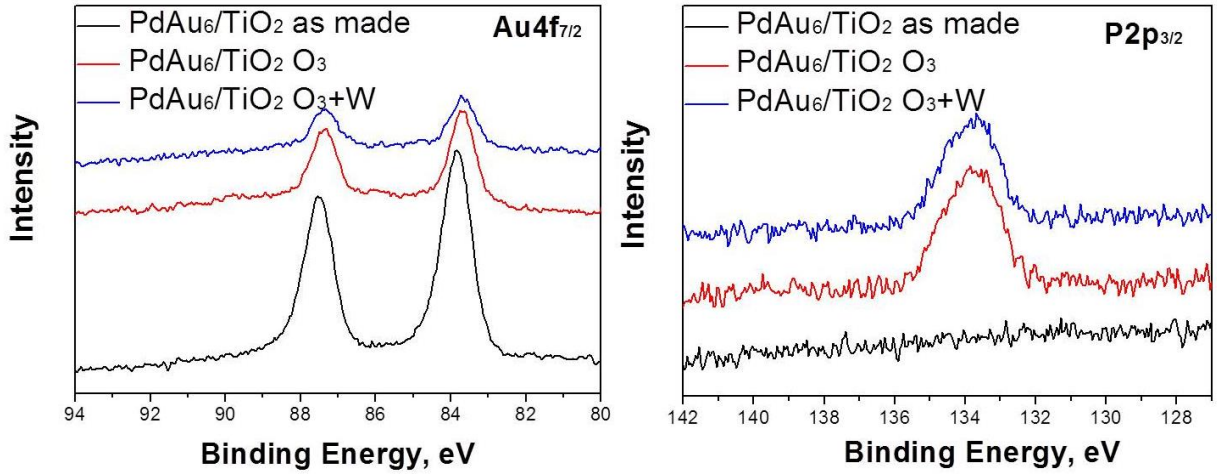

Figure 4.12. $Au4f_{7/2}$ and $P2p_{3/2}$ spectra of $0.5PdAu_6/TiO_2$ before and after treatments.

Finally, DR UV-vis spectra of the $PtAu_8$-based catalysts are depicted in Figure 4.13. As was previously observed for Au_6, Au_8 and Au_9 catalysts, calcination of $PtAu_8/TiO_2$ caused strong particle aggregation, resulting in the appearance of strong SPR band in the spectrum of the calcined catalyst. Very weak SPR band was observed for ozone-treated catalysts, while large particles formed upon subjecting as made $PtAu_8/TiO_2$ to reaction conditions. XPS study of as made $PtAu_8/TiO_2$ showed the presence of two states of gold with $Au4f_{7/2}$ binding energies of 84.9 and 83.8 eV (Figure 4.14). Because pure $PtAu_8$ cluster was previously shown to contain only one signal at higher binding energy of 84.6 eV,[228] the presence of two peaks might indicate partial cluster decomposition on TiO_2. Upon ozone-treatment $Au4f_{7/2}$ peak is shifted towards 83.6 eV due to the formation of metallic Au^0 gold. Similarly to Au_6 and Au_8, toluene wash induces stronger Au-TiO_2 interaction, resulting in the appearance of another $Au4f_{7/2}$ peak at higher binding energy (84.9 eV).

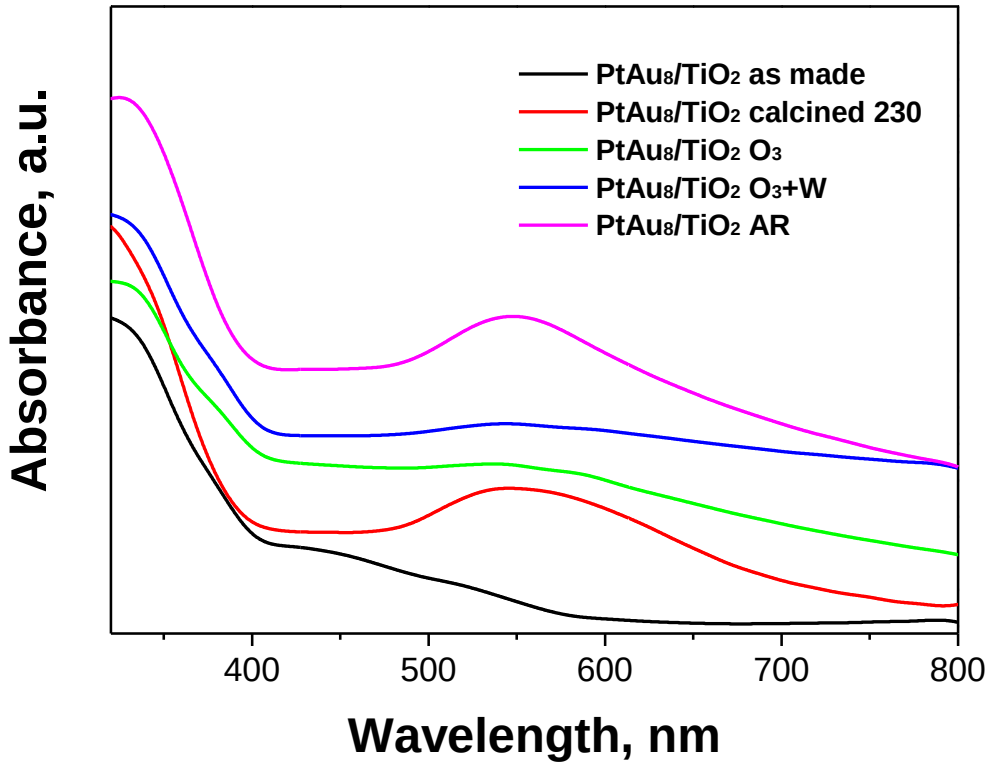

Figure 4.13. Diffuse-reflectance UV-vis spectra of $0.5PtAu_8/TiO_2$ before and after treatments.

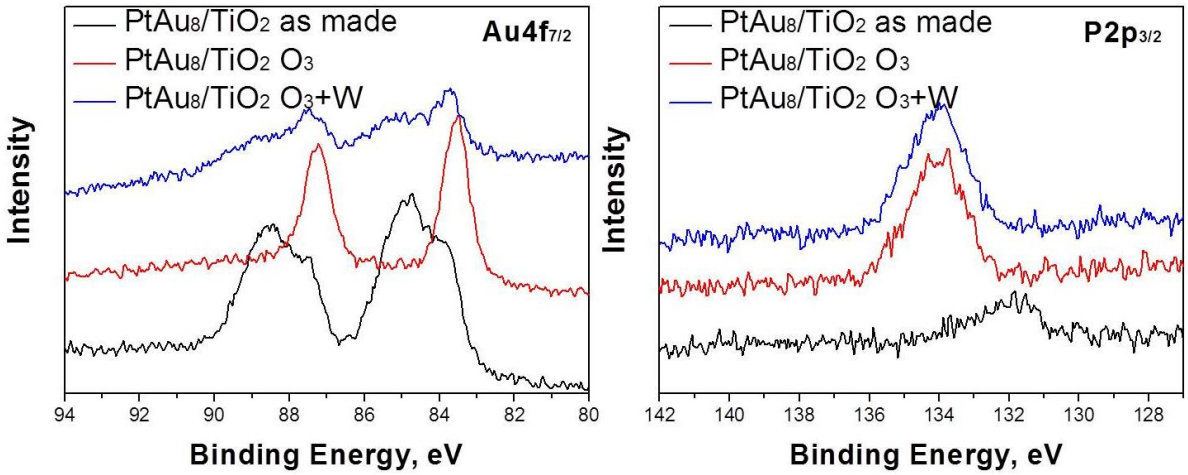

Figure 4.14. $Au4f_{7/2}$ and $P2p_{3/2}$ spectra of $0.5PtAu_8/TiO_2$ before and after treatments.

In summary, the following conclusions could be drawn from DR UV-vis and XPS studies of gold and mixed-metal catalysts (as made and treated in various ways):

1) Clusters of as made catalysts strongly agglomerate under the conditions of the imine synthesis reaction.
2) Based on the results of DR UV-vis study, calcination seems to cause stronger particle aggregation compared to ozonolysis and ozonolysis, followed by toluene reflux at 100 ˚C. However, further studies (HAADF STEM or EXAFS) are necessary to unequivocally confirm this suggestion.
3) During ozonolysis, uncharged metallic gold nanoparticles (Au^0) form from the supported gold clusters. The subsequent wash in toluene induces strong gold-support interaction in some cases, resulting in formation of charged gold indicated by the appearance of $Au4f_{7/2}$ peak at higher binding energy. In some cases (Au_6) catalyst treatment helps to prevent gold leaching.
4) Phosphorous remains on the surface of TiO_2 in its oxidized form after ozonolysis and ozonolysis, followed by toluene wash.

4.3 Study of the activity of pre-treated Au and mixed-metal catalysts in the synthesis of N-benzylidene benzylamine (N-BBA)

Catalytic activity of variously pre-treated catalysts was studied in the one-pot synthesis of N-benzylidene benzylamine (Table 4.5). Catalysts showed activities ranging from low to high depending on the nature of the cluster and pre-treatment method.

Table 4.5. Effect of cluster nature and catalyst pre-treatment on activity in one-pot synthesis of imine.

Catalyst	Treatment	Yield of N-BBA, %	Yield of benzaldehyde, %
$0.5Au_6/TiO_2$	As made	10	-
	Calcined	19	-
	O_3	7	-
	O_3 + reflux (O_3+W)	13	-
$0.5Au_9/TiO_2$	As made	20	-
	Calcined	28	8
	O_3	11	-
	O_3 + reflux (O_3+W)	18	-
$0.5Au_8/TiO_2$	As made	21	-
	Calcined	17	-
	O_3	12	-
	O_3 + reflux(O_3+W)	15	-
$0.5Au_{101}/TiO_2$	As made	84	7
	Calcined	53	-
	O_3	25	-
	O_3 + reflux (O_3+W)	12	-
$0.5PdAu_6/TiO_2$	As made	62	21
	Calcined	71	32
	O_3	37	24
	O_3 + reflux (O_3+W)	56	44
$0.5PtAu_8/TiO_2$	As made	15	-
	Calcined	22	-
	O_3	20	-
	O_3 + reflux (O_3+W)	21	-

Conditions: benzyl alcohol 0.1 mmol, benzyl amine 0.1 mmol, K_2CO_3 0.2 mmol, toluene 3 mL, 19 h, catalyst 50 mg, 100 ˚C, O_2 1 atm, 10 mg of biphenyl (internal standard).

In most cases catalyst activity increased upon calcination of the supported cluster. The yield of N-BBA increased upon calcination from 10 % to 19 % for Au_6/TiO_2, from 20 % to

28 % for Au_9/TiO_2, from 62 % to 71 % for $PdAu_6/TiO_2$ and from 15 % to 22 % for $PtAu_8/TiO_2$. The activity slightly dropped upon calcination for Au_8/TiO_2 - the yield of N-BBA dropped from 21 % to 17 %; and N-BBA yield decreased from 84 % to 53 % for Au_{101}/TiO_2. There was a significant drop in activity upon ozonolysis for most of the studied systems. Yields of N-BBA reduced from 10 % to 7 % for Au_6, from 20 % to 11 % for Au_9, from 21 % to 12 % for Au_8, from 84 % to 25 % for Au_{101} and 62 % to 37 % for $PdAu_6$.

Finally, in most cases, except for Au_{101}, we observed slight increase in catalytic activity of ozone-treated catalysts after they were washed in toluene, however activity of O_3+W catalysts was lower than that of calcined or as made catalysts in most cases. For example, after toluene wash activity of Au_9/TiO_2 O_3 increased from 11 % to 18 %, while the maximum yield of N-BBA achieved within this series of catalysts was 28 % for calcined Au_9/TiO_2. Interestingly, strong gold-support interaction induced in some O_3-treated catalysts upon washing in toluene (Au_6, Au_8, $PtAu_8$) did not lead to notably different activity.

To summarize the trends observed for catalysts upon various treatments, in the majority of cases, the most active catalyst in the series was calcined catalyst, the second active catalyst was as made catalyst, and the least active catalysts within the series were ozone-treated catalysts. Interestingly, only Au_{101} did not follow that pattern and all treatments applied in this study reduced its activity.

To explain the observed trends and activities, it is necessary to discuss the reaction mechanism and factors that might affect activity of gold catalysts in this reaction. The synthesis of imine from alcohols and amines is known to be a two-step process. First, alcohol is oxidized to the corresponding aldehyde in the presence of gold catalyst and base, and then the aldehyde formed reacts with amine to give imine (Figure 4.15).[188, 189, 229]

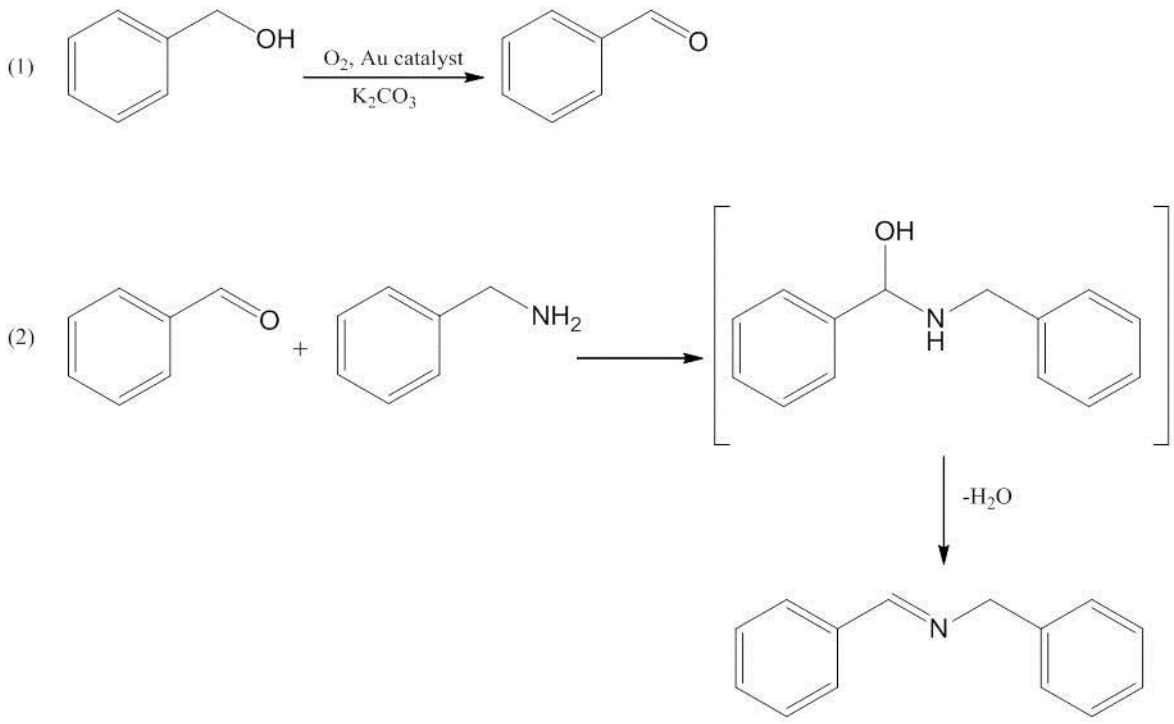

Figure 4.15. Two-step synthesis of N-benzylidene benzylamine from benzyl alcohol and benzylamine.

The first step of the reaction is catalysed by supported gold nanoparticles in the presence of base. The second step usually does not require a catalyst. In particular, mixing benzylamine and benzaldehyde in toluene at room temperature immediately gave N-benzylidene benzylamine, though not quantitatively. Literature data indicates that condensation of amines with aldehydes is somewhat facilitated by metal catalysts and in some cases, *i.e.* when less nucleophilic amines are used, the presence of catalysts is necessary for condensation of amine with aldehyde.[188, 229] Thus, considering such a two-step mechanism of the imine formation, and that the first step of this reaction, *i.e.* alcohol oxidation to aldehyde, is catalysed by gold, the observed effects of the nature of cluster precursor and catalyst pre-treatment should be considered with respect to the oxidation of alcohols.

First, in this study we observed that catalysts derived from $PdAu_6$ cluster were significantly more active compared to catalysts derived from pure Au_6, Au_8 and Au_9 clusters.

It was previously shown that alloy Au-Pd catalysts outperform both gold and palladium catalysts in the oxidation of alcohols in terms of both activity and selectivity.[124, 224, 230, 231] Moreover, it was demonstrated that addition of a very small amount of Pd to Au nanoparticles can drastically increase the activity of the system in alcohol oxidation. For example, Yang *et al.* showed that alloy Au-Pd nanoparticles with the composition of $Pd_{0.05}Au_1$ have 6 times higher activity in the oxidation of benzyl alcohol compared to monometallic Au particles.[230] Tsukuda and co-workers showed that replacement of only one Au atom with Pd in Au_{25} cluster increased conversion of benzyl alcohol from 22 % to 74 %.[124] The effect is believed to be due to the electronic modification of gold by Pd atoms. Thus, the higher activity of catalysts, derived from $PdAu_6/TiO_2$ and studied in this work, is in line with the previously reported results. Such strong activity enhancement is most likely due to the electronic modification of gold by Pd atoms, similarly to the case of the Au_{25} cluster.[124] Additionally, we observed that product selectivity of $PdAu_6$-derived catalysts was somewhat worse compared to pure gold catalysts: benzyl aldehyde was always detected as a by-product. This may be due to the inferior ability of Pd-Au nanoparticles to catalyse condensation of amine and aldehyde compared to pure gold particles.

As made catalysts were less active compared to calcined catalysts with the exception of Au_{101}. Since DR UV-vis study showed that clusters aggregated during the reaction to form larger plasmonic particles, the increase in activity upon calcination could be explained by the fact that active species, *i.e.* phosphine-free aggregated particles, had been pre-formed before the reaction, whereas it took some time during the reaction for as made catalysts to form active gold nanoparticles (*i.e.* induction period). An independent study of benzyl alcohol oxidation in the presence of Au_{101}-derived carbon-based catalysts by Sedigheh Ghadamgahi in the Golovko group showed that the reaction possessed an induction period,[232] indicating that formation of active gold nanoparticles from phosphine-stabilised gold clusters also

occurs during benzyl alcohol oxidation, similarly to the results obtained for cyclohexene oxidation (Chapter 2). Thus, pre-treatment, which leads to the formation of active catalysts, results in higher catalytic activity.

Detailed analysis of the numerous studies, reported in the literature, shows that medium-sized gold nanoparticles (4 - 8 nm) are generally more active in the oxidation of alcohols and polyols compared to the smaller or larger particles (See detailed discussion in the Introduction).[90, 91, 99, 138-143] Thus, there is more or less good agreement among different research groups regarding the optimal size of gold nanoparticles for the oxidation of alcohols. In the light of these data and the results of our DR UV-vis study, the lower activity of ozone-treated catalysts in this work could be explained by the formation of stable Au particles with small size that is below the optimum. Some increase in activity of ozone-treated catalysts upon the subsequent toluene wash could be due to a slight particle size increase, as evidenced by the higher intensity of SPR band of O_3+W catalysts, making particle size closer to the optimal size. It should be noted that the change of activity associated with catalyst pre-treatment and thus with the change in particle size is almost negligible compared to the change in activity upon addition of other metal (Pd). Addition of Pt to Au did not seem to cause substantial change in activity, which is in line with the results previously reported by Soule and co-workers.[194]

In summary, various TiO_2-supported catalysts derived from gold and mixed-metal clusters were prepared, treated by calcination, ozonolysis and ozonolysis, followed by washing with toluene and characterised using diffuse-reflectance UV-visible spectroscopy and Synchrotron-based X-ray photoelectron spectroscopy. The study of catalytic activity of gold catalysts in the one-pot synthesis of N-benzylidene benzylamine showed that activity is moderately affected by the nature of Au cluster precursor: catalysts derived from Au_6, Au_8 and Au_9 showed similar activities. Untreated Au_{101}/TiO_2 showed the highest activity among

all catalysts, however, its activity always deteriorated upon treatments. By studying the activity of $PdAu_6$ and $PtAu_8$ clusters we showed that activity of gold nanoparticles is strongly increased upon the addition of Pd, but no such effect was observed when Pt was added. Pd-Au catalysts obtained from $PdAu_6/TiO_2$ by various treatments were demonstrated to be the most active ones among the studied catalytic systems derived from atomically precise clusters. Finally, we showed that catalyst pre-treatment also affects the activity. Catalyst calcination at elevated temperature was shown to give the most active catalysts in most cases.

Chapter 5. Study of biological activity of gold nanoparticles

5.1 Introduction

Today there is a strong focus on application of nanotechnology to cancer treatment. Several pharmacological companies have got approval from the Food and Drug administration (FDA) for the development and use of nano-drugs.[233] In particular, due to their unique properties, gold nanoparticles have attracted tremendous interest in applications related to diagnosis and treatment of cancer.[233-236] Significant progress has been achieved in understanding of behaviour of gold nanoparticle systems in biological applications in the past years.

The main reasons for a particular attractiveness of gold nanoparticles in cancer research compared to the nanoparticles of other metals/metal oxides are:

1) Gold nanoparticles are generally non-toxic, non-immunogenic, and can penetrate tissue without hampering cell functionality.[105, 237, 238] Some studies, however, indicate that Au particles with certain sizes could be toxic;[105, 239-241]
2) Different Au particles can by synthesised with high degree of control over their size and shape;[233]
3) Gold nanoparticles possess the localised surface plasmon resonance (SPR), which can be easily tuned by changing particles size/shape (see Chapter 1, Figure 1.10). SPR serves as a basis for various bio-nanotechnological applications of gold nanoparticles.
4) Gold nanoparticles can be easily functionalised with various probe molecules, such as antibodies, enzymes, *etc.*

5) Due to its rare occurrence gold could be easily quantified at low concentrations (compared to other metals such as *e.g.* Fe, Cu, *etc.*), making the analysis of the gold uptake by cells more facile.

The main applications of Au nanoparticles in cancer research include imaging/detection of cancer, therapeutical applications and drug delivery. Moreover, all three types of applications can be utilised simultaneously.

5.1.1 Cancer detection and imaging using gold nanoparticles

Metallic nanoparticles can be used for *in vitro* and *in vivo* imaging of cancer cells. They have several advantages for bioimaging compared to other types of nanoparticles (*e.g.* semiconductor, magnetic, polymer, *etc.*). First, metal particles scatter light intensely: they are much brighter compared to molecular fluorophores. Metal particles do not photobleach, are easily detectable and have enhanced light scattering at wavelengths of their localised surface plasmon resonance.[242]

First, particles need to be targeted to cancer cells through either passive or active targeting. Maeda *et al.* showed that nanoparticles < 200 nm tend to passively accumulate in solid tumours through a leaky tumour vasculature due to enhanced permeability and retention effect (EPR effect).[243, 244] Because malignant tumours develop new vasculature very rapidly to supply the expanding tumour mass, these newly developed blood vessels have abnormal structure and irregular shape with inconsistent diameters and large gaps. These large gaps serve as gates for large molecules and nanoparticles in the blood stream to penetrate into the tumour; and since tumour tissue usually lacks effective lymphatic drainage, nanoparticles and large molecules remain inside the tumour. This effect is referred to as EPR effect and it can be observed in almost all human cancers with the exception of hypovascular tumours such as prostate or pancreatic cancers.[243]

Though particles accumulate inside solid tumours through EPR effect, their uptake by cancer cells has been questioned[245] and *active targeting* of nanoparticles can be additionally applied. This is usually achieved by modification of particle surface with the antibodies, targeted against oncoproteins overexpressed on cancer cell surfaces; aptamers or cancer-related substances.[246-249] Nanoparticles with these ligands are recognised by the surface receptors of cancer cells, which leads to particle uptake through receptor-mediated endocytosis.[245]

Folic acid and glucose are often used as common "cancer-related" ligands. While the use of antibodies in clinical applications could be restricted because of the variations from patient to patient and a type of cancer, the use of folic acid and glucose is based on the properties that many cancer types have in common. Folic acid is a basic component of cell metabolism and DNA synthesis/repair and it is an essential vitamin required for both normal and tumour cells.[249] Because cancer cells divide and grow very rapidly, they have an increased requirement for folate to maintain DNA synthesis. This is supported by the observations showing that the cells of some of the malignant tumours of epithelial origin overexpress folate receptor – a membrane-bound protein with high affinity for binding and transporting folate into cells. This property of cancer cells can be used for selective delivery of cytotoxic agents into malignant cells with reduced toxic side effects on non-target tissues.[248, 250-254] The potential use of glucose as a cancer-targeting ligand is based on the fact that cancer cells consume significantly higher amounts of glucose compared to normal cells,[247, 255, 256] because they have higher rate of growth and metabolism, which requires higher glucose uptake. Moreover, cancer cells mainly produce their energy via glycolysis - non-oxidative breakdown of glucose (so called Warburg effect).[256] In contrast, normal cells produce energy via oxidative breakdown of pyruvate (Krebs cycle), an end product of glycolysis.[257] This increased uptake of glucose by tumours now serves as a foundation for detection and

monitoring of human cancers by positron emission tomography using fluorodeoxyglucose (2-^{18}F-2-deoxyglucose) as a radiotracer.[257]

Nanoparticles accumulated inside the cells or tumours can be used as sensors or contrast agents for optical detection due to their enhanced adsorption and scattering. The scattering properties of gold nanospheres have been used for cancer cell imaging using confocal microscopy and dark-field microscopy.[242, 258-260] Due to the high electron density of gold nanoparticles they can be used as contrast agents in transmission electron microscopy.[242]

El-Sayed's group used gold nanoparticles and nanorods, conjugated with antibodies to epidermal growth factor receptor (EGFR), overexpressed in malignant cells, to distinguish malignant and non-malignant cells.[258] As can be seen from the light-scattering images, shown in Figure 5.1, antibody-conjugated particles randomly interact with non-cancerous cells (left column), while both nanospheres and nanorods bind specifically to malignant cells, which overexpress the targeted EGFR (middle and right columns).

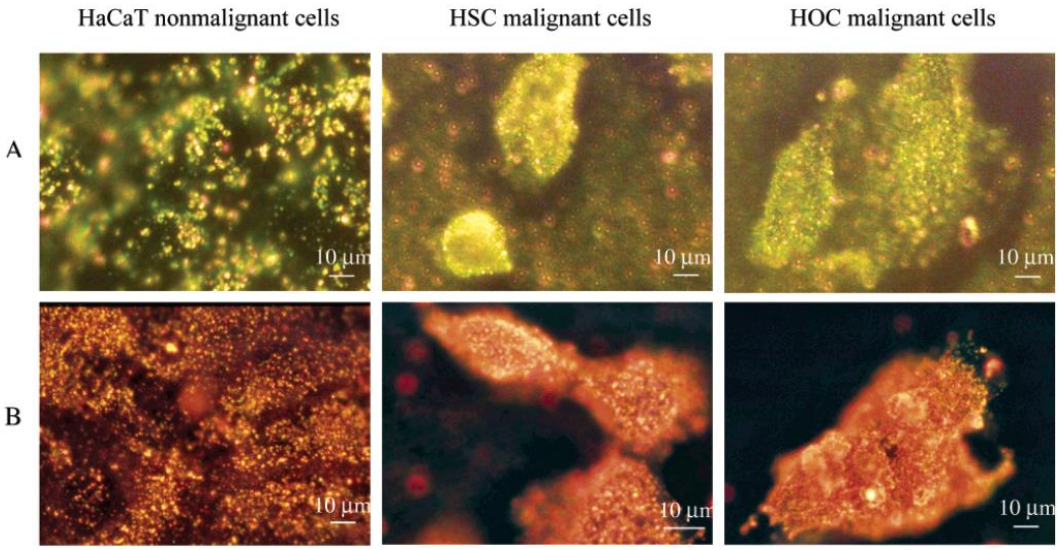

Figure 5.1. Light-scattering images of anti-EGFR/Au nanospheres (A) and anti-EGFR/Au nanorods (B) after incubation with cells for 30 minutes. Reprinted with permission from ref. [258]. Copyright American Chemical Society.

Often imaging of cancer using metal nanoparticles is coupled with either therapeutical applications or enhanced drug delivery using gold nanoparticle carriers, or both, in order to simultaneously detect cancer and treat it in the early stages of development.

5.1.2 Therapeutical applications of gold nanoparticles

Hyperthermia is the use of local heating (42 – 43 ˚C) to cause cell protein denaturation with the following cell death. This area has recently attracted broad attention as an adjunctive cancer treatment option.[261] Gold nanoparticles are the perfect candidates to phototherapeutic agents in cancer treatment. As was shown previously (Figure 1.10), surface plasmon resonance of gold nanoparticles can be easily tuned by changing their size and shape. When particles, which were targeted to a tumour, are irradiated with light of the same wavelength as the wavelength of their SPR band, the energy of light can be converted into heat, thus causing selectively localised hyperthermia and ablation of the located nearby cancer cells. In this respect, gold nanorods are the most attractive types of gold particles because they strongly absorb in the near IR region – a region where body tissue does not absorb, thus no harm can be done to healthy organs and only parts loaded with gold nanorods are subjected to treatment. Photothermal therapy is usually combined with imaging; and such approach was shown to selectively destroy cancerous cells both *in vitro* and *in vivo*.[251, 258, 259, 261-266] Study by Heys *et al.* showed that gold nanorods do not have to be internalised in cells in order to efficiently destroy tumours by photothermal treatment – extracellular hyperthermia, in which particles are maintained in the extracellular space, was shown to be an effective method of inducing cancer cell death.[261] Loo *et al.* demonstrated how Human epidermal growth factor receptor 2 (HER-2)-targeted gold nanoshells can be used for combined imaging and near-IR phototherapy of SKBr3 breast cancer cells (Figure 5.2).[259] As can be seen from Figure 5.2, both SKBr3 cell imaging and efficient photothermal ablation were achieved when gold nanoshells were targeted to HER-2 protein, overexpressed by breast cancer cells.

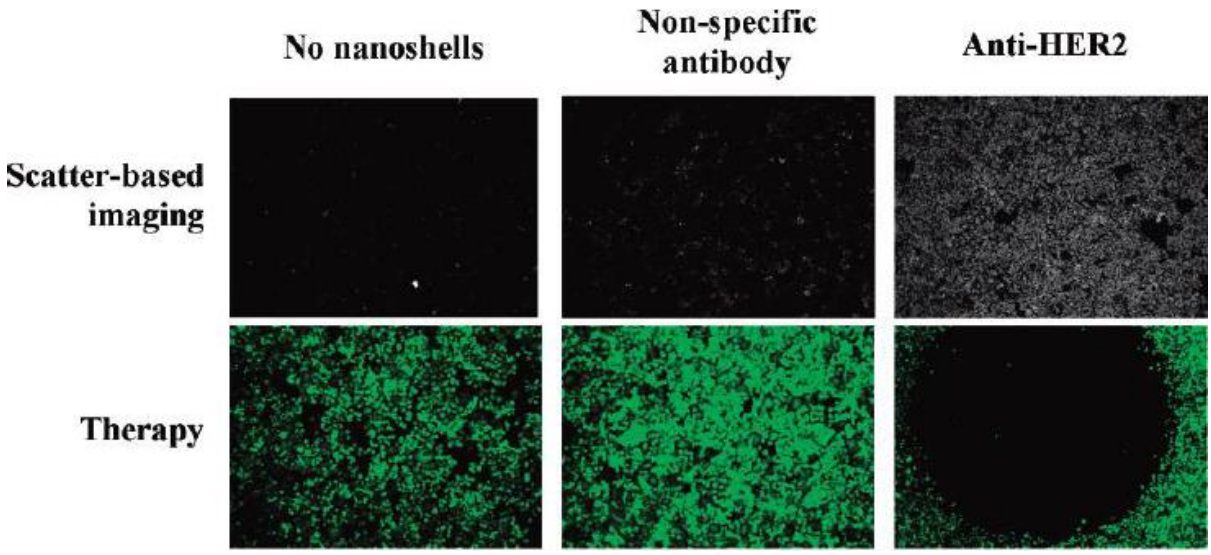

Figure 5.2. Combined imaging and therapy of SKBr3 cells using HER2-targeted gold nanoshells. Reprinted with permission from ref. [259]. Copyright American Chemical Society.

Radiation therapy (radiotherapy) is a method based on employing ionising radiation to destroy cancer cells by DNA damage and their exposure to free radicals.[267-269] Radiotherapy is currently used as a cancer treatment method accompanying chemotherapy. It was shown that the efficiency of the radiotherapy could be significantly enhanced in the presence of high-Z elements[270, 271] by reducing the dose of radiation and drugs while preserving (or enhancing) the destructive power of the treatment. Gold nanoparticles strongly absorb X-rays. This property, combined with their ability to accumulate in solid tumours by EPR effect, makes them an excellent choice as high-Z element constituents in enhanced radiotherapy.[267, 269]

Hainfeld *et al.* employed gold nanoparticles to enhance the effects of the radiation treatment of mice bearing subcutaneous EMT-6 mammary carcinomas.[267] They showed that 86 % of mice survived after 1 year, when the mice were injected with gold nanoparticles and treated with X-ray radiation, while only 20 % and 0 % survived when they were treated with either radiation alone or gold nanoparticles alone, respectively. It was also clearly demonstrated that radiation response is dependent on gold dosage: 50 % of mice survived

when they were injected with 1.35 Au g/kg of gold nanoparticles, while 86 % survived when the dosage was twice as high.

5.1.3 Enhanced drug delivery using gold nanoparticle carriers

In addition to imaging and therapeutic applications, gold nanoparticles can also be used for efficient drug delivery. High drug toxicity is a barrier for the drug application, because strong side-effects limit the drug dosage and therefore its efficiency. Gold nanoparticles can be loaded with large doses of chemotherapeutic drug and simultaneously targeted to cancer cells, thus their use offers improved precision of chemotherapeutic targeting, resulting in lower systemic toxicity.[272] The application of gold nanoparticles in drug delivery has been actively investigated during last ten years.[273-276] Brown *et al.* developed oxaliplatin drug delivery system based on gold nanoparticle carriers (Figure 5.3).[246] Such system showed 6-fold increase of *in vitro* toxicity for lung and colorectal cancer cells compared to unbound oxaliplatin. The increase in toxicity is believed to be due to enhanced cellular uptake of the system.

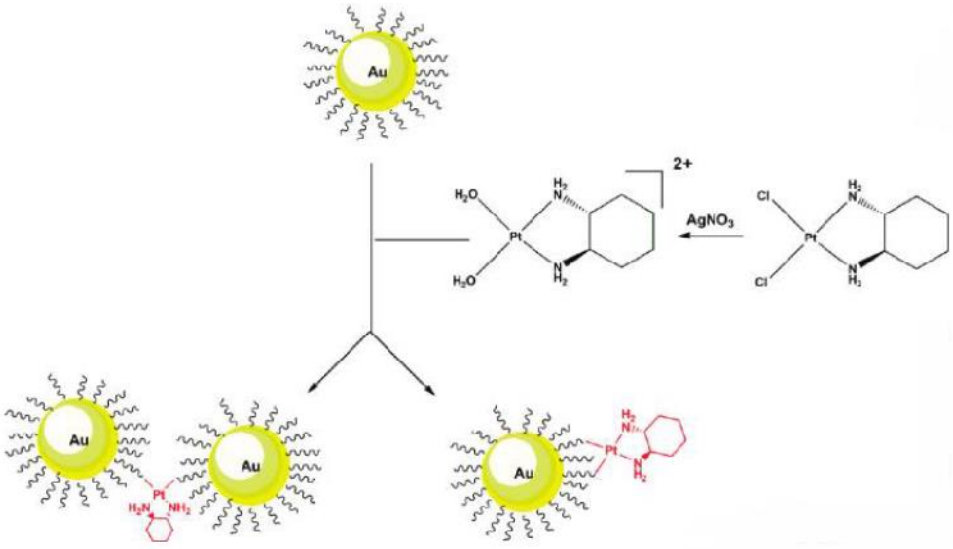

Figure 5.3. Platinum tethered gold nanoparticles. Image reproduced from ref. [246].

Agasti *et al.* demonstrated a light-controlled release of drug from a gold nanoparticle carrier.[277] Such strategy is attractive because the location and extent of drug release can be easily controlled. Gold nanoparticles were also shown to be efficient delivery systems for water-insoluble drugs. For example, silicon phthalocyanine 4 (Pc4) is a hydrophobic drug for photodynamic therapy, which is currently under Phase I clinical trials.[278] Photodynamic therapy employs photosensitizing agents (porphyrins, phtalocyanines) to generate highly reactive oxygen species upon light irradiation to induce apoptosis and necrosis of the surrounding tissue. When Pc4 is injected in vivo, it takes 1 – 2 days to achieve sufficient drug accumulation to employ further irradiation. Cheng *et al.* showed that upon Pc4 conjugation with Au nanoparticles the time of maximum drug accumulation in tumour can be reduced to a few hours.[278]

5.2 Scope of this study

Applications of gold nanoparticles, described above, demonstrate the breadth of their potential uses in the treatment of life threatening diseases, such as cancer. It is important to study behaviour of gold nanoparticles, i.e. biocompatibility or toxicity (depending on the application), stability under physiological conditions, nanoparticle uptake by cells, *etc.*

This work was performed in collaboration with the group of Prof John Evans (University of Otago) and later with the group of Prof Dar-Bin Shieh (National Cheng Kung University). Since this area of research was new for both Christchurch-based groups, the aim of this part of my thesis was to initialise research in the area of application of gold nanoparticles in cancer treatment research, establish procedures and perform preliminary investigations. In this work we studied the biological behaviour of gold nanoparticles derived from Au_{101} cluster and functionalised with two cancer-related substances, *i.e.* folic acid[248, 250] and thio-glucose.[247] In particular, we studied cytotoxicity of Au_{101}-nanoparticles in a wide range of healthy and cancer cell types, gold uptake by cells and particle localisation inside cells. Synthesis, modification and characterisation of gold nanoparticles were performed at the University of Canterbury by Baira Donoeva. Cytotoxicity studies on Ishikawa (endometrial cancer) and C2C12 (normal myoblast) cell lines, their gold uptake and localisation studies were performed at the University of Otago by Baira Donoeva with great help from Dr Kenny Chitcholtan (University of Otago). Cytotoxicity, uptake and localisation studies on the rest of the cell types were performed at the National Cheng Kung University by Kevin Li.

5.3 Experimental

5.3.1 Synthesis of functionalised 1.5nm Au_{101}-nanoparticles

Nanoparticles with the estimated composition of $Au_{101}(PPh_3)_{21}Cl_6$ (denoted as Au_{101}-PPh_3) and the average particle size of 1.5 nm were synthesized and characterized according to the previously published procedure.[279] The exact synthetic procedure is described in the Chapter 2.

Ligand exchange procedure was carried out using method similar to the one reported by Woehrle *et. al.*[280] Thioglucose (TG) stabilised particles were obtained directly via exchange of Au_{101}-PPh_3 with TG (Figure 5.4 (1)). Folate-modified particles were obtained via two-step synthesis: first, phosphine-stabilised particles were exchanged with cysteamine (CYS) (Figure 5.4 (2)) and, second, folic acid (FA, Figure 5.4 (3)) was subsequently attached to cysteamine by amidation.

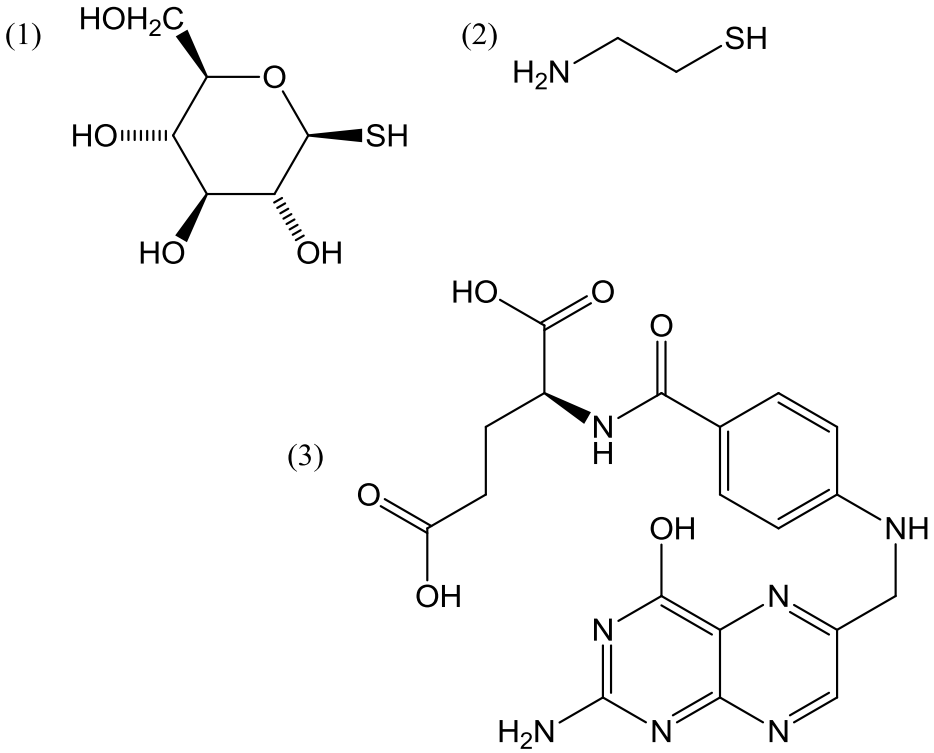

Figure 5.4. Ligands employed in this study: 1) 1-thio-β-D-glucose 2) cysteamine and 3) folic acid.

The general procedure for cysteamine and thio-glucose (Au_{101}-CYS and Au_{101}-TG) ligand exchange was as follows: to a solution of Au_{101}-PPh_3 (20 mg) nanoparticles in CH_2Cl_2 (3 mL) was added a solution of thio-glucose or cysteamine hydrochloride (20 mg) in Milli-Q water (3 mL). The biphasic reaction mixture was stirred rapidly at room temperature until the completion of the ligand exchange reaction (up to 2 days). Completion of ligand exchange was confirmed by colour transfer from organic to aqueous phase. The aqueous layer was then separated from the organic layer and the volume of aqueous solution was reduced using a rotary evaporator. Next, particles were purified twice from the free ligand (cysteamine or thio-glucose) on Sephadex LH-20 column (d 15 mm, length 30 cm) using water as an eluent. Finally, nanoparticle solutions were sterilized using filter with 0.2 μm pores.

Preparation of Au_{101}-folate (Au_{101}-FA)

Folic acid was attached to Au_{101}-CYS through peptide-bond formation in a similar manner to the previously published procedures.[251, 252, 268] To the solution of Au_{101}-CYS in water obtained from 15 mg Au_{101}-PPh_3 and purified on Sephadex LH-20, folic acid in water (0.6 mL of 0.6 g/L, pH 8) was added. Next, 0.1 M N-hydroxysuccinimide (30 μL) and 0.4 M 1-ethyl-3-(3-dimethylaminopropyl)carbodiimide (EDC HCl, 30 μL) were added. The mixture was allowed to stir for 3 hours in an ice bath. Next, solution volume was reduced using a rotary evaporator and particles were purified from other mixture components on Sephadex LH-20, sterilized using filter with 0.2 μm pores. Successful attachment of folic acid was confirmed by FT-IR, UV-visible spectroscopy and ^{1}H NMR.

Preparation of fluorescent Au_{101}-nanoparticles

Fluorescent Au_{101} nanoparticles were synthesized from Au_{101}-CYS by their reaction with fluorescein succinimidyl ester Fluorescein EX-5 (Invitrogen, F-6130). First, several drops of solution containing 0.06 M $Na_2B_4O_7$ and 0.075 M HCl were added to a solution of Au_{101}-CYS (5 mL, Au concentration 3 mg/mL), followed by the addition of fluorescein-EX-5 (0.1

mg) dissolved in minimum amount of DMSO. The mixture was allowed to stir for 1 hour. As prepared particles were purified from unbound fluorescein on Sephadex LH-20 (d 15 mm, length 30 cm) and successful attachment of fluorescein was confirmed using fluorescence spectrometry.

5.3.2 Methods

Particles were characterized using TEM, ^{1}H NMR and fluorescent spectroscopy. Particle size was monitored using TEM after each ligand exchange or modification to ensure that core size remained unchanged. TEM images of Au_{101}-nanoparticles were taken on Philips CM200 (200kV). Samples were deposited on holey-carbon TEM grids (300 mesh) using diluted solutions of Au_{101} nanoparticles in CH_2Cl_2 or water. Gold concentration in as prepared nanoparticle solutions was established using Atomic Absorption spectroscopy (AAS). Aliquot (50 μL) of Au-nanoparticle solution was mixed with 200 μL of freshly prepared *aqua regia*, diluted to 5 mL with Milli-Q water and gold concentration was measured using Varian SpectrAA 220FS instrument. Solutions with known Au concentration were diluted with Milli-Q water to obtain solutions with desired concentration for further use. Fourier transform infrared spectra (FT-IR) and UV-visible spectra were recorded using Bruker ALPHA FT-IR spectrometer and Varian Cary 50 Probe UV-visible spectrophotometer, respectively. Fluorescence spectroscopy was performed using Horiba Jobin-Yvon Fluorolog-3 fluorescence spectrometer. Inductively coupled plasma mass spectrometry (ICP-MS) was performed using ICP-MS Agilent 7500cx. Sunrise, Tecan (Männedorf, Switzerland) microplate reader was used for cytotoxicity studies. Fluorescence microscopy was performed using Confocal Microscope (Olympus FluoView™ FV1000) and epifluorescent microscope AxioVision 4.5 (Carl Zeiss, Oberkochen, Germany).

5.3.3 Cytotoxicity of Au_{101}-nanoparticles

Endometrial cancer cell lines (Ishikawa) at $2x10^4$ cells/well, C_2C_{12} myoblast cells (passage number lower than 25) at $4x10^3$ cells/well and the rest of the cell lines at 10^4 cells/well were cultured in a 96-well culture plate with 200 µL of Dulbecco's Modified Eagle Medium (DMEM F12) culture media supplemented with 10% fetal bovine serum (FBS), Penicillin-Streptomycin (P/S) and Glutamax. Cells were then incubated at 37 ºC, 5% CO_2 atmospheric conditions for 48 hours prior to the treatment with Au_{101} nanoparticles. Culture media was replaced by fresh FBS-free DMEM (low glucose) media (total volume 150 µL) and calculated volume of Au_{101} nanoparticle solutions was added. Cells were then incubated with nanoparticles at 37 ºC, 5% CO_2 atmospheric conditions for 24 hours.

After 24-hour cell incubation with gold nanoparticles, the cell survival rate was established using either Alamar blue or MTT assay.

Alamar Blue Assay (used in New Zealand).[281] After cell incubation with gold nanoparticles, 15 µL of Alamar blue dye was added to culture media and cells were further incubated for 3 hours. The assay is used to assess mitochondrial metabolic activity by reduction of blue-coloured Alamar blue dye (resazurin) to purple-coloured resorufin (Figure 5.5). Figure 5.5 also shows the 96-well plate immediately after addition of Alamar Blue to the culture media (top left) and after 3 h incubation at 37 ºC (bottom left). As can be seen from the figure, initially blue solutions turn pink upon incubation with living cells.

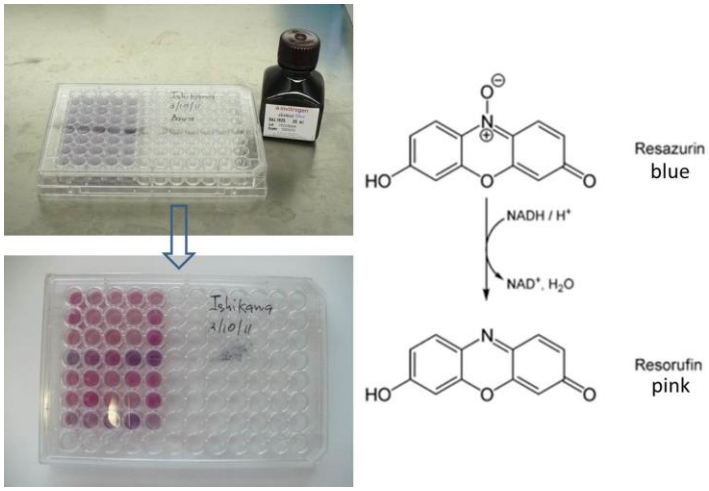

Figure 5.5. Reduction of resazurin to resorufin (Alamar Blue assay)

The cellular activity was determined by the change of colour from blue to purple. The intensity of absorbance of blue and purple colours was measured at 560 and 595 nm, respectively, using fluorescent microplate reader. The final values of cell survival rate were represented as absolute absorbance of Alamar blue ($A = A_{560} – A_{595}$), calculated relatively to control wells (100 %).

MTT assay (used in Taiwan). After cell incubation in the presence gold particles 3-(4,5-dimethylthiazol-2-yl)-2,5-diphenyltetrazolium bromide (MTT, Sigma-Aldrich) was added to cells. The cells were treated with MTT reagent and incubated at 37 °C for 4 h. Cell viability was determined using MTT assay by measuring the enzymatic reduction of yellow tetrazolium MTT to a purple insoluble formazan (Figure 5.6).

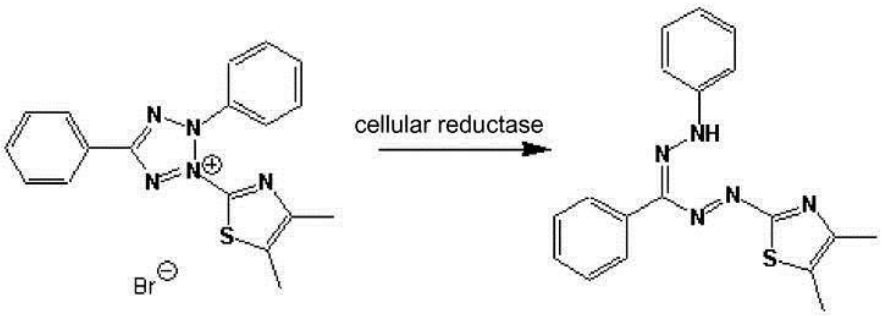

Figure 5.6. Reduction of tetrazolium dye MTT to formazan (MTT assay)

The purple crystals of formazan were then dissolved in dimethyl sulfoxide and the supernatant was transferred to an ELISA plate and the absorbance was quantified at 595 nm using a microplate reader.

Cytotoxicity experiments were performed at least 4 times in pentets.

5.3.4 Study of Au nanoparticle uptake by cells

Ishikawa cells ($1.6 \cdot 10^5$ cells/well), C_2C_{12} ($6 \cdot 10^4$ cells/well) myoblast cells and other cells ($2 \cdot 10^5$) were cultured in a 6-well culture plate with 2 mL of culture media supplemented with 10 % FBS, P/S and Glutamax. Cells were then incubated at 37 ºC, 5% CO_2 atmospheric conditions for 72 hours. After that media was replaced by FBS-free DMEM (low glucose) media and calculated volume of Au-nanoparticle solutions was added. Cells were then incubated with nanoparticles for 24 hours.

In 24 hours culture media was collected from 6-well plates and cells were washed with 1x phosphate buffered saline (PBS) twice and treated with 0.5 mL of 1x trypsin EDTA in PBS. Suspensions with detached cells were collected in Eppendorf tubes and centrifuged (1500 rpm x 5 min). Next, trypsin solution was decanted and cells were re-suspended in culture media. Final cell number in each well was established by cell count using a haemocytometer. After the cell count, cells were separated from culture media by centrifugation and 0.2 mL of freshly prepared *aqua regia* was added to lyse cells and dissolve internalised gold nanoparticles. The solution cleared instantly. The clear solution was carefully transferred to 5 mL volumetric flasks (each Eppendorf tube was rinsed 3 times) and diluted to 5 mL using dilution solution: 2% HNO_3 (AR), 0.5% HCl (AR), 0.5 g/L thiourea in nanopure water. Gold content in the final solutions was established using ICP-MS. Particle number was calculated from gold concentration established from ICP-MS assuming that each gold particle contains *ca.* 100 Au atoms. Finally, the number of particles was normalised to

the number of cells, and the percentage of the gold nanoparticles internalised by cells (uptake %) was calculated.

5.3.5 Study of Au_{101} localization inside the cells

Ishikawa cells ($4 \cdot 10^4$ cells/well), C_2C_{12} ($1.5 \cdot 10^4$ cells/well) myoblast cells and other cells ($2 \cdot 10^4$ cells/well) were cultured on glass cover slips in 12-well culture plate with 1 mL of culture media supplemented with 10% FBS, P/S and Glutamax. Cells were then incubated at 37 ºC, 5 % CO_2 atmospheric conditions for 72 hours. After that media was replaced by FBS-free DMEM (low glucose) media and calculated volume of Au-nanoparticle solutions was added so that the total atomic Au concentration in wells was 20 μM. Cells were incubated with nanoparticles for 24 hours. After incubation, cells were washed with 1 mL of PBS twice and fixed by treating them with 0.5 mL of 4 % formaldehyde in PBS for 20 minutes. After fixation cells were washed with 0.05 % Tween-20 in 1x PBS three times (5 min each time) to remove excess of Au_{101} nanoparticles and, finally, were nuclei- and actin-stained using Hoechst 33342 Fluorescent Stain (or DAPI) and Phalloidin stain solution, respectively. Distribution of the fluorescent particles within the cells was monitored using fluorescent microscopy.

5.4 Results and discussion

5.4.1 Particle synthesis, ligand modification and characterization

Au_{101} particles with mean core diameter of 1.5 nm, stabilised with triphenylphosphine, have been synthesized according to the earlier published procedure.[279] An important property of Au_{101} nanoparticles is that their solubility in a particular solvent is determined by the solubility of their stabilizing ligands in that solvent.[280] Phosphine stabilized particles were subjected to ligand exchange with water-soluble thiol ligands in order to make them water-soluble and modify nanoparticles with targeting ligands. Two targeting ligands were employed in this study – thio-glucose and folic acid. Thio-glucose stabilised Au_{101} nanoparticles were obtained directly by one-step ligand exchange of phosphines in Au_{101}-PPh_3 with TG. Time needed for complete ligand exchange was 2 days, and the successful exchange was evidenced by the transfer of gold nanoparticles from the organic phase to the aqueous phase (Figure 5.7).

Figure 5.7. Biphasic mixture before and after ligand exchange, organic layer (bottom) initially contains dissolved Au_{101}-PPh_3, aqueous layer (top) – thiol ligand. After the ligand exchange particles transfer to the aqueous layer.

Since folic acid does not have any thiol groups, Au_{101} nanoparticles modified with folic acid were obtained via two-step synthesis. First, phosphines of Au_{101}-PPh_3 were exchanged with cysteamine to obtain Au_{101}-CYS. Time needed for particle transfer to aqueous phase was 4 hours. Au_{101}-CYS were also used later for cytotoxicity and uptake studies for comparison.

Folic acid was attached to cysteamine-modified particles through peptide bond formation between carboxylic groups of folate and amino-group of cysteamine in the presence of N-hydroxysuccinimide and 1-ethyl-3-(3-dimethylaminopropyl)carbodiimide (EDC HCl, Figure 5.8).

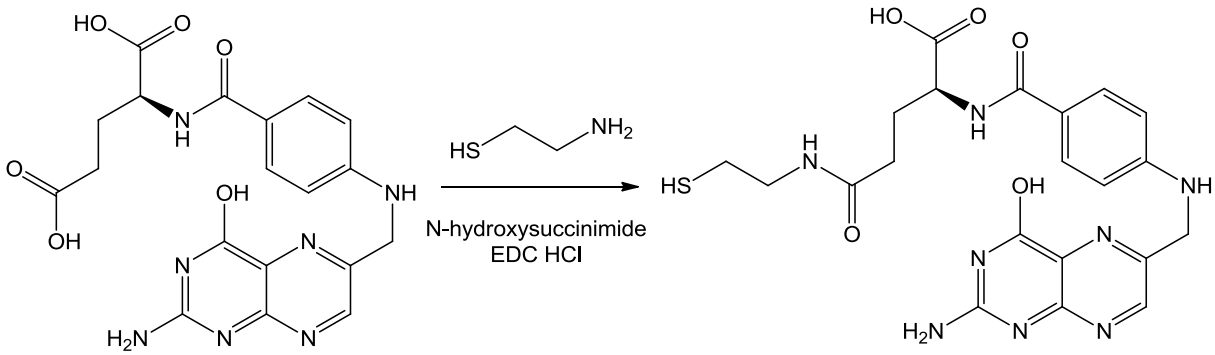

Figure 5.8. Amide bond formation between folic acid and cysteamine in the presence of N-hydroxysuccinimide and EDC HCl

Au_{101}-FA was characterised using FT-IR and UV-vis. Additionally, NMR of the solution of Au_{101}-FA, decomposed with *aqua regia*, was performed. Figure 5.9(a) shows FT-IR spectra of unbound FA, Au_{101}-CYS and Au_{101}-FA. IR absorption spectra of both FA and Au_{101}-FA have absorption bands between *ca.* 1200 and 1690 cm^{-1}, which include characteristic absorption bands attributed to vibrations of pterin and phenyl rings, bending of NH-group and stretching C=O group of folic acid.[251, 268, 282] UV-vis absorption spectra of FA, Au_{101}-CYS and Au_{101}-FA are shown in Figure 5.9(b). UV-vis absorption spectrum of FA possesses pronounced bands at 254, 285 and 370 nm, which can be assigned to $\pi \rightarrow \pi^*$ transitions of FA molecule.[282] All these bands can be observed in the spectrum of Au_{101}-FA,

while none of them are present in the spectrum of Au_{101}-CYS. Thus, we can conclude that folic acid was successfully conjugated to gold nanoparticles. Additionally, ^{1}H NMR spectrum of the solution of Au_{101}-FA decomposed by *aqua regia*, showed signals at 6.9, 7.7 and 8.5 ppm indicating the presence of folic acid in Au_{101}-FA (see Appendix 18).

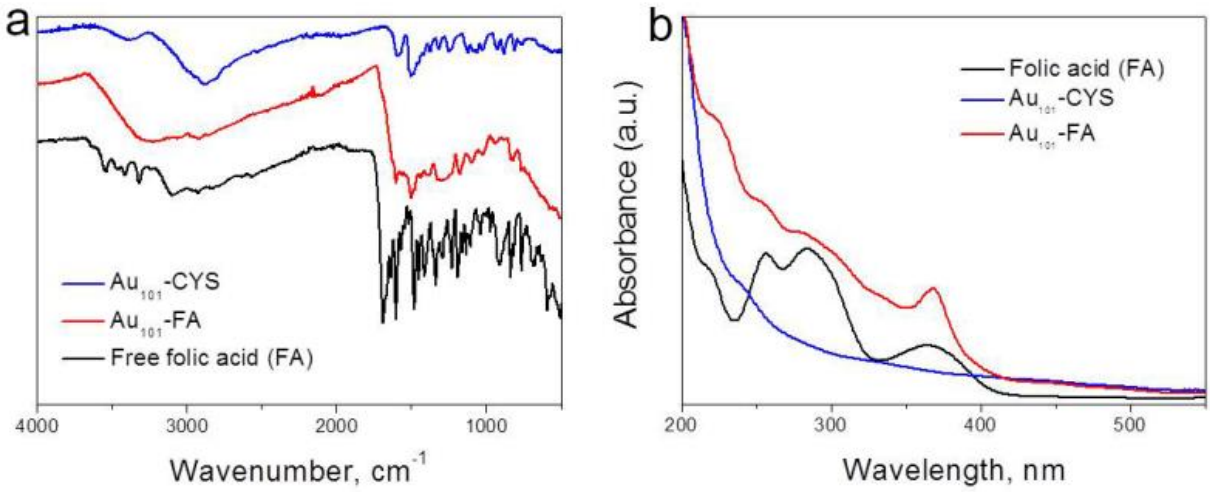

Figure 5.9. a) FT-IR absorption spectra of free folic acid, Au_{101}-CYS and Au_{101}-FA b) UV-vis spectra of aqueous solution of folic acid, Au_{101}-CYS and Au_{101}-FA.

The size of gold particles after ligand exchange with TG, CYS and FA attachment was monitored using TEM. In all cases no significant change in the gold core size was detected upon ligand exchange. Mean gold core diameter remained 1.5 ± 0.3 nm, which demonstrated high stability of Au_{101} particles upon ligand exchange.

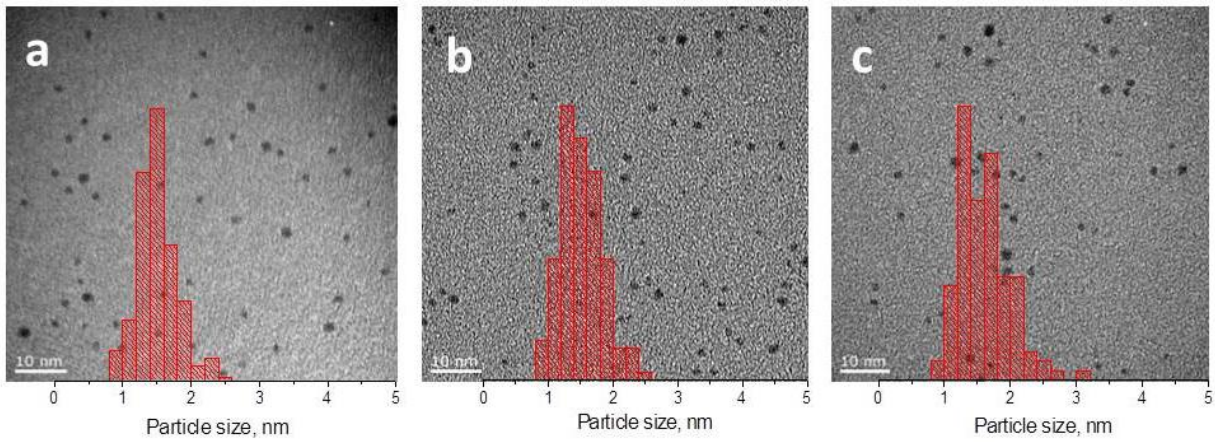

Figure 5.10. Representative TEM images and corresponding particle size distributions of Au_{101}-PPh_3 (a), Au_{101}-FA (b) and Au_{101}-TG (c).

Stability of Au_{101}-TG in Dulbecco's Modified Eagle Medium (DMEM) was studied using TEM. Figure 5.11 shows TEM micrograph of Au_{101}-TG after its incubation in culture media (DMEM) for 24 hours at 37 ˚C and the corresponding particles size distribution. As can be seen from the Figure 5.11, particle size slightly increased to 2.7 ± 0.7 nm and particles retained their spherical shape. Since culture media is a complex mixture, various interactions between the mixture components and gold nanoparticles are possible, which may cause slight particle agglomeration.[283]

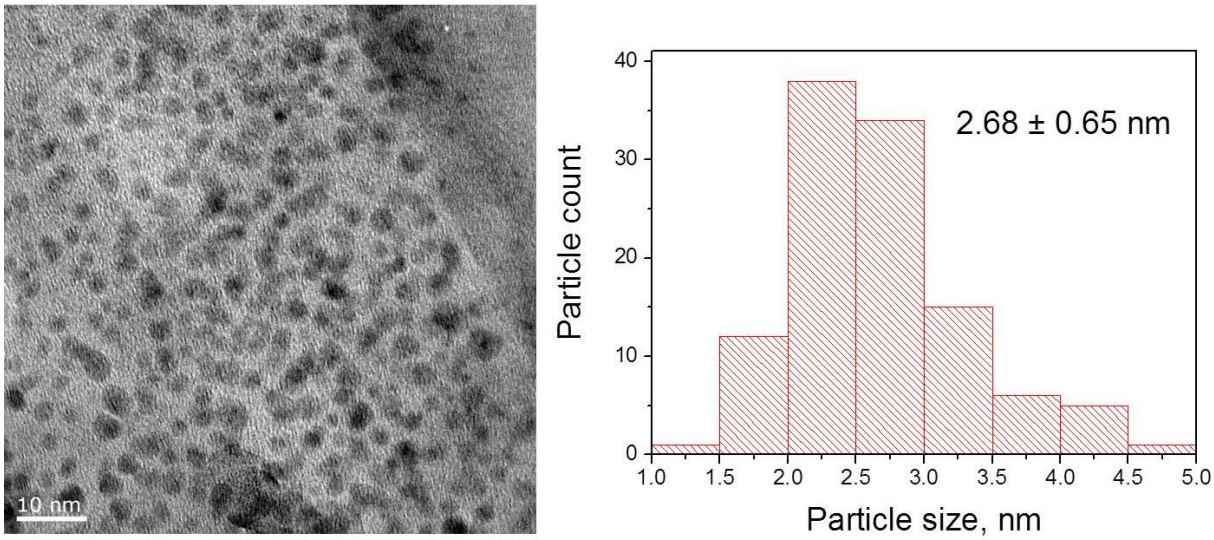

Figure 5.11. Representative TEM micrograph of Au_{101}-TG particles after 24 h incubation in DMEM media (left) and corresponding particle size distribution (right).

Fluorescent nanoparticles Au_{101}-fluorescein were prepared using the same principle of peptide bond formation which was employed for the synthesis of Au_{101}-FA (Figure 5.12). Amino-reactive Fluorescein-EX-5 N-hydroxysuccinimide ester (Invitrogen) was employed to obtain fluorescent nanoparticles. The aqueous solution of Au_{101}-CYS was alkalised using borate buffer in order to deprotonate amino groups of cysteamine, since the succinimidyl ester reacts with deprotonated form of the amino group only.

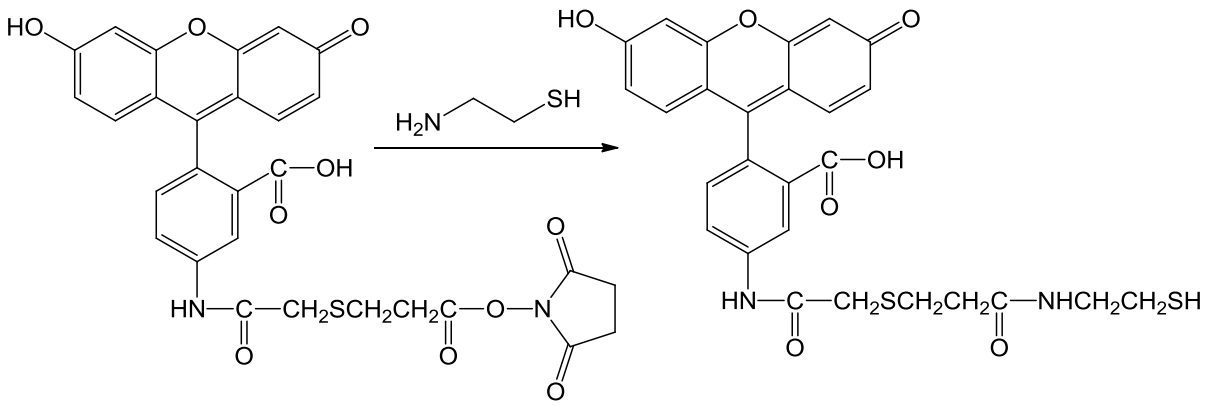

Figure 5.12. Amide bond formation between Fluorescein-5-EX and cysteamine.

Figure 5.13(a) shows fluorescence spectra of aqueous solution of Au_{101}-Fluorescein, purified from the unbound Fluorescein EX-5 using size-exclusion chromatography (Sephadex LH-20). As can be seen from Figure 5.13 the spectra of Au_{101}-Fluorescein nanoparticles match fluorescence spectra of pure Fluorescein EX-5 (Figure 5.13(b)) with the excitation band positioned at 492 nm and emission band at 515 nm. Since Au_{101}-CYS particles are not fluorescent, we can conclude that fluorescein has been successfully attached to Au_{101}-CYS.

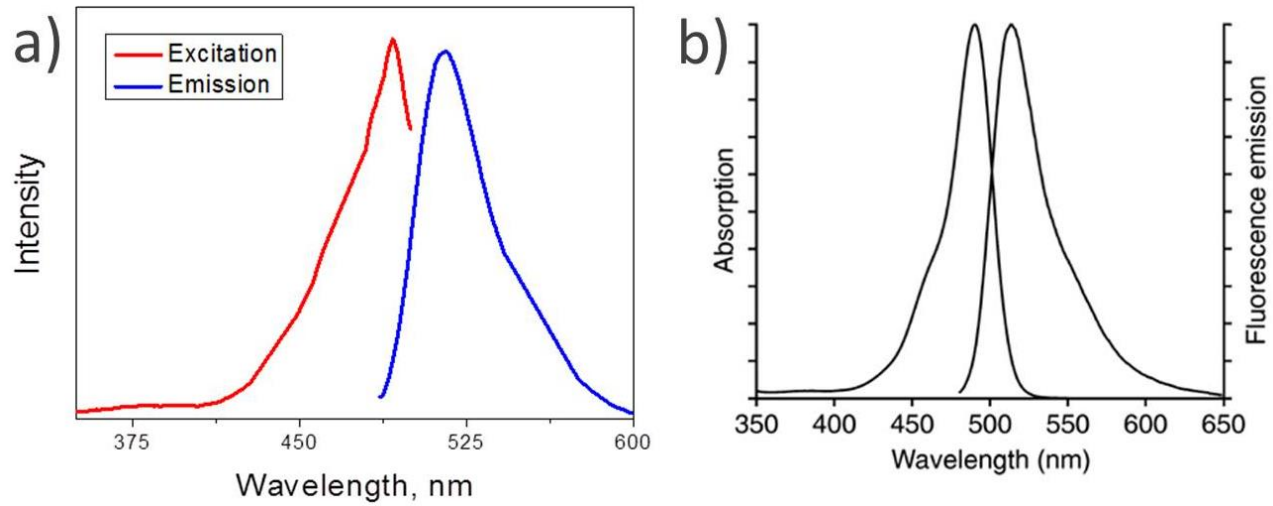

Figure 5.13. Fluorescence spectra of Au_{101}-fluorescein (a) and pure Fluorescein EX-5(b) in water.

5.4.2 Cytotoxicity, uptake and imaging of Au-nanoparticles

In vitro cytotoxicity and uptake of gold nanoparticles were studied on 11 different normal and cancer cell lines (Table 5.1). Normal cell lines tested in this work included NIH3T3 (mouse embryonic fibroblast), HUVEC (endothelium of veins from the umbilical cord, human) and C2C12 (mouse myoblast). Cancer cell lines included OC3, OC2, OEC-M1, SCC-15, SAS – all of which are human oral cancer cell lines, MDA-MB-468 (human breast cancer), Ishikawa (human endometrial cancer) and HepG2 (human hepatocarcinoma).

Cytotoxicity of three different types of particles at different Au concentrations (0.2, 2 and 20 μM, atomic [Au] by AAS) after 24 hour incubation was studied in terms of Au nanoparticle effects on cell proliferation. Cell survival rates were established using Alamar Blue and MTT assays. Both untreated cells and cells, treated with 0.2, 2 and 20 μM Au_{101}-TG, Au_{101}-FA and Au_{101}-CYS, were subjected to Alamar Blue or MTT assay for determination of the cell viability. Cytotoxicity of unconjugated ligands (TG, FA and CYS) was also tested. The results showed no reduction of the viability of all studied cell types in the presence of unbound TG, FA or CYS.

Table 5.1. Cell lines studied in this work

Normal cell line	Cancer cell line
NIH3T3	OC3
HUVEC	OEC-M1
C2C12[a]	SCC-15
	MDA-MB-468
	Ishikawa[a]
	OC2
	HepG2
	SAS

[a]cell lines studied in Christchurch, the rest of the cell lines were tested at the National Cheng Kung University in Taiwan.

Study of the viability of three normal cell lines (NIH3T3, HUVEC and C2C12) in the presence of Au_{101}-TG, Au_{101}-FA and Au_{101}-CYS showed that the viability of these cell types

was not altered significantly in the presence of gold particles at Au concentrations up to 20 μM (Figure 5.14 - Figure 5.16) with more than 90 % cell survival in all cases.

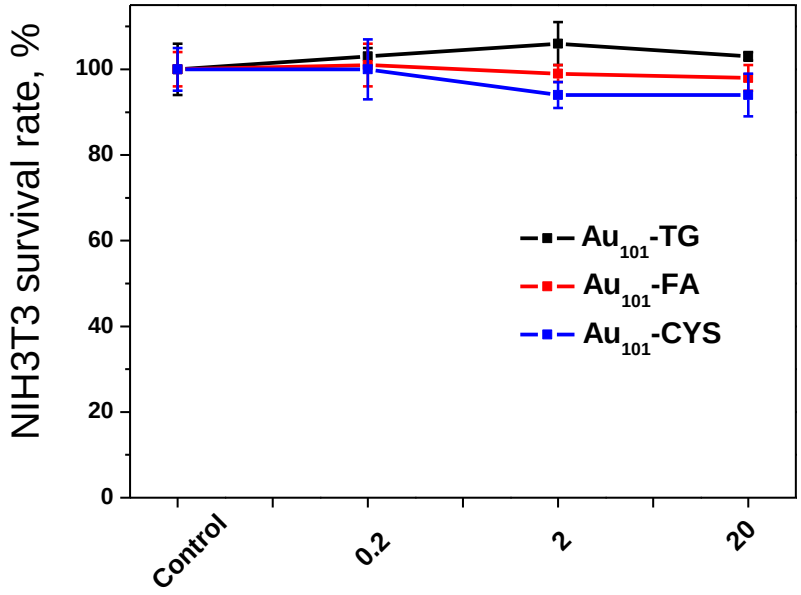

Figure 5.14. Survival rate of NIH3T3 cells treated with 0.2, 2 and 20 μM Au_{101}-TG, Au_{101}-FA and Au_{101}-CYS.

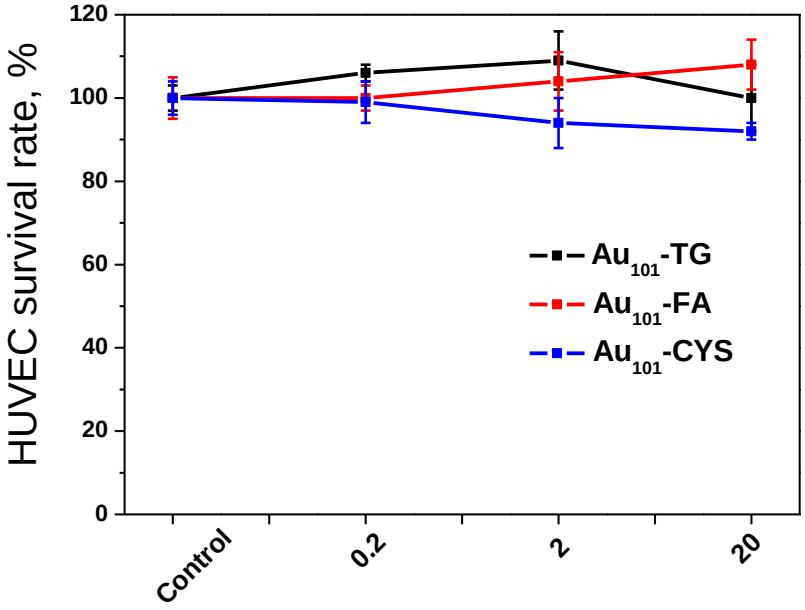

Figure 5.15. Survival rate of HUVEC cells treated with 0.2, 2 and 20 μM Au_{101}-TG, Au_{101}-FA and Au_{101}-CYS.

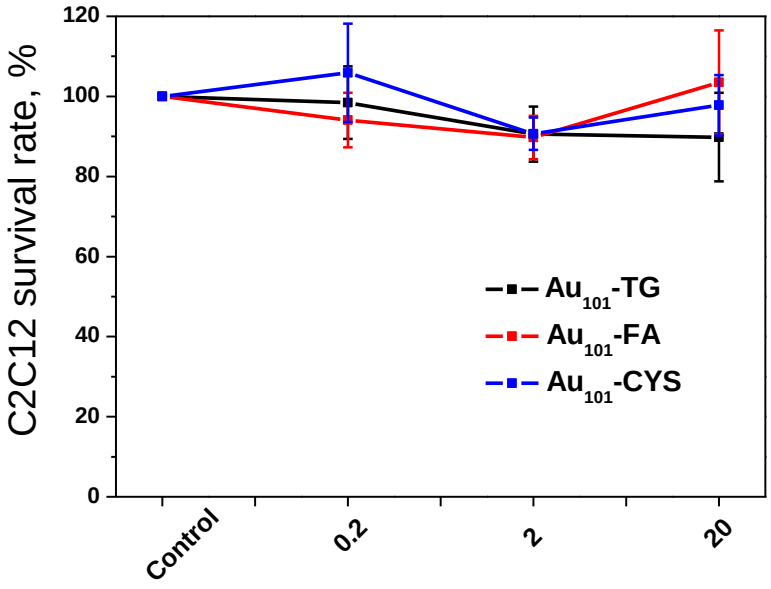

Figure 5.16. Survival rate of C2C12 cells treated with 0.2, 2 and 20 μM Au_{101}-TG, Au_{101}-FA and Au_{101}-CYS.

Au_{101} cytotoxicity study on cancer cell lines SCC15, MDA-MB468 and Ishikawa showed no significant cellular toxicity of the three particles types at three studied concentrations (Figure 5.17 - Figure 5.19) with cell survival values exceeding 95 %, except for Au_{101}-FA treatment (20 μM) of Ishikawa cells. In this case cell viability dropped to 84 %.

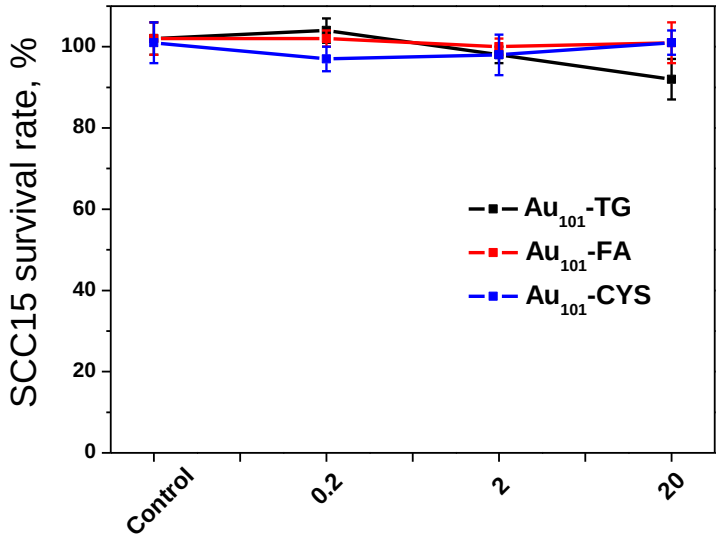

Figure 5.17. Survival rate of SCC15 cells treated with 0.2, 2 and 20 μM Au_{101}-TG, Au_{101}-FA and Au_{101}-CYS.

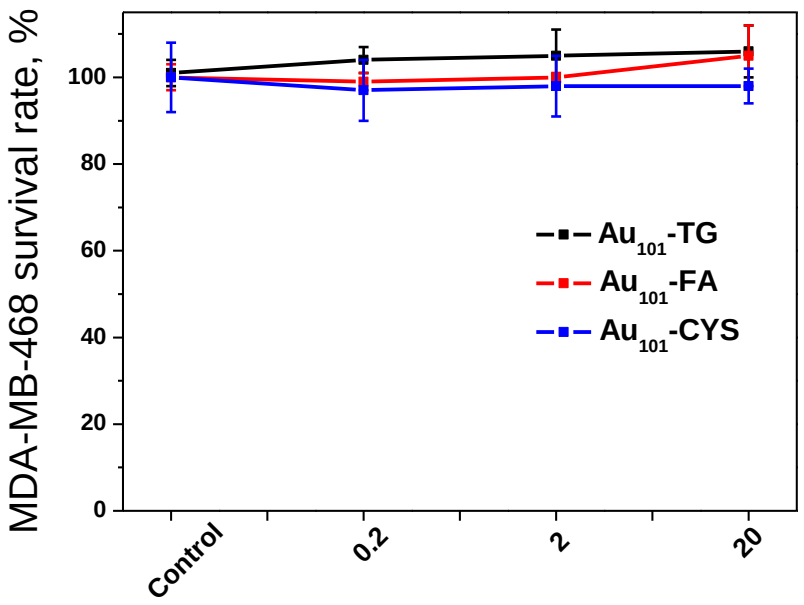

Figure 5.18. Survival rate of MDA-MB-468 cells treated with 0.2, 2 and 20 μM Au_{101}-TG, Au_{101}-FA and Au_{101}-CYS.

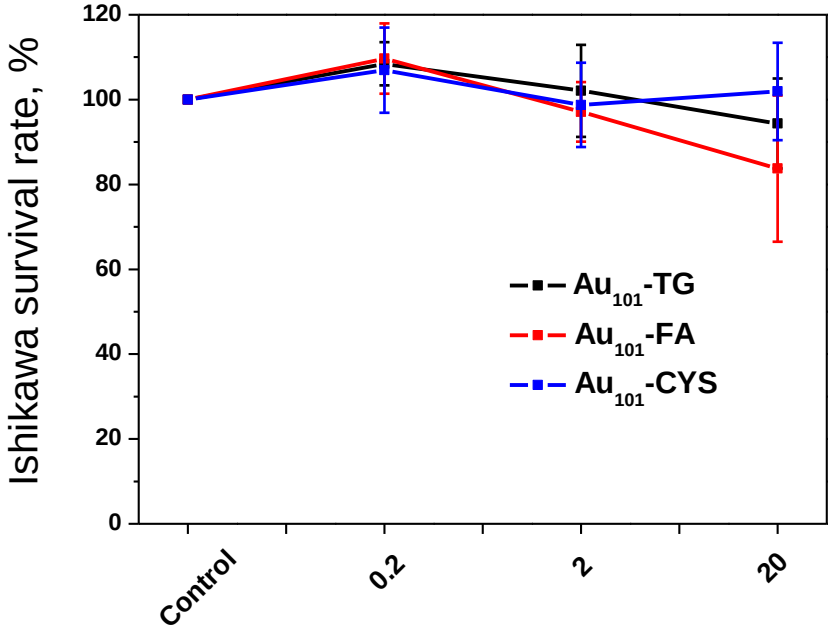

Figure 5.19. Survival rate of Ishikawa cells treated with 0.2, 2 and 20 μM Au_{101}-TG, Au_{101}-FA and Au_{101}-CYS.

Study of the cell viability of OEC-M1 and OC3 lines showed that Au_{101}-FA and Au_{101}-CYS were not significantly toxic at all studied concentrations with cell viabilities being close to 100 % (Figure 5.20 and Figure 5.21). However, moderate cytotoxicity was observed when

cells were treated with Au_{101}-TG. OEC-M1 and OC3 cell viability rate gradually decreased upon increase in concentration of Au_{101}-TG. Cell survival rates were 82 and 75 % for OEC-M1 and OC3, respectively, when they were treated with 20 µM solution of Au_{101}-TG.

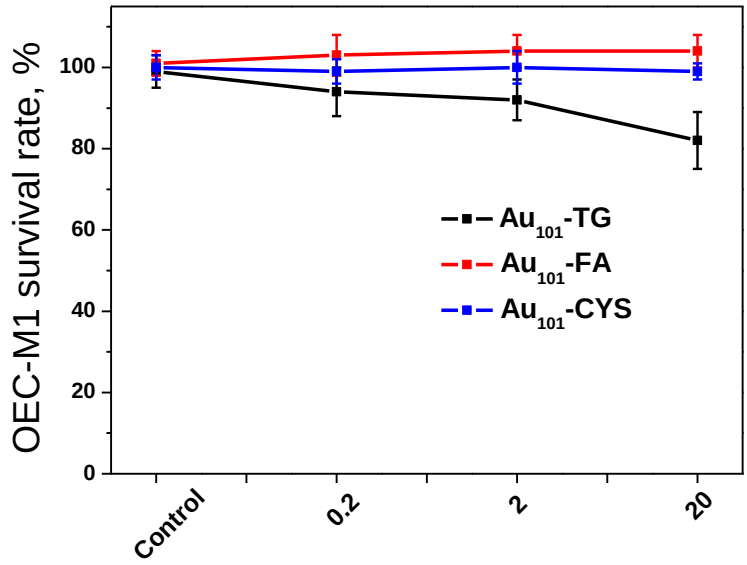

Figure 5.20. Survival rate of OEC-M1 cells treated with 0.2, 2 and 20 µM Au_{101}-TG, Au_{101}-FA and Au_{101}-CYS.

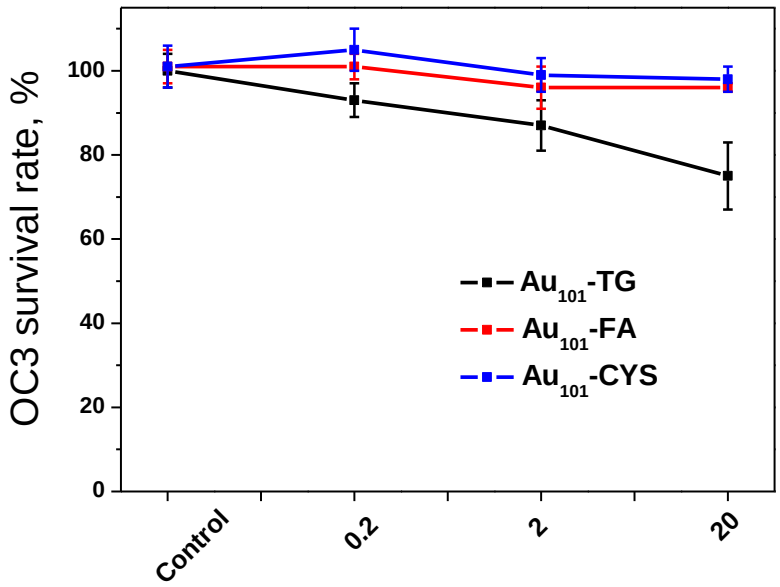

Figure 5.21. Survival rate of OC3 cells treated with 0.2, 2 and 20 µM Au_{101}-TG, Au_{101}-FA and Au_{101}-CYS.

Cell viability study performed on HepG2 cell line in the presence of Au_{101}-TG with Au concentrations ranging from 0.02 to 40 μM showed gradual decrease in cell survival rate to 80 % upon increase in Au concentration (Figure 5.22).

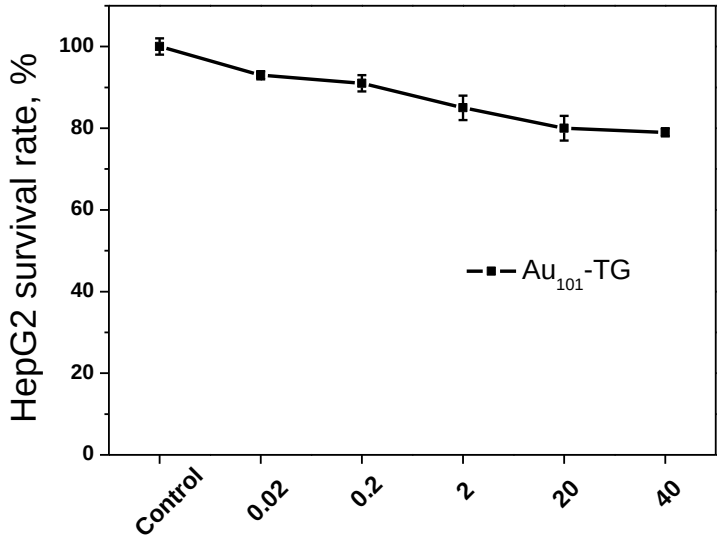

Figure 5.22. Survival rate of HepG2 cells treated with 0.02, 0.2, 2, 20 and 40 μM Au_{101}-TG.

Proliferation of OC2 cells was not significantly affected by the presence of Au_{101}-TG at Au concentrations ranging from 0.02 μM to 20 μM and cell survival rates exceeded 90 (Figure 5.23).

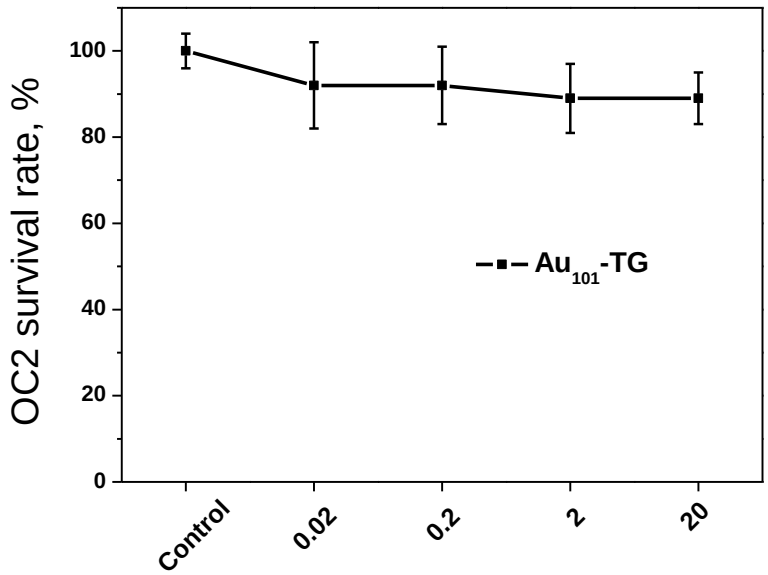

Figure 5.23. Survival rate of OC2 cells treated with 0.02, 0.2, 2 and 20 μM Au101-TG.

The morphology of C2C12 and Ishikawa cell lines in the presence of 0.2 – 20 μM Au_{101}-TG was monitored using optical microscopy. Microscopy study showed no significant change in the morphology of both C2C12 and Ishikawa cells upon incubation in the presence of gold nanoparticles (Figure 5.24 and Figure 5.25), which is consistent with the results of cytotoxicity study.

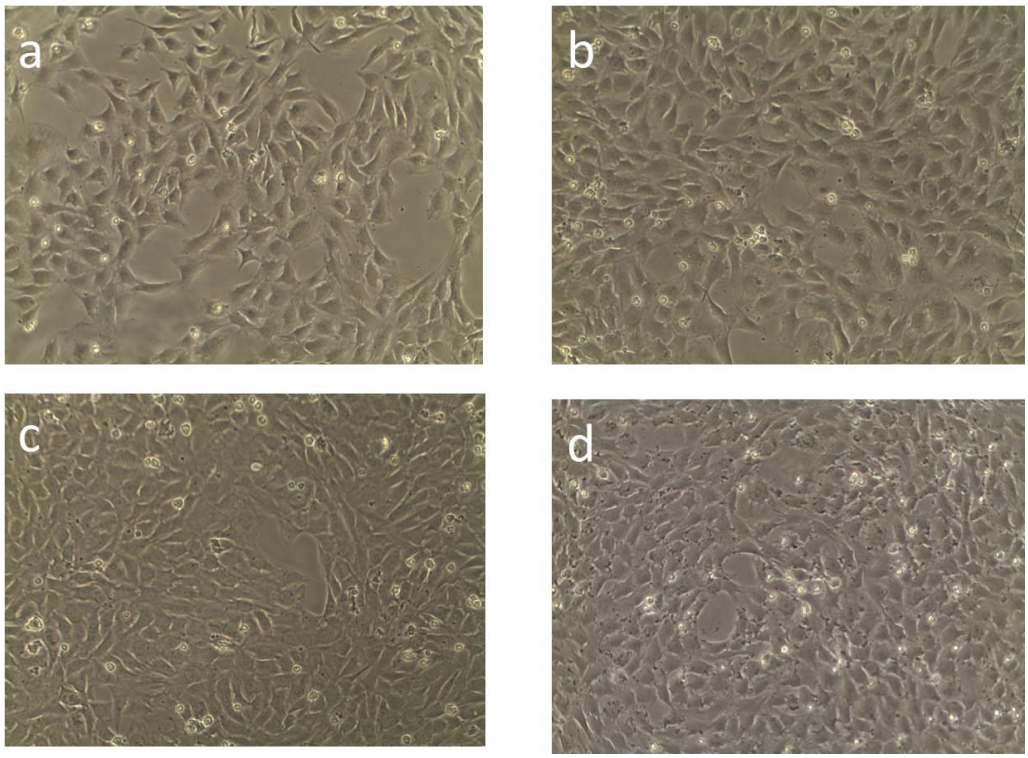

Figure 5.24. Morphology of C2C12 cells treated with Au_{101}-TG: a) no Au_{101} added b) [Au] 0.2 μM c) [Au] 2 μM and d) [Au] 20 μM.

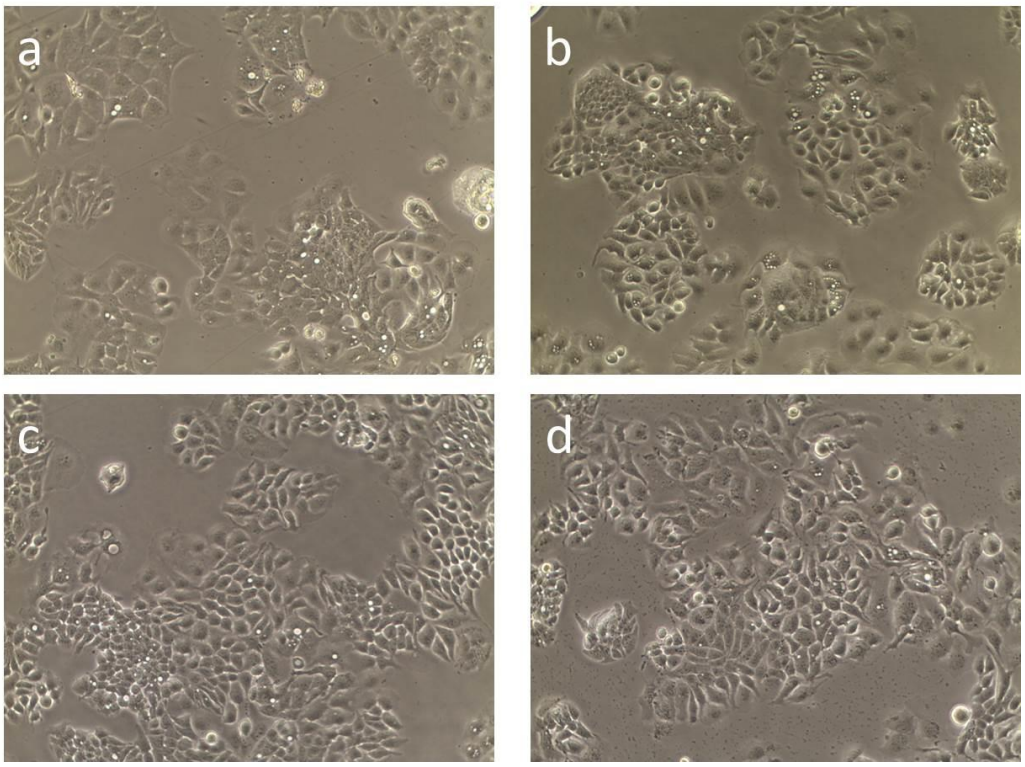

Figure 5.25. Morphology of Ishikawa cells treated with Au_{101}-TG: a) no Au_{101} added b) [Au] 0.2 μM c) [Au] 2 μM and d) [Au] 20 μM.

Fluorescent gold nanoparticles Au_{101}-fluorescein were employed to study particle internalisation and localisation in the cells using fluorescent microscopy. This study was performed on C2C12, Ishikawa and OC3 cell lines.

We observed internalisation of fluorescent Au_{101} particles in all three cell types after 24 h incubation (Figure 5.26 - Figure 5.28). Fluorescent gold nanoparticles can be seen as bright green dots on fluorescent images, whereas cell nuclei are seen as blue objects. As can be seen from the figures, nanoparticles were primarily located in cytoplasm around cell nuclei. Cross-section images demonstrated that particles mostly do not enter cell nuclei (top and right line on fluorescent images). It is known that nanoparticles < 100 nm mainly enter cells by non-specific endocytosis.[237, 284] Shukla et al. studied the pathway of the uptake of Au nanoparticles (3 - 8 nm) by RAW264.7 macrophage cells using various microscopy techniques.[237] The study showed that nanoparticles were internalised in cells through

pinocytosis and localised in lysosomes. The lysosomal bodies slowly moved from cell membranes towards nuclei and eventually arranged around the nuclei without entering them. Gold aggregation was observed inside lysosomes, whereas no Au nanoparticle aggregation was spotted outside macrophage cells. Presumably, nanoparticles in this study go through similar pathway of non-specific pinocytosis with the following localisation in lysosomes. Lysosomal aggregation of gold nanoparticles, functionalised with drug or gene, could in principle release the ligands, thus allowing efficient drug/gene delivery.

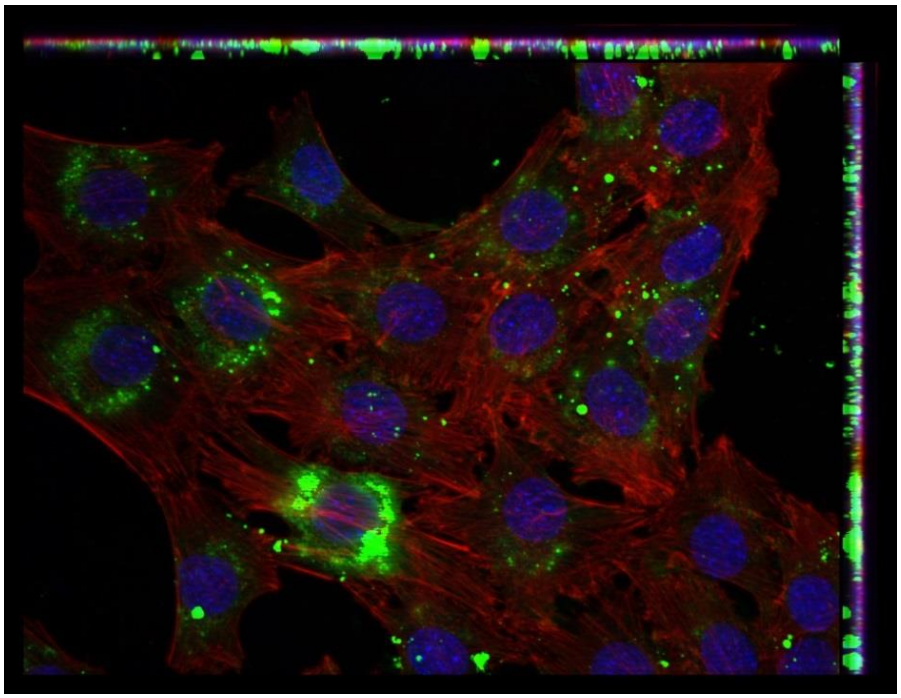

Figure 5.26. Fluorescent Au_{101} nanoparticles in C2C12 cells. Green - gold particles, blue - cell nuclei and red - cell membranes

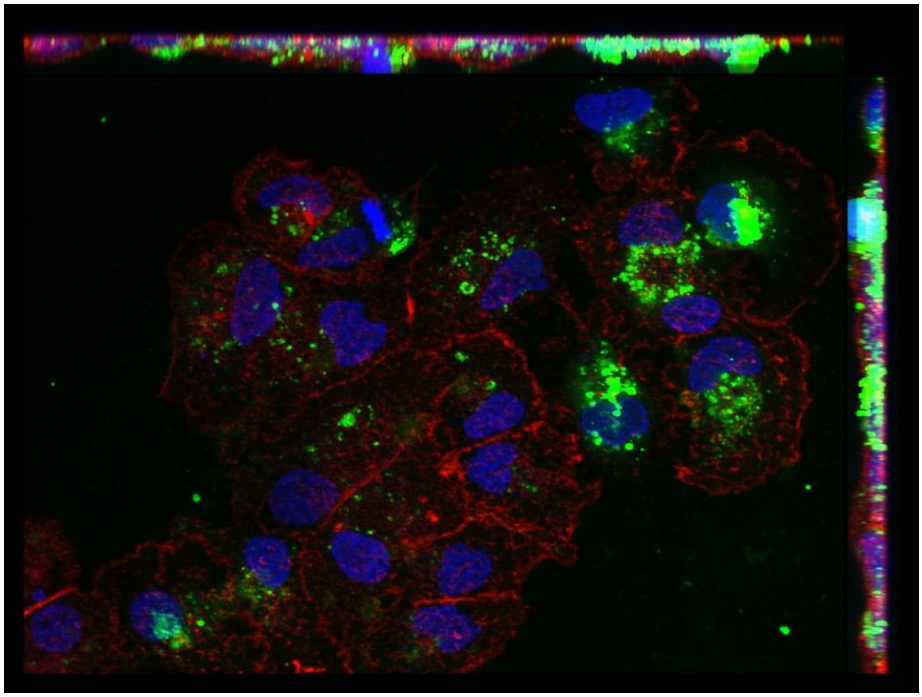

Figure 5.27. Fluorescent Au_{101} nanoparticles in Ishikawa cells. Green - gold particles, blue – cell nuclei and red - cell membranes.

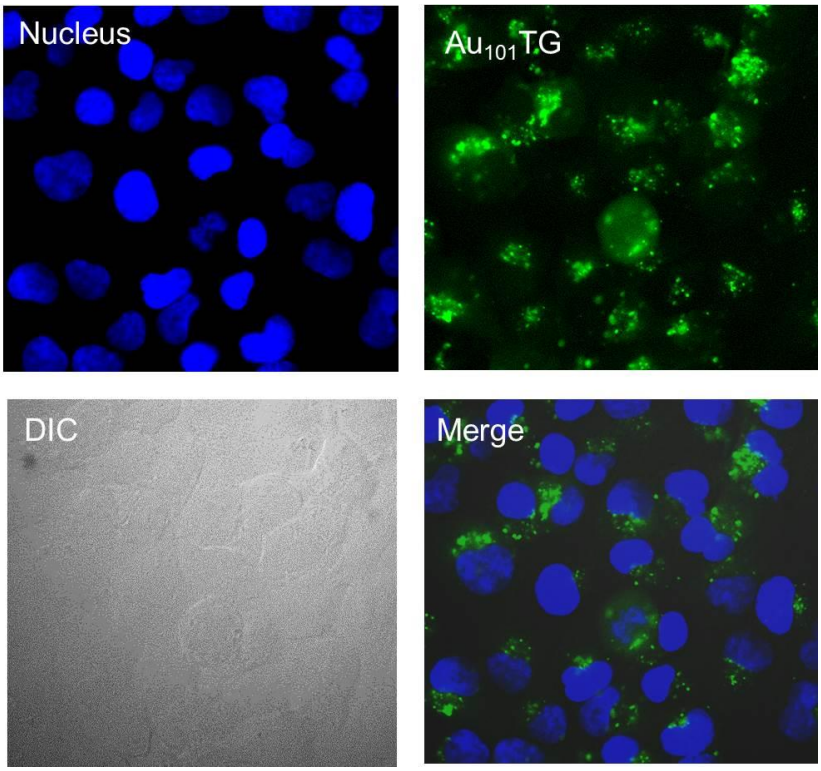

Figure 5.28. Fluorescent Au_{101} nanoparticles in OC3 cells. Each fluorescent image and phase image are shown separately and overlapped (right bottom).

C2C12 and Ishikawa cells were also cultured in the presence of unbound fluorescein. Figure 5.29 shows phase and fluorescent images of Ishikawa and C2C12 cells treated with aqueous fluorescein EX-5 for 24 hours. No fluorescein internalisation by the two types of living cells was observed when it was not bound to gold nanoparticles. Some fluorescence can be observed in Figure 5.29(2b). This is because fluorescein can be cytotoxic and induce cell death. The membranes of the dying cells become leaky; and compounds, such as fluorescein, can easily enter the cells. Thus, the results of the study with unbound fluorescein confirm that fluorescence shown earlier in Figure 5.26 - Figure 5.28 is due to Au_{101}-fluorescein, internalised by cells.

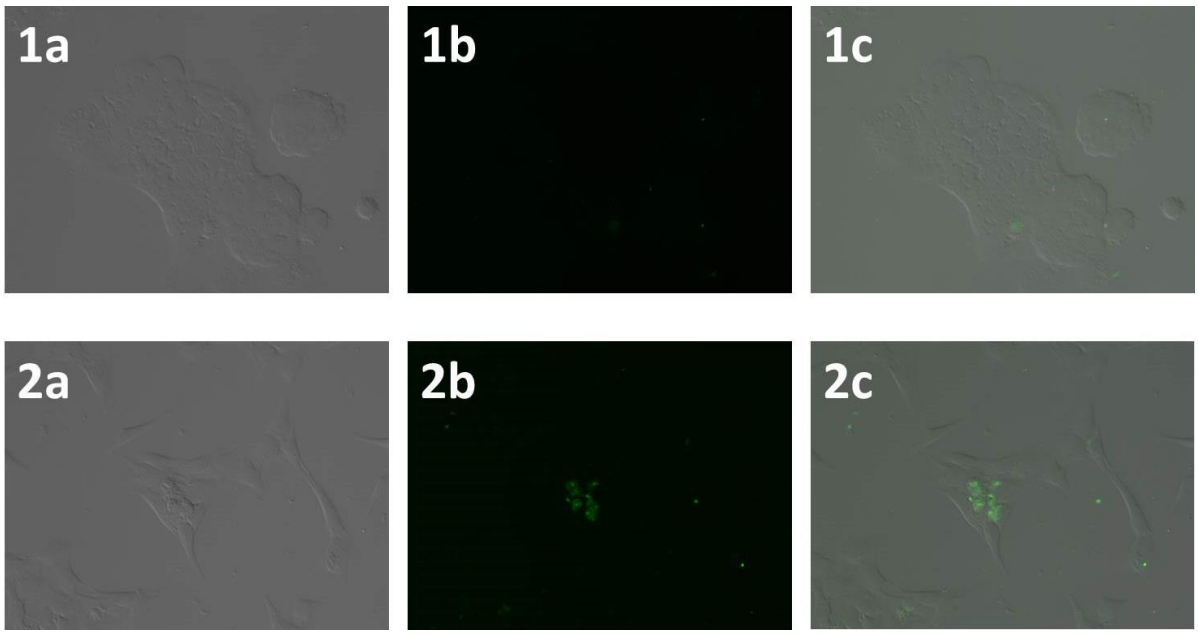

Figure 5.29. Ishikawa (1) and C2C12 (2) cells treated with unbound Fluorescein EX-5. a) phase images b) fluorescent images c) fluorescent image overlapped with phase image.

The cytotoxicity study performed on 10 different normal and cancer cell lines showed that in most cases cell viability was not significantly altered by the presence of Au-nanoparticles stabilized by TG, CYS and FA at Au concentrations reaching 20 μM. Au_{101}-TG showed moderate toxicity, increasing upon the increase in gold concentration, in the case of three cancer cell lines – OEC-M1, OC3 and HepG2. Good biocompatibility of gold

nanoparticles was also confirmed by the unchanged morphology of selected cell lines upon incubation in the presence of 20 μM Au_{101} nanoparticles.

Even though gold particles are generally considered to be non-toxic, previous studies show that some gold nanoparticles could reduce cell viability, depending on their core size, type of stabilizing ligands and concentration.[240, 284-287] Schmid *et al.* studied cytotoxicity of phosphine-stabilised 1.4 nm Au particles and compared it to the cytotoxicity of cisplatin, a routinely applied chemotherapeutic drug.[283] IC_{50} value is the concentration of drug, required to reduce cell survival by 50 % compared to control. The IC_{50} value of 1.4 nm particles after 24 h incubation with a series of different cell lines was lower than that of cisplatin after 72 h incubation, which indicated a significantly higher toxicity of gold particles compared to cisplatin. The suggested reason for such a high toxicity of gold nanoparticles was their strong interaction with DNA. Earlier molecular modelling study showed that naked 1.4 nm Au particles have the same dimensions as the major groves of DNA, which are 0.9 nm in depth and 1.43 nm in length (Figure 5.30).[288] Such geometry favours strong interaction between 1.4 nm nanoparticles and negatively charged oxygen atoms of the phosphate groups of DNA. Gold nanoparticles of different sizes (0.8, 1.2, 1.8 and 15 nm) stabilised with the same ligand were shown to be less toxic, compared to 1.4 nm Au nanoparticles, presumably because of the worse size fit with the major groves of DNA. Importantly, the stabilising ligand was shown to play significant role in particle toxicity: weakly interacting phosphine ligands can be easily replaced with other stronger interacting ligands (such as DNA), whereas thiol-stabilised particles were shown to be completely non-toxic because of the strong interaction between gold and sulphur in thiol which does not allow gold nanoparticle-DNA interaction.[283]

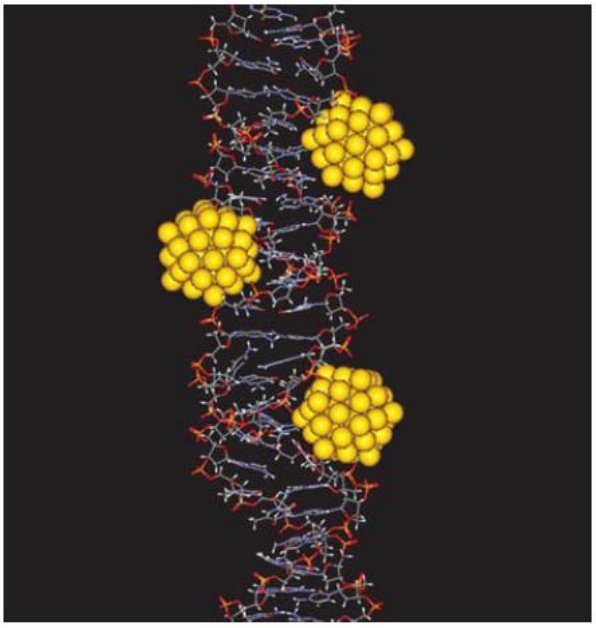

Figure 5.30. Modelling of interaction of 1.4 nm Au particles with the major groves of DNA. Reprinted with permission from ref. [288]. Copyright WILEY-VCH Verlag GmbH & Co. KGaA.

The general non-toxicity of the gold nanoparticles studied in this work could possibly be explained by the slightly larger size (compared to 1.4 nm), greater stability due to strong interaction of the gold core with thiol-ligands and the fact, that Au particles mostly do not enter cell nuclei.

To understand whether higher gold uptake induces greater cytotoxicity, the uptake of Au_{101}-TG by normal and cancer cells was studied. The knowledge of uptake is also important for drug and gene-delivery applications. Figure 5.31 shows data on gold uptake by 9 different cell lines. The initial concentration of Au_{101}-TG was kept the same in all cases ([Au] 20 μM).

The results of the Au_{101}-TG uptake study by various cell lines show that gold uptake varied depending on the cell line and no correlation can be drawn between the extent of the gold uptake and cell line type (cancer or normal). Ishikawa cells showed the highest gold uptake among studied cell lines with $1.8 \cdot 10^8$ Au_{101} particles internalised by one cell. MDA-MB-468, NIH3T3 and HUVEC cell lines showed uptake values of $1.1 \cdot 10^8$, 10^8 and $9.3 \cdot 10^7$ particles/cell, respectively. Interestingly, all the oral cancer cell lines (OEC-M1, SAS, OC2

and OC3) showed relatively low gold uptake with values below $5 \cdot 10^7$ particles/cell. Unfortunately, no other comparative studies on nanoparticle uptake by oral cancer cell lines *vs.* other cancer cell lines were reported in the literature to compare with the results of this study. C2C12 also demonstrated relatively low gold uptake of $2 \cdot 10^7$ particle/cell.

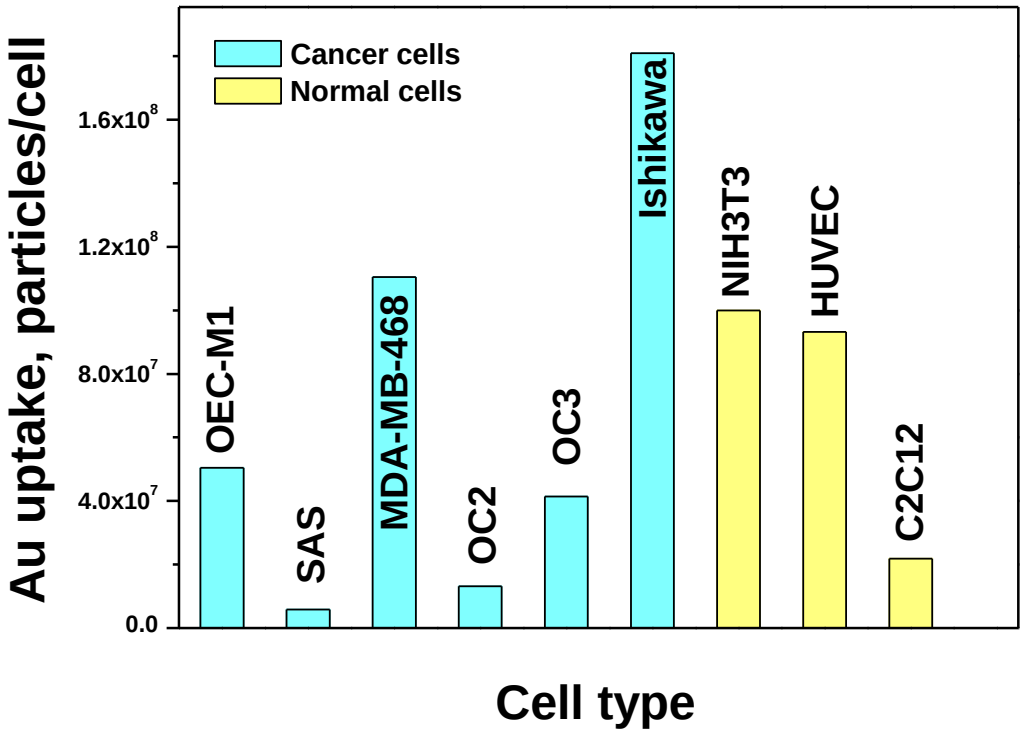

Figure 5.31. Au uptake by normal and cancer cells ([Au] 20 μM).

Comparison of gold uptake results with cytotoxicity data shows that higher uptake does not necessarily induce stronger cytotoxicity. The viability of all four cell lines (Ishikawa, MDA-MB-468, NIH3T3 and HUVEC) with high gold uptake was not altered substantially after cells were treated with 20 μM Au_{101} (Figure 5.14,Figure 5.15, Figure 5.18, Figure 5.19 and Figure 5.31), whereas, gold uptake was relatively low for OEC-M1 and OC3, for which Au_{101}-TG showed some cytotoxicity (Figure 5.20 and Figure 5.21).

The high uptake of gold demonstrated by normal cell lines, along with the biocompatibility of the studied Au nanoparticles could be potentially used for gene, DNA or RNA delivery applications.[273, 289, 290]

We further studied how initial gold concentration affects particle uptake by cells. Ishikawa and C2C12 cells were incubated for 24 h in the presence of gold nanoparticles with Au concentrations 2 and 20 μM. Uptake of three types of gold nanoparticles (2 and 20 μM) by C2C12 and Ishikawa cell lines is shown in Figure 5.32.

Gold nanoparticle uptake at [Au] 2 μM is shown in Figure 5.32A. Both cell types internalised slightly less Au_{101}-CYS compared to Au_{101}-TG and Au_{101}-FA. Gold uptake by Ishikawa cells was significantly (*ca.* 2 – 2.5 times) lower compared to that by C2C12 cells.

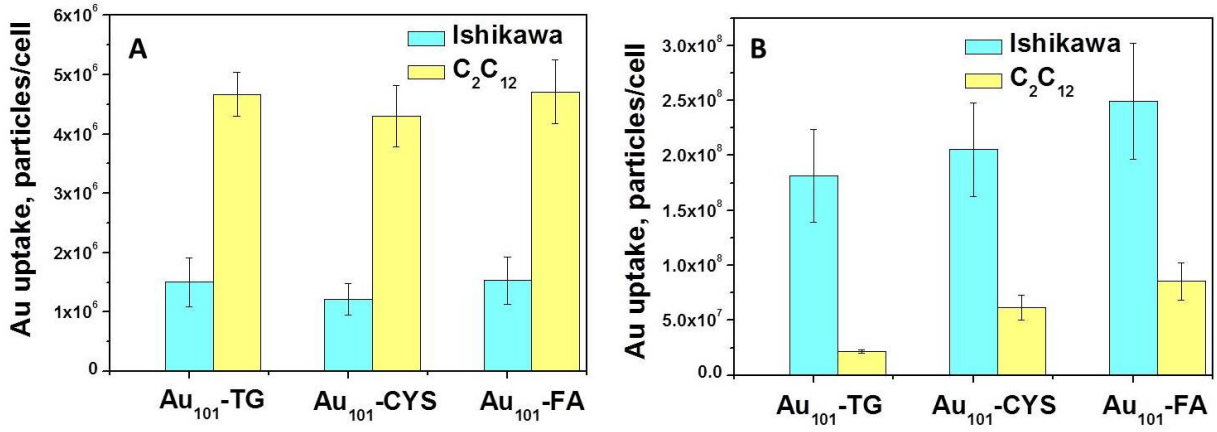

Figure 5.32. Uptake of Au_{101}-TG, Au_{101}-CYS and Au_{101}-FA by Ishikawa and C2C12 cells. Initial Au concentration 2 μM (A) and 20 μM (B).

Interestingly, when the total Au concentration was increased to 20 μM, the trend of gold uptake changed drastically: both cell lines internalised Au_{101} nanoparticles in the following order Au_{101}-FA > Au_{101}-CYS > Au_{101}-TG; and the uptake by Ishikawa cells was significantly higher than that by C2C12 cells (Figure 5.32B).

The same experimental data plotted as a percentage of added gold internalised by cells is shown in Figure 5.33. As can be seen from the Figure 5.33(top), at both concentrations C2C12 cell line internalised very close percentages of gold particles with most values in the range of 10 - 20 %.

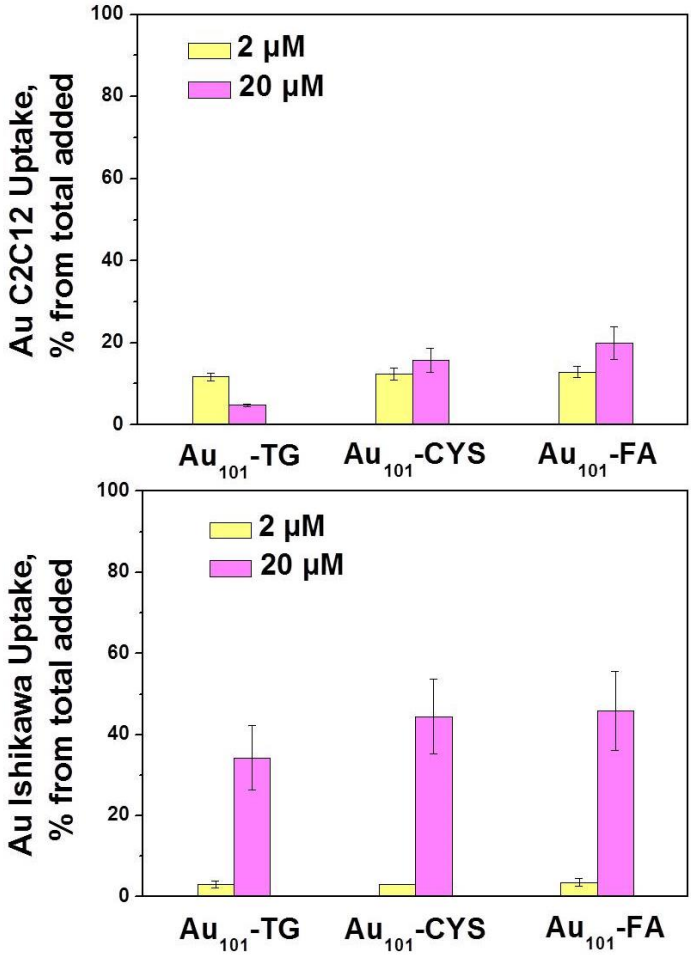

Figure 5.33. Percentage of the total added amount of gold which was internalized by cells (C2C12 top, Ishikawa bottom).

In the case of Ishikawa cell line, 10-fold increase in Au concentration drastically changed the percentage of the gold uptake from *ca.* 3 % to *ca.* 40 %, showing that gold uptake by Ishikawa cells is concentration-dependent. Thus, at lower Au concentration, C2C12 cells internalised higher amount of gold relative to Ishikawa cells, whereas at higher concentration the opposite behaviour was observed. Such a different concentration dependency of gold nanoparticle uptake by C2C12 (normal) and Ishikawa (cancer) cell lines, demonstrated in this work, could be potentially used to deliver higher relative number of particles to either normal or cancer cells depending on the task.

5.5 Summary

In summary, synthesis and characterisation of thiol-stabilised water-soluble gold nanoparticles, derived from $Au_{101}(PPh_3)_{21}Cl_6$ and stabilised with thio-glucose, cysteamine and folic acid, were performed. These particles were used to conduct the study of cytotoxicity, uptake and cell localisation of the gold nanoparticles using a range of normal and cancer cell lines. The following conclusions could be drawn from the results of this study:

1) The cores of Au_{101} nanoparticles were demonstrated to be stable upon ligand exchange and modification; however, they slightly increase to 2.7 nm upon incubation in the culture media at 37 ˚C.
2) Au_{101}, nanoparticles stabilised with different ligands (thio-glucose, cysteamine and folic acid) showed high biocompatibility with the majority of the studied normal and cancer cell lines at Au concentrations up to 20 μM. Au_{101}-TG at high concentration showed some moderate cytotoxicity with 2 oral cancer cell lines.
3) Both fluorescent microscopy and ICP-MS studies demonstrated high cell permeability of gold nanoparticles. Fluorescent microscopy study showed perinuclear localisation of gold nanoparticles. Comparison of the cytotoxicity and gold uptake results showed that there was no correlation between the extent of gold uptake and cytotoxicity.
4) A gold uptake study, performed at two different Au concentrations using Ishikawa (cancer) and C2C12 (normal) cell lines, showed that C2C12 and Ishikawa demonstrated different uptake behaviour: C2C12 internalised a similar percentage of gold independently of the initial gold concentration, whereas the fraction of internalised gold drastically increased for Ishikawa cell upon increase in Au

concentration. Further study is needed for better understanding of the reasons behind such a different behaviour.

5) Gold nanoparticles studied in this work are suitable for further investigation of treatment development due to their high uptake, general biocompatibility and selective toxicity.

In the future similar studies can be performed to study the effect of particle size, cell exposure time on toxicity/uptake of gold nanoparticles and the range of studied concentrations, cell types and ligands can be broadened. Methods and procedures, established in this study, would be highly useful for the following work.

Final remarks and future work

The discovery of catalytic activity of gold nanoparticles was an important finding in catalytic science which triggered extensive research focused on both understanding the physical origins of catalytic activity of gold and exploring new possible industrial applications of gold catalysts. Oxidation processes are among the most promising applications of gold catalysts, for which either exceptional catalytic activity or selectivity of gold were demonstrated.

In this work, small phosphine stabilised atomically precise gold and mixed metal clusters were employed as precursors to highly active supported gold catalysts. The use of the small clusters allowed a better understanding of the optimal size of gold nanoparticles in the aerobic oxidation of cyclohexene. It was found that small phosphine-stabilised clusters, supported on SiO_2, gradually lost their ligand shell and increased in size during catalytic reaction. Comparison of the induction period of cyclohexene oxidation and the formation of large Au particles showed that small Au particles < 2 nm were inactive and the activity appeared only after sufficient number of metallic particles larger than 2 nm formed. The activity was shown to be proportional to the surface of gold exposed to the reagents. Thus, the optimal size of gold nanoparticles for aerobic oxidation of cyclohexene is *ca.* 2 nm. In the future similar studies can be performed to establish the threshold in size of active gold nanoparticles in other reactions.

The nature of catalysis in cyclohexene oxidation was shown to be truly heterogeneous; and catalytic support was found to affect both catalytic activity and selectivity. Study of Au particle size aggregation on two different supports at various gold loadings during catalytic oxidation of cyclohexene showed indications of different mechanisms of particle sintering for small (< 1 nm) and larger (> 1.5 nm) gold clusters. In the future more detailed study could be

performed to establish mechanisms of sintering for particles with different sizes, which in turn will facilitate a rational design of heterogeneous Au catalysts for liquid-phase reactions.

The activity of gold and mixed-metal catalysts was studied in one-pot imine synthesis. Catalysts derived from Au_6, Au_8 and Au_9 demonstrated similarly low activities. Comparison of gold and mixed metal clusters showed strong enhancement of the catalytic activity upon the addition of Pd atoms in one-pot synthesis of imines, whereas no such effect was observed upon the addition of Pt atoms. Catalysts were treated in different ways and the nature of catalyst pre-treatment was shown to affect the activity of catalysts – calcination was shown to produce the most active catalysts among the studied treatments. Further studies of the effect of pre-treatment on the size of gold particles can be performed by either using more sophisticated techniques, such as HAADF STEM, or by studying catalysts with high gold loading (4 – 5 wt%).

Finally, in this project a preliminary study of biological applications of gold nanoparticles derived from Au_{101}-cluster has been performed. Nanoparticles stabilised with four different ligands have been successfully synthesised. Cytotoxicity of the gold nanoparticles was studied on 11 different cancer and normal cell lines. In most cases nanoparticles demonstrated good biocompatibility, with cell survival rates exceeding 90 – 95 %. Au nanoparticles stabilised with thio-glucose showed moderate toxicity on two OC3 and OEC-M1 oral cancer cell lines. Uptake study demonstrated that toxicity is not proportional to the gold uptake: normal cell lines with high survival rate showed high gold uptake, while cancer OC3 and OEC-M1 had relatively low gold uptake. Ishikawa cancer cells and C2C12 cells showed different concentration-dependency of the gold uptake. In the future, this work can be extended to study the effect of particle size, Au concentration, duration of cell exposure to gold nanoparticles on their toxicity/uptake, while the range of studied cell types and targeting ligands can also be broadened.

Bibliography

1. I. Chorkendorff and J. W. Niemantsverdriet, in *Concepts of Modern Catalysis and Kinetics*, Wiley-VCH Verlag GmbH & Co. KGaA, 2005, pp. 1-21.
2. G. Ertl, H. Knoezinger, F. Schueth, J. Weitkamp and Editors, *Handbook of Heterogeneous Catalysis; Volume 1*, Wiley-VCH Verlag GmbH & Co. KGaA, 2008.
3. L. Canali and D. C. Sherrington, *Chemical Society Reviews*, 1999, **28**, 85-93.
4. B. C. Gates, *Chemical Reviews*, 1995, **95**, 511-522.
5. J. A. Anderson, World Scientific Publishing Company, Singapore, 2 edn., 2011.
6. P. Mulvaney, *MRS Bulletin*, 2001, **26**, 1009-1014.
7. M. Faraday, *Philos. Trans. R. Soc. London*, 1857, **147**.
8. J. Turkevich, P. C. Stevenson and J. Hillier, *Discuss. Faraday Soc.*, 1951, **No. 11**, 55-75.
9. C. L. Geoffrey C. Bond, David T. Thompson, *Catalysis by gold*, Imperial College Press, 2006.
10. G. Schmid, R. Pfeil, R. Boese, F. Brandermann, S. Meyer, G. H. M. Calis and d. V. J. W. A. Van, *Chem. Ber.*, 1981, **114**, 3634-3642.
11. F. Wen, U. Englert, B. Gutrath and U. Simon, *European Journal of Inorganic Chemistry*, 2008, 106-111.
12. B. D. Alexander, B. J. Johnson, S. M. Johnson, A. L. Casalnuovo and L. H. Pignolet, *J. Am. Chem. Soc.*, 1986, **108**, 4409-4417.
13. A. M. Mueting, W. Bos, B. D. Alexander, P. D. Boyle, J. A. Casalnuovo, S. Balaban, L. N. Ito, S. M. Johnson and L. H. Pignolet, *New Journal of Chemistry*, 1988, **12**, 505-527.
14. L. N. Ito, B. J. Johnson, A. M. Mueting and L. H. Pignolet, *Inorganic Chemistry*, 1989, **28**, 2026-2028.
15. M. Haruta, T. Kobayashi, H. Sano and N. Yamada, *Chem. Lett.*, 1987, 405-408.
16. M. Haruta, H. Kageyama, N. Kamijo, T. Kobayashi and F. Delannay, *Stud. Surf. Sci. Catal.*, 1989, **44**, 33-42.
17. K. Blick, T. D. Mitrelias, J. S. J. Hargreaves, G. J. Hutchings, R. W. Joyner, C. J. Kiely and F. E. Wagner, *Catal. Lett.*, 1998, **50**, 211-218.
18. S. D. Lin, M. Bollinger and M. A. Vannice, *Catal. Lett.*, 1993, **17**, 245-262.
19. M. Haruta, *CATTECH*, 2002, **6**, 102-115.
20. H. H. Kung, M. C. Kung and C. K. Costello, *J. Catal.*, 2003, **216**, 425-432.
21. M. Haruta, S. Tsubota, T. Kobayashi, H. Kageyama, M. J. Genet and B. Delmon, *J. Catal.*, 1993, **144**, 175-192.
22. R. Zanella, L. Delannoy and C. Louis, *Appl. Catal., A*, 2005, **291**, 62-72.
23. L. Prati and G. Martra, *Gold Bull. (London)*, 1999, **32**, 96-101.

24. R. Zanella, S. Giorgio, C. R. Henry and C. Louis, *J. Phys. Chem. B*, 2002, **106**, 7634-7642.

25. M. Okumura, S. Tsubota and M. Haruta, *J. Mol. Catal. A: Chem.*, 2003, **199**, 73-84.

26. R. V. W. William Arthur Bone, *Philosophical transactions of the royal society A*, 1906, **206**, 1-67.

27. G. C. Bond, *Gold Bull.*, 1972, **5**, 11-13.

28. R. J. Mikovsky, M. Boudart and H. S. Taylor, *J. Am. Chem. Soc.*, 1954, **76**, 3814-3819.

29. H. Wise and K. M. Sancier, *Journal of Catalysis*, 1963, **2**, 149-151.

30. P. A. Sermon, G. C. Bond and P. B. Wells, *Journal of the Chemical Society, Faraday Transactions 1: Physical Chemistry in Condensed Phases*, 1979, **75**, 385-394.

31. J. Erkelens, C. Kemball and A. K. Galwey, *Transactions of the Faraday Society*, 1963, **59**, 1181-1191.

32. P. Claus, *Topics in Catalysis*, 1998, **5**, 51-62.

33. R. Zanella, C. Louis, S. Giorgio and R. Touroude, *Journal of Catalysis*, 2004, **223**, 328-339.

34. P. Claus, *Applied Catalysis A: General*, 2005, **291**, 222-229.

35. M. Shibata, N. Kawata, T. Masumoto and H. Kimura, *Journal of the Chemical Society, Chemical Communications*, 1988, 154-156.

36. J. E. Bailie and G. J. Hutchings, *Chemical Communications*, 1999, 2151-2152.

37. J. E. Bailie, H. A. Abdullah, J. A. Anderson, C. H. Rochester, N. V. Richardson, N. Hodge, J.-G. Zhang, A. Burrows, C. J. Kiely and G. J. Hutchings, *Physical Chemistry Chemical Physics*, 2001, **3**, 4113-4121.

38. Y. Segura, N. López and J. Pérez-Ramírez, *Journal of Catalysis*, 2007, **247**, 383-386.

39. S. H. Inami, B. J. Wood and H. Wise, *Journal of Catalysis*, 1969, **13**, 397-403.

40. J. Słoczyński, R. Grabowski, A. Kozłowska, P. Olszewski, J. Stoch, J. Skrzypek and M. Lachowska, *Applied Catalysis A: General*, 2004, **278**, 11-23.

41. R. A. Koeppel, A. Baiker, C. Schild and A. Wokaun, *Journal of the Chemical Society, Faraday Transactions*, 1991, **87**, 2821-2828.

42. H. Sakurai and M. Haruta, *Applied Catalysis A: General*, 1995, **127**, 93-105.

43. M. Haruta, T. Kobayashi, H. Sano and N. Yamada, *Chemistry Letters*, 1987, 405-408.

44. G. J. Hutchings and M. Haruta, *Applied Catalysis A: General*, 2005, **291**, 2-5.

45. M. Haruta, *J. New Mater. Electrochem. Syst.*, 2004, **7**, 163-172.

46. M. Haruta, *Gold Bull. (London, U. K.)*, 2004, **37**, 27-36.

47. M. Haruta, *J. New Mater. Electrochem. Syst.*, 2004, **7**, 163-172.

48. M. Haruta, *Catal. Today*, 1997, **36**, 153-166.

49. M. Valden, X. Lai and D. W. Goodman, *Science*, 1998, **281**, 1647-1650.

50. M. M. Schubert, S. Hackenberg, V. A. C. van, M. Muhler, V. Plzak and R. J. Behm, *J. Catal.*, 2001, **197**, 113-122.

51. T. V. Choudhary, C. Sivadinarayana, C. C. Chusuei, A. K. Datye, J. P. Fackler, Jr. and D. W. Goodman, *J. Catal.*, 2002, **207**, 247-255.

52. J. Chou, N. R. Franklin, S.-H. Baeck, T. F. Jaramillo and E. W. McFarland, *Catalysis Letters*, 2004, **95**, 107-111.

53. S.-H. Wu, X.-C. Zheng, S.-R. Wang, D.-Z. Han, W.-P. Huang and S.-M. Zhang, *Catalysis Letters*, 2004, **96**, 49-55.

54. S. H. Overbury, V. Schwartz, D. R. Mullins, W. Yan and S. Dai, *J. Catal.*, 2006, **241**, 56-65.

55. M. C. Kung, R. J. Davis and H. H. Kung, *J. Phys. Chem. C*, 2007, **111**, 11767-11775.

56. Tana, F. Wang, H. Li and W. Shen, *Catal. Today*, 2011, **175**, 541-545.

57. G. C. Bond and D. T. Thompson, *Gold Bull. (London)*, 2000, **33**, 41-51.

58. C. K. Costello, J. H. Yang, H. Y. Law, Y. Wang, J. N. Lin, L. D. Marks, M. C. Kung and H. H. Kung, *Appl. Catal., A*, 2003, **243**, 15-24.

59. S. T. Daniells, A. R. Overweg, M. Makkee and J. A. Moulijn, *J. Catal.*, 2005, **230**, 52-65.

60. T. V. W. Janssens, B. S. Clausen, B. Hvolbaek, H. Falsig, C. H. Christensen, T. Bligaard and J. K. Norskov, *Topics in Catalysis*, 2007, **44**, 15-26.

61. http://www.prweb.com/releases/hydrogen_peroxide/bleaching_pulp_paper/prweb9268178.htm.

62. P. Landon, P. J. Collier, A. J. Papworth, C. J. Kiely and G. J. Hutchings, *Chemical Communications*, 2002, 2058-2059.

63. J. K. Edwards, B. E. Solsona, P. Landon, A. F. Carley, A. Herzing, C. J. Kiely and G. J. Hutchings, *Journal of Catalysis*, 2005, **236**, 69-79.

64. J. K. Edwards, B. Solsona, P. Landon, A. F. Carley, A. Herzing, M. Watanabe, C. J. Kiely and G. J. Hutchings, *Journal of Materials Chemistry*, 2005, **15**, 4595-4600.

65. R. A. Sheldon, *Pure and Applied Chemistry*, 2000, **72**, 1233-1246.

66. C. Parmeggiani and F. Cardona, *Green Chemistry*, 2012, **14**, 547-564.

67. C. Della Pina, E. Falletta, L. Prati and M. Rossi, *Chemical Society Reviews*, 2008, **37**, 2077-2095.

68. T. Hayashi, K. Tanaka and M. Haruta, *Journal of Catalysis*, 1998, **178**, 566-575.

69. B. S. Uphade, T. Akita, T. Nakamura and M. Haruta, *Journal of Catalysis*, 2002, **209**, 331-340.

70. C. Qi, T. Akita, M. Okumura, K. Kuraoka and M. Haruta, *Applied Catalysis A: General*, 2003, **253**, 75-89.

71. A. K. Sinha, S. Seelan, T. Akita, S. Tsubota and M. Haruta, *Applied Catalysis A: General*, 2003, **240**, 243-252.

72. C. Qi, M. Okumura, T. Akita and M. Haruta, *Applied Catalysis A: General*, 2004, **263**, 19-26.

73. B. Taylor, J. Lauterbach and W. N. Delgass, *Applied Catalysis A: General*, 2005, **291**, 188-198.

74. M. D. Hughes, Y.-J. Xu, P. Jenkins, P. McMorn, P. Landon, D. I. Enache, A. F. Carley, G. A. Attard, G. J. Hutchings, F. King, E. H. Stitt, P. Johnston, K. Griffin and C. J. Kiely, *Nature (London, U. K.)*, 2005, **437**, 1132-1135.

75. P. Lignier, F. Morfin, S. Mangematin, L. Massin, J.-L. Rousset and V. Caps, *Chem. Commun. (Cambridge, U. K.)*, 2007, 186-188.

76. P. Lignier, F. Morfin, L. Piccolo, J.-L. Rousset and V. Caps, *Catal. Today*, 2007, **122**, 284-291.

77. P. Lignier, S. Mangematin, F. Morfin, J.-L. Rousset and V. Caps, *Catal. Today*, 2008, **138**, 50-54.

78. J. Edwards, P. Landon, A. F. Carley, A. A. Herzing, M. Watanabe, C. J. Kiely and G. J. Hutchings, *J. Mater. Res.*, 2007, **22**, 831-837.

79. N. S. Patil, B. S. Uphade, P. Jana, R. S. Sonawane, S. K. Bhargava and V. R. Choudhary, *Catal. Lett.*, 2004, **94**, 89-93.

80. N. S. Patil, R. Jha, B. S. Uphade, S. K. Bhargava and V. R. Choudhary, *Appl. Catal., A*, 2004, **275**, 87-93.

81. M. Turner, O. P. H. Vaughan and R. M. Lambert, *Chem. Commun. (Cambridge, U. K.)*, 2008, 2316-2318.

82. Y. Zhu, H. Qian and R. Jin, *Chemistry – A European Journal*, 2010, **16**, 11455-11462.

83. P. C. Della, E. Falletta and M. Rossi, *Chemical Society Reviews*, 2012, **41**, 350-369.

84. K. Zhu, J. Hu and R. Richards, *Catal. Lett.*, 2005, **100**, 195-199.

85. Y. Liu, H. Tsunoyama, T. Akita, S. Xie and T. Tsukuda, *ACS Catal.*, 2011, **1**, 2-6.

86. S. E. Davis, M. S. Ide and R. J. Davis, *Green Chemistry*, 2013, **15**, 17-45.

87. H. Tsunoyama, H. Sakurai, Y. Negishi and T. Tsukuda, *J. Am. Chem. Soc.*, 2005, **127**, 9374-9375.

88. T. Hayashi, T. Inagaki, N. Itayama and H. Baba, *Catal. Today*, 2006, **117**, 210-213.

89. N. Dimitratos, J. A. Lopez-Sanchez, D. Morgan, A. Carley, L. Prati and G. J. Hutchings, *Catal. Today*, 2007, **122**, 317-324.

90. V. R. Choudhary, A. Dhar, P. Jana, R. Jha and B. S. Uphade, *Green Chem.*, 2005, **7**, 768-770.

91. P. Haider, B. Kimmerle, F. Krumeich, W. Kleist, J.-D. Grunwaldt and A. Baiker, *Catalysis Letters*, 2008, **125**, 169-176.

92. Y. Liu, H. Tsunoyama, T. Akita and T. Tsukuda, *Chem. Lett.*, 2010, **39**, 159-161.

93. M. Zahmakiran and S. Oezkar, *Mater. Chem. Phys.*, 2010, **121**, 359-363.

94. W. Fang, J. Chen, Q. Zhang, W. Deng and Y. Wang, *Chem.--Eur. J.*, 2011, **17**, 1247-1256, S1247/1241-S1247/1243.

95. S. Carrettin, P. McMorn, P. Johnston, K. Griffin, C. J. Kiely and G. J. Hutchings, *Phys. Chem. Chem. Phys.*, 2003, **5**, 1329-1336.

96. S. Carrettin, P. McMorn, P. Johnston, K. Griffin, C. J. Kiely, G. A. Attard and G. J. Hutchings, *Top. Catal.*, 2004, **27**, 131-136.

97. A. Villa, G. M. Veith and L. Prati, *Angew. Chem., Int. Ed.*, 2010, **49**, 4499-4502, S4499/4491-S4499/4413.

98. E. Skrzynska, J. Ftouni, J.-S. Girardon, M. Capron, L. Jalowiecki-Duhamel, J.-F. Paul and F. Dumeignil, *ChemSusChem*, 2012, **5**, 2065-2078.

99. W. C. Ketchie, Y.-L. Fang, M. S. Wong, M. Murayama and R. J. Davis, *J. Catal.*, 2007, **250**, 94-101.

100. S. Sarina, E. R. Waclawik and H. Zhu, *Green Chem.*, 2013, **15**, 1814-1833.

101. A. R. Sadrolhosseini, A. S. M. Noor and M. M. Moksin, *Application of Surface Plasmon Resonance Based on a Metal Nanoparticle*, 2012.

102. P. V. Kamat, *Journal of Physical Chemistry B*, 2002, **106**, 7729-7744.

103. K. L. Kelly, E. Coronado, L. L. Zhao and G. C. Schatz, *Journal of Physical Chemistry B*, 2003, **107**, 668-677.

104. A. Henglein, *Langmuir*, 1999, **15**, 6738-6744.

105. A. M. Alkilany and C. J. Murphy, *J. Nanopart. Res.*, 2010, **12**, 2313-2333.

106. A. Primo, A. Corma and H. Garcia, *Phys. Chem. Chem. Phys.*, 2011, **13**, 886-910.

107. S. Zhu, S. Liang, Q. Gu, L. Xie, J. Wang, Z. Ding and P. Liu, *Appl. Catal., B*, 2012, **119-120**, 146-155.

108. J. Lee, S. Mubeen, X. Ji, G. D. Stucky and M. Moskovits, *Nano Lett.*, 2012, **12**, 5014-5019.

109. M. Gonzalez-Bejar, K. Peters, G. L. Hallett-Tapley, M. Grenier and J. C. Scaiano, *Chemical Communications*, 2013, **49**, 1732-1734.

110. A. Furube, L. Du, K. Hara, R. Katoh and M. Tachiya, *Journal of the American Chemical Society*, 2007, **129**, 14852-14853.

111. X. Chen, H.-Y. Zhu, J.-C. Zhao, Z.-F. Zheng and X.-P. Gao, *Angew. Chem., Int. Ed.*, 2008, **47**, 5353-5356.

112. X. Zhang, X. Ke and H. Zhu, *Chem. - Eur. J.*, 2012, **18**, 8048-8056.

113. K.-H. Chen, Y.-C. Pu, K.-D. Chang, Y.-F. Liang, C.-M. Liu, J.-W. Yeh, H.-C. Shih and Y.-J. Hsu, *J. Phys. Chem. C*, 2012, **116**, 19039-19045.

114. H. Zhu, X. Chen, Z. Zheng, X. Ke, E. Jaatinen, J. Zhao, C. Guo, T. Xie and D. Wang, *Chem. Commun. (Cambridge, U. K.)*, 2009, 7524-7526.

115. H. Zhu, X. Ke, X. Yang, S. Sarina and H. Liu, *Angewandte Chemie International Edition*, 2010, **49**, 9657-9661.

116. X. Ke, S. Sarina, J. Zhao, X. Zhang, J. Chang and H. Zhu, *Chemical Communications*, 2012, **48**, 3509-3511.

117. S. Sarina, H. Zhu, E. Jaatinen, Q. Xiao, H. Liu, J. Jia, C. Chen and J. Zhao, *Journal of the American Chemical Society*, 2013, **135**, 5793-5801.

118. A. Wang, X. Y. Liu, C.-Y. Mou and T. Zhang, *J. Catal.*, 2013, **308**, 258-271.

119. H.-L. Jiang and Q. Xu, *J. Mater. Chem.*, 2011, **21**, 13705-13725.

120. C. L. Bracey, P. R. Ellis and G. J. Hutchings, *Chem. Soc. Rev.*, 2009, **38**, 2231-2243.

121. D. Wang, A. Villa, F. Porta, L. Prati and D. Su, *J. Phys. Chem. C*, 2008, **112**, 8617-8622.

122. X. Liu, A. Wang, L. Li, T. Zhang, C.-Y. Mou and J.-F. Lee, *J. Catal.*, 2011, **278**, 288-296.

123. X. Liu, A. Wang, X. Yang, T. Zhang, C.-Y. Mou, D.-S. Su and J. Li, *Chem. Mater.*, 2009, **21**, 410-418.

124. S. Xie, H. Tsunoyama, W. Kurashige, Y. Negishi and T. Tsukuda, *ACS Catal.*, 2012, **2**, 1519-1523.

125. G. X. Pei, X. Y. Liu, A. Wang, L. Li, Y. Huang, T. Zhang, J. W. Lee, B. W. L. Jang and C.-Y. Mou, *New J. Chem.*, 2014, **38**, 2043-2051.

126. T. Deronzier, F. Morfin, M. Lomello and J.-L. Rousset, *J. Catal.*, 2014, **311**, 221-229.

127. L. Zhang, W. Wang, A. Wang, Y. Cui, X. Yang, Y. Huang, X. Liu, W. Liu, J.-Y. Son, H. Oji and T. Zhang, *Green Chem.*, 2013, **15**, 2680-2684.

128. J. W. Lee, X. Liu and C.-Y. Mou, *J. Chin. Chem. Soc. (Weinheim, Ger.)*, 2013, **60**, 907-914.

129. X. Huang, X. Wang, X. Wang, X. Wang, M. Tan, W. Ding and X. Lu, *J. Catal.*, 2013, **301**, 217-226.

130. P. Liu and J. K. Norskov, *Phys. Chem. Chem. Phys.*, 2001, **3**, 3814-3818.

131. B. Hvolbæk, T. V. W. Janssens, B. S. Clausen, H. Falsig, C. H. Christensen and J. K. Nørskov, *Nano Today*, 2007, **2**, 14-18.

132. M. M. Schubert, S. Hackenberg, A. C. van Veen, M. Muhler, V. Plzak and R. J. Behm, *Journal of Catalysis*, 2001, **197**, 113-122.

133. F. Boccuzzi, A. Chiorino, M. Manzoli, P. Lu, T. Akita, S. Ichikawa and M. Haruta, *J. Catal.*, 2001, **202**, 256-267.

134. G. Mills, M. S. Gordon and H. Metiu, *Journal of Chemical Physics*, 2003, **118**, 4198-4205.

135. M. Turner, V. B. Golovko, O. P. H. Vaughan, P. Abdulkin, A. Berenguer-Murcia, M. S. Tikhov, B. F. G. Johnson and R. M. Lambert, *Nature (London, U. K.)*, 2008, **454**, 981-983.

136. L. Wang, B. Zhang, W. Zhang, J. Zhang, X. Gao, X. Meng, D. S. Su and F.-S. Xiao, *Chem. Commun. (Cambridge, U. K.)*, 2013, **49**, 3449-3451.

137. M. Boronat, A. Corma, F. Illas, J. Radilla, T. Rodenas and M. J. Sabater, *J. Catal.*, 2011, **278**, 50-58.

138. K.-Q. Sun, S.-W. Luo, N. Xu and B.-Q. Xu, *Catalysis Letters*, 2008, **124**, 238-242.

139. L. Prati and M. Rossi, *J. Catal.*, 1998, **176**, 552-560.

140. P. Haider, J.-D. Grunwaldt and A. Baiker, *Catal. Today*, 2009, **141**, 349-354.

141. F. Porta, L. Prati, M. Rossi, S. Coluccia and G. Martra, *Catal. Today*, 2000, **61**, 165-172.

142. L. Prati and F. Porta, *Appl. Catal., A*, 2005, **291**, 199-203.

143. S. Biella, F. Porta, L. Prati and M. Rossi, *Catal. Lett.*, 2003, **90**, 23-29.

144. P. Haider, A. Urakawa, E. Schmidt and A. Baiker, *J. Mol. Catal. A: Chem.*, 2009, **305**, 161-169.

145. Y. Guan and E. J. M. Hensen, *Applied Catalysis A: General*, 2009, **361**, 49-56.

146. G. J. Hutchings, M. Brust and H. Schmidbaur, *Chemical Society Reviews*, 2008, **37**, 1759-1765.

147. Y. Ofir, B. Samanta and V. M. Rotello, *Chemical Society Reviews*, 2008, **37**, 1814-1825.

148. R. A. Sperling, P. Rivera Gil, F. Zhang, M. Zanella and W. J. Parak, *Chemical Society Reviews*, 2008, **37**, 1896-1908.

149. F. Chemnitius, *Chem.-Ztg.*, 1927, **51**, 823.

150. M. L. Malvano, *Atti della Reale Accademia dei Lincei*, 1908, **17**, 857.

151. L. Malatesta, L. Naldini, G. Simonetta and F. Cariati, *Coord. Chem. Rev.*, 1966, **1**, 255-262.

152. N. H. Takata, A. M. P. Felicissimo and V. G. Young, *Inorg. Chim. Acta*, 2001, **325**, 79-84.

153. J. J. Bour, R. P. F. Kanters, P. P. J. Schlebos and J. J. Steggerda, *Recueil Des Travaux Chimiques Des Pays-Bas-Journal of the Royal Netherlands Chemical Society*, 1988, **107**, 211-215.

154. R. P. F. Kanters, J. J. Bour, P. P. J. Schlebos, W. P. Bosman, H. Behm, J. J. Steggerda, L. N. Ito and L. H. Pignolet, *Inorganic Chemistry*, 1989, **28**, 2591-2594.

155. R. Ugo, F. Cariati and G. La Monica, *Inorg. Synth.*, 1990, **28**, 123-126.

156. d. V. J. W. A. Van, J. J. Bour, W. P. Bosman and J. H. Noordik, *Inorganic Chemistry*, 1983, **22**, 1913-1918.

157. J. W. A. Van der Velden, J. J. Bour, J. J. Steggerda, P. T. Beurskens, M. Roseboom and J. H. Noordik, *Inorganic Chemistry*, 1982, **21**, 4321-4324.

158. M. N. Martin, J. I. Basham, P. Chando and S.-K. Eah, *Langmuir*, 2010, **26**, 7410-7417.

159. D. Zhao, Q. Huo, J. Feng, B. F. Chmelka and G. D. Stucky, *Journal of the American Chemical Society*, 1998, **120**, 6024-6036.

160. L. Bromberg, Y. Diao, H. Wu, S. A. Speakman and T. A. Hatton, *Chemistry of Materials*, 2012, **24**, 1664-1675.

161. Y. Liu, H. Tsunoyama, T. Akita and T. Tsukuda, *The Journal of Physical Chemistry C*, 2009, **113**, 13457-13461.

162. D. A. Shirley, *Phys. Rev. B*, 1972, **[3]5**, 4709-4714.

163. H. P. Hughes and J. A. Scarfe, *J. Phys.: Condens. Matter*, 1996, **8**, 1421-1438.

164. R. D. Mair and A. J. Graupner, *Analytical Chemistry*, 1964, **36**, 194-204.

165. G. B. Shul'pin, *Journal of Molecular Catalysis A: Chemical*, 2002, **189**, 39-66.

166. Y. Liu, H. Tsunoyama, T. Akita and T. Tsukuda, *J. Phys. Chem. C*, 2009, **113**, 13457-13461.

167. J. Kilmartin, R. Sarip, R. Grau-Crespo, T. D. Di, G. Hogarth, C. Prestipino and G. Sankar, *ACS Catal.*, 2012, **2**, 957-963.

168. G. H. Woehrle and J. E. Hutchison, *Inorganic Chemistry*, 2005, **44**, 6149-6158.

169. D. Zhao, J. Feng, Q. Huo, N. Melosh, G. H. Frederickson, B. F. Chmelka and G. D. Stucky, *Science (Washington, D. C.)*, 1998, **279**, 548-552.

170. G. C. Bond and D. T. Thompson, *Catalysis Reviews*, 1999, **41**, 319-388.

171. R. Vankayala, A. Sagadevan, P. Vijayaraghavan, C.-L. Kuo and K. C. Hwang, *Angew. Chem., Int. Ed.*, 2011, **50**, 10640-10644, S10640/10641-S10640/10646.

172. M. Sun and H. Xu, *Small*, 2012, **8**, 2777-2786.

173. P. Christopher, H. Xin and S. Linic, *Nat. Chem.*, 2011, **3**, 467-472.

174. C. Battistoni, G. Mattogno, F. Cariati, L. Naldini and A. Sgamellotti, *Inorganica Chimica Acta*, 1977, **24**, 207-210.

175. C. H. A. Tsang, Y. Liu, Z. Kang, D. D. D. Ma, N.-B. Wong and S.-T. Lee, *Chemical Communications*, 2009, 5829-5831.

176. Z.-Y. Cai, M.-Q. Zhu, J. Chen, Y.-Y. Shen, J. Zhao, Y. Tang and X.-Z. Chen, *Catalysis Communications*, 2010, **12**, 197-201.

177. L. Alves, B. Ballesteros, M. Boronat, J. R. Cabrero-Antonino, P. Concepción, A. Corma, M. A. Correa-Duarte and E. Mendoza, *Journal of the American Chemical Society*, 2011, **133**, 10251-10261.

178. S. M. Mahajani, M. M. Sharma and T. Sridhar, *Chemical Engineering Science*, 1999, **54**, 3967-3976.

179. M. Conte, X. Liu, D. M. Murphy, K. Whiston and G. J. Hutchings, *Physical Chemistry Chemical Physics*, 2012, **14**, 16279-16285.

180. G. Lue, D. Ji, G. Qian, Y. Qi, X. Wang and J. Suo, *Appl. Catal., A*, 2005, **280**, 175-180.

181. H. E. B. Lempers and R. A. Sheldon, *Journal of Catalysis*, 1998, **175**, 62-69.

182. C. Venturello, R. D'Aloisio, J. C. J. Bart and M. Ricci, *Journal of Molecular Catalysis*, 1985, **32**, 107-110.

183. R. Bera and S. Koner, *Inorganica Chimica Acta*, 2012, **384**, 233-238.

184. A. T. Bolsoni, J. S. dos Santos, M. D. Assis and H. P. Oliveira, *Journal of Non-Crystalline Solids*, 2011, **357**, 3301-3306.

185. K. Kamata, K. Yonehara, Y. Sumida, K. Hirata, S. Nojima and N. Mizuno, *Angewandte Chemie International Edition*, 2011, **50**, 12062-12066.

186. N. V. Maksimchuk, O. V. Zalomaeva, I. Y. Skobelev, K. A. Kovalenko, V. P. Fedin and O. A. Kholdeeva, *Proceedings of the Royal Society A: Mathematical, Physical and Engineering Science*, 2012.

187. I. Y. Skobelev, A. B. Sorokin, K. A. Kovalenko, V. P. Fedin and O. A. Kholdeeva, *Journal of Catalysis*, 2013, **298**, 61-69.

188. L. Jiang, L. Jin, H. Tian, X. Yuan, X. Yu and Q. Xu, *Chemical Communications*, 2011, **47**, 10833-10835.

189. H. Tian, X. Yu, Q. Li, J. Wang and Q. Xu, *Advanced Synthesis & Catalysis*, 2012, **354**, 2671-2677.

190. H. Sun, F.-Z. Su, J. Ni, Y. Cao, H.-Y. He and K.-N. Fan, *Angewandte Chemie International Edition*, 2009, **48**, 4390-4393.

191. E. Zhang, H. Tian, S. Xu, X. Yu and Q. Xu, *Organic Letters*, 2013, **15**, 2704-2707.

192. M. S. Kwon, S. Kim, S. Park, W. Bosco, R. K. Chidrala and J. Park, *The Journal of Organic Chemistry*, 2009, **74**, 2877-2879.

193. Y. Shiraishi, M. Ikeda, D. Tsukamoto, S. Tanaka and T. Hirai, *Chemical Communications*, 2011, **47**, 4811-4813.

194. J.-F. Soule, H. Miyamura and S. Kobayashi, *Chemical Communications*, 2013, **49**, 355-357.

195. S. F. Martin, *Pure Appl. Chem.*, 2009, **81**, 195-204.

196. N. Li, X. Lang, W. Ma, H. Ji, C. Chen and J. Zhao, *Chemical Communications*, 2013, **49**, 5034-5036.

197. S.-i. Naya, K. Kimura and H. Tada, *ACS Catalysis*, 2012, **3**, 10-13.

198. A. Grirrane, A. Corma and H. Garcia, *Journal of Catalysis*, 2009, **264**, 138-144.

199. B. Zhu, M. Lazar, B. G. Trewyn and R. J. Angelici, *Journal of Catalysis*, 2008, **260**, 1-6.

200. A. Zanardi, J. A. Mata and E. Peris, *Chemistry – A European Journal*, 2010, **16**, 10502-10506.

201. R. D. Patil and S. Adimurthy, *Advanced Synthesis & Catalysis*, 2011, **353**, 1695-1700.

202. C. Xu, L. Y. Goh and S. A. Pullarkat, *Organometallics*, 2011, **30**, 6499-6502.

203. J. W. Rigoli, S. A. Moyer, S. D. Pearce and J. M. Schomaker, *Org. Biomol. Chem.*, 2012, **10**, 1746-1749.

204. S. Sithambaram, R. Kumar, Y.-C. Son and S. L. Suib, *J. Catal.*, 2008, **253**, 269-277.

205. Q. Kang and Y. Zhang, *Green Chem.*, 2012, **14**, 1016-1019.

206. S. Kegnaes, J. Mielby, U. V. Mentzel, C. H. Christensen and A. Riisager, *Green Chemistry*, 2010, **12**, 1437-1441.

207. J. A. Lopez-Sanchez, N. Dimitratos, C. Hammond, G. L. Brett, L. Kesavan, S. White, P. Miedziak, R. Tiruvalam, R. L. Jenkins, A. F. Carley, D. Knight, C. J. Kiely and G. J. Hutchings, *Nat. Chem.*, 2011, **3**, 551-556.

208. L. D. Menard, F. Xu, R. G. Nuzzo and J. C. Yang, *J. Catal.*, 2006, **243**, 64-73.

209. P. Wagener, A. Schwenke and S. Barcikowski, *Langmuir*, 2012, **28**, 6132-6140.

210. C. Della Pina, E. Falletta, M. Rossi and A. Sacco, *J. Catal.*, 2009, **263**, 92-97.

211. K. Chen, H. Wu, Q. Hua, S. Chang and W. Huang, *Physical Chemistry Chemical Physics*, 2013, **15**, 2273-2277.

212. A. Quintanilla, V. C. L. Butselaar-Orthlieb, C. Kwakernaak, W. G. Sloof, M. T. Kreutzer and F. Kapteijn, *J. Catal.*, 2010, **271**, 104-114.

213. M. Zhang, Q. Wang, C. Chen, L. Zang, W. Ma and J. Zhao, *Angewandte Chemie International Edition*, 2009, **48**, 6081-6084.

214. X. Lang, H. Ji, C. Chen, W. Ma and J. Zhao, *Angewandte Chemie International Edition*, 2011, **50**, 3934-3937.

215. J.-D. Grunwaldt, C. Kiener, C. Wogerbauer and A. Baiker, *J. Catal.*, 1999, **181**, 223-232.

216. J.-D. Grunwaldt, M. Maciejewski, O. S. Becker, P. Fabrizioli and A. Baiker, *J. Catal.*, 1999, **186**, 458-469.

217. J. Llorca, M. Dominguez, C. Ledesma, R. J. Chimentao, F. Medina, J. Sueiras, I. Angurell, M. Seco and O. Rossell, *J. Catal.*, 2008, **258**, 187-198.

218. K. Y. Ho and K. L. Yeung, *J. Catal.*, 2006, **242**, 131-141.

219. S. H. Overbury, L. Ortiz-Soto, H. Zhu, B. Lee, M. D. Amiridis and S. Dai, *Catalysis Letters*, 2004, **95**, 99-106.

220. D. P. Anderson, J. F. Alvino, A. Gentleman, H. A. Qahtani, L. Thomsen, M. I. J. Polson, G. F. Metha, V. B. Golovko and G. G. Andersson, *Physical Chemistry Chemical Physics*, 2013, **15**, 3917-3929.

221. Z. Zhang, H. Li, F. Zhang, Y. Wu, Z. Guo, L. Zhou and J. Li, *Langmuir*, 2014, **30**, 2648-2659.

222. S. Deki, K. Akamatsu, Y. Hatakenaka, M. Mizuhata and A. Kajinami, *Nanostruct. Mater.*, 1999, **11**, 59-65.

223. N. Toshima, M. Harada, Y. Yamazaki and K. Asakura, *J. Phys. Chem.*, 1992, **96**, 9927-9933.

224. S. Marx and A. Baiker, *The Journal of Physical Chemistry C*, 2009, **113**, 6191-6201.

225. P. Weinberger, L. Szunyogh and B. I. Bennett, *Phys. Rev. B: Condens. Matter*, 1993, **47**, 10154-10157.

226. P. A. P. Nascente, S. G. C. De Castro, R. Landers and G. G. Kleiman, *Phys. Rev. B: Condens. Matter*, 1991, **43**, 4659-4666.

227. T.-U. Nahm, R. Jung, J.-Y. Kim, W. G. Park, S. J. Oh, J. H. Park, J. W. Allen, S. M. Chung, Y. S. Lee and C. N. Whang, *Phys. Rev. B: Condens. Matter Mater. Phys.*, 1998, **58**, 9817-9825.

228. Y. M. Shulga, A. V. Bulatov, R. A. T. Gould, W. V. Konze and L. H. Pignolet, *Inorganic Chemistry*, 1992, **31**, 4704-4706.

229. W. Cui, H. Zhu, M. Jia, W. Ao, Y. Zhang and B. Zhaorigetu, *Reac Kinet Mech Cat*, 2013, **109**, 551-562.

230. X. Yang, C. Huang, Z. Fu, H. Song, S. Liao, Y. Su, L. Du and X. Li, *Appl. Catal., B*, 2013, **140-141**, 419-425.

231. Y. Chen, H. Lim, Q. Tang, Y. Gao, T. Sun, Q. Yan and Y. Yang, *Appl. Catal., A*, 2010, **380**, 55-65.

232. S. Ghadamgahi, 2014.

233. M. S. Khan, G. D. Vishakante and H. Siddaramaiah, *Adv. Colloid Interface Sci.*, 2013, **199-200**, 44-58.

234. M. Z. Ahmad, S. Akhter, Z. Rahman, S. Akhter, M. Anwar, N. Mallik and F. J. Ahmad, *J. Pharm. Pharmacol.*, 2013, **65**, 634-651.

235. S. R. Butle and P. R. Baheti, *Int. J. Pharm. Sci. Rev. Res.*, 2011, **10**, 54-59.

236. K. S. Shiva, T. P. Shukla, P. S. Vara, C. H. Priyanka and K. Ramanjaneyulu, *Int. J. Pharm. Sci. Rev. Res.*, 2012, **12**, 15-21.

237. R. Shukla, V. Bansal, M. Chaudhary, A. Basu, R. R. Bhonde and M. Sastry, *Langmuir*, 2005, **21**, 10644-10654.

238. L. Vigderman, P. Manna and E. R. Zubarev, *Angew. Chem., Int. Ed.*, 2012, **51**, 636-641, S636/631-S636/638.

239. Y.-S. Chen, Y.-C. Hung, I. Liau and G. S. Huang, *Nanoscale Res. Lett.*, 2009, **4**, 858-864.

240. W.-S. Cho, M. Cho, J. Jeong, M. Choi, H.-Y. Cho, B. S. Han, S. H. Kim, H. O. Kim, Y. T. Lim, B. H. Chung and J. Jeong, *Toxicol. Appl. Pharmacol.*, 2009, **236**, 16-24.

241. Y. Pan, S. Neuss, A. Leifert, M. Fischler, F. Wen, U. Simon, G. Schmid, W. Brandau and W. Jahnen-Dechent, *Small*, 2007, **3**, 1941-1949.

242. R. Hu, K.-T. Yong, I. Roy, H. Ding, S. He and P. N. Prasad, *J. Phys. Chem. C*, 2009, **113**, 2676-2684.

243. H. Maeda, G. Y. Bharate and J. Daruwalla, *Eur. J. Pharm. Biopharm.*, 2009, **71**, 409-419.

244. S. Lal, S. E. Clare and N. J. Halas, *Accounts of Chemical Research*, 2008, **41**, 1842-1851.

245. M. Wang and M. Thanou, *Pharmacol. Res.*, 2010, **62**, 90-99.

246. S. D. Brown, P. Nativo, J. A. Smith, D. Stirling, P. R. Edwards, B. Venugopal, D. J. Flint, J. A. Plumb, D. Graham and N. J. Wheate, *Journal of the American Chemical Society*, 2010, **132**, 4678-4684.

247. F. Geng, K. Song, J. Z. Xing, C. Yuan, S. Yan, Q. Yang, J. Chen and B. Kong, *Nanotechnology*, 2011, **22**, 285101/285101-285101/285108, S285101/285101.

248. B. Asadishad, M. Vosoughi, I. Alamzadeh and A. Tavakoli, *J. Dispersion Sci. Technol.*, 2010, **31**, 492-500.

249. L. E. Kelemen, *Int. J. Cancer*, 2006, **119**, 243-250.

250. K. S. Brandenburg, A. Shakeri-Zadeh, R. Hashemian and G. A. Mansoori, Folate-conjugated gold nanoparticles for cancer nanotechnology applications, 2011.

251. H. Jin, P. Yang, J. Cai, J. Wang and M. Liu, *Appl. Microbiol. Biotechnol.*, 2012, **94**, 1199-1208.

252. J. Park, W. I. Jeon, S. Y. Lee, K.-S. Ock, J. H. Seo, J. Park, E.-O. Ganbold, K. Cho, N. W. Song and S.-W. Joo, *J. Biomed. Mater. Res., Part A*, 2012, **100A**, 1221-1228.

253. B. Stella, V. Marsaud, S. Arpicco, G. Geraud, L. Cattel, P. Couvreur and J.-M. Renoir, *J. Drug Targeting*, 2007, **15**, 146-153.

254. J. Weng, Z. Zhang, L. Sun and J. A. Wang, *Biosensors & Bioelectronics*, 2011, **26**, 1847-1852.

255. R. A. Gatenby and R. J. Gillies, *Nat. Rev. Cancer*, 2004, **4**, 891-899.

256. O. Warburg, *Science*, 1956, **123**, 309-314.

257. J.-w. Kim and C. V. Dang, *Cancer Research*, 2006, **66**, 8927-8930.

258. X. Huang, I. H. El-Sayed, W. Qian and M. A. El-Sayed, *J. Am. Chem. Soc.*, 2006, **128**, 2115-2120.

259. C. Loo, A. Lowery, N. J. Halas, J. West and R. Drezek, *Nano Letters*, 2005, **5**, 709-711.

260. C. Loo, A. Lin, L. Hirsch, M. H. Lee, J. Barton, N. J. Halas, J. West and R. Drezek, *Technology in Cancer Research & Treatment*, 2004, **3**, 33-40.

261. H. C. Huang, K. Rege and J. J. Heys, *Acs Nano*, 2010, **4**, 2892-2900.

262. C. S. Rejiya, J. Kumar, V. Raji, M. Vibin and A. Abraham, *Pharmacological Research*, 2012, **65**, 261-269.

263. D. P. O'Neal, L. R. Hirsch, N. J. Halas, J. D. Payne and J. L. West, *Cancer Letters*, 2004, **209**, 171-176.

264. E. Y. Hleb, J. H. Hafner, J. N. Myers, E. Y. Hanna, B. C. Rostro, S. A. Zhdanok and D. O. Lapotko, *Nanomedicine (London, U. K.)*, 2008, **3**, 647-667.

265. B. Khlebtsov, V. Zharov, A. Melnikov, V. Tuchin and N. Khlebtsov, *Nanotechnology*, 2006, **17**, 5167-5179.

266. J. Choi, J. Yang, D. Bang, J. Park, J.-S. Suh, Y.-M. Huh and S. Haam, *Small*, 2012, **8**, 746-753.

267. J. F. Hainfeld, D. Slatkin and H. M. Smilowitz, *Phys. Med. Biol.*, 2004, **49**, N309-N315.

268. P. Huang, L. Bao, C. Zhang, J. Lin, T. Luo, D. Yang, M. He, Z. Li, G. Gao, B. Gao, S. Fu and D. Cui, *Biomaterials*, 2011, **32**, 9796-9809.

269. C. J. Liu, C. H. Wang, S. T. Chen, H. H. Chen, W. H. Leng, C. C. Chien, C. L. Wang, I. M. Kempson, Y. Hwu, T. C. Lai, M. Hsiao, C. S. Yang, Y. J. Chen and G. Margaritondo, *Physics in Medicine and Biology*, 2010, **55**, 931-945.

270. H. Matsudaira, A. M. Ueno and I. Furuno, *Radiat. Res.*, 1980, **84**, 144-148.

271. D. F. Regulla, L. B. Hieber and M. Seidenbusch, *Radiat. Res.*, 1998, **150**, 92-100.

272. Y. Malam, M. Loizidou and A. M. Seifalian, *Trends in Pharmacological Sciences*, 2009, **30**, 592-599.

273. Z. P. Xu, Q. H. Zeng, G. Q. Lu and A. B. Yu, *Chemical Engineering Science*, 2006, **61**, 1027-1040.

274. G. F. Paciotti, D. G. I. Kingston and L. Tamarkin, *Drug Development Research*, 2006, **67**, 47-54.

275. G. F. Paciotti, L. Myer, D. Weinreich, D. Goia, N. Pavel, R. E. McLaughlin and L. Tamarkin, *Drug Delivery*, 2004, **11**, 169-183.

276. N. G. Portney and M. Ozkan, *Analytical and Bioanalytical Chemistry*, 2006, **384**, 620-630.

277. S. S. Agasti, A. Chompoosor, C.-C. You, P. Ghosh, C. K. Kim and V. M. Rotello, *Journal of the American Chemical Society*, 2009, **131**, 5728-5729.

278. Y. Cheng, A. C. Samia, J. D. Meyers, I. Panagopoulos, B. W. Fei and C. Burda, *Journal of the American Chemical Society*, 2008, **130**, 10643-10647.

279. W. W. Weare, S. M. Reed, M. G. Warner and J. E. Hutchison, *J. Am. Chem. Soc.*, 2000, **122**, 12890-12891.

280. G. H. Woehrle, L. O. Brown and J. E. Hutchison, *J. Am. Chem. Soc.*, 2005, **127**, 2172-2183.

281. S. Al-Nasiry, N. Geusens, M. Hanssens, C. Luyten and R. Pijnenborg, *Hum. Reprod.*, 2007, **22**, 1304-1309.

282. Y. Y. He, X. C. Wang, P. K. Jin, B. Zhao and X. Fan, *Spectrochim. Acta, Part A*, 2009, **72A**, 876-879.

283. G. Schmid, *Chemical Society Reviews*, 2008, **37**, 1909-1930.

284. W. Jiang, B. Y. S. Kim, J. T. Rutka and W. C. W. Chan, *Nature Nanotechnology*, 2008, **3**, 145-150.

285. T. Mironava, M. Hadjiargyrou, M. Simon, V. Jurukovski and M. H. Rafailovich, *Nanotoxicology*, 2010, **4**, 120-137.

286. Y. Pan, A. Leifert, D. Ruau, S. Neuss, J. Bornemann, G. Schmid, W. Brandau, U. Simon and W. Jahnen-Dechent, *Small*, 2009, **5**, 2067-2076.

287. C. M. Goodman, C. D. McCusker, T. Yilmaz and V. M. Rotello, *Bioconjugate Chemistry*, 2004, **15**, 897-900.

288. Y. Liu, W. Meyer-Zaika, S. Franzka, G. Schmid, M. Tsoli and H. Kuhn, *Angew. Chem., Int. Ed.*, 2003, **42**, 2853-2857.

289. C. Zhang, S. Gao, W. Jiang, S. Lin, F. Du, Z. Li and W. Huang, *Biomaterials*, 2010, **31**, 6075-6086.

290. S. H. Lee, K. H. Bae, S. H. Kim, K. R. Lee and T. G. Park, *International Journal of Pharmaceutics*, 2008, **364**, 94-101.

Appendix

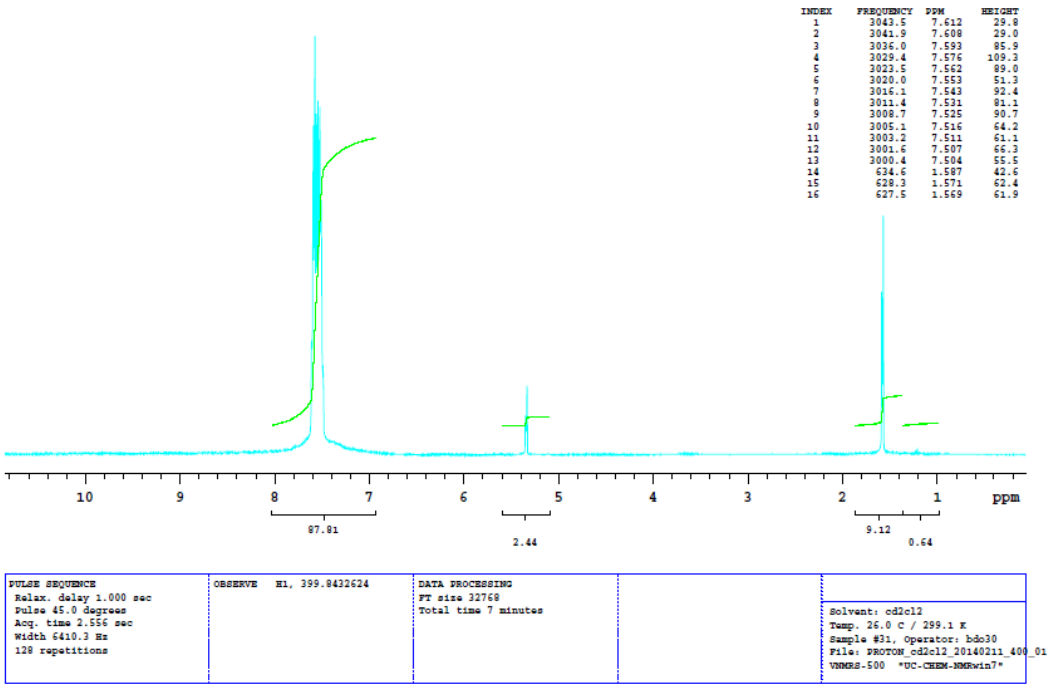

Appendix 1. ^{1}H NMR of $AuPPh_3Cl$ in CD_2Cl_2

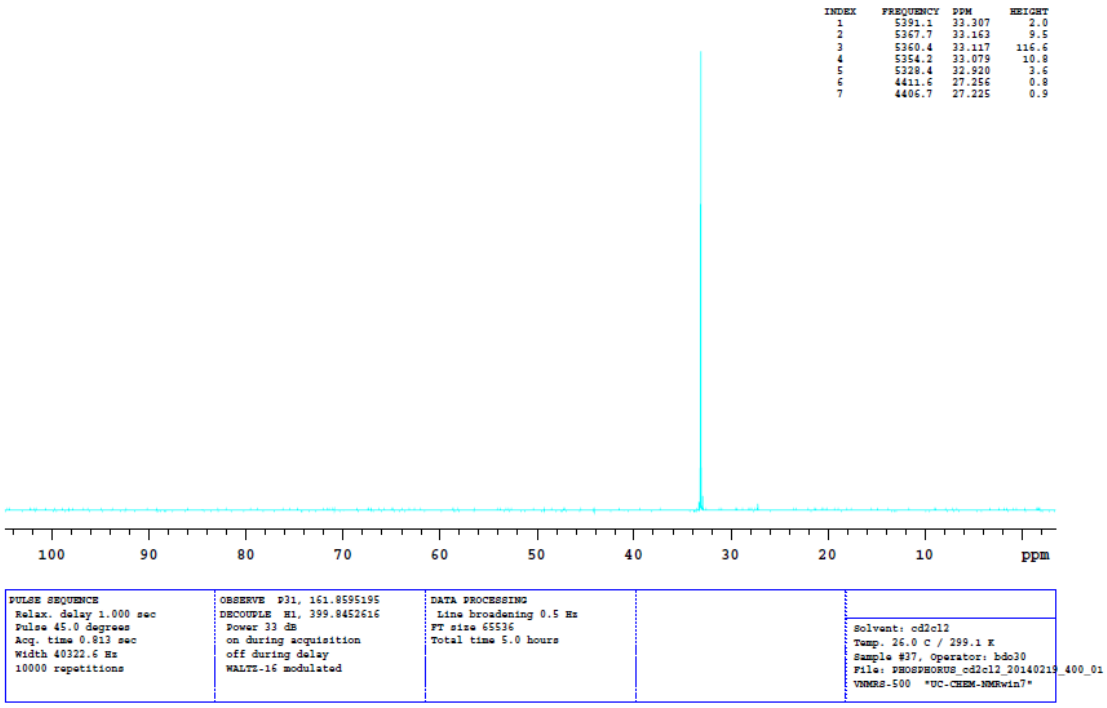

Appendix 2. ^{31}P NMR of $AuPPh_3Cl$ in CD_2Cl_2

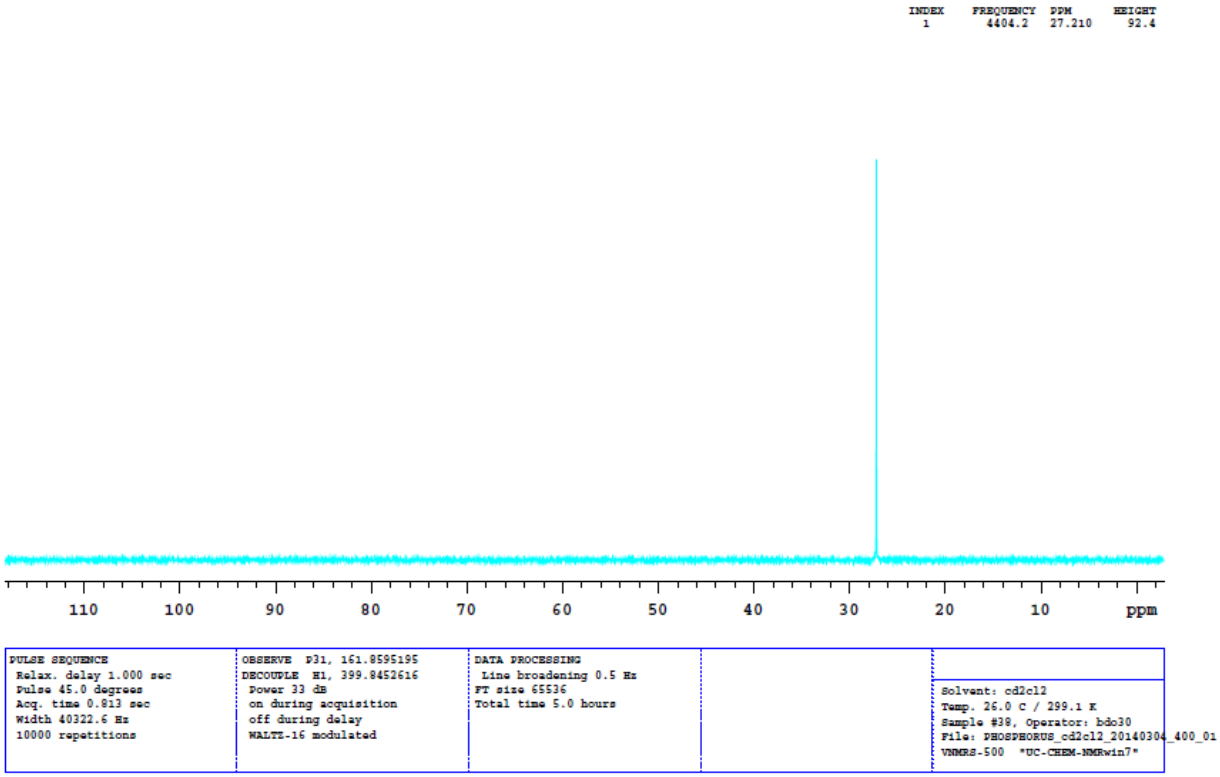

Appendix 3. ^{31}P NMR of $AuPPh_3NO_3$ in CD_2Cl_2

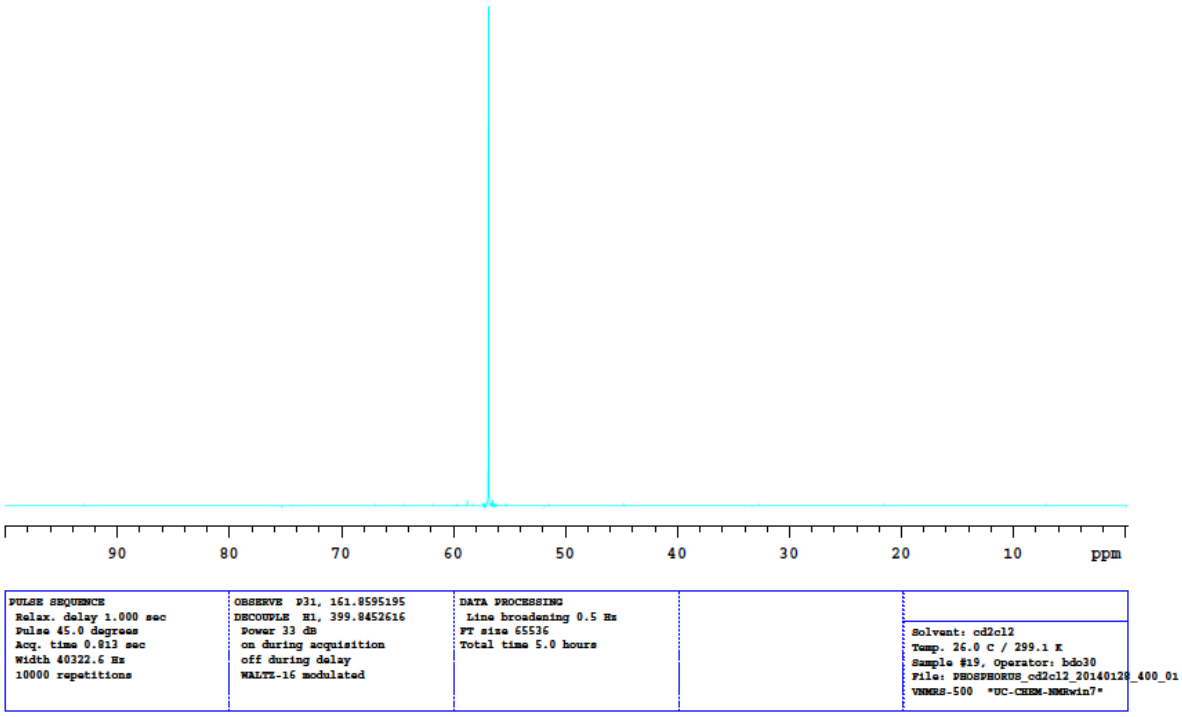

Appendix 4. ^{31}P NMR of $Au_9(PPh_3)_8(NO_3)_3$ in CD_2Cl_2

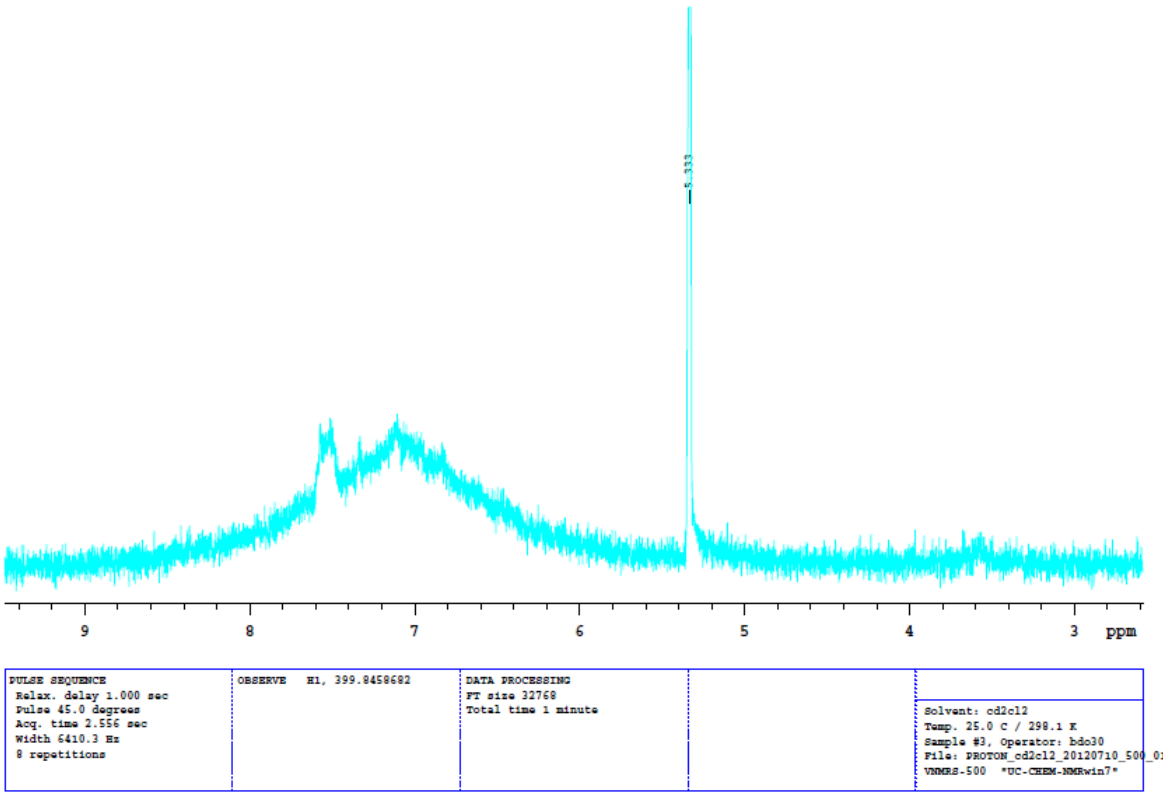

Appendix 5. ^{1}H NMR of $Au_{101}(PPh_3)_{21}Cl_6$ in CD_2Cl_2

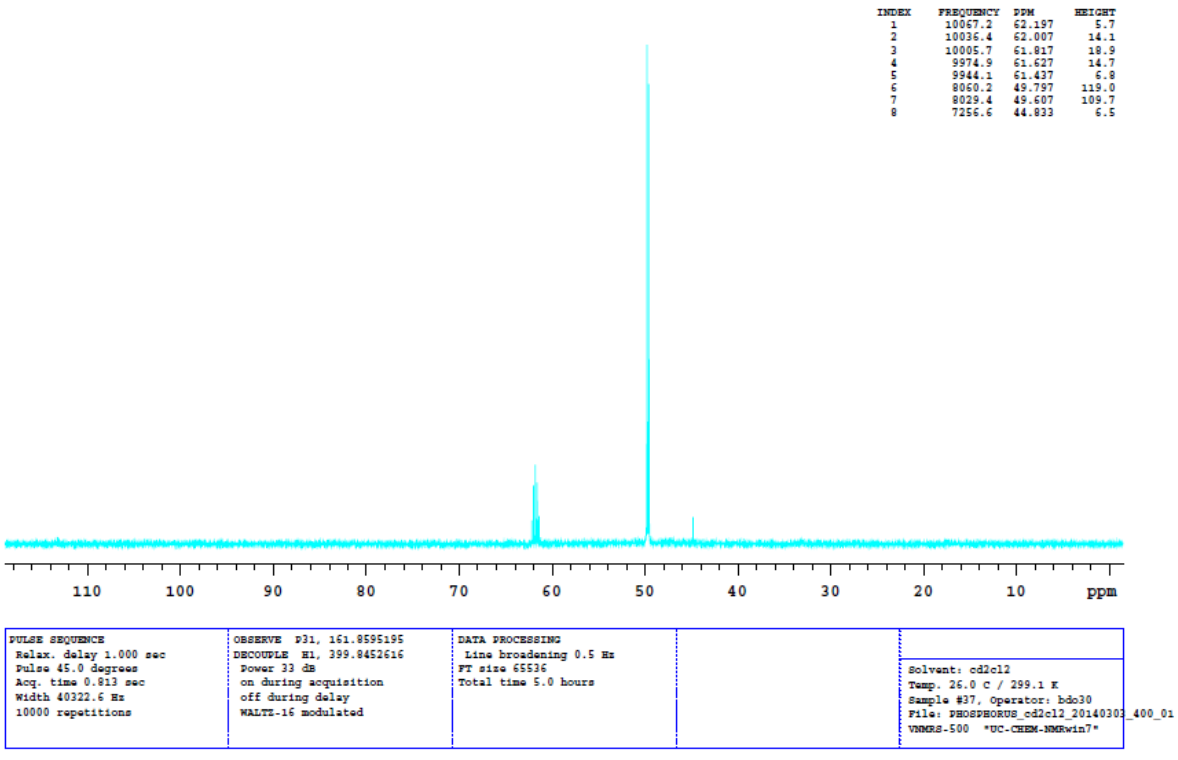

Appendix 6. ^{31}P NMR of $PdAu_6(PPh_3)_7(NO_3)_2$ in CD_2Cl_2

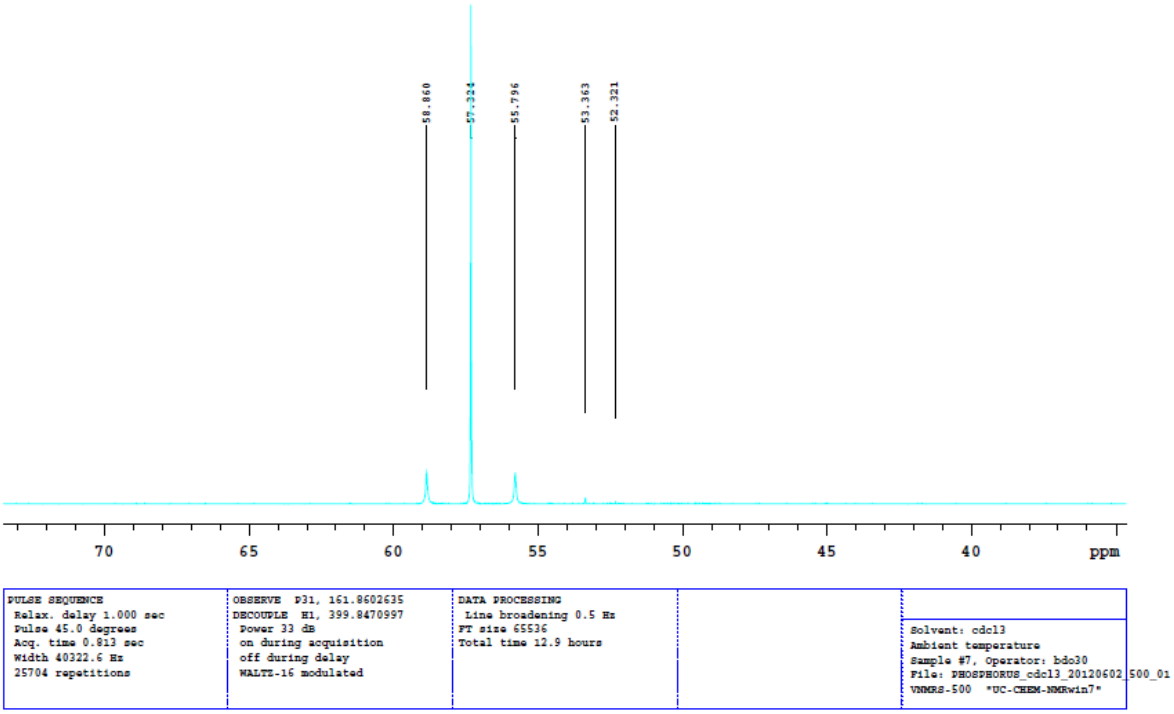

Appendix 7. ^{31}P NMR of $PtAu_8(PPh_3)_8(NO_3)_2$ in $CDCl_3$

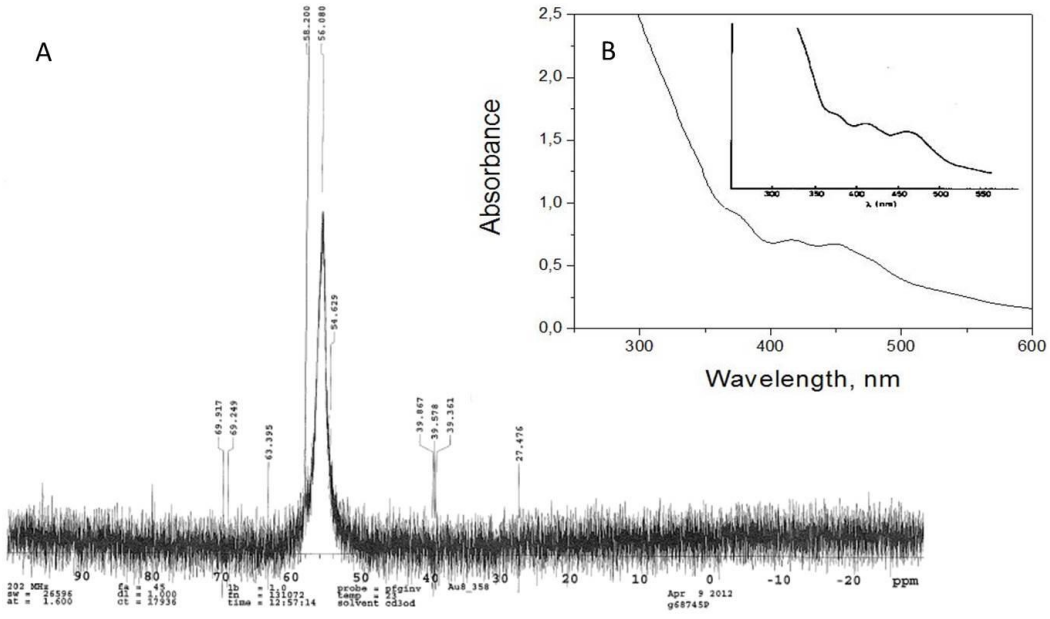

Appendix 8. ^{31}P NMR of $Au_8(PPh_3)_8(NO_3)_2$ in CD_3OD (A) and UV-vis of $Au_8(PPh_3)_8(NO_3)_2$ in CH_2Cl_2 (B, inset shows the earlier reported UV-vis spectrum of Au_8)

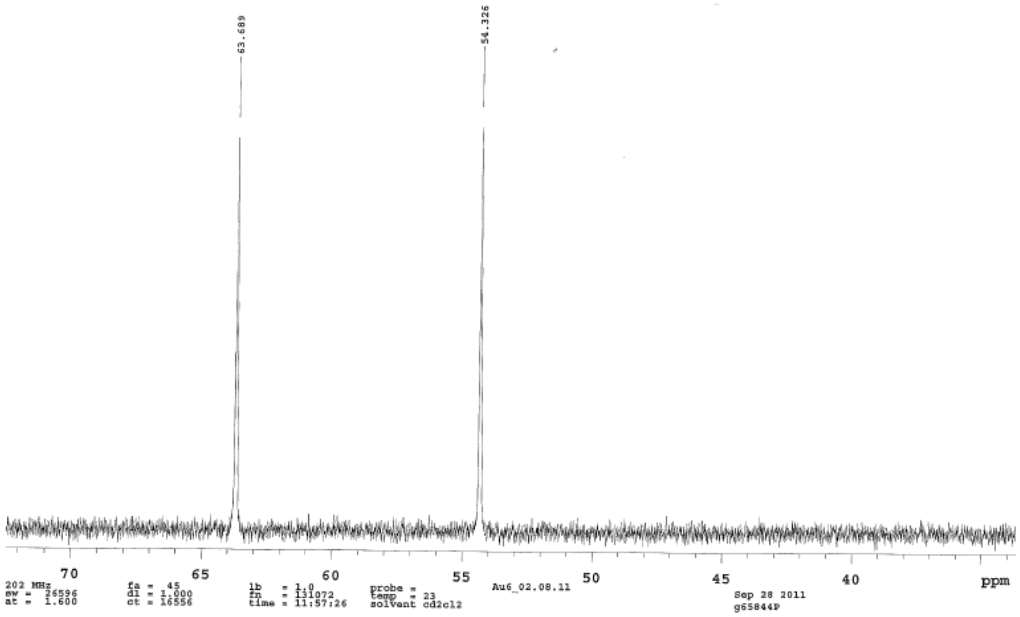

Appendix 9. ^{31}P NMR of $Au_6(dppp)_4(NO_3)_2$ in CD_2Cl_2

Trace products in cyclohexene oxidation by mass-spectrometry

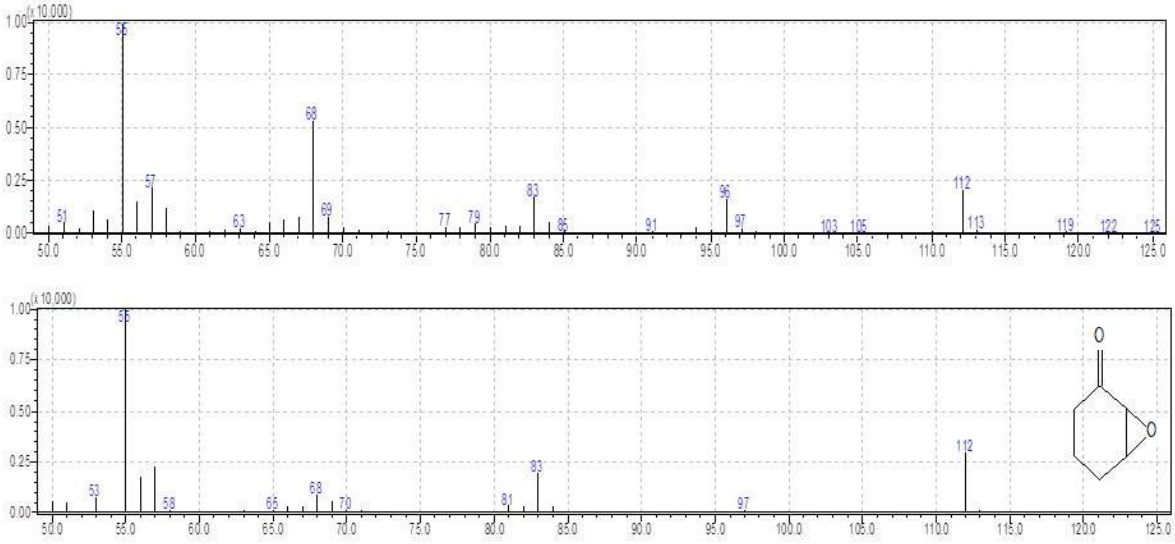

Appendix 10. Mass-spectrum of 2,3-Epoxycyclohexenone. Top – experimental data, bottom – library data.

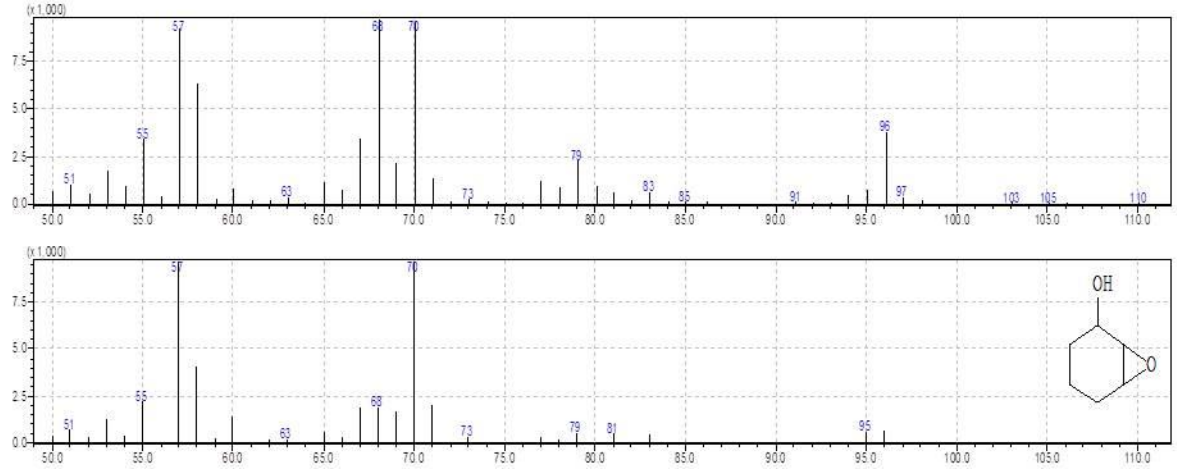

Appendix 11. Mass-spectrum of 2,3-Epoxycyclohexenol. Top – experimental data, bottom – library data.

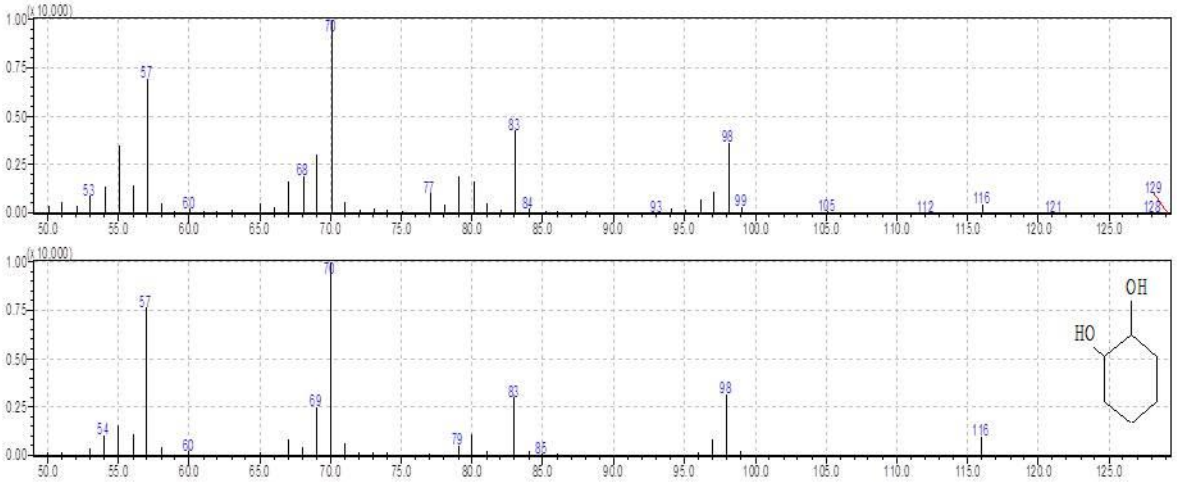

Appendix 12. Mass-spectrum of 1,2-Cyclohexanediol. Top – experimental data, bottom – library data.

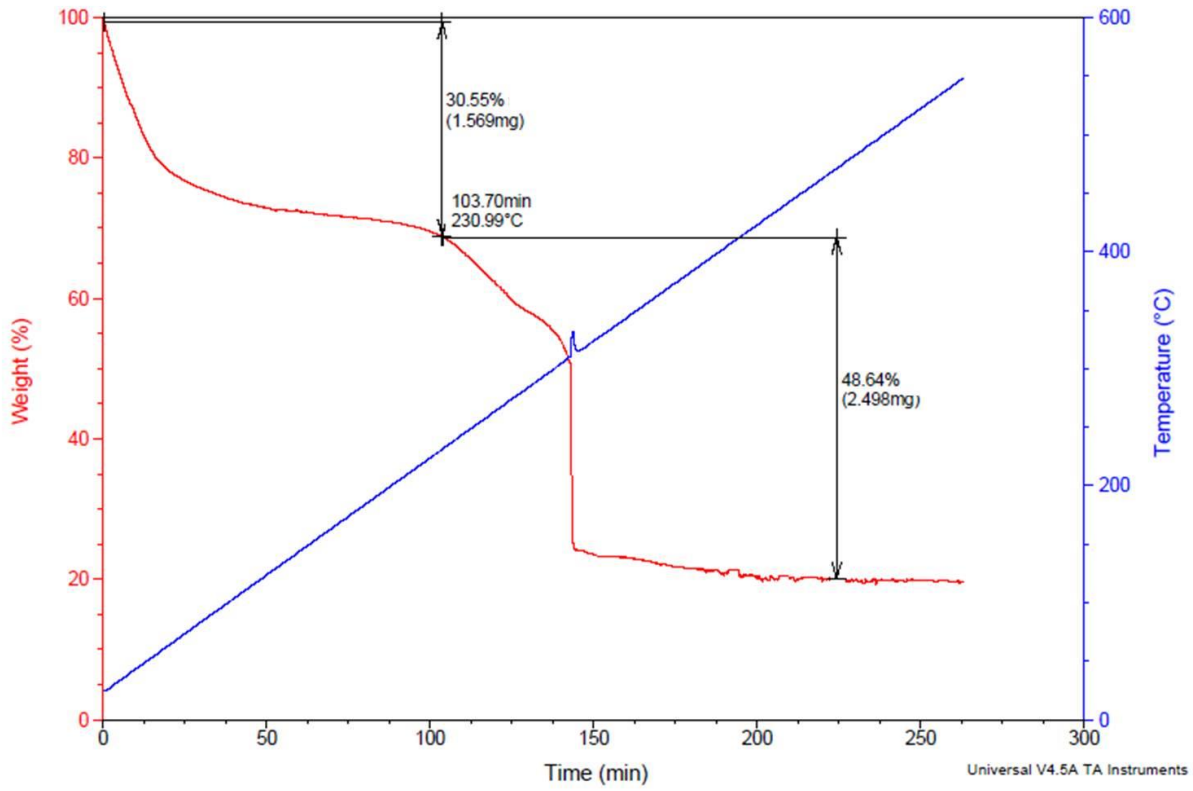

Appendix 13. TGA of CrMIL-101.

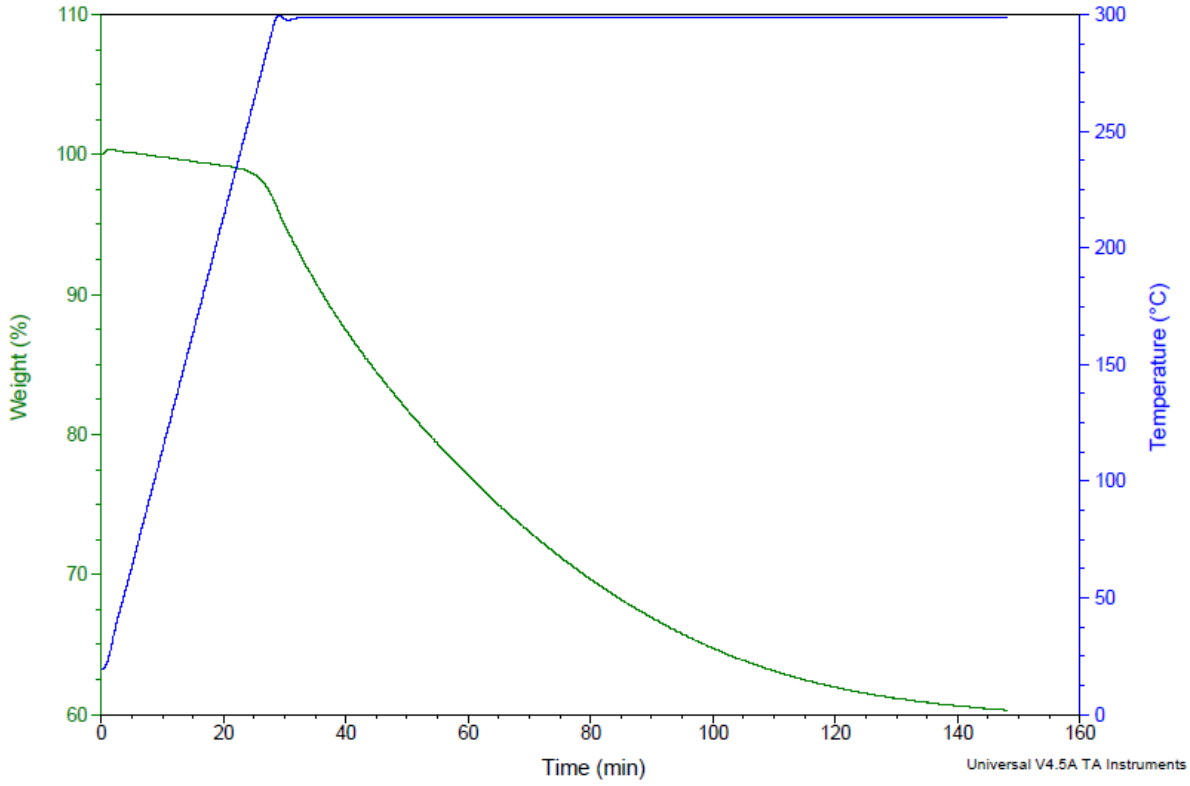

Appendix 14. TGA of $Au_6(dppp)_4(NO_3)_2$

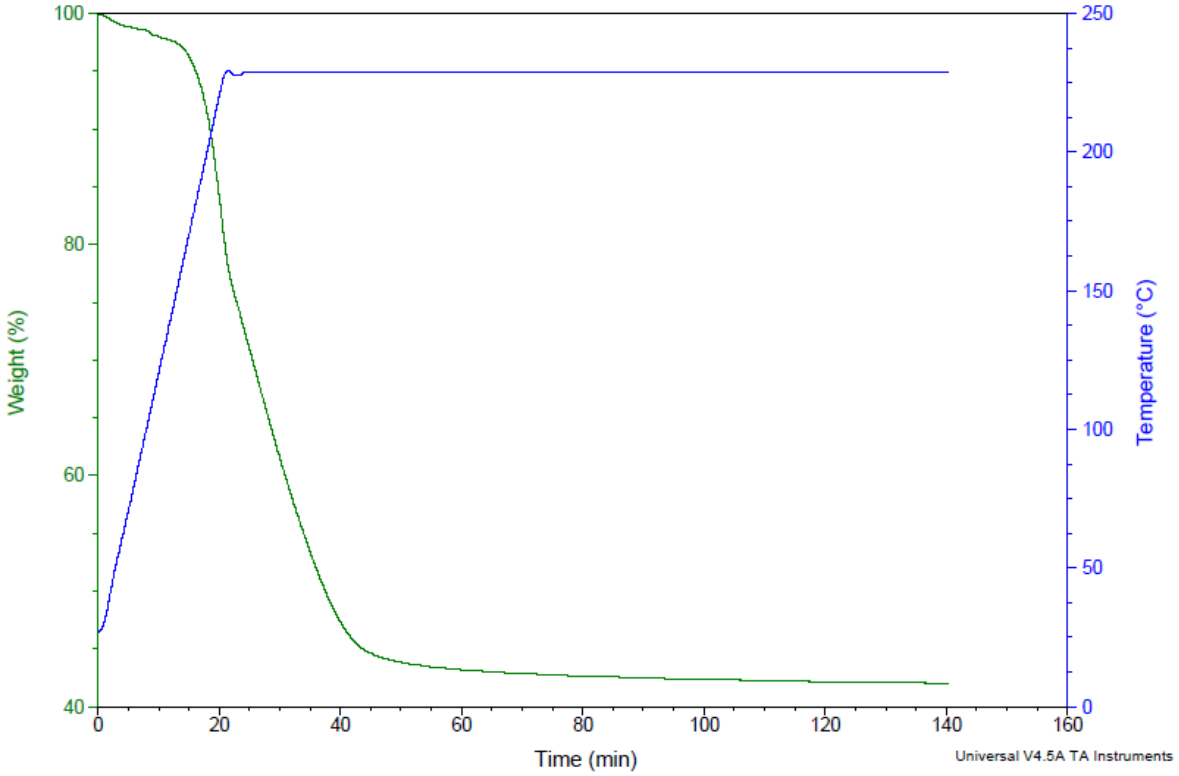

Appendix 15. TGA of $Au_8(PPh_3)_8(NO_3)_2$

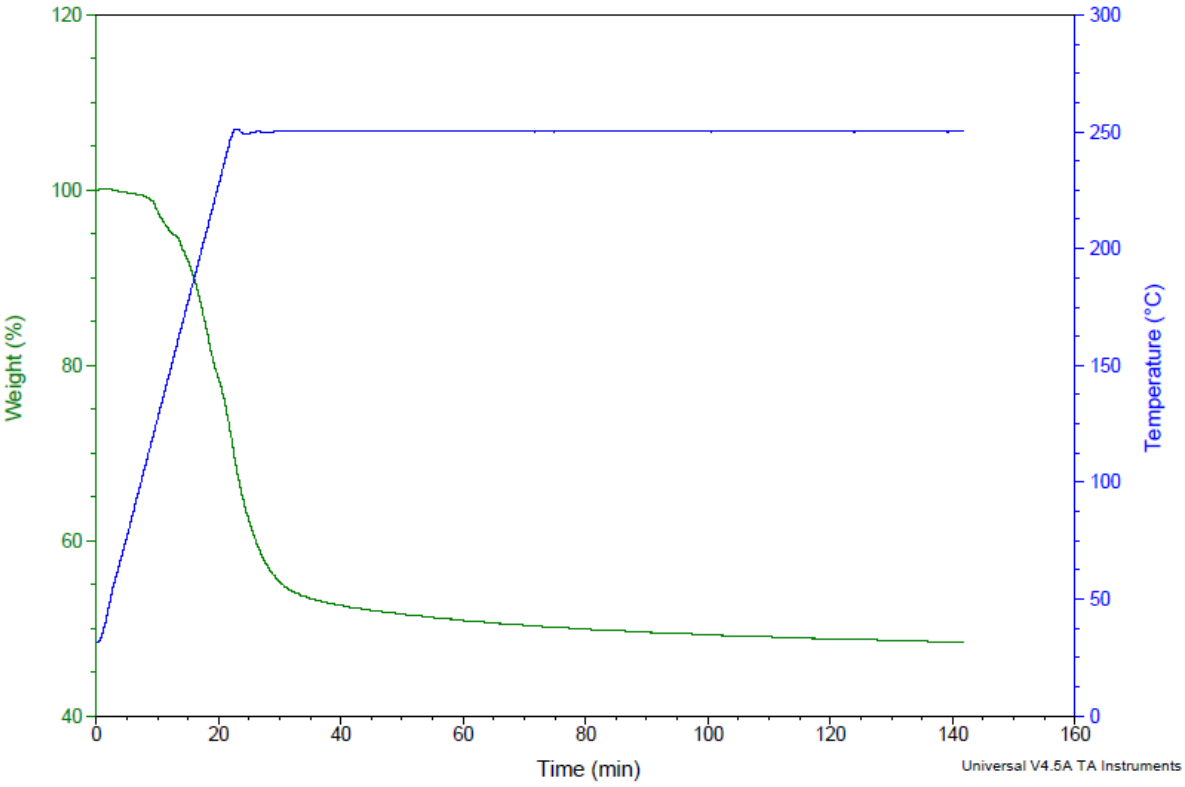

Appendix 16. TGA of $PdAu_6(PPh_3)_7(NO_3)_2$

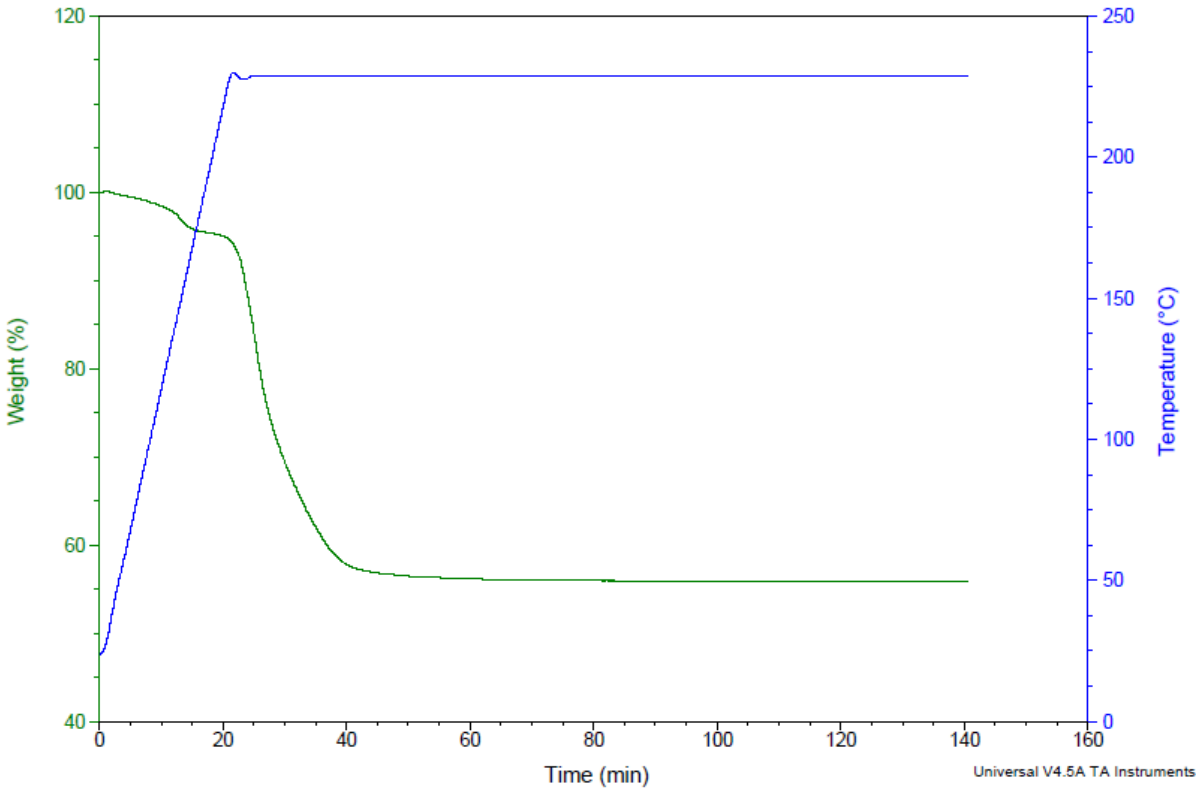

Appendix 17. TGA of $PtAu_8(PPh_3)_8(NO_3)_2$.

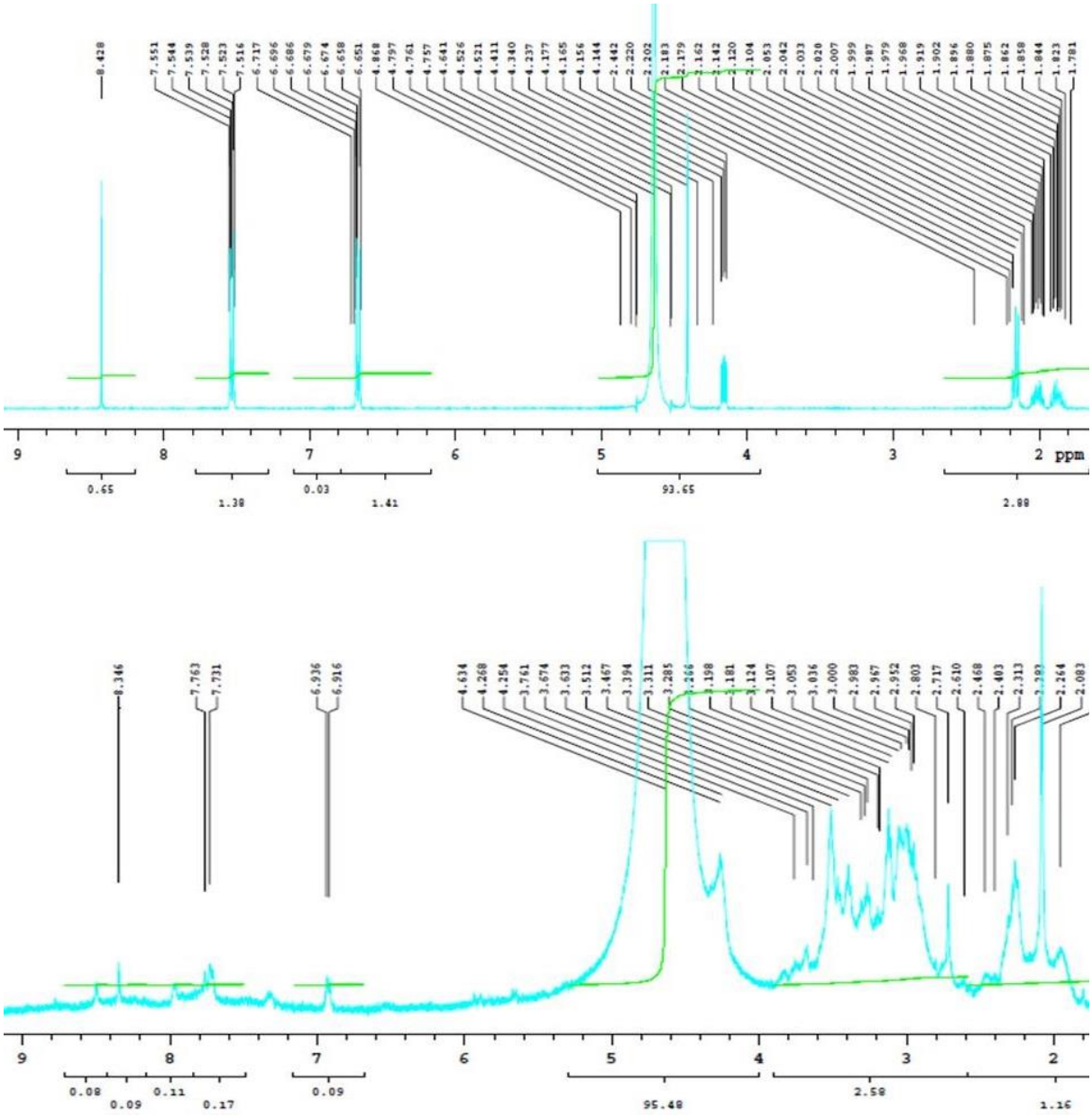

Appendix 18. ^{1}H NMR of folic acid (top) and decomposed Au_{101}-FA (bottom) in D_2O.

Appendix 19. Kinetic model for the oxidation of cyclohexene.

The following mechanism could be suggested:

1) $Au + C_6H_{10} \rightarrow Au\text{-}H + C_6H_9\cdot$
2) $C_6H_9\cdot + O_2 \rightarrow C_6H_9\text{-}OO\cdot$
3) $C_6H_9\text{-}OO\cdot + C_6H_{10} \rightarrow C_6H_9\text{-}OOH + C_6H_9\cdot$
4) $C_6H_9\text{-}OO\cdot + C_6H_9\text{-}OOH \rightarrow C_6H_9\text{-}OOH + C_6H_8\cdot\text{-}OOH$
5) $C_6H_8\cdot\text{-}OOH \rightarrow C_6H_8{=}O + \cdot OH$
6) $C_6H_9\text{-}OOH \rightarrow C_6H_9\text{-}O\cdot + \cdot OH$

7) $C_6H_9\text{-}O\cdot + C_6H_{10} \rightarrow C_6H_9OH + C_6H_9\cdot$

8) $C_6H_9\text{-}O\cdot + C_6H_{10} \rightarrow C_6H_{10}O + C_6H_9\cdot$

9) $2\ C_6H_9\text{-}OO\cdot \rightarrow C_6H_8{=}O + C_6H_9OH + O_2$

10) $C_6H_9\text{-}OO\cdot + C_6H_{10} \rightarrow C_6H_{10}O + C_6H_9\text{-}O\cdot$

11) $2Au\text{-}H + O_2 \rightarrow 2Au + 2\cdot OH$

12) $\cdot OH + C_6H_9\cdot \rightarrow C_6H_9OH$

13) $\cdot OH + C_6H_{10} \rightarrow C_6H_9\cdot + H_2O$

14) $Au + C_6H_9\text{-}OOH \rightarrow Au\text{-}H + \cdot C_6H_8\text{-}OOH$

15) $\cdot C_6H_8\text{-}OOH + O2 \rightarrow \cdot OO\text{-}C_6H_8\text{-}OOH$

16) $2\cdot OO\text{-}C_6H_8\text{-}OOH \rightarrow O{=}C_6H_7\text{-}OOH + HO\text{-}C_6H_8\text{-}OOH + O_2$

$$\alpha := \begin{pmatrix} -1 & -1 & 1 & 1 & 0 & 0 & 0 & 0 & 0 & 0 & 0 & 0 & 0 & 0 & 0 & 0 & 0 \\ 0 & 0 & 0 & -1 & -1 & 1 & 0 & 0 & 0 & 0 & 0 & 0 & 0 & 0 & 0 & 0 & 0 \\ 0 & -1 & 0 & 1 & 0 & -1 & 1 & 0 & 0 & 0 & 0 & 0 & 0 & 0 & 0 & 0 & 0 \\ 0 & 0 & 0 & 0 & 0 & -1 & 0 & 1 & 0 & 0 & 0 & 0 & 0 & 0 & 0 & 0 & 0 \\ 0 & 0 & 0 & 0 & 0 & 0 & 0 & -1 & 1 & 1 & 0 & 0 & 0 & 0 & 0 & 0 & 0 \\ 0 & 0 & 0 & 0 & 0 & 0 & -1 & 0 & 0 & 1 & 1 & 0 & 0 & 0 & 0 & 0 & 0 \\ 0 & -1 & 0 & 1 & 0 & 0 & 0 & 0 & 0 & 0 & -1 & 1 & 0 & 0 & 0 & 0 & 0 \\ 0 & -1 & 0 & 1 & 0 & 0 & 0 & 0 & 0 & 0 & -1 & 0 & 1 & 0 & 0 & 0 & 0 \\ 0 & 0 & 0 & 0 & 1 & -2 & 0 & 0 & 1 & 0 & 0 & 1 & 0 & 0 & 0 & 0 & 0 \\ 0 & -1 & 0 & 0 & 0 & -1 & 0 & 0 & 0 & 0 & 1 & 0 & 1 & 0 & 0 & 0 & 0 \\ 2 & 0 & -2 & 0 & -1 & 0 & 0 & 0 & 0 & 2 & 0 & 0 & 0 & 0 & 0 & 0 & 0 \\ 0 & 0 & 0 & -1 & 0 & 0 & 0 & 0 & 0 & -1 & 0 & 1 & 0 & 0 & 0 & 0 & 0 \\ 0 & -1 & 0 & 1 & 0 & 0 & 0 & 0 & 0 & -1 & 0 & 0 & 0 & 1 & 0 & 0 & 0 \\ -1 & 0 & 1 & 0 & 0 & 0 & -1 & 0 & 0 & 0 & 0 & 0 & 0 & 0 & 1 & 0 & 0 \\ 0 & 0 & 0 & 0 & -1 & 0 & 0 & 0 & 0 & 0 & 0 & 0 & 0 & 0 & -1 & 1 & 0 \\ 0 & 0 & 0 & 0 & 1 & 0 & 0 & 0 & 0 & 0 & 0 & 0 & 0 & 0 & -2 & 1 & 1 \end{pmatrix}$$

$$\text{Model}(k, x) := \alpha^{T} \begin{pmatrix} k_1 x_1 x_2 \\ k_2 x_4 x_5 \\ k_3 x_6 x_2 \\ k_4 x_6 x_7 \\ k_5 x_8 \\ k_6 x_7 \\ k_7 x_{11} x_2 \\ k_8 x_{11} x_2 \\ k_9 x_6 x_6 \\ k_{10} x_6 x_2 \\ k_{11} x_3 x_3 x_5 \\ k_{12} x_{10} x_4 \\ k_{13} x_{10} x_2 \\ k_{14} x_1 x_7 \\ k_{15} x_{15} x_5 \\ k_{16} x_{16} x_{16} \end{pmatrix} \rightarrow \begin{bmatrix} 2 \cdot k_{11} \cdot x_5 \cdot (x_3)^2 - k_1 \cdot x_1 \cdot x_2 - k_{14} \cdot x_1 \cdot x_7 \\ -k_1 \cdot x_1 \cdot x_2 - k_3 \cdot x_2 \cdot x_6 - k_{10} \cdot x_2 \cdot x_6 - k_7 \cdot x_2 \cdot x_{11} - k_8 \cdot x_2 \cdot x_{11} - k_{13} \cdot x_2 \cdot x_{10} \\ k_1 \cdot x_1 \cdot x_2 - 2 \cdot k_{11} \cdot x_5 \cdot (x_3)^2 + k_{14} \cdot x_1 \cdot x_7 \\ k_1 \cdot x_1 \cdot x_2 - k_2 \cdot x_4 \cdot x_5 + k_3 \cdot x_2 \cdot x_6 + k_7 \cdot x_2 \cdot x_{11} + k_8 \cdot x_2 \cdot x_{11} + k_{13} \cdot x_2 \cdot x_{10} - k_{12} \cdot x_4 \cdot x_{10} \\ k_9 \cdot (x_6)^2 - k_{11} \cdot x_5 \cdot (x_3)^2 + k_{16} \cdot (x_{16})^2 - k_2 \cdot x_4 \cdot x_5 - k_{15} \cdot x_5 \cdot x_{15} \\ k_2 \cdot x_4 \cdot x_5 - 2 \cdot k_9 \cdot (x_6)^2 - k_3 \cdot x_2 \cdot x_6 - k_4 \cdot x_6 \cdot x_7 - k_{10} \cdot x_2 \cdot x_6 \\ k_3 \cdot x_2 \cdot x_6 - k_6 \cdot x_7 - k_{14} \cdot x_1 \cdot x_7 \\ k_4 \cdot x_6 \cdot x_7 - k_5 \cdot x_8 \\ k_9 \cdot (x_6)^2 + k_5 \cdot x_8 \\ 2 \cdot k_{11} \cdot x_5 \cdot (x_3)^2 + k_5 \cdot x_8 + k_6 \cdot x_7 - k_{13} \cdot x_2 \cdot x_{10} - k_{12} \cdot x_4 \cdot x_{10} \\ k_6 \cdot x_7 + k_{10} \cdot x_2 \cdot x_6 - k_7 \cdot x_2 \cdot x_{11} - k_8 \cdot x_2 \cdot x_{11} \\ k_9 \cdot (x_6)^2 + k_7 \cdot x_2 \cdot x_{11} + k_{12} \cdot x_4 \cdot x_{10} \\ k_{10} \cdot x_2 \cdot x_6 + k_8 \cdot x_2 \cdot x_{11} \\ k_{13} \cdot x_2 \cdot x_{10} \\ k_{14} \cdot x_1 \cdot x_7 - k_{15} \cdot x_5 \cdot x_{15} \\ k_{15} \cdot x_5 \cdot x_{15} - 2 \cdot k_{16} \cdot (x_{16})^2 \\ k_{16} \cdot (x_{16})^2 \\ k_{16} \cdot (x_{16})^2 \end{bmatrix}$$

$$\text{CyH0} := 1$$

$$inC := \begin{pmatrix} 0.005 \\ CyH0 \\ 0 \\ 0 \\ 50 \\ 0 \\ 0 \\ 0 \\ 0 \\ 0 \\ 0 \\ 0 \\ 0 \\ 0 \\ 0 \\ 0 \\ 0 \end{pmatrix}$$

$k_1 := 2\ k_2 := 1.0\ k_3 := 2.0\ k_4 := 3.2\ k_5 := 2.5\ k_6 := 0.0\ k_7 := 5\ k_8 := 2.1\ k_9 := 1.2\ k_{10} := 0.00\ k_{11} := 5$

$k_{12} := 0.02\ k_{13} := 0.02\ k_{14} := 5\ k_{15} := 10\ k_{16} := 10$

$Func(t, x) := Model(k, x)$

$S := rkfixed(inC, 0, 25, 5000, Func)$

$t := S^{\langle 1 \rangle}$ $\quad Conv := 100 \cdot \dfrac{CyH0 - S^{\langle 3 \rangle}}{CyH0}$, $\quad YieldTotal := YieldOne + YieldOl + YieldH + YieldOx$

$YieldOne := 100 \cdot \dfrac{S^{\langle 10 \rangle}}{CyH0}$, $\quad YieldOl := 100 \cdot \dfrac{S^{\langle 13 \rangle}}{CyH0}$,

$YieldH := 100 \cdot \dfrac{S^{\langle 8 \rangle}}{CyH0}$, $\quad YieldOx := 100 \cdot \dfrac{S^{\langle 14 \rangle}}{CyH0}$

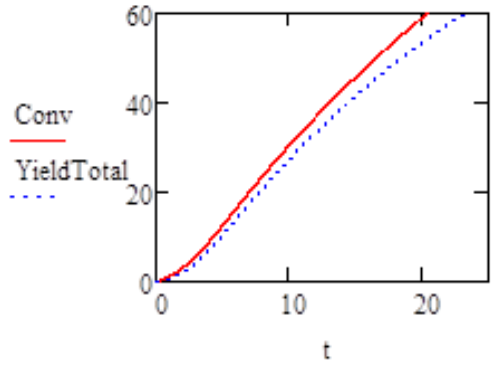
Conv
YieldTotal
60
40
20
0
0
10
20
t

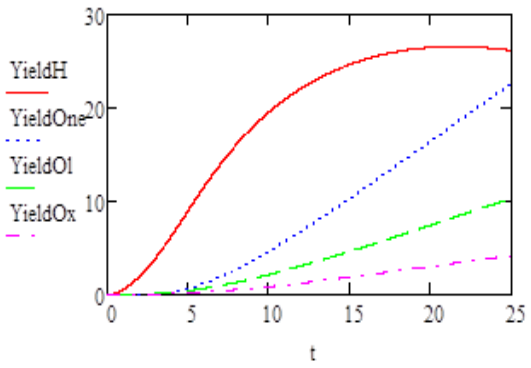
YieldH
YieldOne
YieldOl
YieldOx
30
20
10
0
0
5
10
15
20
25
t